AD-A190 503

DTIC FILE COPY

INTERACTION OF A TWO-DIMENSIONAL BLUFF BODY AND INCOMPRESSIBLE JET AND ANNULUS FLOWS

THESIS

Christopher A. Boedicker
Captain, USAF

AFIT/GAE/AA/87D-2

DTIC
ELECTE
MAR 0 3 1988
H

DEPARTMENT OF THE AIR FORCE
AIR UNIVERSITY
AIR FORCE INSTITUTE OF TECHNOLOGY

Wright-Patterson Air Force Base, Ohio

DISTRIBUTION STATEMENT A
Approved for public release;

88 3 01 128

AFIT/GAE/AA/87D-2

INTERACTION OF A TWO-DIMENSIONAL BLUFF BODY AND INCOMPRESSIBLE JET AND ANNULUS FLOWS

THESIS

Christopher A. Boedicker
Captain, USAF

AFIT/GAE/AA/87D-2

Approved for public release; distribution unlimited

DTIC
ELECTE
MAR 0 3 1988
S D
H

AFIT/GAE/AA/87D-2

INTERACTION OF A TWO-DIMENSIONAL BLU F BODY AND INCOMPRESSIBIE JET AND ANNULUS FLOWS

THESIS

Presented to the Faculty of the School of Engineering
of the Air Force Institute of Technology
Air University
In Partial Fulfillment of the
Requirements for the Degree of
Master of Science in Aeronautical Engineering

Christopher A. Boedicker, B.S.
Captain, US F

December 1987

Approved for public release; distribution unlimited

Preface

The objective of this investigation was to try to better understand the interactions of jet and annulus flows in the presence of a bluff body. These interactions are very important in combustors and injectors, and a greater understanding of flow interaction can be ultimately used to increase the efficiency and performance of these devices. This investigation, however, was conducted from a scientific viewpoint, not an engineering one.

A unique apparatus was used to determine the nature of the interactions. A two-dimensional bluff body surrounded a planar slot jet which exhausted into a parallel, moving stream, the annulus flow. Flow visualization provided qualitative insight into flowfield occurrences. Laser Doppler Anemometry was used to measure axial and transverse velocities for the two-dimensional configuration. Light scattering, Mie scattering, was used to determine the shedding frequency of the large vortex structures present in the flow. The results of these experiments were compiled, and a description of the jet and annulus interaction was developed. As in any problem in fluid mechanics, there will be some doubt concerning the applicability of the description for conditions and geometries different than those tested. Further studies, then, should test the "robustness" of the physical description provided herein.

DTIC COPY INSPECTED 1

ion For
GRA&I
B
nced
cation

By
Distribution/
Availability Codes
Dist | Avail and/or Special
A-1

"Original contains color plates: All DTIC reproductions will be in black and white"

As in any endeavor of this magnitude, there is a list of those to whom I owe at least the debt of gratitude. My faculty advisor, Lt James B. Planeaux, was very patient and helpful, and he kept steering me along the right path just as I would begin to veer. I would also like to thank Professors William C. Elrod and James E. Hitchcock for their assistance, especially with regard to the comments provided for this thesis. Dr W. Mel Roquemore, sponsor of the project, of the Aero Propulsion Lab provided invaluable assistance and lively discussions throughout the course of the investigation. The help of Mr Ron Britton, also from the Aero Propulsion Lab, is greatly appreciated. Ron's technical expertise and creative genius are only matched by his enthusiasm. It was also a pleasure to work with Professor Richard S. Tankin from Northwestern University during his short summer tour in the Aero Propulsion Lab. In the test cell where the experiments were performed, four individuals from the University of Dayton Research Institute provided assistance which was indicative of their superb professionalism. Mr W. John Schmoll provided help in every aspect of the experimentation, and without his help the investigation would never have been completed on time. Dr T.-H. Chen provided assistance in reducing and preparing the raw LDA data. Mr Darryl D. Trump handled all problems peculiar to the flow visualization set-up, and Mr James Heinrichs provided materiel support in the test cell. Assistance provided by Dr Roquemore and Ms Cindy Obringer

in preparing this document is greatly appreciated. I would also like to thank my wife Kim for typing part of this manuscript. Finally, I must thank my wife Kim and son Stephen for their unerring patience. I know this has not been easy for you, but you must surely know that you are the ones to whom I devote my life.

Christopher A. Boedicker

TABLE OF CONTENTS

	Page
Preface	ii
List of Figures	vi
List of Tables	ix
Notation	x
Abstract	xii
I. Introduction	1
II. Description of Experimental Techniques	10
III. Experimental Apparatus	20
IV. Preliminary Investigations	35
V. Flow Conditions and Experimental Procedure	42
VI. Results and Discussion	50
Flow Visualization	50
LDA Measurements	60
Mie Scattering	69
Discussion	69
VII. Conclusions and Recommendations	93
Appendix A: Determination of $TiCl_4$ Concentration	96
Appendix B: Validation of Mie Scattering Method	109
Appendix C: LDA Data Summary	116
Bibliography	147
Vita	150

List of Figures

Figure		Page
2.1.	Flow Visualization Test Set-Up	11
2.2.	Reactive Flow Visualization Examples	12
2.3.	Optical Arrangement for Flow Visualization . .	12
2.4.	Mie Scattering Test Set-Up	15
2.5.	Mie Scattering Results	18
3.1.	Co-Flowing Test Arrangement	20
3.2.	Two-Dimensional Centerbody	21
3.3.	Laboratory Test Facility Layout	23
3.4.	Flow Visualization Test Arrangement	24
3.5.	Two-Component LDA System (Optics)	25
3.6.	Data Acquisition and Processing System	26
3.7.	Three-Axis Burner Traversing Platform	29
3.8.	Spatial Coordinate System	30
3.9.	Velocity Coordinate System	30
3.10.	LDA Flow System Arrangement	31
3.11.	Low Output Tube Seeder	33
3.12.	Low Output Cyclone Seeder	34
4.1.	Flow Visualization from Tankin (1987)	36
4.2.	Flow Visualization Terminology	39
5.1.	Potential Misinterpretation of Mie Scattering Results	48
6.1.	Lateral Plane Flow Visualization	51
6.2.	Horizontal Flow Visualization (U_j = 18.5 cm/s)	55
6.3.	Horizontal Flow Visualization (U_j = 37.0 cm/s)	56
6.4.	Vertical Plane Flow Visualization	59

Figure		Page

6.5. Idealized Instantaneous Transverse Velocity for Two Solid Body Rotators Translating Uniformly 62

6.6. Axial Velocity Profiles 64

6.7. Transverse Velocity Profiles 65

6.8. u_{rms} Profiles 66

6.9. v_{rms} Profiles 67

6.10. Covariance Profiles 68

6.11. Vortex Shedding Frequencies 70

6.12. Mean Velocity Distribution (Sato, 1960) . . . 71

6.13. Estimation of Vortex Angular Rotation Rate . . 73

6.14. Duct Flow 75

6.15. Variation of Strouhal Number with Reynolds Number 78

6.16. Stable Configurations 81

6.17. Frequency Spectra from Tankin (1987) 83

6.18. Vortex Shedding Rate for the Two-Dimensional Centerbody 85

6.19. Axial Velocity Profile, Transverse Scan Exit Profile (U_j = 22.2 cm/s) 87

6.20. Axial Velocity Profile, Transverse Scan z = 60 mm (U_j = 37.0 cm/s) 89

6.21. Conception of the Reason for Asymmetric Vortex Shedding in a Thin Slot Jet 91

6.22. Vortex Shedding Frequency z = 20 mm (U_j = 33.3 cm/s) 92

A-1. Flow Visualization Test Arrangement 97

A-2. $TiCl_4$ Seeding Vessel 97

A-3. $TiCl_4$ Vapor Pressure 102

Figure Page

B-2. Optical Arrangement for Mie Scattering Method Validation 112

B-1. Flow System for Mie Scattering Method Validation 111

B-3. Natural Jet Vortex Shedding Frequency Spectrum (Axisymmetric Jet, U_j = 4 m/s) 114

B-4. Forced Jet Vortex Shedding Frequency Spectrum (Axisymmetric Jet, U_j = 4 m/s) 114

List of Tables

Table		Page
I.	Flow Conditions	42
II.	Transverse Scan Locations	44
III.	Photographic Summary	46
A-I.	Lydersen's Critical Contributions	101
A-II.	$TiCl_4$ Properties	101
A-III.	Concentration of $TiCl_4$	108
C-I.	LDA Run Summary	117

Notation

Symbols

b	Slot half width
f	Frequency
r	Radius
slpm	Standard liters per minute
u	Axial velocity
v	Transverse (radial) velocity
w	Lateral velocity
x	Lateral position
y	Transverse position
z	Axial position
A	Area
D	Slot width
Q	Volumetric flow rate
U	Theoretical (1-D) exit velocity
Re	Reynolds number
St	Strouhal number
ω	Angular rotation rate

Subscripts

a	Annulus
j	Jet
max	Maximum
r	Rotation
rms	Root-mean-square

Superscripts

~	Instantaneous value
-	Overbar denotes mean quantity

Acronyms

LDA	Laser Doppler Anenometry
JFM	Journal of Fluid Mechanics

Chemical Compounds

HCl	Hydrochloric Acid
H_2O	Water
$TiCl_4$	Titanium Tetrachloride
TiO_2	Titanium Dioxide

ABSTRACT

A particular interaction of bluff body and jet flows was studied using a two-dimensional slot jet (aspect ratio = 50) surrounded by a two-dimensional bluff body. The co-flowing system used air in the annulus and nitrogen in the jet. Flow visualization identified flow patterns containing large vortex structures. With a fixed annulus velocity, drastic changes in the flow's structure were observed as jet velocities changed. Laser Doppler Anenometry measurements of instantaneous velocities were examined to characterize the flowfield details, and high speed movies provided qualitative insight into flow dynamics. The concept of jet and annulus "fields" is introduced. The "jet field" is the region above the bluff body that extends six or seven slot widths downstream, and the "annulus field" is the region above the jet field. The annulus flow dictates the flowfield dynamics in the annulus field up to jet-to-annulus velocity ratios of 1.45. The jet is responsible for the formation of the large-scale structures and dominates the flow in the jet field. Jet domination of the entire flowfield is seen at velocity ratios of 1.45 and above. Mie scattering was used to determine shedding frequencies of the large-scale structures; Strouhal number based on jet velocity and slot width was a constant 0.098.

I. Introduction

Many studies of wakes, plumes, and jets have been accomplished. With the recent attention given to coherent structures in turbulent flow, many studies have begun to focus on the deterministic character of the flow. It had been felt that turbulent flows could only be analyzed using statistical tools. Some people believe now, however, that the character of the flow is completely determined by occurrences in the near field, where the coherent structures exist (List, 1982; Laufer, 1981; Hussain, 1986). Hussain reports that coherent structures may be the tractable part of turbulence and may contain most of the essential physics of turbulence. Laufer says that the initial instability has a strong influence on subsequent jet development. In his review article, List tells us that there is now overwhelming evidence that the initial growth of turbulent jets is a direct result of large-scale motions generated at jet boundaries. This emphasis has only recently shifted to the region near the flow's point of initiation (near field). For turbulent flows, the near field of plane jets is considered to extend from the jet exit to $z/D = 30$ or 40, where z is the axial dimension and D the slit width. The near field of axisymmetric jets is considered to end at approximately $z/D = 8$, where D is now the jet exit diameter.

Thousands of papers on turbulence have been written, but most of these efforts focused on the far field. Also,

nearly all work has been accomplished for geometries that are not complicated (i.e., jets, shear layers, bluff bodies, etc are studied, but combinations like a jet flowing into a moving stream are relatively rare). Studies that did investigate co-flowing systems showed that the parallel flow has a significant impact on the jet flow. Bradbury (1965) studied a turbulent plane jet exhausting into a slow-moving parallel flow and found self-similarity of the flow was achieved much further downstream when a parallel flow (even a very weak one) was used. Everitt and Robins (1978) have recently confirmed this result. Their experiments on a plane jet exhausting into a moving airstream proposed a concept of "strong" and "weak" jets. The weak jet is one whose velocity is small compared to the parallel flow and results in a slow development of the flow.

Some recent work on various combustor configurations has introduced unique geometries which may be used to better characterize the events in the near and far fields of jets and co-flowing systems. Roquemore et al (1986) studied an axisymmetric bluff body combustor, and Ballal and Chen (1986) and Tankin (1987) tested a two-dimensional slot jet surrounded by a bluff body (the configuration will be referred to as the 2-D centerbody, and it can be seen in Figure 3.1). This configuration represents the two-dimensional analogue of an afterburner's fuel ring (Ballal and Chen, 1986). The bluff body is used to provide

stability. The high aspect ratio jet exhausts into a moving airstream, referred to as the annulus flow. Flame stabilization is greatly enhanced by the fluid dynamic processes that occur in the near field. This configuration is indeed unique since it incorporates a jet, a bluff body, and a parallel annulus flow. Previous research on another configuration like this has not been identified. This set-up is also important in that it provides a geometry which simplifies advanced Computational Fluid Dynamics (CFD) models.

Ballal and Chen studied a jet flow and used CO_2 as the working fluid. Annulus velocity was only 10 percent of the jet velocity, and this ensured they had a jet flow. From the Laser Doppler Anenometry (LDA) data they obtained, which focused on the near field, they were able to provide a physical description of the flowfield development. Attempts to verify this description using flow visualization failed. Since CO_2 is negatively buoyant, the flow is highly unstable, and two-dimensional visualization of the flow did not provide any evidence of the large-scale structure they had predicted.

Tankin used the same configuration as Ballal and Chen to perform an extensive flow visualization study. Air was used in the annulus, while N_2, He, and CO_2 were used separately in the jet. Wide ranges of annulus and jet flows were investigated. Tankin was also able to use a special

technique that used light scattering, Mie scattering, to determine the shedding frequencies of the large vortex structures evident in some of the flows.

As evidenced by Tankin's work, velocities low enough to avoid homogeneous turbulence produce large-scale vortex structures which persist far downstream of the jet's exit plane. These flow patterns closely resemble the patterns seen in the wake of a cylinder at low Reynolds number (a von Karman vortex street), and some of these patterns are shown in Figure 4.1. If the annulus velocity is fixed, central jet velocity increments result in flow pattern changes, some of which are quite remarkable. These changes, called bifurcations, are the result of interactions between the jet and annulus flows and the bluff body.

To understand the occurrences in the flow regime under investigation, flow visualization, LDA measurements, and frequency information from light scattering would be needed. Flow conditions at and around the bifurcation points had to be investigated quantitatively as well as qualitatively. Extensive LDA measurements could provide important statistical quantities that would help characterize the details of the flowfield. As mentioned earlier, Ballal and Chen (1986) used the distribution of turbulent quantities in the near field of the slot jet/bluff body flow to devise a physical description of the flow development. Knowing the flow structure in the present investigation, one could use

the statistical quantities to better characterize the flow which is depicted so well in the visualizations.

Flow visualization, to include high speed movies, would be done not in one plane but in all three planes of the jet. Sheet lighting the y-z (vertical) plane (spatial coordinates are shown in Figure 3.8) shows the large-scale structures in the flowfield. Lighting the x-z (lateral) plane would provide a qualitative estimate of the three-dimensionality of the flow, as would lighting the x-y (horizontal) plane. Looking at the horizontal plane might also show how instabilities in the third dimension interact to cause or assist in the observed transitions. Along these lines, Ghoniem et al (1987) used three-dimensional vortex simulation to model the shear layer for an axisymmetric jet. They found that the vortex rings formed in the near field became unstable (wavy) to a certain azimuthal perturbation, and this caused the eventual breakdown of the vortex ring. The azimuthal plane for axisymmetric jets corresponds to the horizontal plane of a planar jet. Disturbances in the horizontal plane might indicate the onset of an instability that leads to the bifurcations.

Mie scattering might provide information on the shedding frequencies of the large-scale structures which may provide important clues about how this configuration compares with other configurations in terms of a parameter like Strouhal number. This comparison might also help

explain the flow dynamics and the important factors in jet development since analyses on the simpler configurations are so abundant. If valid analogies can be made for the range of jet velocities investigated, one or several pictures of how the annulus and jet flows interact when in the presence of the bluff body might emerge. The Strouhal number for a planar jet is given by

$$St = \frac{f\,D}{U_j} \tag{1.1}$$

where f is frequency, D is the slot width, and U_j is the jet exit velocity. This is a very important parameter for categorizing a flow with frequency content. Sato (1960) tested a plane jet and observed that Strouhal number was independent of Reynolds number (Re) for low Re (1500-8000). Beavers and Wilson (1970) used two-dimensional and axisymmetric jets with Re from 500 to 3000 and also showed that Strouhal numbers were independent of Re. If Reynolds numbers are high enough, however, Strouhal numbers for plane jets (Sato, 1960) and axisymmetric jets (Becker and Massaro, 1968) vary as the square root of Reynolds number. These results have been verified by many other investigators. The Reynolds numbers for the present experiment (based on slot width and theoretical (1-D) jet exit velocity) range from 35 to 105. Although these are quite low, one cannot be sure of what to expect since the consequences of interactions between the jet and annulus flows are unknown.

The objectives of this investigation are to characterize the interactions of jet and annulus flows in the presence of a bluff body. With these objectives, a set of experiments was devised to analyze the flow pattern changes and attempt to define flow dynamics for this two-dimensional slot jet/bluff body configuration. For the present investigation, air was used in the annulus. Nitrogen was chosen for the jet so buoyancy would be negligible. With a fixed annular velocity, jet velocity increments that produced the expected bifurcations were determined using a laser sheet lighting technique. Six jet velocities, with a fixed annulus velocity, were chosen for investigation. These six conditions included jet velocities prior to, at, and beyond the observed bifurcation points. Flow visualization in two other planes of the jet would then be used to assess the three-dimensionality of the jet. Laser anenometry would provide important statistical information about the flowfields. Mie scattering could be used to identify the frequencies at which the large structures are shed. This information would be compiled in order to provide a detailed picture of the flowfield and its dynamics. With this plan of attack, then, the complete character of the slot jet/annulus flow interaction might be better understood.

Even with this extensive test plan that includes some sophisticated techniques, several cautions should be noted.

Analyses of LDA measurements of instantaneous velocity provide various statistical descriptions of flow parameters (e.g., mean and root mean square velocities, Reynolds stresses, turbulent kinetic energy, etc). Some of these quantities will have an entirely different interpretation for a non-turbulent flow, and some may have no meaning at all. Also important is the fact that there are two velocity scales and two, possibly three, length scales for this configuration. The jet and annulus velocities are important, and one might imagine that the full width of the bluff body and slot, the width of the bluff body on only one side of the slot, and the slot width could all be important length scales. This fact may make the search for meaningful non-dimensional parameters, like Strouhal and Reynolds numbers, more difficult. This certainly does not rule out their use, but these peculiarities are important and must not be ignored.

In order to best describe the investigation, the structure of this thesis will be as follows. First, due to the unique nature of some of the experimental techniques, one chapter will be devoted to explaining the techniques and their usefulness. The next chapter will be used to describe in detail the experimental apparatus. Chapter IV will present the background information that motivated the present investigation; a summary and discussion of previous results obtained using the 2-D centerbody is given.

Chapter V is a short section describing the flow conditions chosen for investigation and the procedures used in the experiments. Results of all work will be presented in Chapter VI, as will the discussion of these results. The conclusions and recommendations will complete the thesis.

II. Description of Experimental Techniques

The unique nature of some of the experimental techniques used in this study demands that a thorough explanation be given. Flow visualization which relies upon a chemical reaction to produce submicron particles, a light scattering technique to determine important shedding frequencies, and Laser Doppler Anemometry (LDA) to determine mean and fluctuating velocity components were used in the present investigation.

The flow visualization technique has been described elsewhere in detail (Chen and Roquemore, 1986). In this section, the details of the technique applicable to the investigation will be given. Titanium tetrachloride ($TiCl_{4(g)}$) is added to a dry flow, such as the one shown in Figure 2.1. As the mixture exhausts into the ambient air, the $TiCl_4$ reacts spontaneously and nearly instantaneously with water vapor ($H_2O_{(g)}$) to form $TiO_{2(s)}$, submicron particles which create a light, white smoke. The chemical reaction is

$$TiCl_4 + 2H_2O \rightleftharpoons 4HCl + TiO_2 \qquad (2.1)$$

Particles formed by this reaction can then be illuminated by various light sources (laser, strobe, etc) to provide precise visualization. This technique relies on having a dry fluid in the flow channel so preformed seed will not be

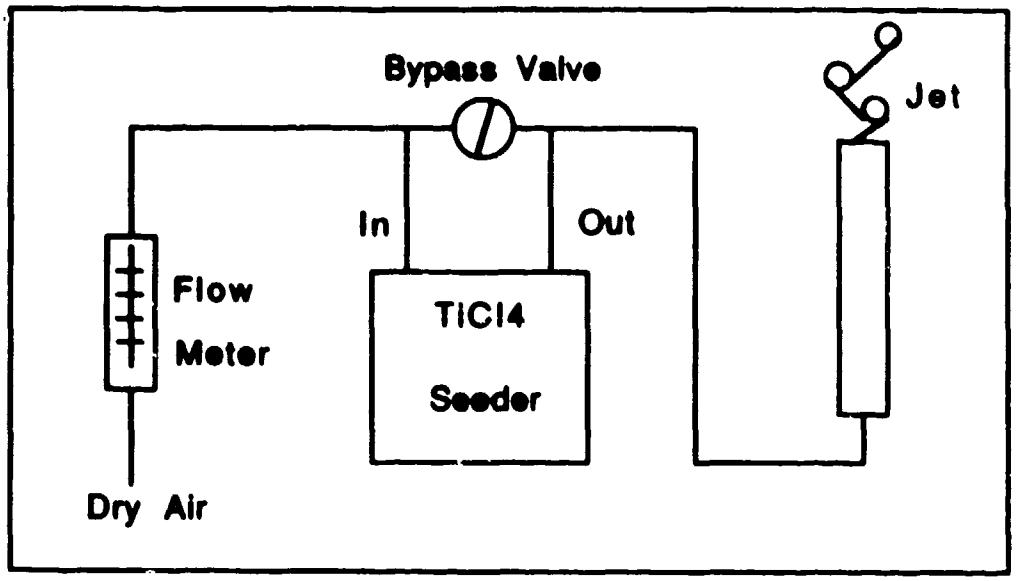

Figure 2.1 Flow Visualization Test Set-Up

created. The dew point temperature of the fluid should be checked, and the value should be below -40°C (Britton, 1987). It should also be noted that the TiO_2 particles are near one micron in size and respond nearly instantaneously to flow variations. The reaction given in Eq (2.1) occurs under nearly isothermal conditions, so relatively little energy is lost or gained by the flow. If flow rates are very low, however, this last statement is invalid. This point will be discussed in greater detail later.

Flow patterns revealed by this technique can be quite interesting. For example, Figure 2.2 shows some of the flow patterns from Tankin's work (1987). Illumination with a sheet of laser light allows one to photograph the flow. The important feature of the reactive flow visualization technique is that surfaces which have clear physical

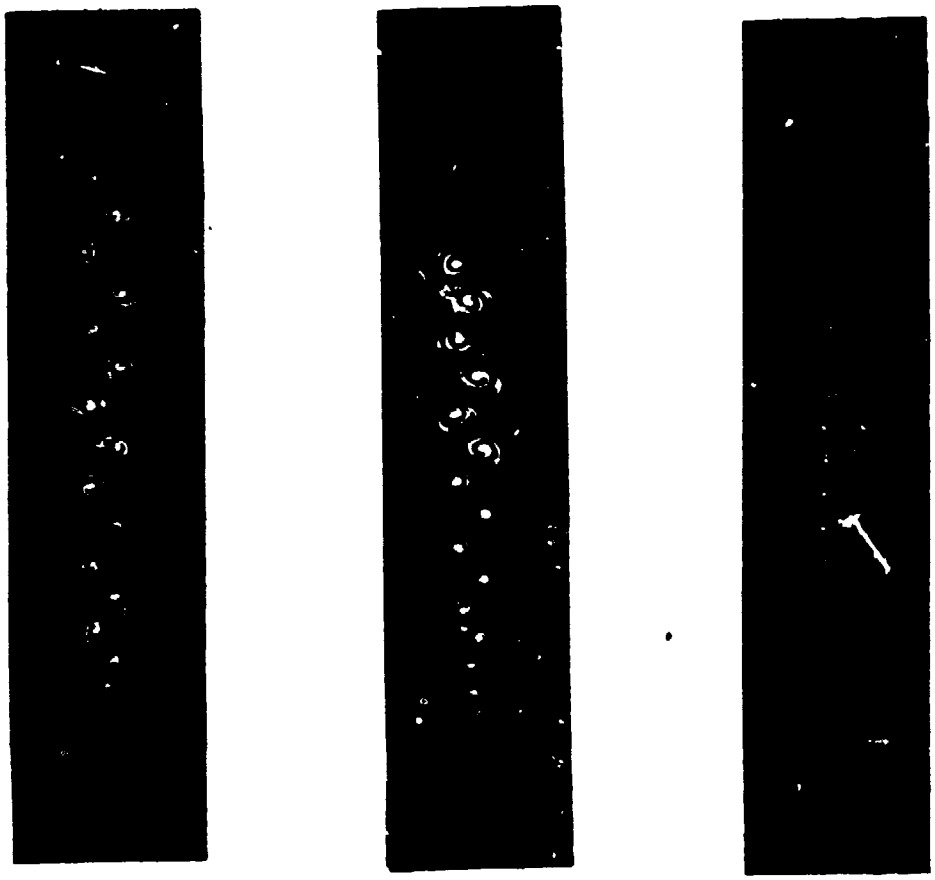

Figure 2.2 Reactive Flow Visualization Examples From Tankin (1987)

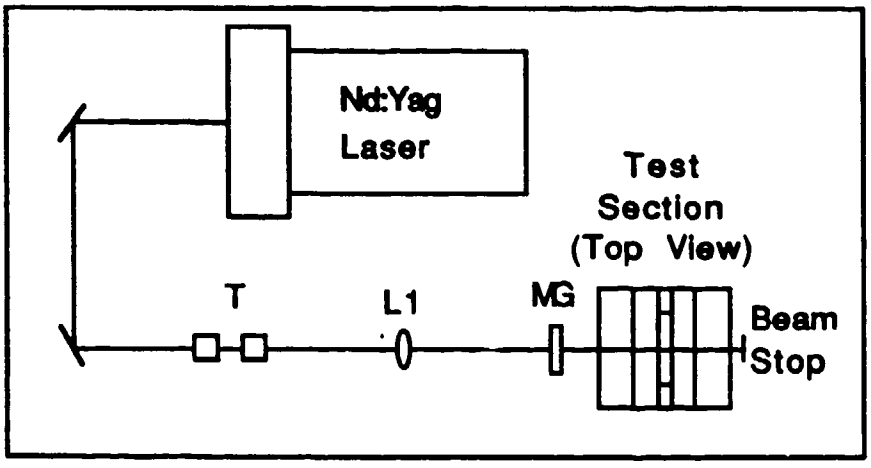

Figure 2.3 Optical Arrangement for Flow Visualization

significance are illuminated. Particles appear only at those places where the main flow has contacted ambient fluid. The lines seen in the visualization, then, indicate the interfaces between jet and ambient fluids.

The optical arrangement is shown in Figure 2.3. A Nd:Yag laser (Quanta Ray Model DCR-2A) serves as the light source for the visualization. For photographs, such as the one shown in Figure 2.2, the camera shutter is synchronized with a 10 ns pulse from the laser. The pulse acts like a flash for the camera. Photographs can also be taken using time exposures of flow fields "frozen" by adjusting the pulse rate of the laser. The sheet of light needed to visualize the plane perpendicular to the slot jet is created by passing the laser output beam through a telescope (T), a cylindrical lens (L1), and a magnifying glass (MG). The magnifying glass is used to narrow the beam into a thin sheet. A mirror can be used to reflect the light sheet back onto itself, thereby increasing beam intensity. To visualize the plane parallel to that of the jet's exit plane, one merely has to rotate the cylindrical lens 90 degrees.

Effects of the seed particles on density and density gradients had been assumed negligible (Roquemore, 1987), but this had never been verified. A model, described in detail in Appendix A, was developed and verified the assumption that the concentration of $TiCl_4$ was small, thus ensuring

that this form of reactive flow visualization is non-intrusive (i.e., does not alter the flow field that would develop under "natural" circumstances). It should be noted here that seeding effects are not negligible if the flow velocities are extremely small (< 5 cm/s). Changes in flow patterns have been observed when high seeding concentrations (i.e., no flow is being bypassed around the $TiCl_4$ seeder) are used in combination with the lowest velocities. Seed concentrations are greatest when flow rates are lowest, and the heat of reaction and density gradient effects are the largest since there is greater time over which the effects are felt. In these instances, natural convection cannot be ignored. For this investigation, velocities greater than 18.5 cm/s were chosen. Also, seed concentrations were minimized by setting the valves on the seeder so that as little flow as possible went to the seeder. These two facts guaranteed that no pronounced effects would be seen for the chosen conditions.

A special type of light scattering, Mie scattering, can be used to determine important shedding frequencies. Large scale structures, often known as coherent structures, are seen in the near field of jet flows and are shed at various frequencies; this method helps determine these frequencies. A typical test arrangement is shown in Figure 2.4. The reactive flow visualization technique just described supports the scattering analysis by providing the particles

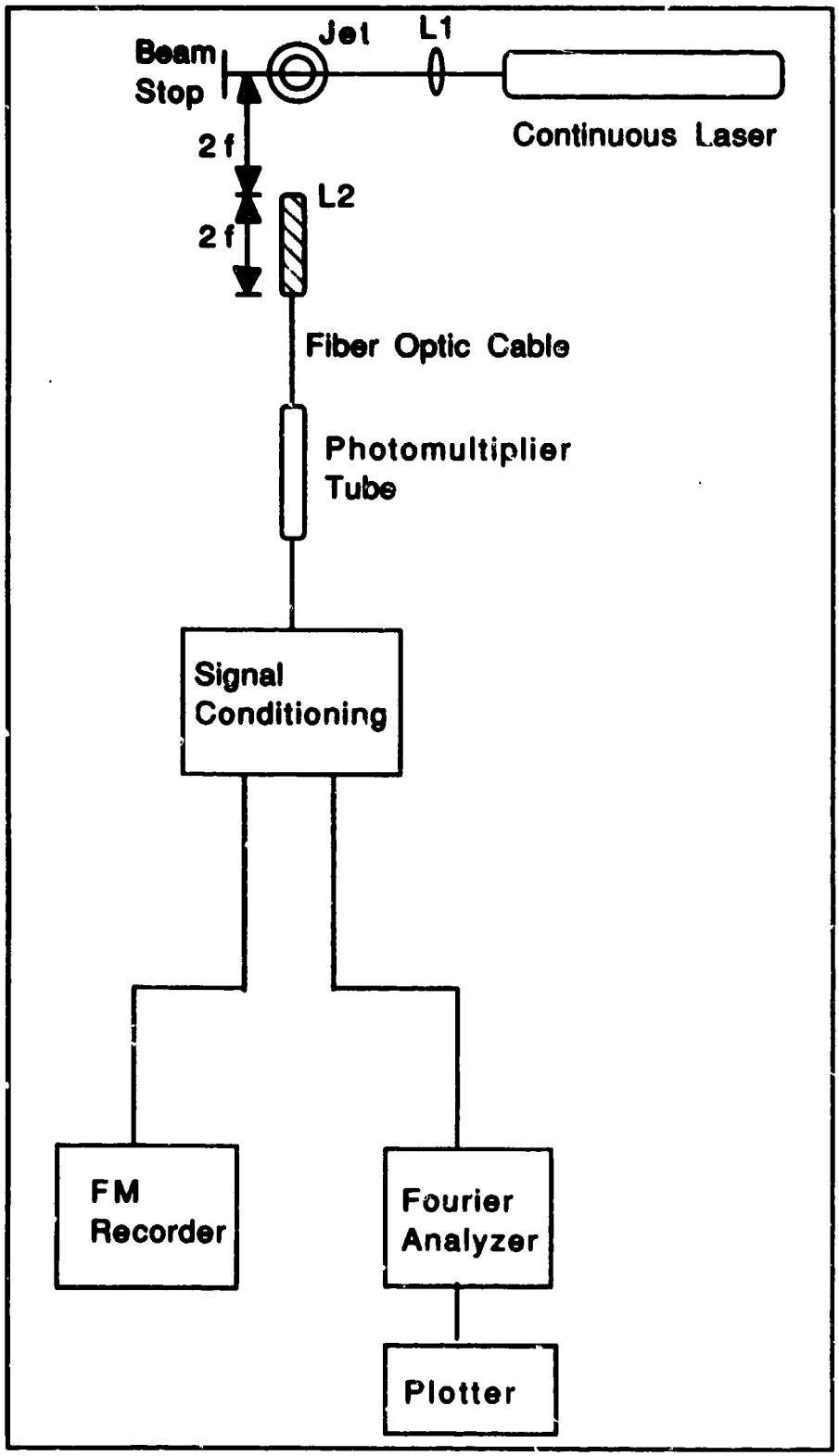

Figure 2.4 Mie Scattering Test Set-Up

required to scatter the laser light. The intersection of the laser beam and an imaginary circle (one whose diameter is that of the fiber optic cable) is located 4 focal lengths (f) from the end of the optic cable. This intersection creates a small spot which will be called the measurement spot. This spot must be located somewhere inside the flowfield (i.e., at a location through which TiO_2 particles will pass). As the TiO_2 particles pass the measurement spot, the laser light is scattered. This light is then transmitted to a photomultiplier via the fiber optic cable. The signal from the photomultiplier is then amplified and sent to either a Fast Fourier Transform analyzer or a tape recorder, or both. The tape recorder allows analysis of the signals at a later time. The resulting analog signal can be analyzed for its frequency content. A similar method for determining shedding frequencies of an axisymmetric jet was used by Becker and Massaro (1968). The method, explained by Becker et al (1967) used an oil condensation smoke to mark the flow. Their scattered-light technique used a photocell and appropriate optics to generate a signal that was proportional to the instantaneous point concentration of the marking smoke. Spectral analysis provided the shedding frequency.

The measurement spot can be located at various downstream and transverse positions, so one could determine

the frequencies at any location in the flowfield where particles pass. A sample time trace and its corresponding frequency spectrum are shown in Figure 2.5. As evidenced by the time trace, there is only one meaningful frequency, 5 Hz. The large peaks are separated by approximately 0.2 s, as are the smaller peaks, and this yields the frequency of 5 Hz. The frequency spectrum contains higher harmonics only as a result of the Fourier transform. The time trace shown in Figure 2.5(a) resembles a square wave, and Fourier transforms of finite square waves contain harmonic frequency components which are the result of attempting to match the abrupt changes at the leading and trailing edges of the square wave (Malmstadt et al, 1981). Validation of the Mie scattering method as an effective means of determining shedding frequencies had not been previously accomplished. Appendix B contains the details of a set of experiments designed to validate the Mie scattering technique. An important factor to remember when analyzing Mie scattering information is that interpretation of the results requires the analog signal (time trace), frequency spectrum, and a flow visualization photograph. These three pieces of information are all required to provide a complete picture of what is occurring; lack of one or more pieces of this information often leads to unwanted guess-work.

Laser Doppler Anenometry (LDA) was used to determine mean and fluctuating components of velocity. The laser

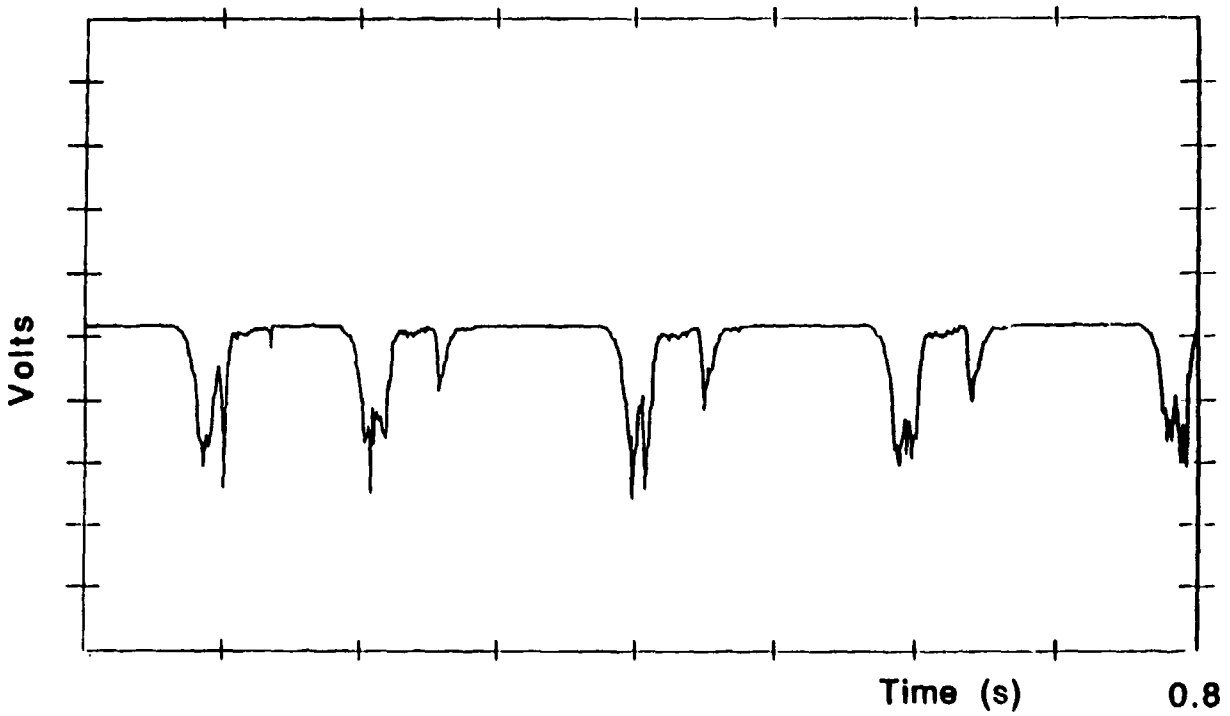

(a) Mie Scattering Time Trace

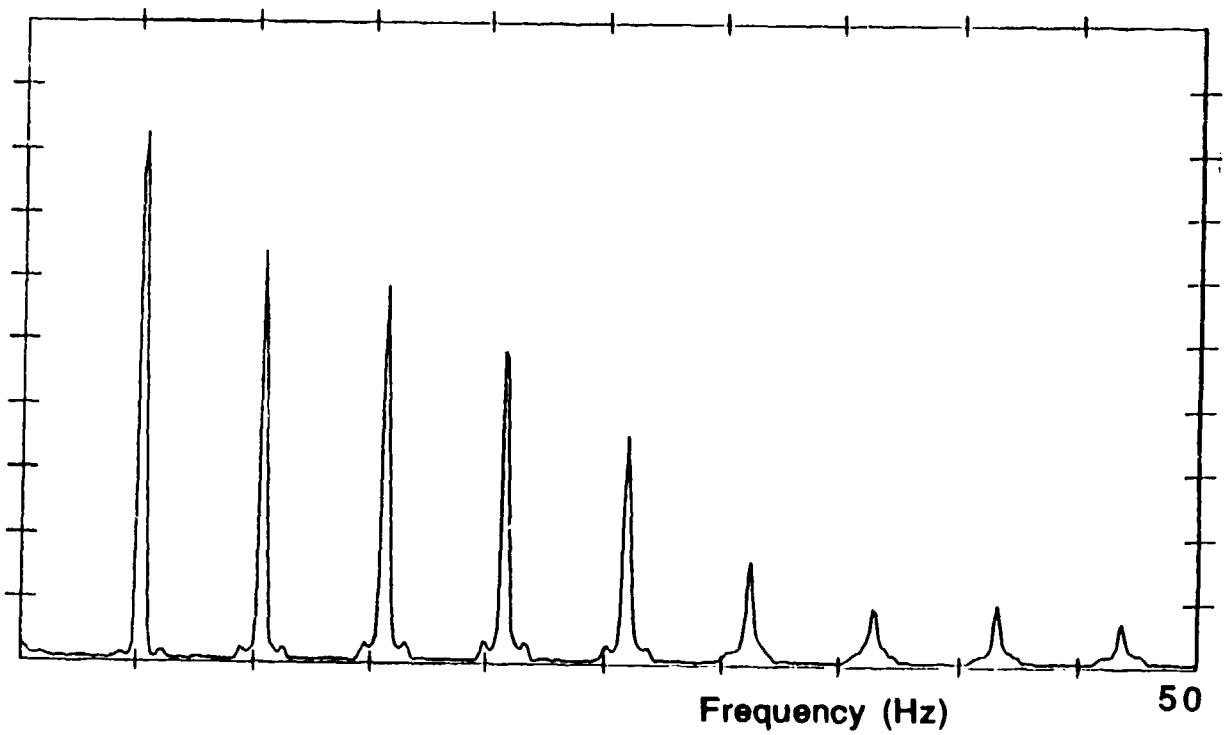

(b) Frequency Spectrum of Signal in (a)

Figure 2.5 Mie Scattering Results

anenometer is a non-intrusive device which can provide precise quantitative measurement of velocity. Measurement is based on the principle of the Doppler shift of the frequency of radiation when scattered from a moving object. Small particles must be distributed in the flow to scatter the light. If the particles are sufficiently small, the slip velocity between the particle and the fluid will be small, and the measurement is a valid measure of the fluid velocity. Optical arrangements vary considerably based on specific requirements; for example, see Holman (1984). The arrangement used in the present investigation will be described in the following chapter.

III. Experimental Apparatus

The unique test configuration used in the present investigation is shown in Figures 3.1 and 3.2. A slot (3 mm x 150 mm, aspect ratio = 50) is surrounded by a bluff body (width of the bluff body is 6 mm on either side of the slot). The plexiglass centerbody, shown in greater detail in Figure 3.2, is housed in a large chimney section which ends in a 24 cm square section. Annulus flows are brought around the outside of the centerbody through the chimney. Two contraction sections are used to minimize boundary layer effects in the annulus; contraction ratio is 2.68. A square plexiglass section sits atop the chimney to minimize outside disturbances.

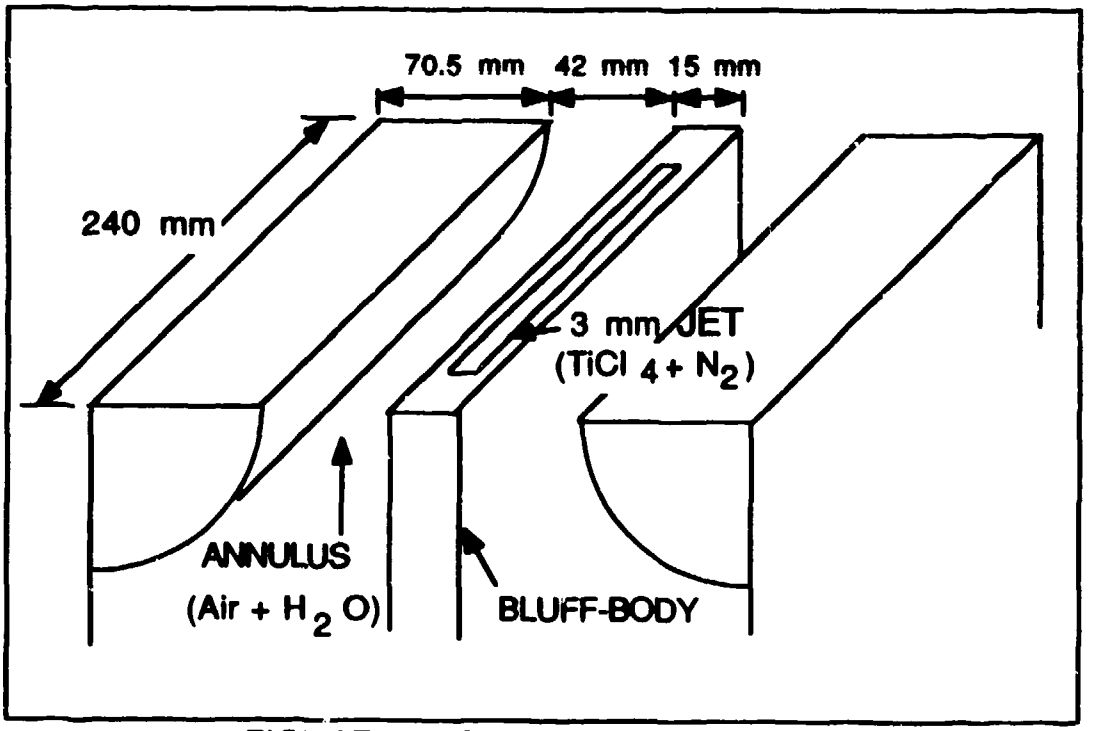

FIGURE 3.1 Co-Flowing Test Arrangement

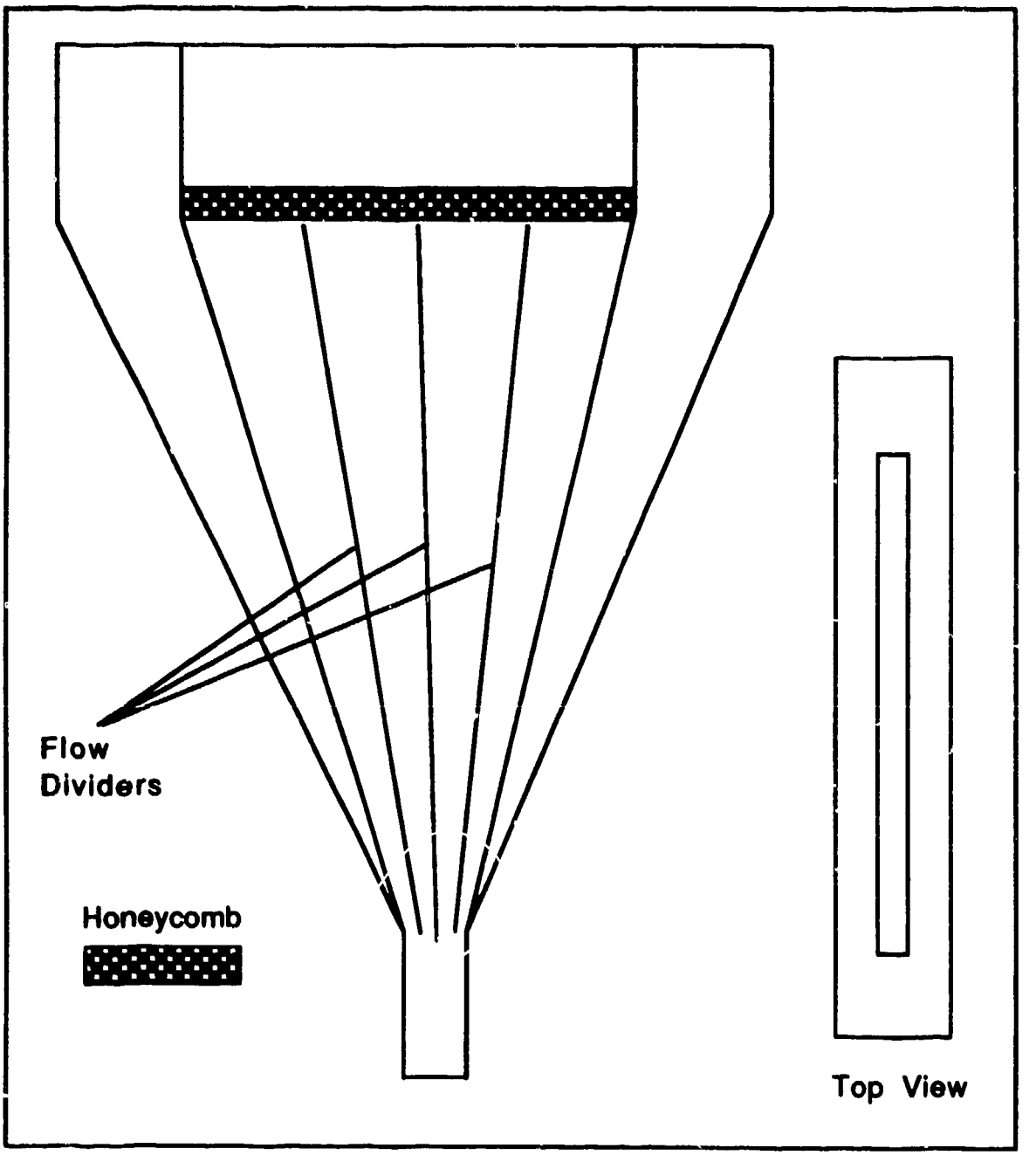

Figure 3.2 Two-Dimensional Centerbody

Cell 153 in Building 490 of the Aero Propulsion Laboratory houses the facility where all experiments were performed. A layout of the cell is given in Figure 3.3. Air was used in the annulus and nitrogen was used in the slot. The effect of buoyancy will be negligible with this choice (various gases could be used in the central jet to study buoyancy effects, and the facility can handle combusting flows; however, natural convection effects were not studied). Air could not be used in the central jet since facility air could not be dried adequately for use with the flow visualization and LDA seeding. If the fluid is too moist and one uses the $TiCl_4$ for flow visualization, seed particles are preformed. This hinders clear visualization of the flow structures. In addition, deposits may form on the centerbody and annulus surfaces and causes the system to be shut down quite often for cleaning. This would add an additional uncertainty in the results since the deposit's effects are unknown.

The flow visualization arrangement is shown in Figure 3.4. The optical system for visualization was described in Chapter II. The annulus air is saturated with water vapor to ensure the air is humid enough for complete reaction of the $TiCl_4$. Three Technology Incorporated electronic flow control units (Model DMF) are used to set and regulate the required volumetric flow rates to within $\pm$ 1 percent.

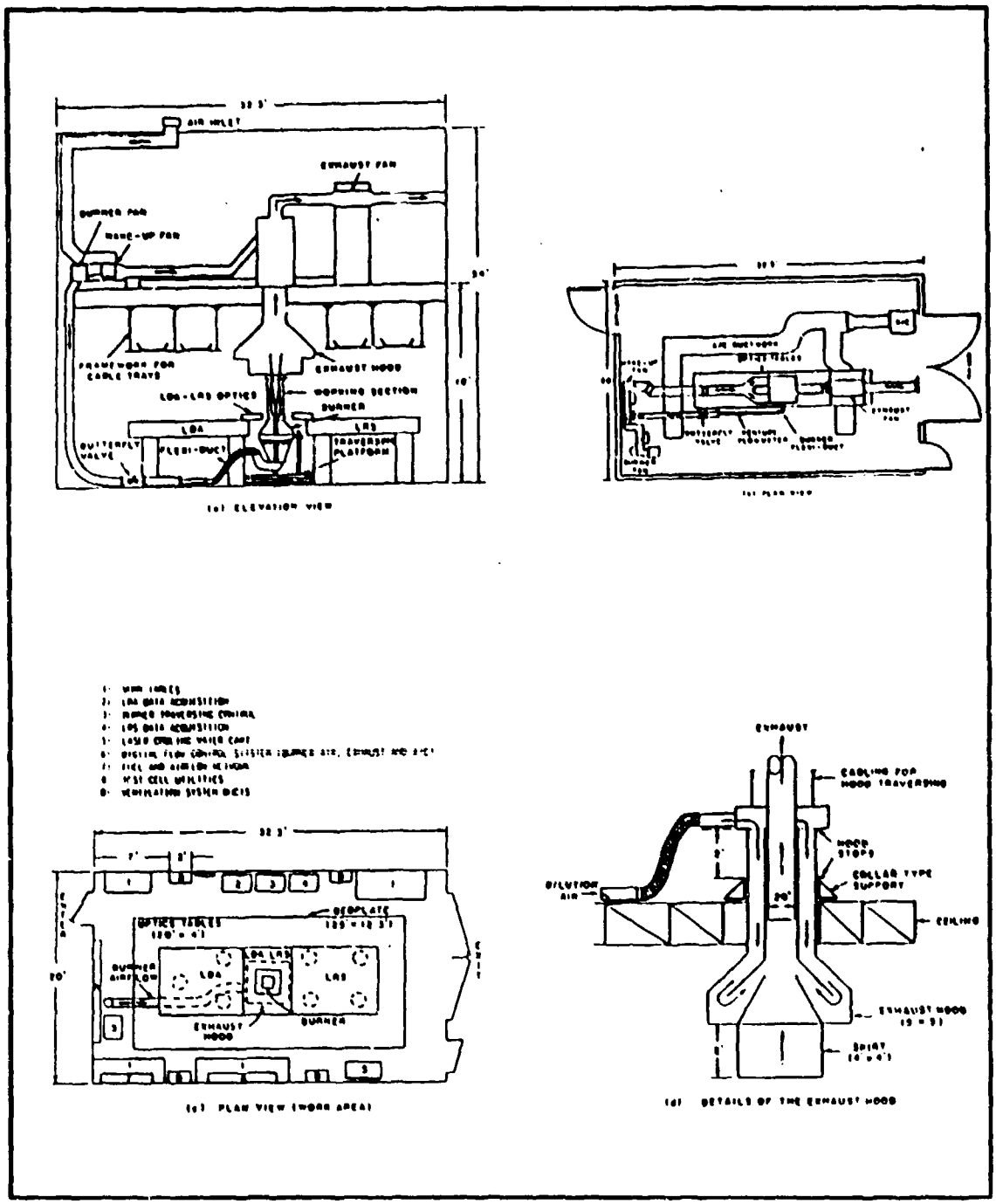

Figure 3.3 Laboratory Test Facility Layout

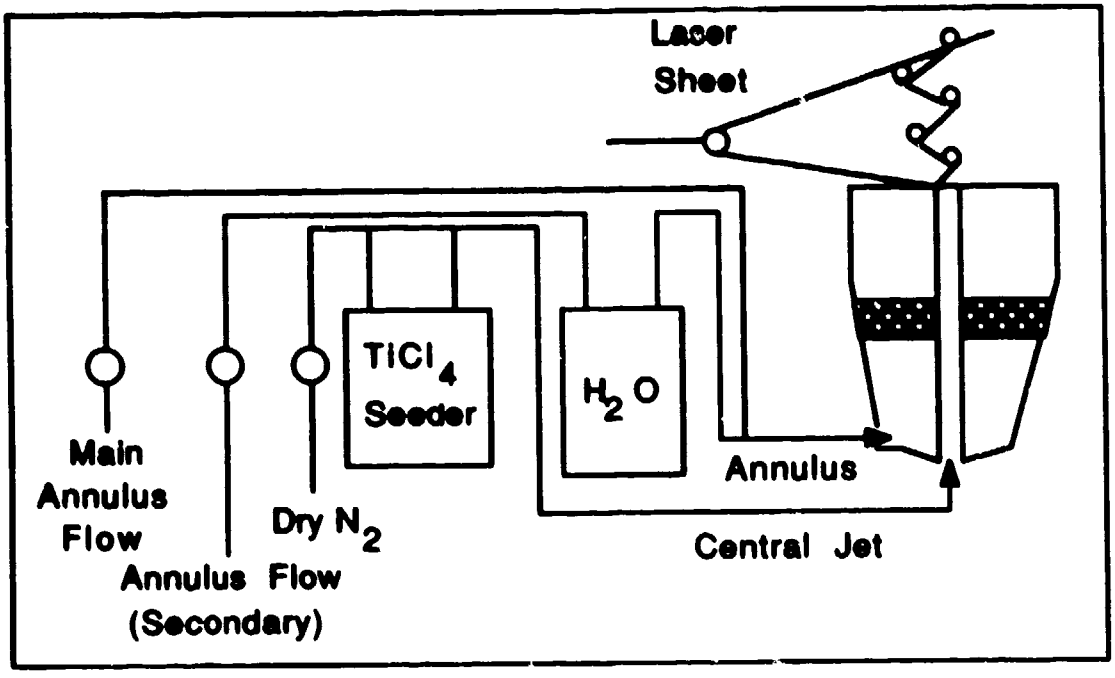

Figure 3.4 Flow Visualization Test Arrangement

The optical arrangement for the LDA is shown in Figure 3.5. This arrangement has been described in detail by Ballal et al (1986). This LDA is able to provide simultaneous measurement of two velocity components. An 8 Watt Argon ion laser (514.5 nm) is the source for the LDA system. Two measurement channels are separated by polarization. The scattered laser radiation is collected 10 degrees off-axis since other systems on the optics table prohibit using 0 degrees. The off-axis configuration did not affect results (Ballal et al, 1986).

The data acquisition and processing system is shown in Figure 3.6. The counter-processors analyze the signals

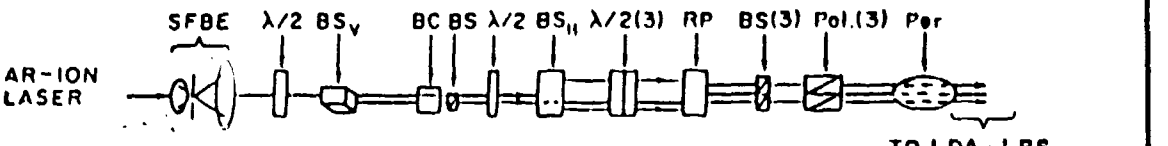

SFBE : SPATIAL FILTER BEAM EXPANDER
λ/2 : HALF-WAVE PLATE
BC : BRAGG CELL
BS : BEAM STEERING PRISM
BS_H, BS_V = BEAM SPLITTER (HORIZONTAL, VERTICAL)
Pol : POLARIZER
RP : RHOMB PRISM SET
Per : PERISCOPE

(a) SCHEMATIC DIAGRAM OF THE LDA OPTICS ARRANGEMENT

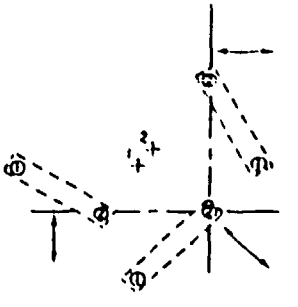

(b) SCHEMATIC OF RHOMB PRISM SET SHOWING INCOMING BEAMS (POSITION 1), OUTGOING BEAMS (POSITION 2) AND THEIR RESPECTIVE CENTERS.

Figure 3.5 Two-Component LDA System (Optics)

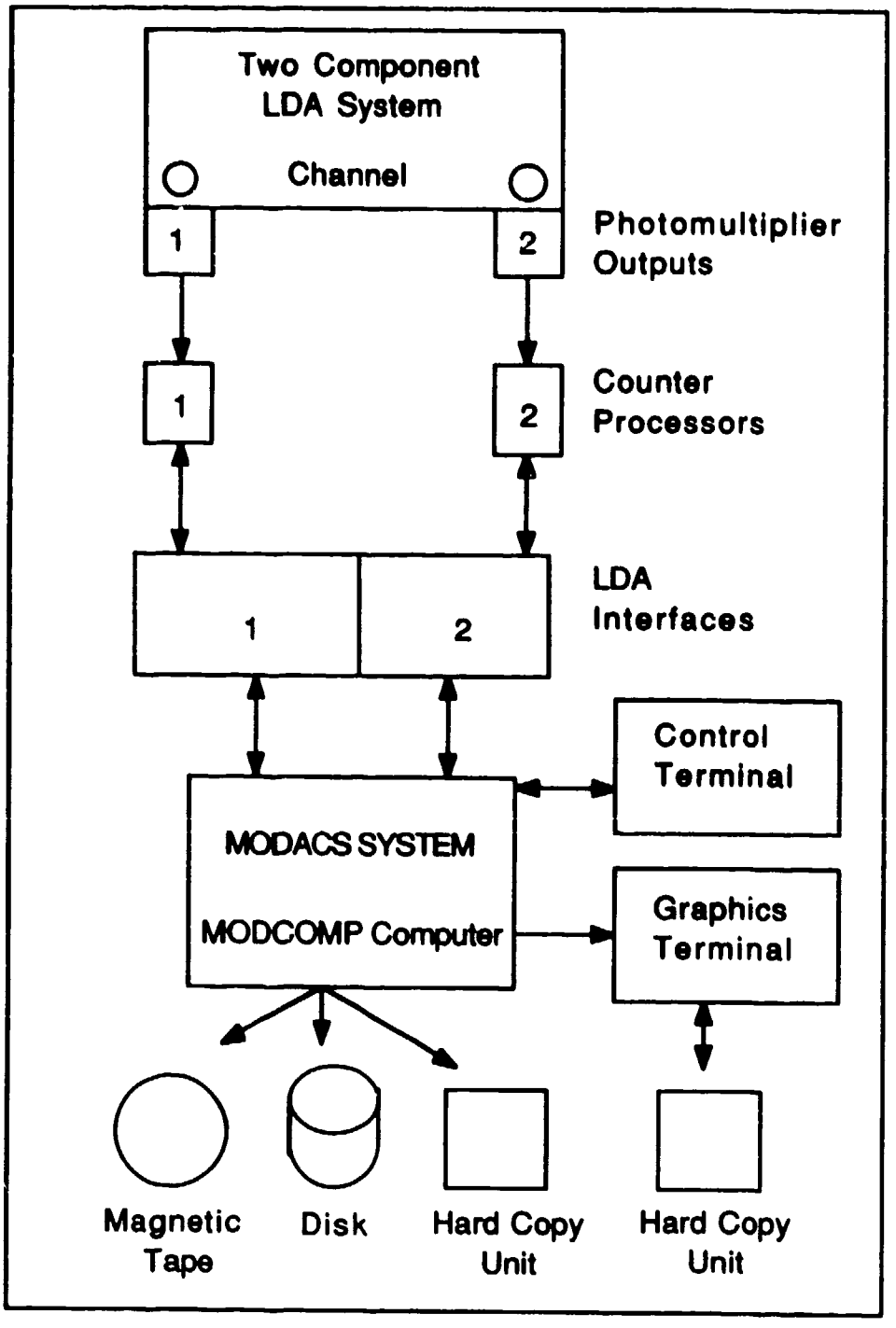

Figure 3.6 Data Acquisition and Processing System

provided by each photodetector (one for each of the two channels) of the LDA. The Doppler signal from the photodetector is amplified, filtered, and then converted into a pulse for digital processing by the counter-processors. These units process only those signals that have exceeded some threshold, thus ensuring good signal quality. The processor requires 32 cycles in an LDA burst (a burst occurs when a particle passes through the measurement volume). The Bragg cell shown in Figure 3.5 helps meet this criterion. The cell operates at 40 MHz, thus shifting the zero velocity signal to 40 MHz. The Doppler signal lies on one side or the other of this frequency, depending on the scatterer's direction. The frequency shift also increases the number of cycles available for analysis. For example, 5 m/s velocities would yield Doppler bursts with a maximum of 10 μs. A typical burst would be 3 μs; at 40 MHz, 120 cycles would be provided for analysis. This set-up provides poor resolution for low speed flows (<1 m/s), so a phase-locked down-mixer electronically shifts the signal from 40 MHz to 5 MHz or 10 MHz (user selectable). At 10 MHz, velocity resolutions of 1.1 cm/s vertically and 1.4 cm/s horizontally are obtained.

The processed signals are then sent to the LDA interfaces which record arrival time and the number of cycles in the burst. The counter-processor and clock data are sent to a mini-computer where, when 4096 data points at

a specific location have been recorded, a preliminary analysis is done which provides estimates of mean velocity and the root mean square (rms) of the fluctuating velocities. Data are then saved on magnetic tape, and the system moves to the next point and begins to take data again. This process is all computer-controlled.

The chimney and centerbody are located on a traversing table which is shown in Figure 3.7. Vertical traverse of 2 feet and horizontal traverses of 9 inches (both ways) are possible. By moving the burner and not the optics, complexity of the optics is minimized and repeated realignments and inaccuracies are avoided. The traverse mechanism controls position within $\pm$ 10 μm. The spatial coordinate system is shown in Figure 3.8, and the corresponding coordinates for velocity are given in Figure 3.9. These systems should be noted well. Also, the terms transverse and radial will be used interchangeably. This notational inconvenience may arise at a later time, but all attempts will be made to ensure clarity in data presentation and discussions.

The seeding used for the LDA deserves special attention. Seeders must produce a steady flux of micron or submicron size particles and must be controllable. Adequate and steady seeding of proper size particles ensures good signal quality and accurate velocity measurement. High seeding rates must be avoided since multiple particles will

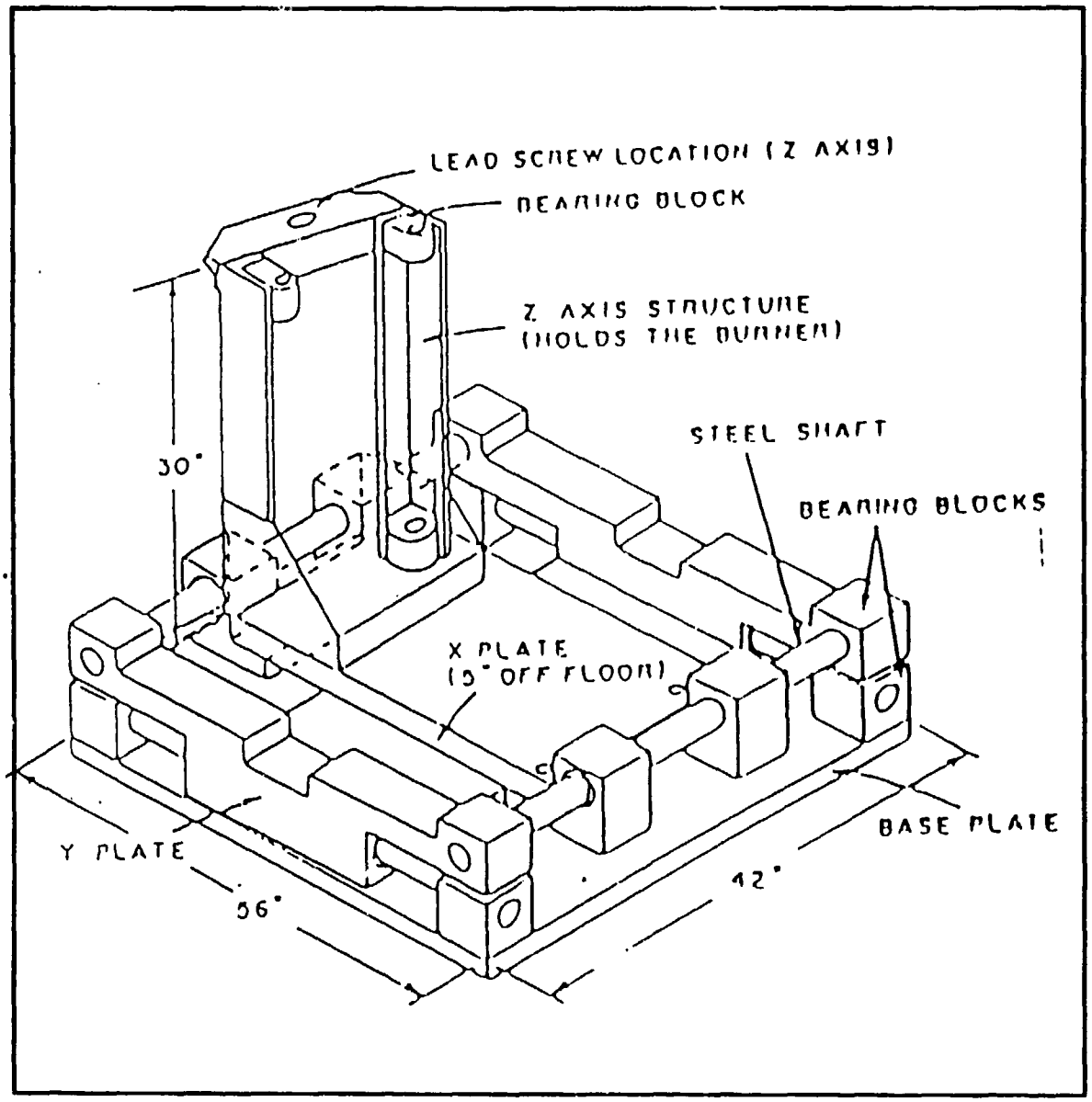

Figure 3.7 Three-Axis Burner Traversing Platform

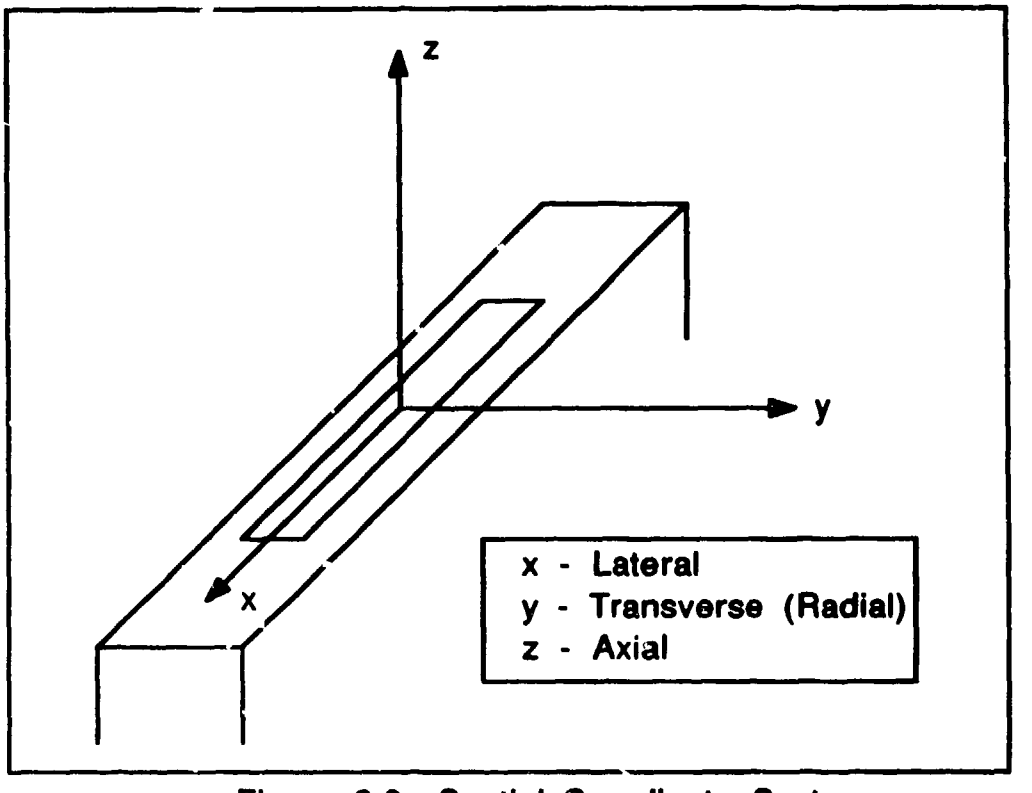

Figure 3.8 Spatial Coordinate System

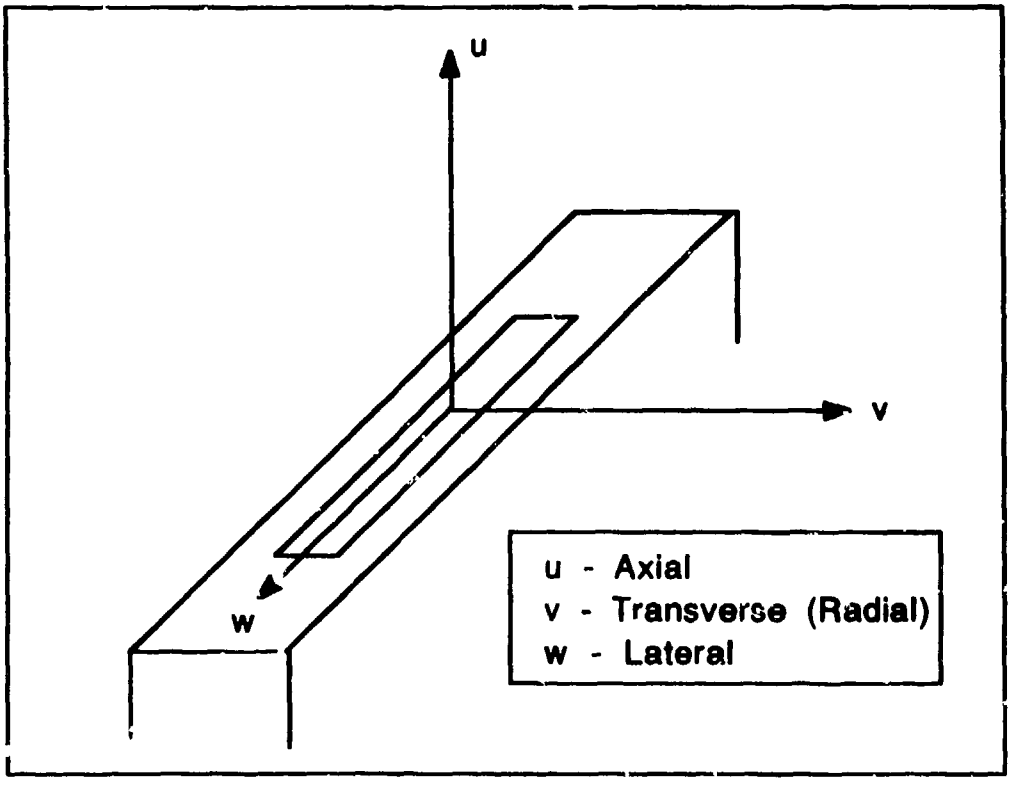

Figure 3.9 Velocity Coordinate System

scatter radiation in different fashions and yield unusable results. Low seeding rates result in data acquisition which is very slow, so time to acquire the desired information can become very large. Spectral information is also often important in analyses, and low seeding gives data rates inadequate to get frequency or power spectra. These problems are amplified when low velocity flows are under study.

The test arrangement used for LDA measurements is shown in Figure 3.10. The high output fluidized bed seeder was used for the annulus flow and provided consistent seeding. The major drawback of many fluidized bed seeders is their inability to obtain the desired particle generation rate.

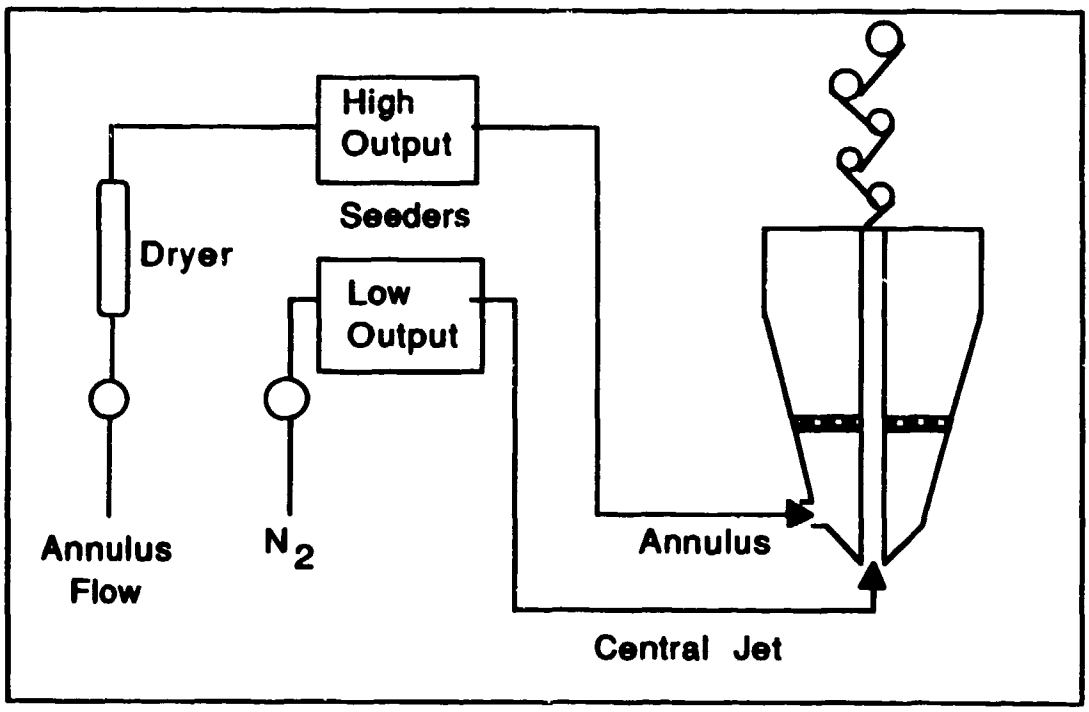

Figure 3.10 LDA Flow System Arrangement

This experiment was done at a constant annular velocity, so after the initial setting, there were no more adjustments and the problem was avoided. The low output seeder used for the central jet was a significant problem for the LDA measurements. Very low volumetric rates (~ 5-15 slpm) made it nearly impossible to get adequate seeding rates. At first, the pipe shown in Figure 3.11 was used. Some of the jet flow could be bypassed around the seeder if necessary. Frequent clogging of the screens soon prohibited its use. A cyclone-type seeder was then created by Mr Ron Britton of the Aero Propulsion Laboratory. This device, shown in Figure 3.12, uses a motor to stir a bed of Al_2O_3 particles. Air is brought in the seeder so a cyclone is created which will take with it the aluminum oxide particles. Flow could also be bypassed around the seeder to whatever degree desired. This configuration worked extremely well and provided excellent seeding over the range of flows investigated.

When data have been collected, various computer programs are available to analyze the data. These programs have been developed by personnel from the University of Dayton Research Institute (UDRI). The user has great flexibility since all the programs are menu driven. Various averaging schemes and/or data smoothing can be used, and statistical descriptions of the data such as mean velocity, root mean square (rms) of the fluctuating velocity,

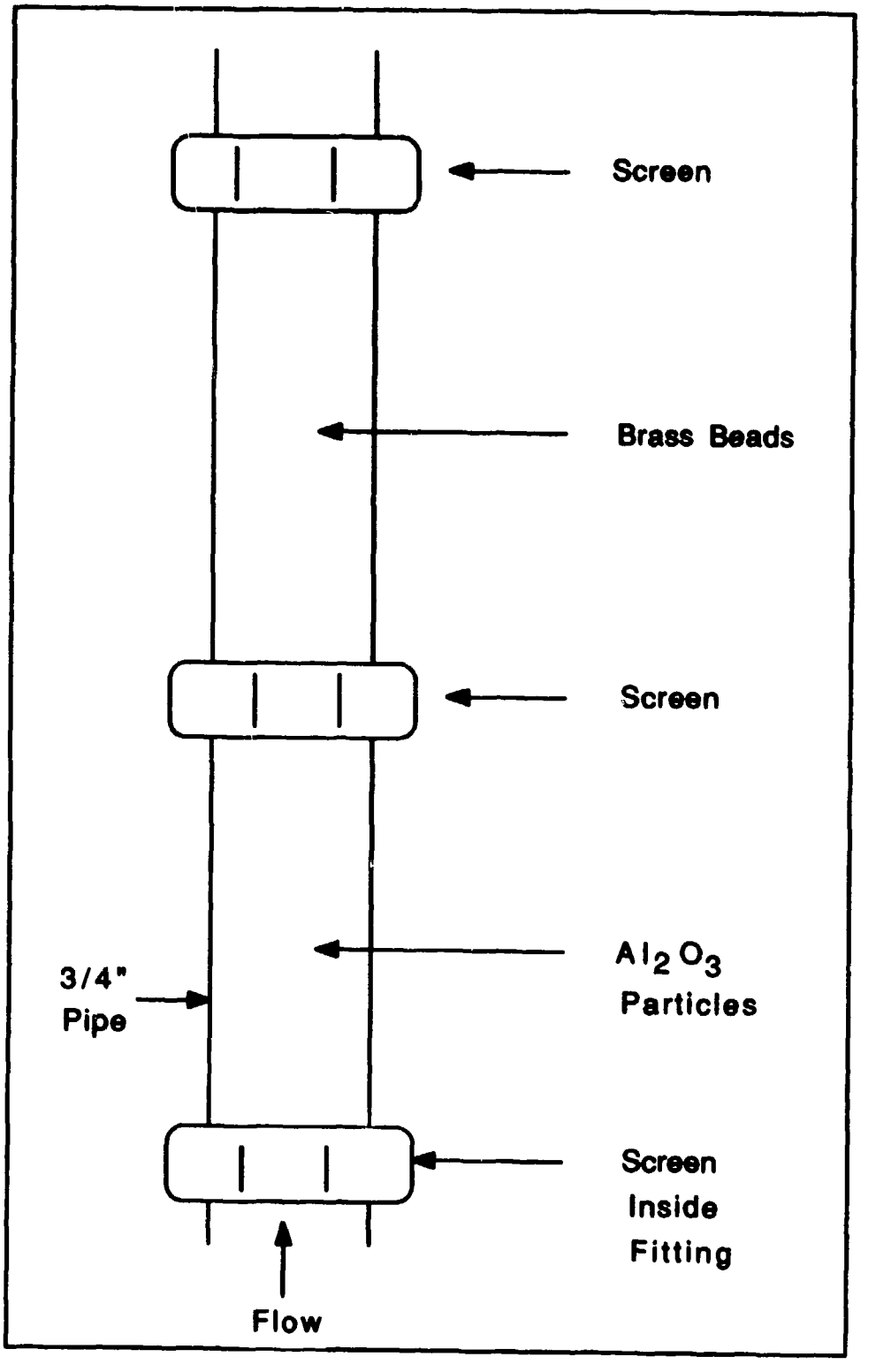

Figure 3.11 Low Output Tube Seeder

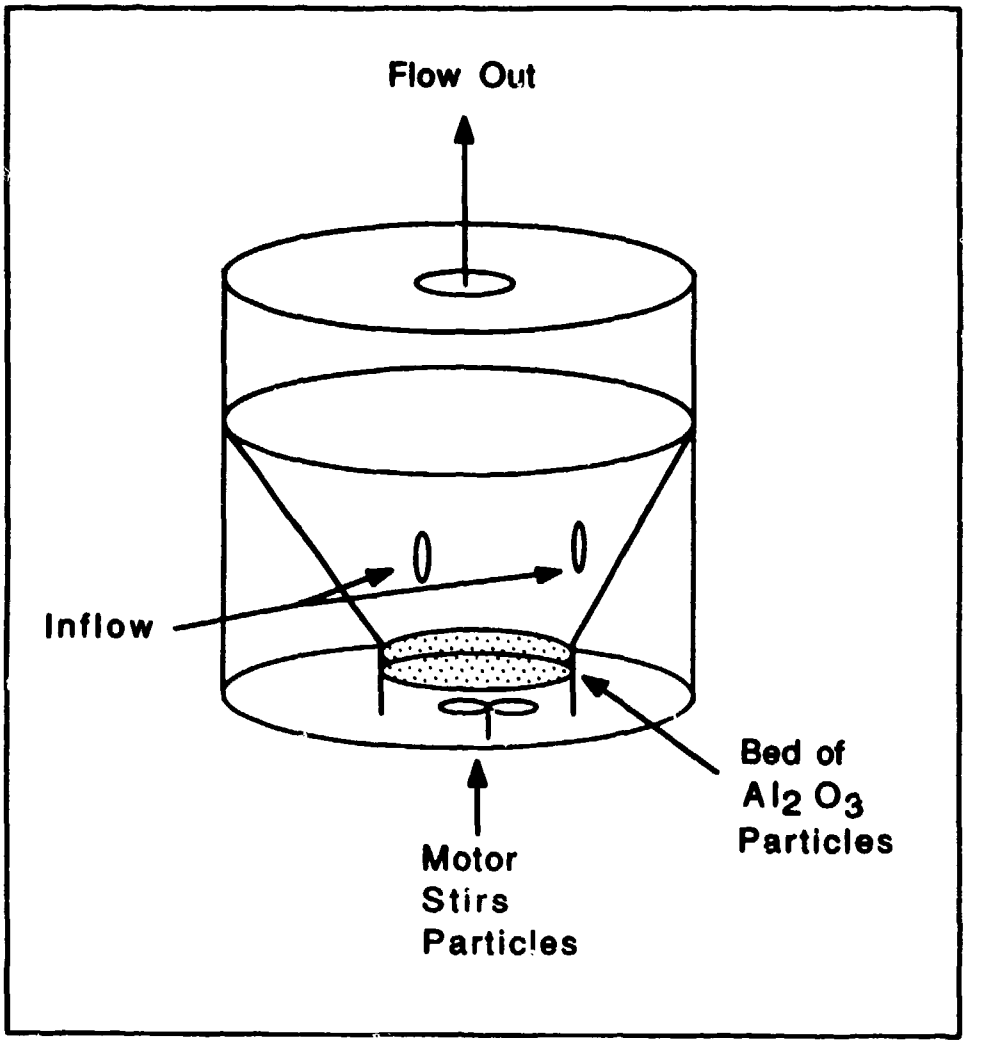

Figure 3.12 Low Output Cyclone Seeder

covariance, turbulent kinetic energy, skewness, kurtosis, probability density functions, and spectral information can be obtained. Techniques for data analysis and presentation will be described as appropriate throughout the remainder of this text.

IV. Preliminary Investigations

Motivation for the present investigation came from the work of Tankin (1987). The centerbody previously described was used in Tankin's work, and the primary emphasis was on flow visualization. Only a small portion of quantitative data was taken. Various annulus velocities were run, and jet gases of He, N_2, and CO_2 were run over a broad range of velocities. A typical sequence of photographs is shown in Figure 4.1. These photographs show N_2 in the central jet. After the annulus velocity is set at its prescribed value, the jet flow is increased from its minimum value until all jet flows have been run. Jet to annulus velocity ratios typically varied from 0.25 up to 5.0 or greater to ensure wide coverage of flow conditions. Photographs were taken at each condition using the laser sheet lighting technique described in Chapter II. Theoretical (1-D) exit velocities for the jet and annulus, those calculated using

$$U = \frac{Q}{A} \tag{4.1}$$

where Q is volumetric flow rate and A is area, will be denoted by U_j and U_a, respectively.

Several key features of the flow visualization technique should be pointed out here. As discussed in Chapter II, the areas where the TiO_2 particles appear mark the boundaries between jet and annulus fluid. Several

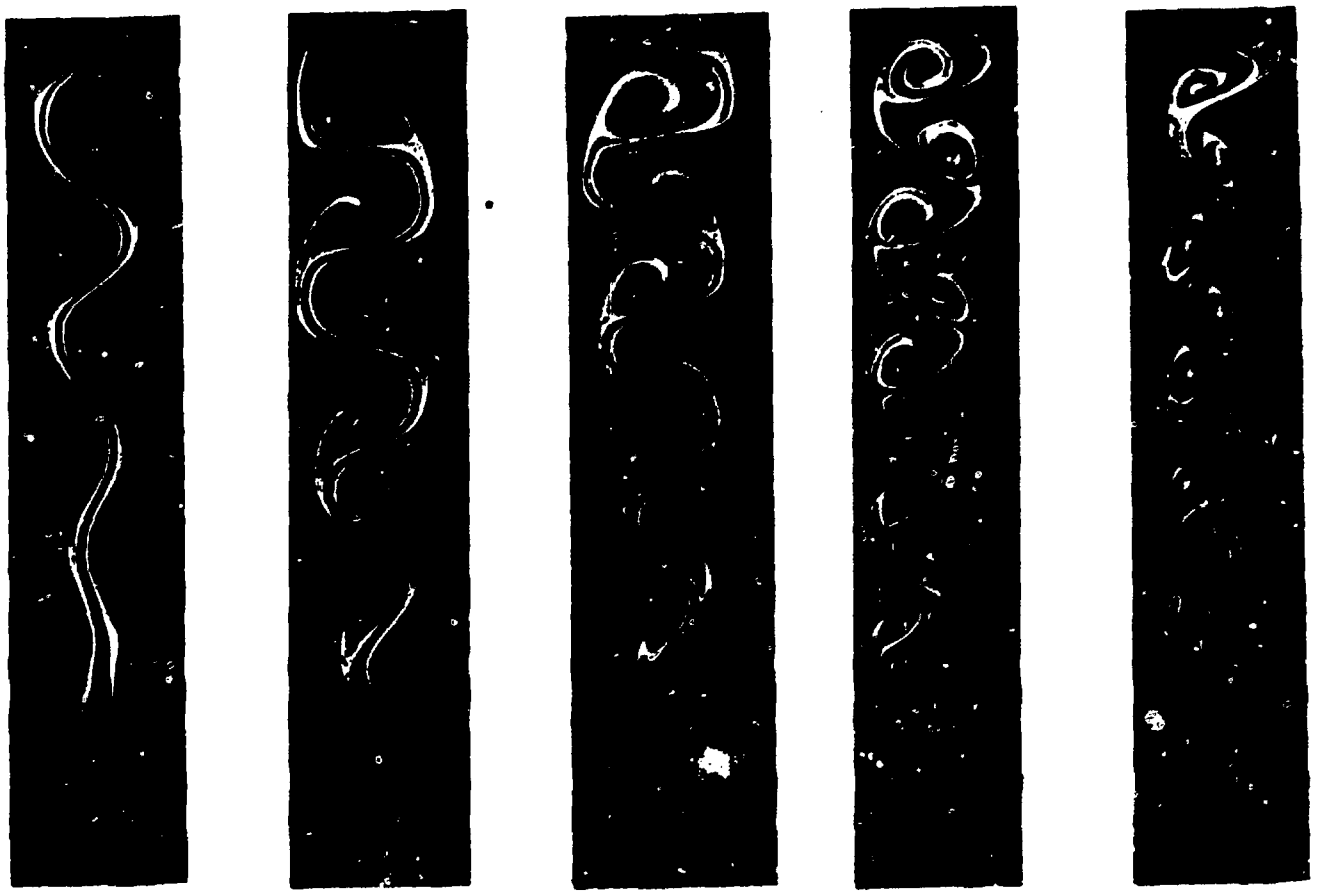

Uj = 4.1 (cm/s) (a) 8.5 (b) 12.6 (c) 18.5 (d) 22.2 (e)

Ua = 27.5 cm/s

Figure 4.1 Flow Visualization from Tankin (1987)

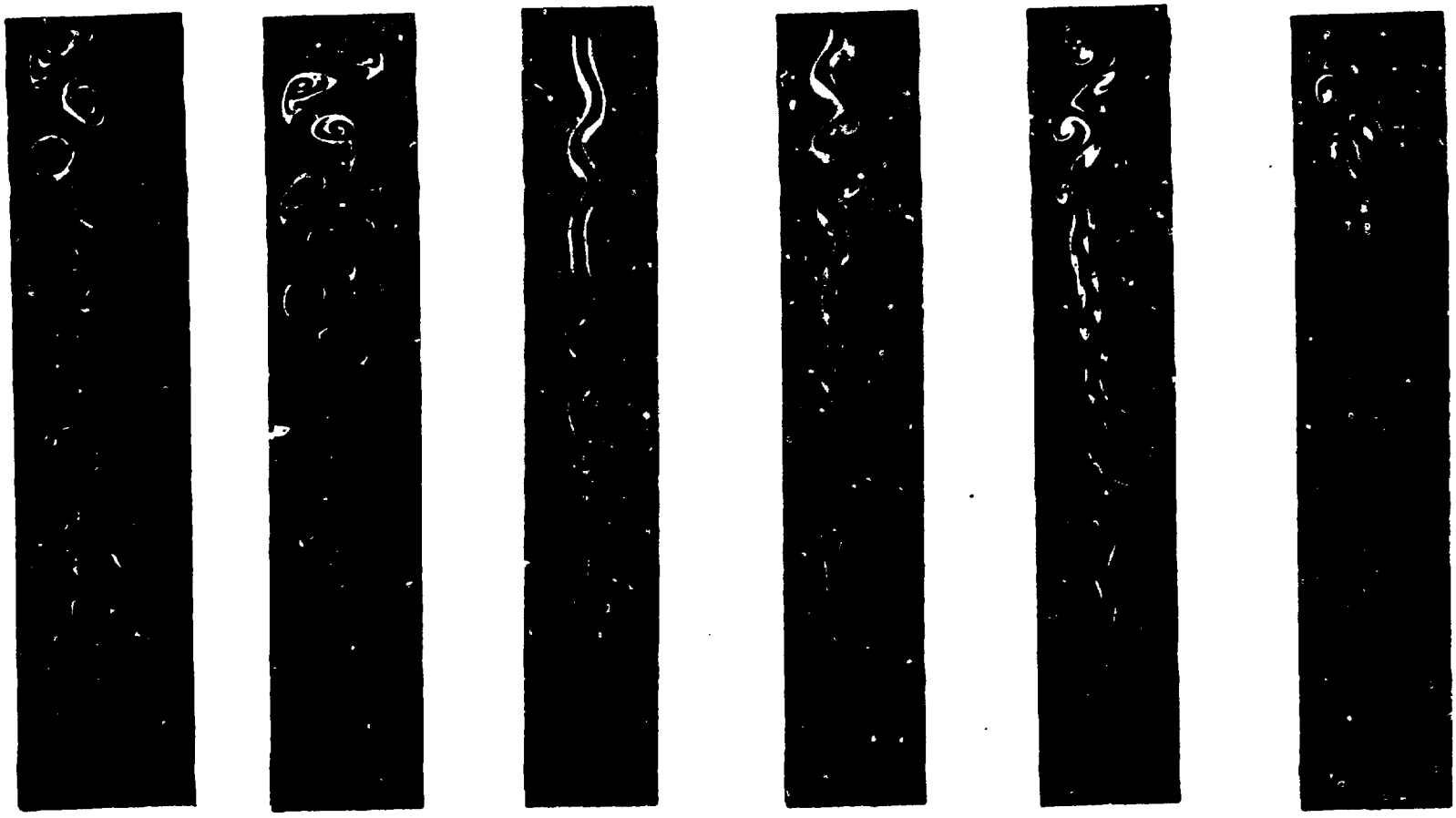

Uj = 27.8 (cm/s) 33.3 37.0 40.4 44.4 51.8

(f) (g) (h) (i) (j) (k)

Ua = 27.5 cm/s

Figure 4.1 Flow Visualization from Tankin (1987)

important terms will be used when analyzing the flow visualization photographs, and these are provided in Figure 4.2. One can clearly see that vortex orientation is "down" for $U_j > 37.0$ cm/s, while it is "up" for $U_j < 37.0$ cm/s. The "trunk" varies considerably for the eleven cases. When $U_j = 37.0$ cm/s, a trunk does not even exist, only interface lines. Familiarity with these terms will be important in later analyses of photographs.

The large scale structures in Figure 4.1 are quite interesting. More intriguing, however, are the drastic flow pattern changes which are seen. The cases where $U_j = 22.2$ cm/s and $U_j = 37.0$ cm/s are particularly interesting. At $U_j = 22.0$ cm/s, the trunk has become quite large, and there appears to be a stagnation point located at the base of the trunk (this apparent stagnation was identified when viewing the high speed movies). At $U_j = 37.0$ cm/s, almost parallel interface lines are produced. Small perturbations (ones that are obviously not amplified) prevent the lines from being perfectly straight.

The two flow patterns just discussed are very sensitive to changes in jet velocity. The patterns can change drastically with only a small change in jet velocity. Once the pattern is established, however, it is very stable. The pattern can be perfectly frozen using the variable pulse rate of the laser or a variable frequency strobe. The laser provides a thin, two-dimensional sheet of light, while the

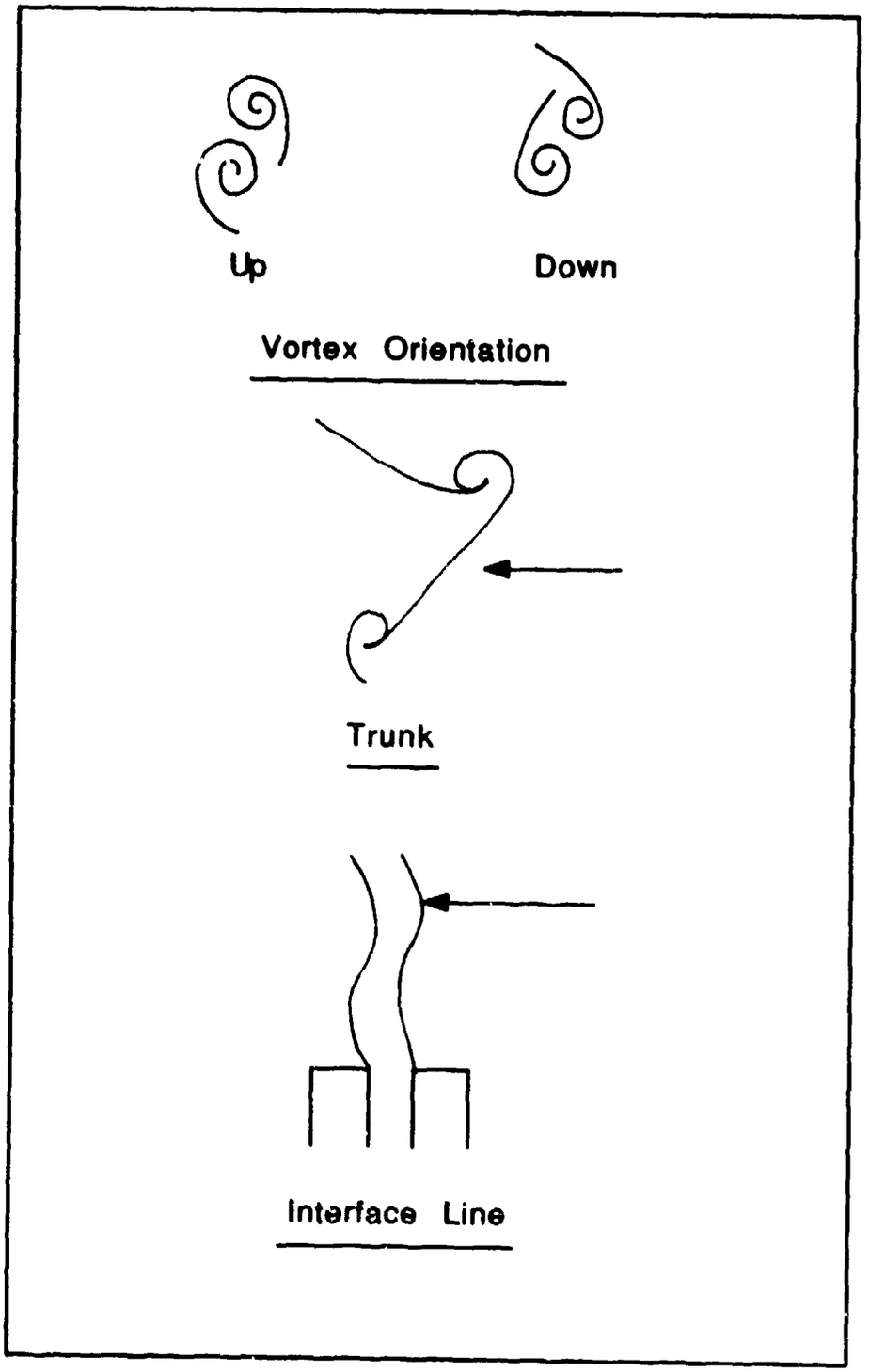

Figure 4.2 Flow Visualization Terminology

strobe can be used to illuminate the flow from a broad perspective. These strong points can be used in combination to provide a detailed picture of the flow in all dimensions. The pulse rate of the laser can be selected in a small range of frequencies (these vary depending on the desired pulse strength which is in Joules per pulse) which are very close to the frequencies at which the observed structures are shed; frequency of the strobe could be varied from 1.67 to 416.67 Hz. Varying the source's pulse rate results in structures which appear to be going forward or backward or can be exactly frozen. The apparent velocity of the structures depends on the difference between the source and shedding frequencies. If shedding is very repetitive, the flow can be perfectly frozen by proper selection of the light source frequency. The ability to freeze a certain pattern, then, suggests a particular stability of the flow.

The other flow patterns of Figure 4.1 change as flow velocities change, but the basic patterns remain the same. For example, the cases where U_j = 27.8 and 33.3 cm/s show patterns which are not identical, but certainly qualitatively similar. Using the terminology of Perry and Chong (1987), patterns are considered topologically equivalent if they can be distorted into one another by a stretching process. If we picture each pattern on a rubber sheet, then the first four patterns could be created by arbitrarily stretching the first pattern. The fifth

pattern, however, could not be created by stretching of any of the other patterns. This drastic flow pattern change, a bifurcation, is indicative of a structurally unstable critical point (Perry and Chong, 1987). Another bifurcation seems to have occurred when U_j = 37 cm/s. It was also noted by Perry and Chong (1987) that near a structurally unstable point, a slight change in one of the relevant parameters could cause a spectacular change in the way a jet or wake distributes and transports (transfers) its mass, momentum, and energy. Although the work of Perry et al has not focused on configurations like the one under investigation, it was felt that the physics of the flows might be similar enough to provide at least some insight into flowfield dynamics. Interpretation in terms of bifurcations may help in understanding the interaction of the bluff body and jet flows. Unfortunately, no quantitative analyses could be done since they are extremely complex.

Having established the motivation for the present experiment, flow conditions and experimental procedure had to be specified. Since flow visualization, LDA, and Mie scattering would be used, conditions had to be chosen judiciously because of time constraints. These factors and the experimental procedures are discussed in the next chapter.

V. Test Conditions and Experimental Procedure

To accomplish the objectives stated in Chapter I, a test plan was selected that would provide adequate characterization of the flowfield interactions. The limiting factor in choosing the number of cases to investigate was the LDA measurements. Because of low seeding rates, a test plan had to be created that would be coarse enough to ensure deadlines were met but fine enough to guarantee adequate coverage of the flow. Six conditions were chosen for investigation and are given in Table I. These captured both bifurcation points as well as conditions before and after these points.

TABLE I Flow Conditions

Condition	U_a (cm/s)	U_j (cm/s)	(Q_a/Q_j) slpm
1	27.5	18.5	(330/5)
2	27.5	22.2	(330/6)
3	27.5	27.8	(330/7.5)
4	27.5	33.3	(330/9)
5	27.5	37.0	(330/10)
6	27.5	51.8	(330/14)

It was decided to repeat six of Professor Tankin's conditions, partly because of the familiarity with his work. Different annular velocities were tried in preliminary visualization studies, but jet flow variations led to the same sequence of patterns observed earlier. A given pattern, however, would not repeat itself at a specified

velocity ratio U_j/U_a for different values of U_a. This behavior was caused by the turbulence intensity in the annulus. The turbulence intensity for the annulus was directly proportional to the volumetric flow rate. Therefore, even though the patterns were highly repeatable, they were also very susceptible to variations in annulus turbulence levels. For the 2-D centerbody configuration, complete break-up of structures was seen at approximately Q_a = 500 slpm (the annulus had become "fully turbulent" at this point). Although one would like as high a velocity as possible to ensure good data rates for the LDA, it was decided to avoid high volumetric flow rates in the annulus. Professor Tankin's conditions offered good middle ground.

Another factor may contribute to the discrepancy that a specific velocity ratio does not produce the same flow pattern when U_a is changed. For a fixed U_j/U_a, U_j must change when U_a is changed. At low velocities, one might expect a parabolic jet exit profile, while high jet velocities should tend toward a top-hat profile. Therefore, it may be important to look at exit mean velocity profiles in order to ascertain the correct exit velocity.

The repeatability of the sequence of flow patterns has been mentioned several times and deserves a short comment here. The qualitative evolution of these patterns at different annular velocities is nearly identical. Quantitative results will differ, but the test conditions

are representative of a general evolution of the flow. Studying one set of conditions instead of another, then, should not lead to different characterizations of the flowfield dynamics -- an encouraging result. It should also be noted here that the repeatability of the flow patterns for a particular U_j (with a fixed U_a) is perfect. In other words, for a fixed annular velocity, if one obtains a certain pattern at a U_j, changes flow conditions, then returns to the original U_j, the original pattern will always return.

Once the flow conditions were determined, the LDA data acquisition grid was chosen. It may be appropriate at this time to review Figure 3.8 since it contains the spatial coordinate system. Only one lateral position, the center of the slot, was used. At a given axial position, a "run" consists of a transverse (Y direction) scan. The Y positions chosen for each run are summarized in Table II.

TABLE II Transverse Scan Locations

Y RANGE (mm)	INCREMENT ΔY(mm)
(-30) to (-15)	5
(-15) to (-9)	2
(-9) to (+9)	1
(+9) to (+15)	2

The edge of the annulus extends to -42 mm, but it was shown by Tankin that edge effects for $|Y| > 30$ mm did not impact the flow near the bluff body. The contraction section was

effective in providing a top-hat velocity profile at the annulus edge. Due to the symmetry of the configuration, a full transverse scan was not necessary. Each scan consisted of 26 points where the u and v (axial and transverse, respectively) velocities would be measured. Lateral velocity could not be measured since the LDA system could only measure two velocity components. Axial positions where the transverse scans would be taken were chosen at z = 6, 10, 20, 40, and 60 mm. A true exit profile (z=0) could not be obtained because the centerbody interfered with the LDA beams below 6 mm. The combination of transverse scans at 5 axial positions resulted in measurements at 130 points in the flowfield. This provided coverage dense enough to indicate how quantities are changing. Because of the lack of structures at low z for U_j = 51.8 cm/s (see Figure 4.1), data were taken at z = 10, 20, 60, and 120 mm for this case only.

Flow visualization in all three planes of the jet was accomplished for the conditions given in Table I. For the vertical sheet lighting, photographs at each of the six conditions were taken. This was also done for the lateral sheet lighting. For the horizontal sheet lighting, photographs were taken at each of the z locations specified earlier, thus providing a picture of the influence of the third dimension as axial position increased. The photographic summary is provided in Table III.

TABLE III Photographic Summary

Sheet Light Orientation	U_a (cm/s)	U_j (cm/s)	z (mm)
VERTICAL	27.5	18.5	N/A
		22.2	
		27.8	
		33.3	
		37.0	
		51.8	
LATERAL		18.5	N/A
		22.2	
		27.8	
		33.3	
		37.0	
		51.8	
HORIZONTAL		18.5	6
			10
			20
			40
			60
		22.2	6
			10
			20
			40
			60
		27.8	6
			10
			20
			40
			60
		33.3	6
			10
			20
			40
			60
		37.0	6
			10
			20
			40
			60
		51.8	6
			10
			20
			60
			120

The Mie Scattering Method (MSM) was used to determine the shedding frequencies of the large-scale structures. The optics for the LDA were used instead of the arrangement described in Chapter II (which was only used to validate this technique). The technique itself is unchanged. Stroboscopic lighting was first used to ensure the measurement spot was in a region where the vortices would pass. Once in this region, the centerbody traverse was moved until maximum signal strength was observed on the oscilloscope (which was part of the LDA arrangement). The high voltage source was then adjusted to provide a signal having a 1.5 volt peak which would be sent to the FM tape recorder. Data were recorded at axial positions of 20, 40, and 60 mm for the first five jet velocities (up to 37.0 cm/s), and at 40, 60, and 120 mm for the case where U_j = 51.8 cm/s. This distribution of stations was chosen to coincide with LDA measurement locations, but measurements at lower z locations (z < 20 mm) were deleted since information about the large structures is desired, and these are not evident very near the jet.

A case that illustrates the possible interpretation errors in using frequency analysis will be discussed here. Figure 5.1 shows the time trace and its associated frequency spectrum at z = 40 mm for the case where U_j = 18.5 cm/s. The shedding frequency, while it appears from the frequency spectrum to be 12.25 Hz, is actually 6.125 Hz. Looking at

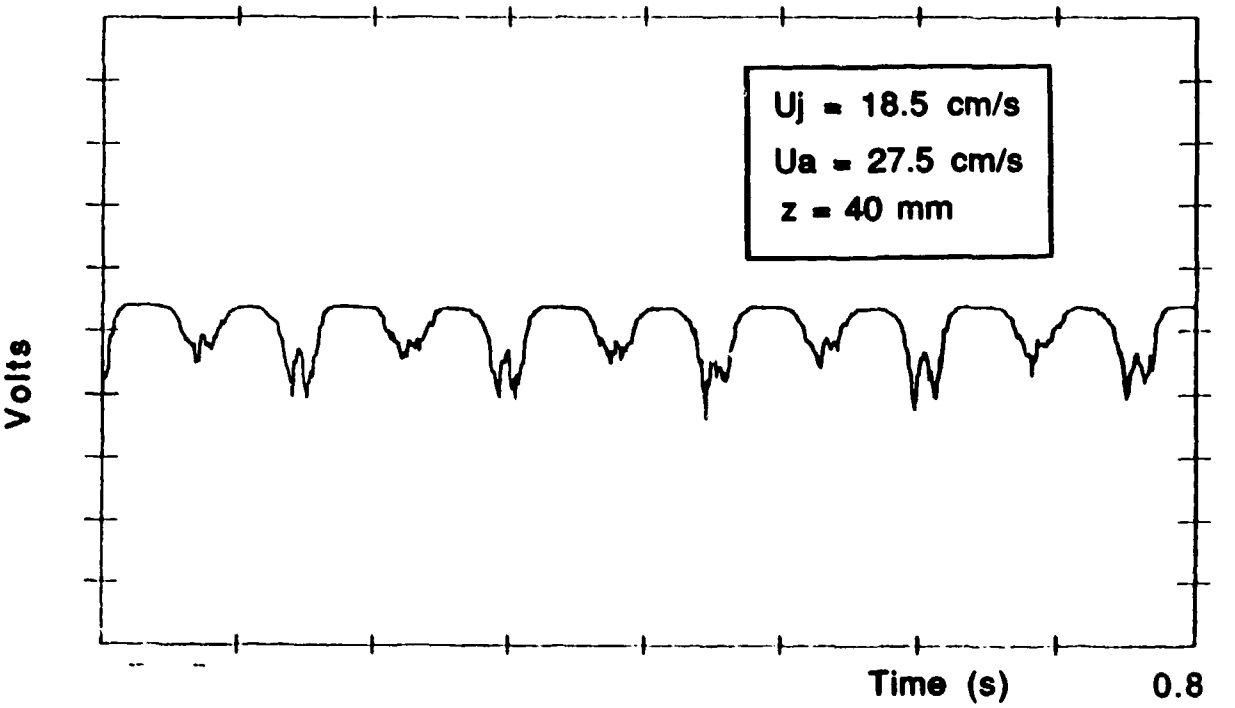

(a) Mie Scattering Time Trace

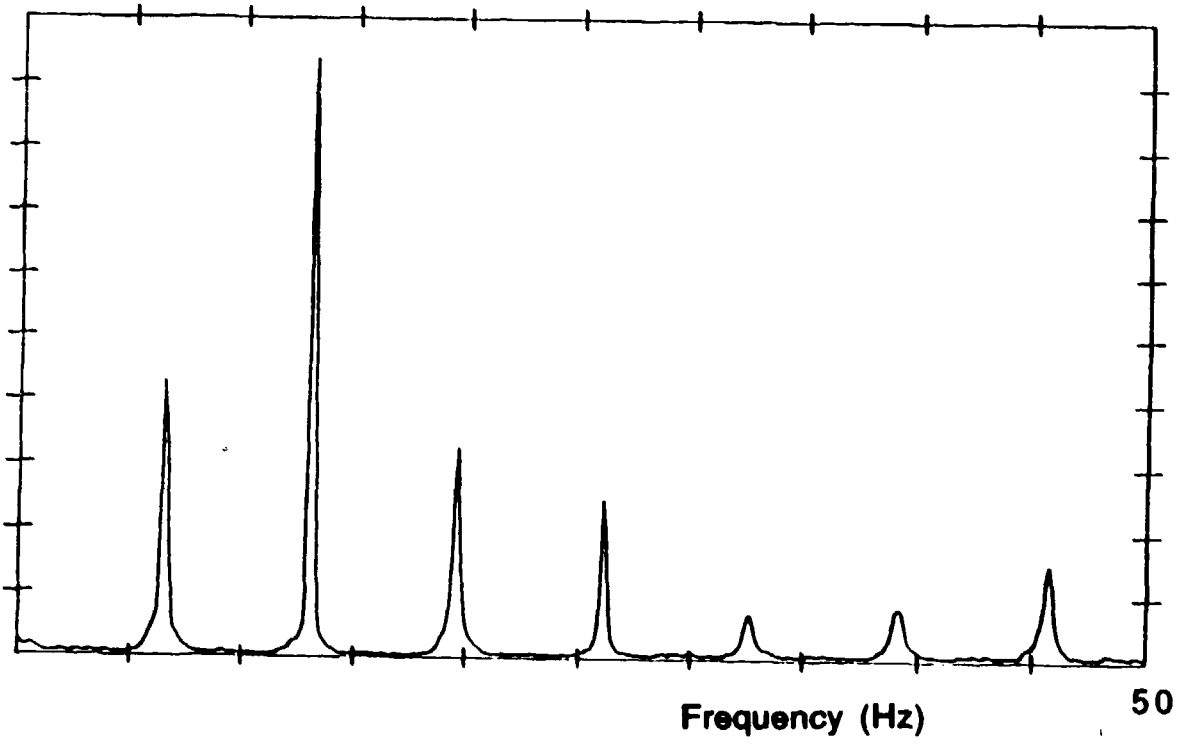

(b) Frequency Spectrum of Signal in (a)

Figure 5.1 Potential Misinterpretation of Mie Scattering Results

the time trace in Figure 5.1(a), one can see that a full waveform (which in this example consists of two peaks of two different amplitudes) repeats itself every 0.16 seconds, thus a frequency of 6.125 Hz. The Fourier analyzer, however, has seen the flat zones at the top of the signal (two per period) and correlated them so that they have a frequency of 12.25 Hz. This correlation is a strong one, and the frequency spectrum indicates this. For a full discussion of Fourier transforms of finite signals, see Malmstadt et al (1981). In most other cases, the Mie scattering data required proper interpretation to determine the shedding frequency. This emphasizes the need to examine the signal's time trace. Photographs were also important in resolving this apparent discrepancy. Measuring the spacing of the structures passing at 40 mm, a shedding frequency of 12.25 Hz would imply that the convecting velocity of the structure was greater than both the annulus and jet velocities. Using 6.125 Hz gives a result consistent with the photograph and the mean axial velocity.

VI. Results and Discussion

Flow Visualization

Flow visualization in the three planes of the jet were done. Since the photographs taken in the y-z plane (those that show the large-scale structures) were expected to be very similar to those of Tankin, it is more interesting to view visualizations in the other two planes first. The lateral (x-z) plane visualizations are shown in Figure 6.1. These photographs identify a problem with the centerbody which had been noted previously under stroboscopic lighting. The flow is not two-dimensional (i.e., there is not a top-hat profile in the lateral direction), particularly at low velocities. When the problem was first noted, it was felt that the flow dividers (see Figure 3.2) were not equispaced, thus distributing the flow improperly. This problem was fixed by realigning the dividers at the bottom of the centerbody. When reinstalled, the flow patterns of Figure 6.1 were unchanged. The problem may be one of flow diffusion. The area ratio of each of the 4 flow segments is greater than 4.0. At very low velocities, low energies, the flow cannot diffuse efficiently. The honeycomb and screens in the chimney section should remove any lateral swirl present in the annulus flow, but this too could be contributing to the problem. This problem was not investigated further. It is interesting to note that the flow for the worst case, U_j = 18.5 cm/s, still maintained a

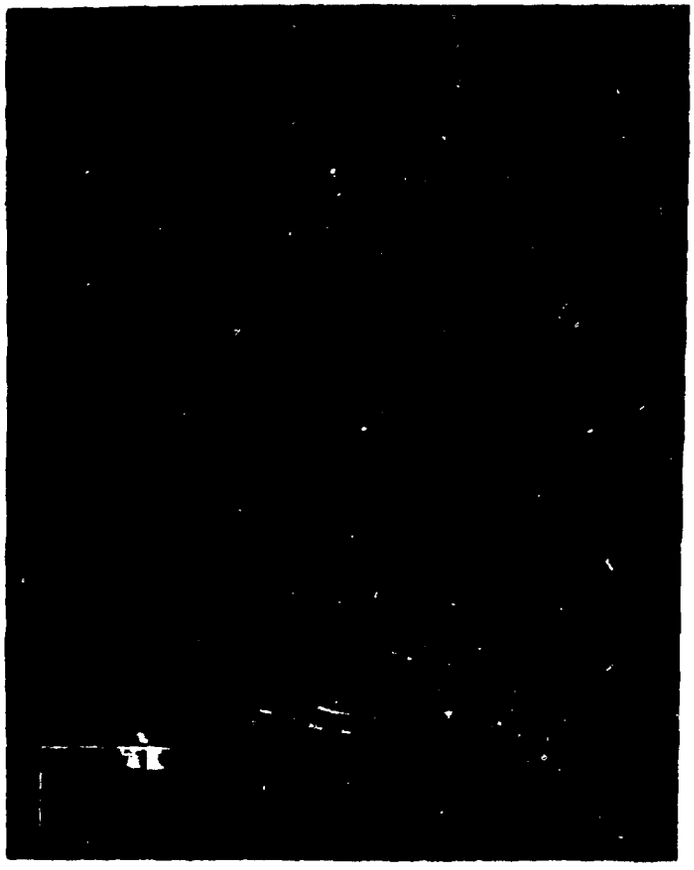

(a) Uj = 18.5 cm/s

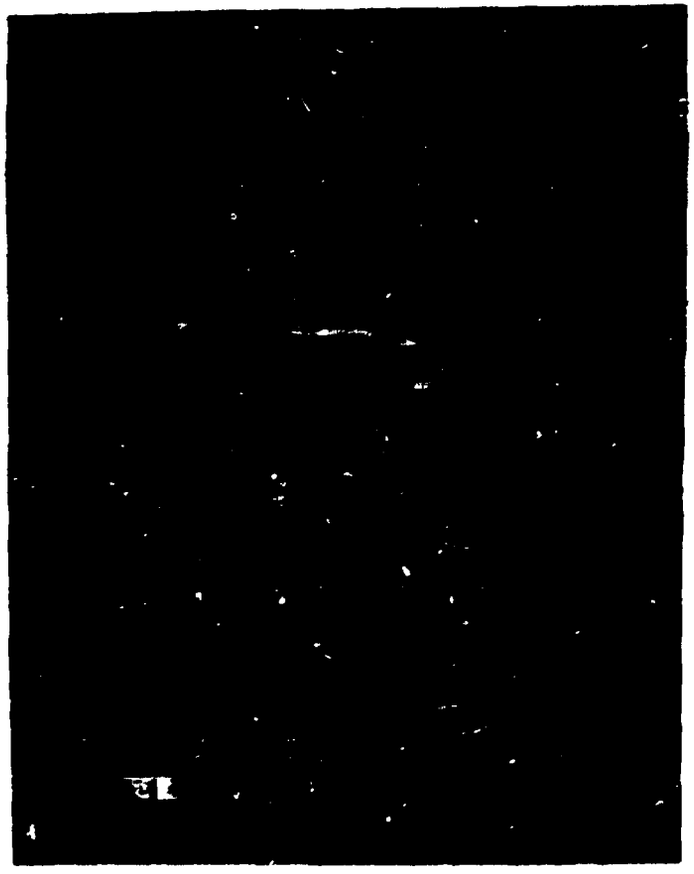

(b) Uj = 22.2 cm/s

Figure 6.1 Lateral Plane Flow Visualization

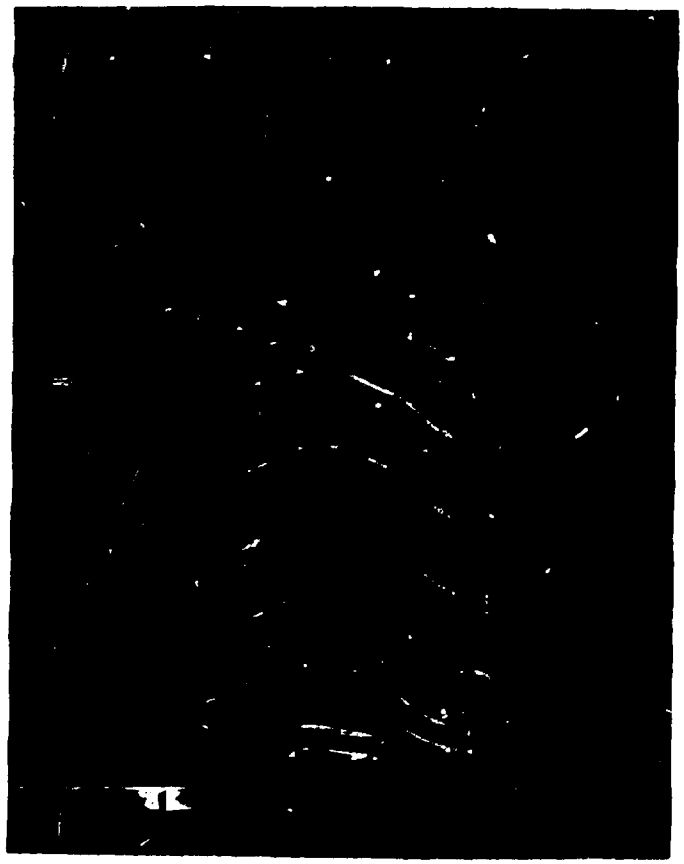

(c) Uj = 27.8 cm/s

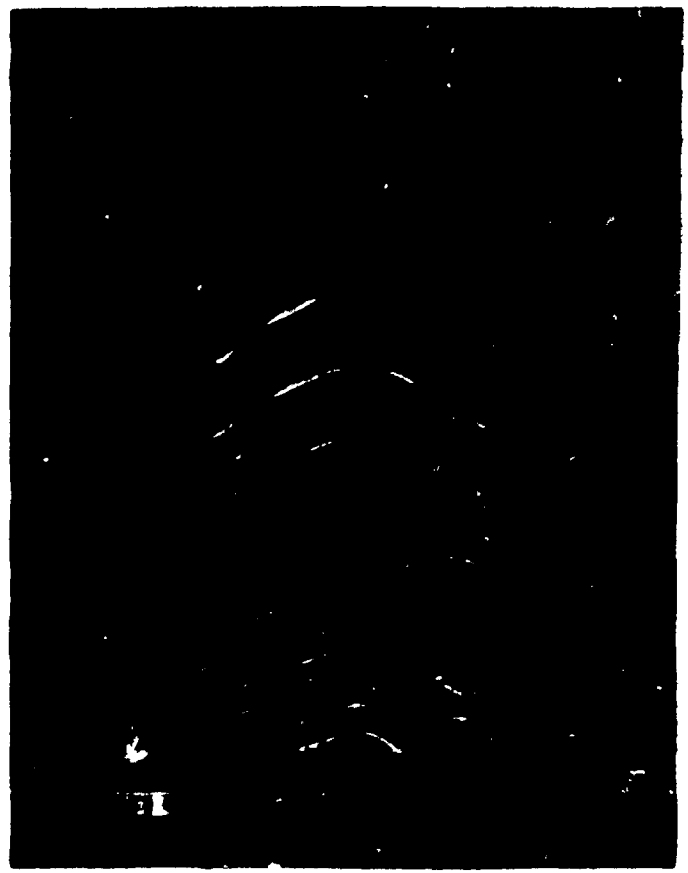

(d) Uj = 33.3 cm/s

Figure 6.1 Lateral Plane Flow Visualization

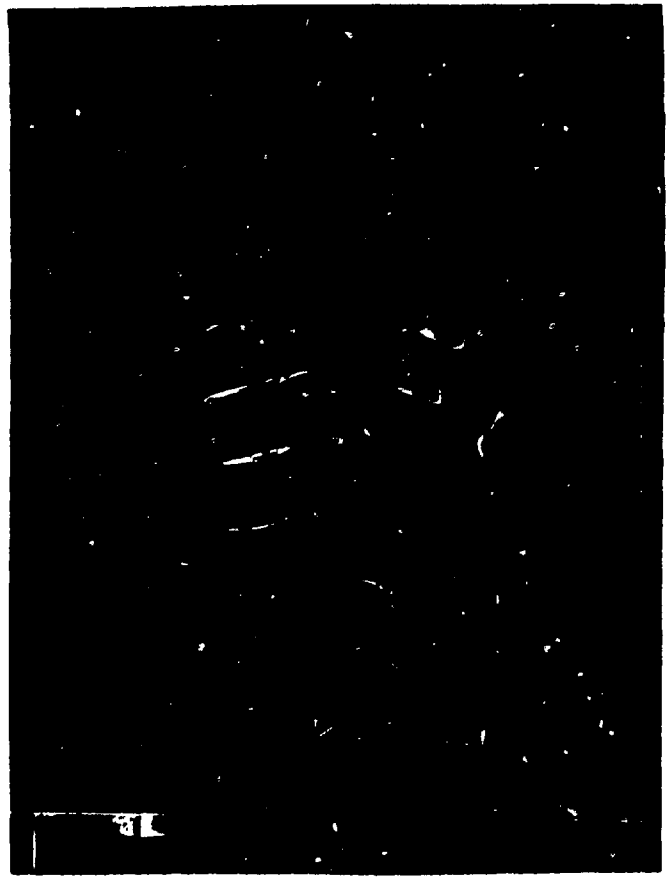

(e) Uj = 37.0 cm/s

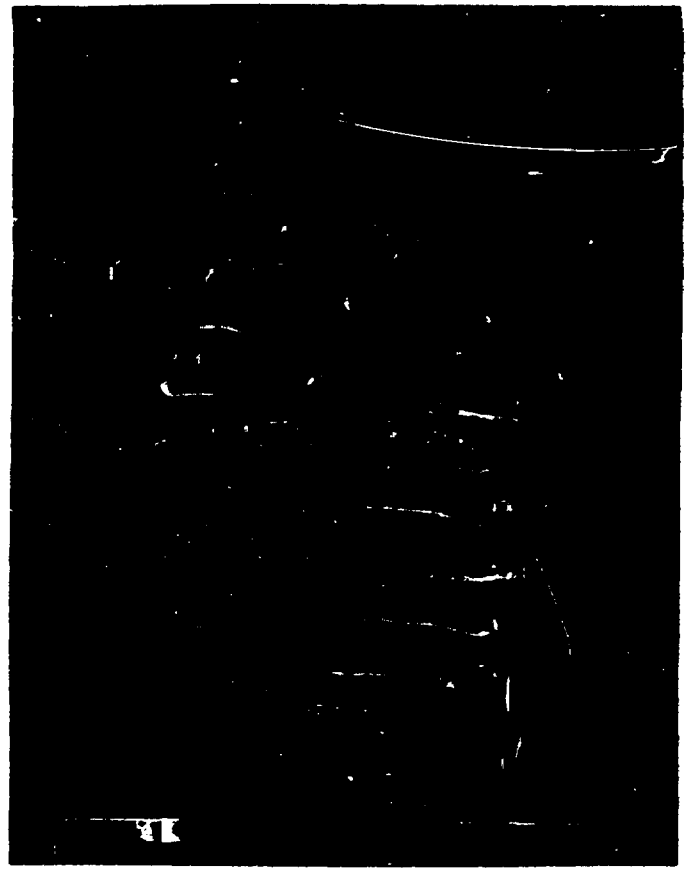

(f) Uj = 51.8 cm/s

Figure 6.1 Lateral Plane Flow Visualization

two-dimensionality (away from the edges), just that it occurred in a plane that now had the slope of the lines shown in Figure 6.1. Using the strobe as a light source, one could look down the centerline of the vortex sheet (viewing from the left looking at Figure 6.1) at the appropriate angle, and it was evident the flow was two-dimensional. It is best to use a term like "quasi-2-D" or "piecewise 2-D" to describe the flows in this experiment. In their study of a free shear layer, Lasheras et al (1986) found that the characteristics of the Kelvin-Helmholtz roll-ups in the shear layer were virtually unaffected by the presence of three-dimensionality. Although true two-dimensionality may never be achieved for this configuration, all attempts were made to minimize spurious contributions to the three-dimensional behavior. It was felt that this had been at least roughly achieved, so the experiments proceeded using the existing ccnfiguration and test conditions.

Because of the three-dimensionality (tilt) of the flow, the photographs in the horizontal plane were not able to provide much insight to how instabilities in that plane affected the transitions. The photographs at the various z locations for U_j = 18.5 cm/s and 37.0 cm/s are given in Figures 6.2 and 6.3, respectively. For U_j = 18.5 cm/s, it is nearly impossible to tell if the observed pattern is a result of a true instability and vortex roll-up (analogous

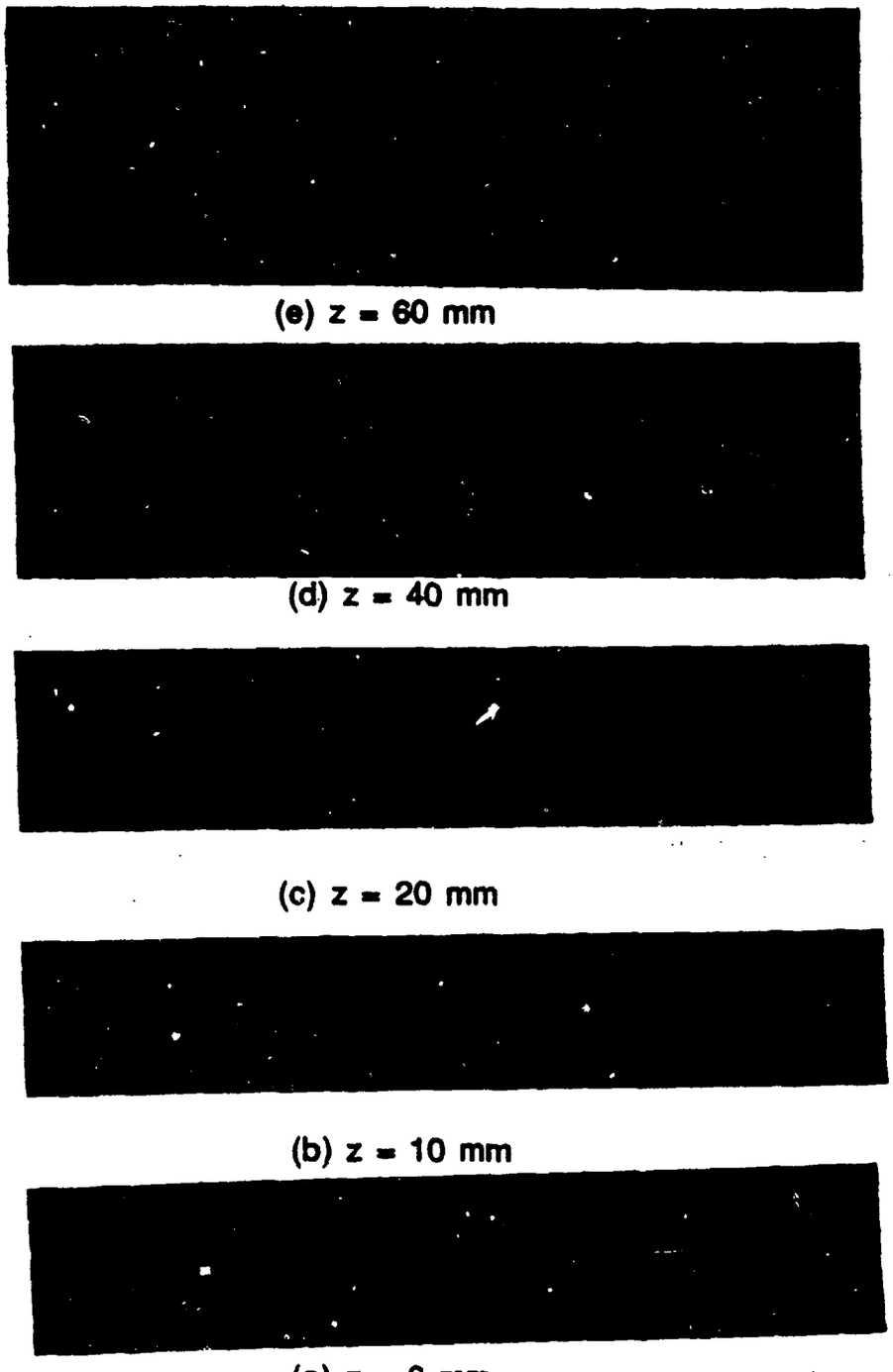

(e) z = 60 mm

(d) z = 40 mm

(c) z = 20 mm

(b) z = 10 mm

(a) z = 6 mm

Figure 6.2 Horizontal Flow Visualization
(Uj = 18.5 cm/s)

(e) z = 60 mm

(d) z = 40 mm

(c) z = 20 mm

(b) z = 10 mm

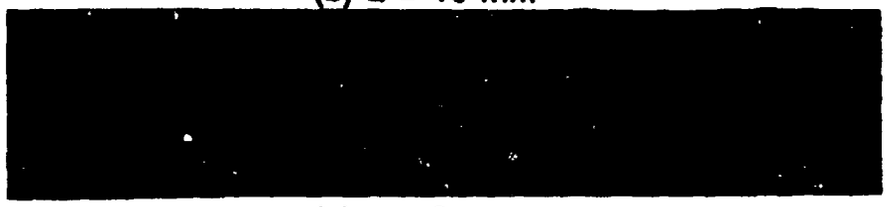

(a) z = 6 mm

Figure 6.3 Horizontal Flow Visualization
(Uj = 37.0 cm/s)

to a Tollmein-Schlichting wave), or the result of fluid motion in the lateral direction induced by the experimental imperfections. Unfortunately, it seems to be the latter. Viewing Figure 6.3 does show, as did Figure 6.1, that the jet is well-behaved and two-dimensional at the high flow rates (even as high as z = 60 mm). Due to the three-dimensional nature of the flow, however, specific analyses would be pure speculation at this time and are avoided.

Some general comments on these visualizations are appropriate. As alluded to earlier, one can see how far downstream the two-dimensionality of the flow prevails. 2-D flow would imply that we would see a rectangle in the horizontal plane. As one can see in Figure 6.2, flow at U_j = 18.5 cm/s already has developed a small amount of waviness at z = 6 mm. The same is true, but to a lesser degree, for jet velocities of 22.2 and 27.8 cm/s (these photographs are not shown here). Higher velocities result in "two-dimensional" flows at this z location. As one goes to greater and greater axial positions, the influence of the third dimension becomes larger and larger.

An interesting behavior is observed in all photographs of the horizontal plane. At the ends of the slot, a rounding has occurred which makes the shape of the illuminated particles much like a dog's bone. One might think about this effect in the following way. Imagine

starting with an axisymmetric jet. The pattern seen in its horizontal plane would be a circle. Distortion of the jet by squeezing its two sides would begin to produce ovals which would become more and more oblong as the squeezing continued. At some point a rectangle (similar to the plane jet) could be achieved. At the ends, some rounding would still exist, but these effects will have been confined to a small region if squeezing was stopped at a high aspect ratio. The analogy here is only meant as a tool; this picture of the plane jet may be useful for conceptualizing various aspects of the flow.

The vertical sheet photographs are given in Figure 6.4. These compare quite well with Tankin's work (see Figure 4.1), as they should. The case where U_j = 37.0 cm/s is where a bifurcation occurs, and the new test conditions produced the pattern seen in Tankin's photograph at a slightly different jet velocity (<2 cm/s difference). There were subtle differences between the present configuration and the one used by Tankin, and this would explain the observed differences in flow patterns. The contraction sections used in the two experiments were different. The contraction ratio for Tankin's work was 4.5, and it was 2.68 in the present work. This difference meant the annular flow rate Q_a had to be increased to meet the requirement that velocities in the two experiments were the same. As discussed earlier, this will change the turbulence intensity

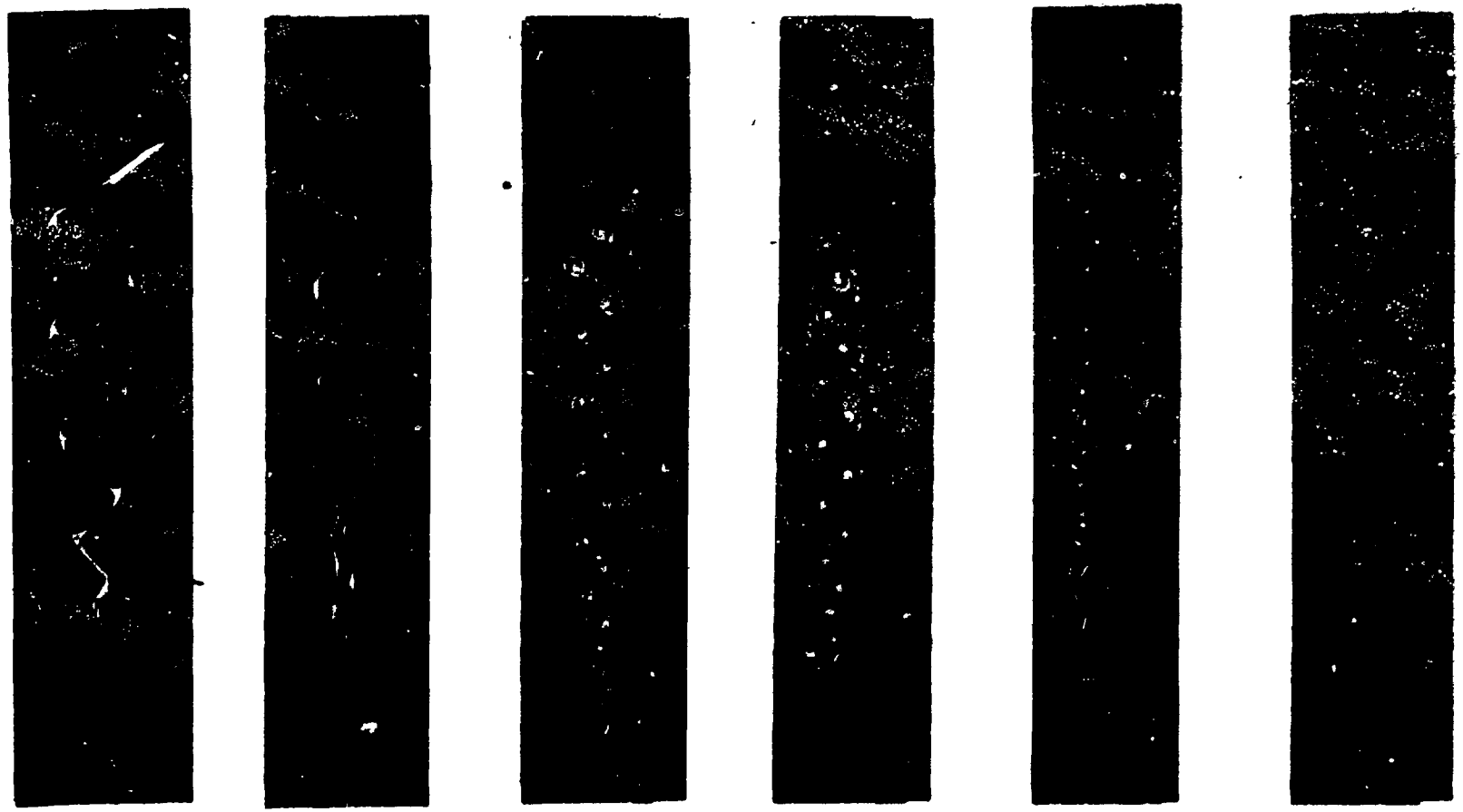

Uj = 18.5 (cm/s) 22.2 27.8 33.3 37.0 51.8

(a) (b) (c) (d) (e) (f)

Ua = 27.5 cm/s

Figure 6.4 Vertical Plane Flow Visualization

in the annulus. Even with these differences, the degree to which the flows are similar indicates that a similar qualitative evolution of these flowfields is occurring.

LDA Measurements

The LDA system described earlier was used to gather instantaneous axial and transverse velocity data. With the data obtained, one could evaluate mean velocities, the root mean square of the velocity fluctuations, normalized Reynolds stress (covariance), turbulent kinetic energy, kurtosis, and skewness. One could also get the probability density function (PDF) and the spectral information from data obtained. Many methods of data presentation were available.

The first problem which is evident is that, while the flow is clearly non-turbulent, only quantities typically used to analyze turbulent flows are available. Except for mean velocities and spectral analyses, these quantities demand new interpretation if they will be used to help determine the character of the flow.

Mean values have a straightforward interpretation. The present significance of root mean square velocities can be analyzed by considering the following idealized case. Consider the transverse velocity for a 2-D vortex (assumed to be a solid body) translating in only the axial direction. If the measurement volume splits the vortex as it

translates, one might expect the instantaneous velocity signal to look like a sine wave. The concept is shown for two vortices in Figure 6.5. The tilda denotes an instantaneous value. At t_o, the first vortex passes the measurement spot with its minimum velocity. Velocity then increases through zero (center of vortex) until the bottom of the first vortex is reached. The space between vortices is assumed to produce a smooth velocity gradient when going from the maximum (end of the first vortex) back to the minimum (beginning of the second vortex) velocity. The process then repeats itself for the second vortex. Since v_{rms} is obtained from the data analysis, and a functional form for $\tilde{v}$ has been assumed, v_{rms} can be related to the rotation speeds of the vortices. For a sine wave, the maximum amplitude and its root mean square are related. Using the analogy to the rigid rotator, one can say

$$|v_{max}| = \sqrt{2}\ v_{rms} \tag{6.1}$$

Flow visualization can provide vortex size, r. Angular speed, ω, could be estimated using

$$\omega = \frac{|v_{max}|}{r} \tag{6.2}$$

A non-zero mean velocity will affect this calculation slightly since this means the solid body is also translating

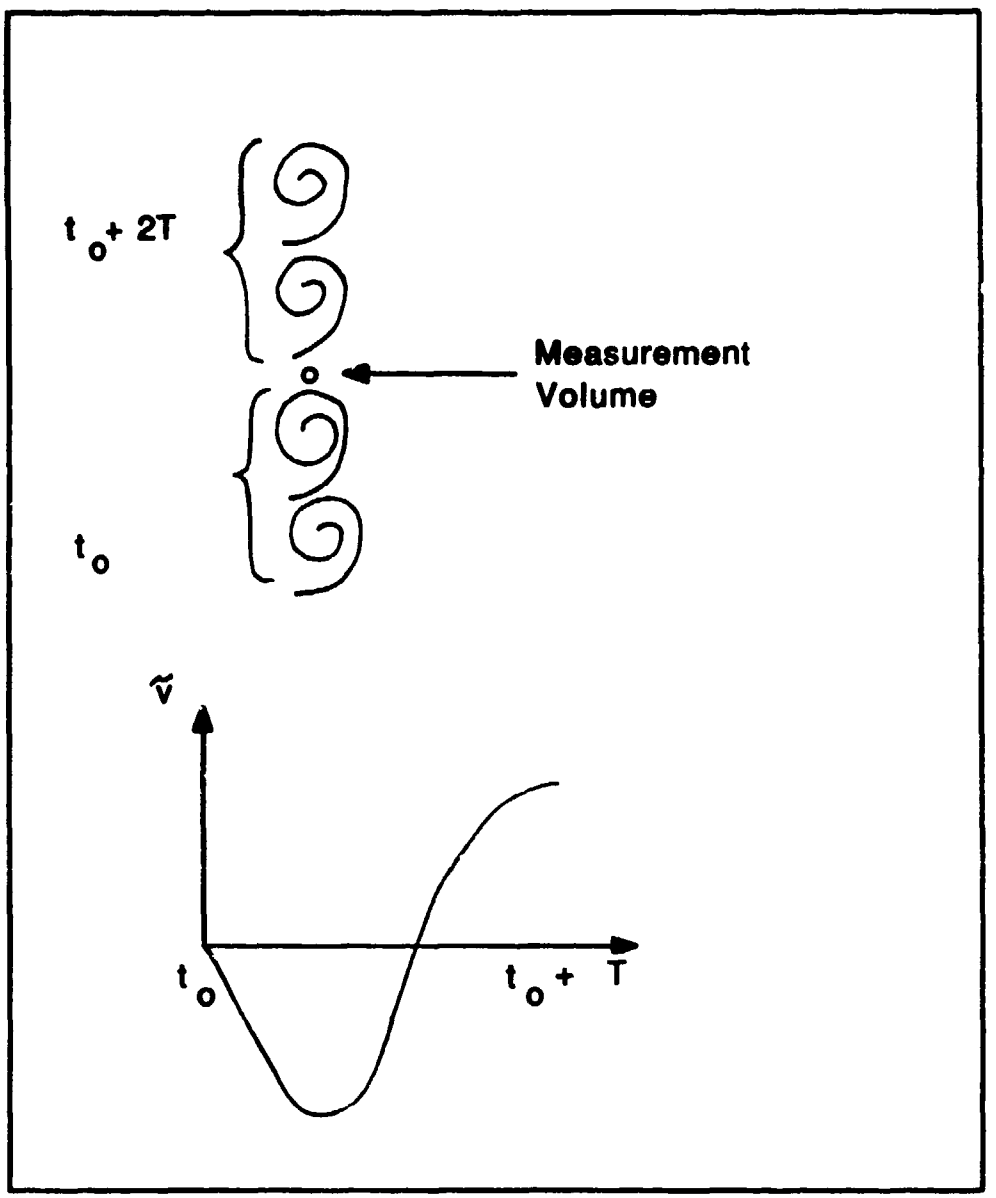

Figure 6.5 Idealized Instantaneous Transverse Velocity for Two Solid Body Rotators Translating Uniformly

in the Y direction. For this analysis, however, the effect will be ignored. This method could provide insight into the dynamics of the vortices.

The Reynold stress, $\overline{u'v'}$, normalized by the product $(\overline{u'^2} \cdot \overline{v'^2})$, the variances of u and v, is called the covariance. It is a value between 0 and ± 1 that identifies the degree to which u_{rms} and v_{rms} are correlated. If a and b represent two signals, if a is always positive when b is negative, then the parameters are perfectly negatively correlated (i.e. covariance is -1). If the signals are both positive most of the time, the signals are said to be strongly positively correlated (i.e. covariance greater than zero and near unity). Two completely random signals should yield a covariance of zero. For non-turbulent flows, it will be important to look at covariance as a correlation parameter only, not as a Reynolds stress.

With these ideas in mind, the data are presented in Figures 6.6 through 6.10. All data have been smoothed using a Gaussian filter. The Gaussian factor was selectable and was chosen as 2.5. The 4096 data points taken at each position represent instantaneous velocities and are used to form a probability density function (PDF). This PDF is assumed to be a Gaussian distribution. All data outside 2.5 standard deviations of the mean are eliminated, and a new distribution is generated. All data lying outside 2.5 standard deviations for the new PDF are eliminated. A new

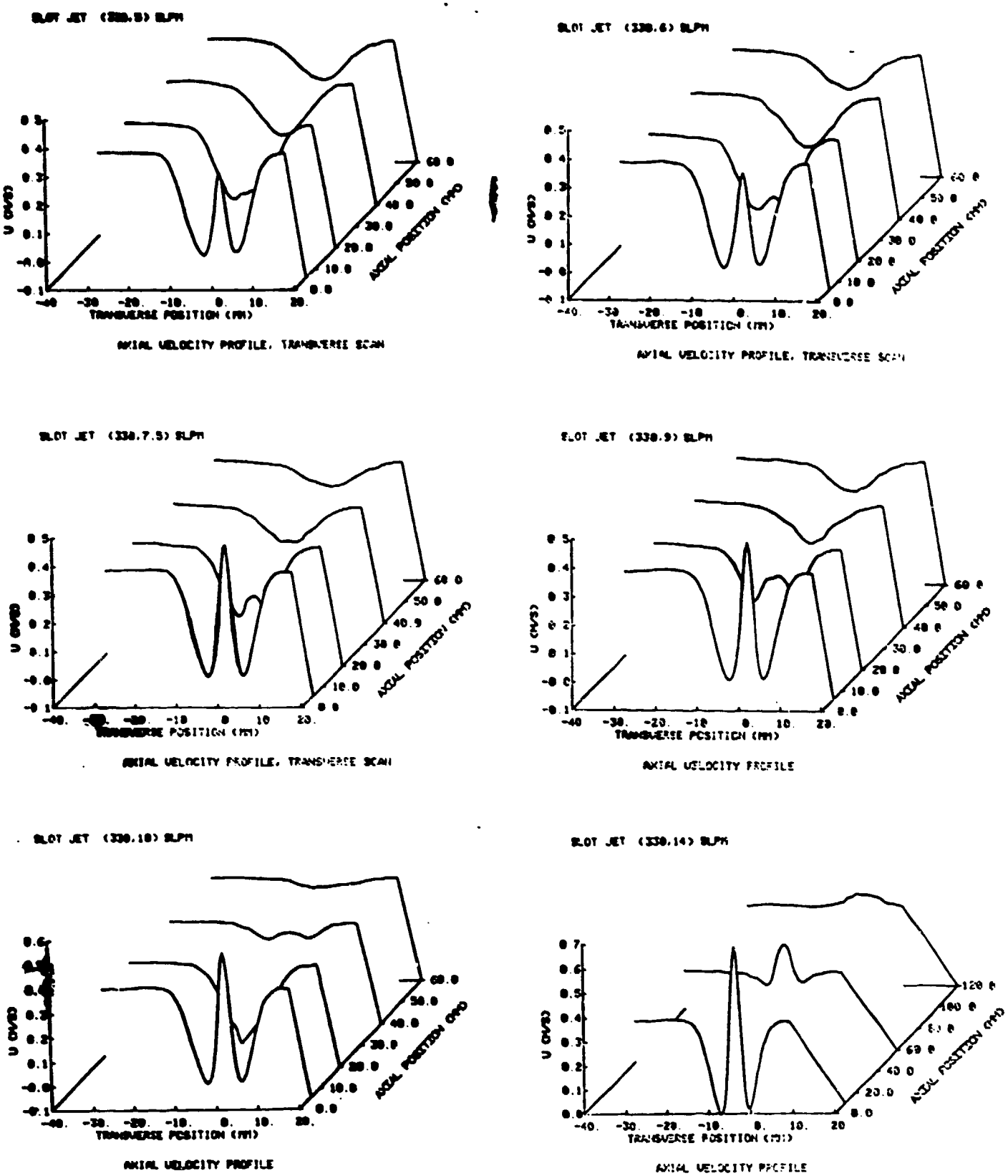

Figure 6.6 Axial Velocity Profiles

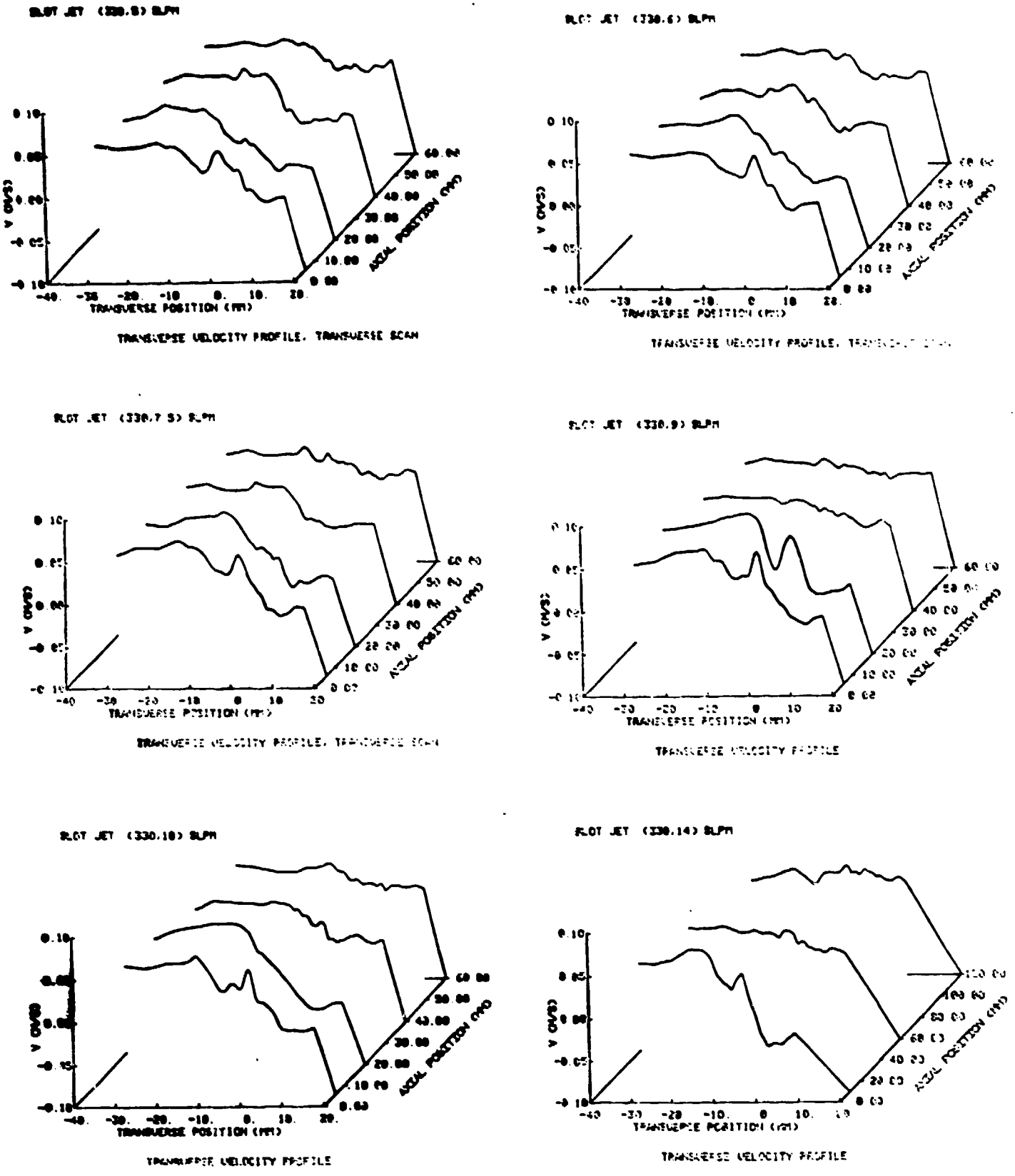

Figure 6.7 Transverse Velocity Profiles

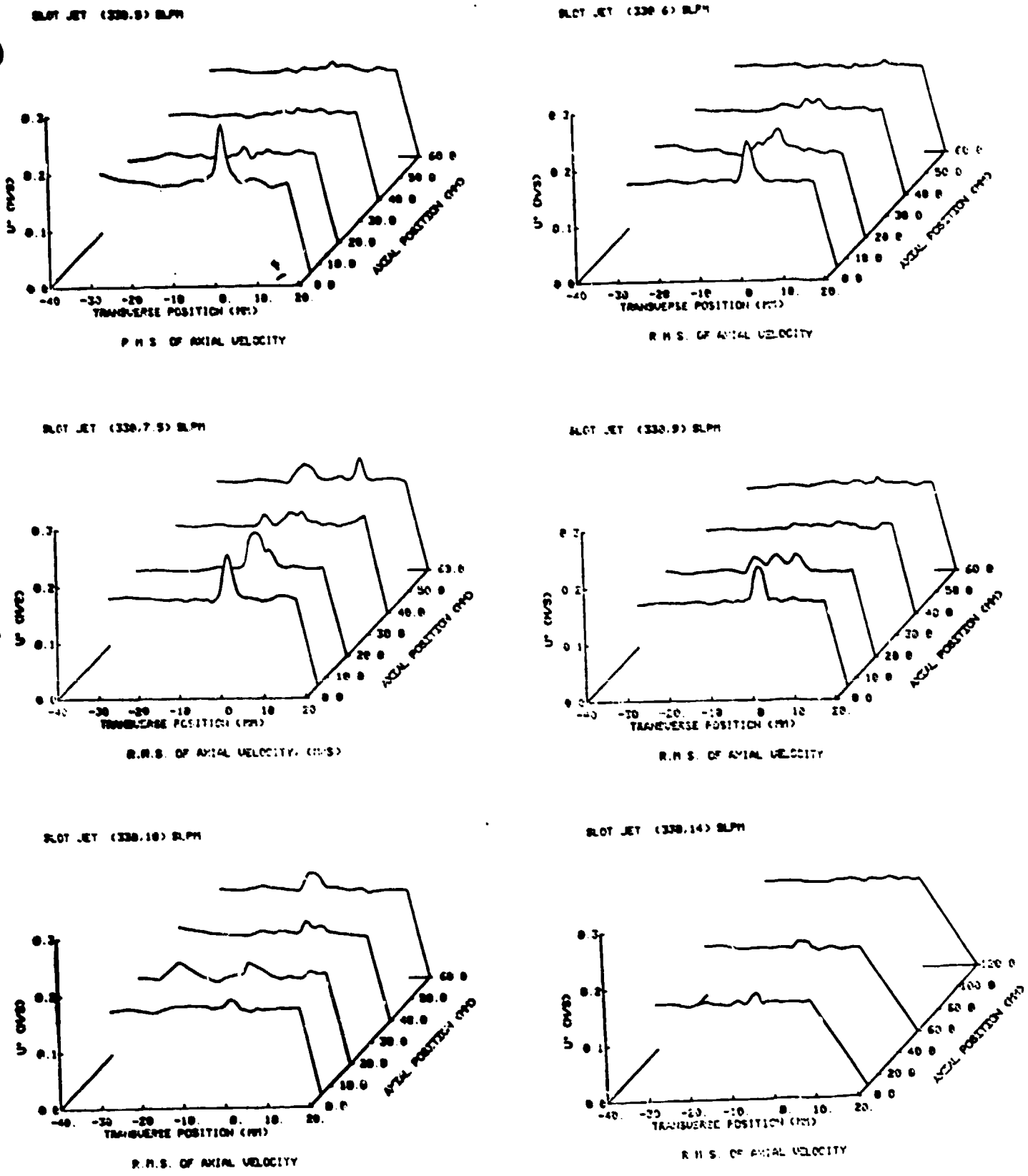

Figure 6.8 u_{rms} Profiles

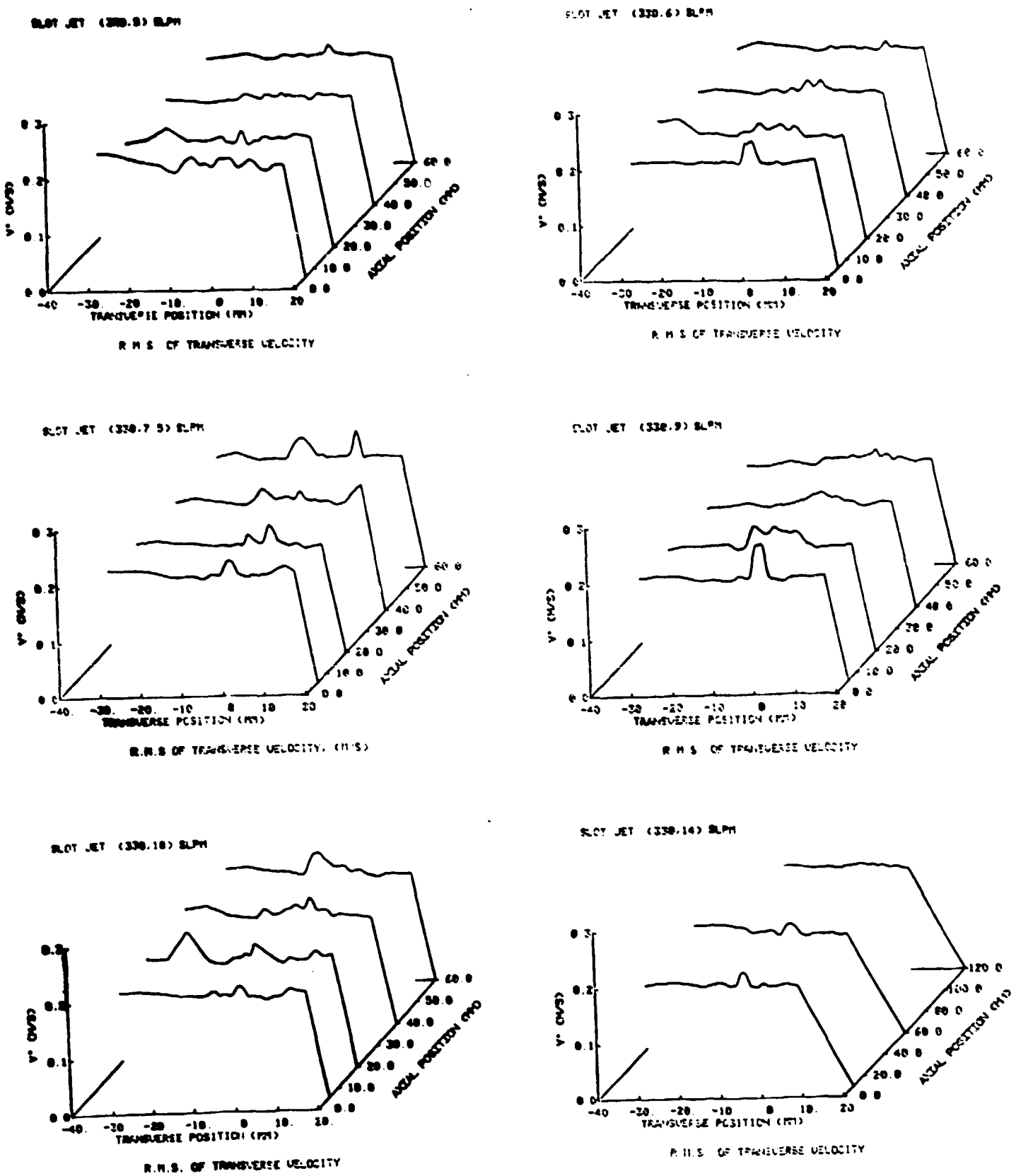

Figure 6.9 v_{rms} Profiles

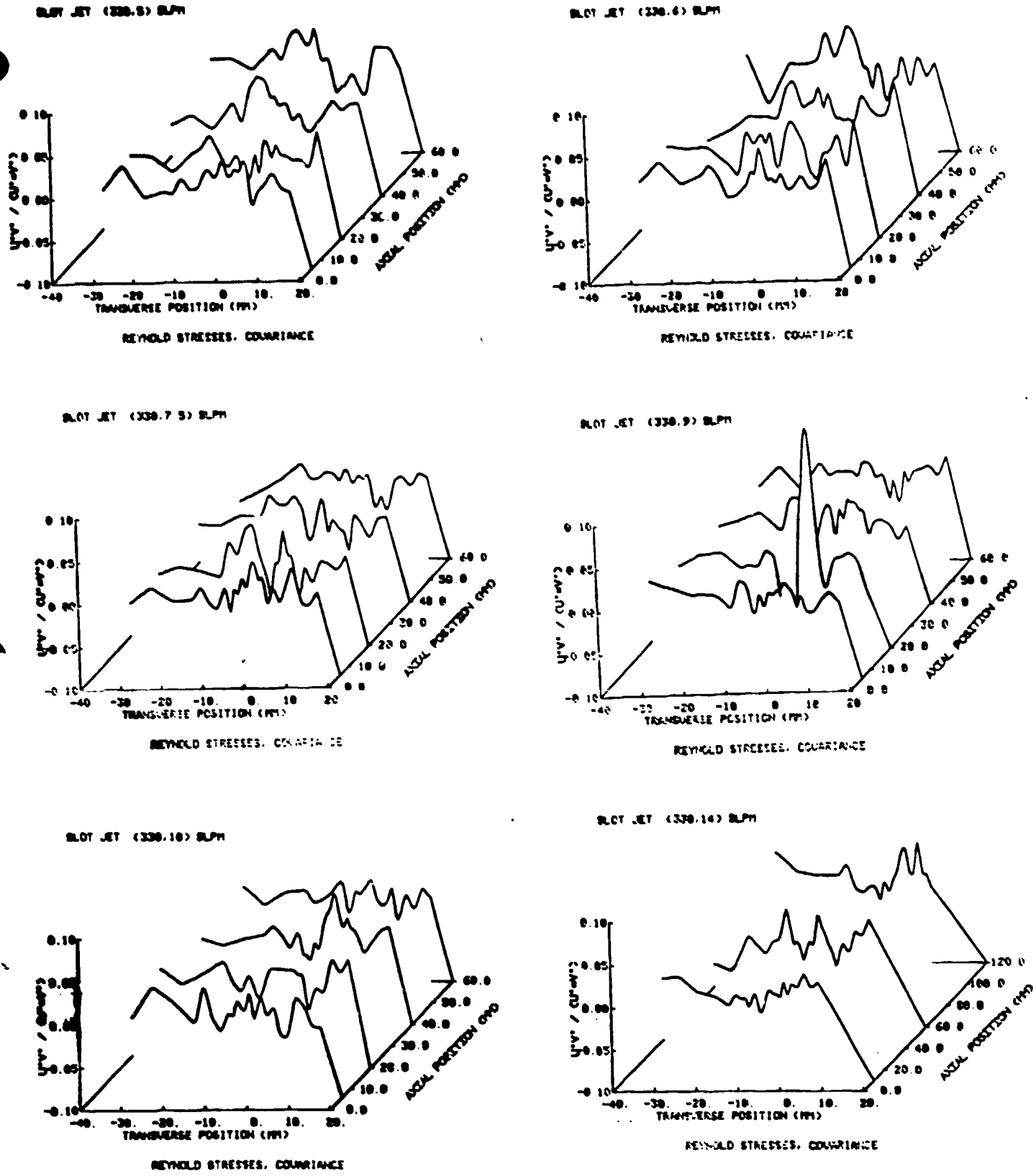

Figure 6.10 Covariance Profiles

PDF is created, and the process is complete. Figures 6.6 through 6.10 show how each of the flow variables change with axial position. Test conditions are given in the header of each plot (refer to Table I). The data are presented here to provide a summary of results. Discussion of the results will be given as appropriate later in this section. Attempts to perform spectral analyses of the data were unsuccessful because seeding rates were too low at nearly all conditions. The Mie Scattering Method would have to be used to obtain the information about vortex shedding frequencies.

Mie Scattering

The Mie Scattering Method (MSM) was used to determine the shedding frequencies of the large-scale structures. The Mie scattering results are summarized in Figure 6.11. Shedding frequencies are shown for z = 60 mm. Shedding rates were the same at all locations (for a given U_j), except where z = 120 mm and U_j = 51.8 cm/s, where no distinct frequency is observed. Discussion of these results will follow.

Discussion

To assess the character of the bluff body/jet interaction, we first look at the results from the LDA

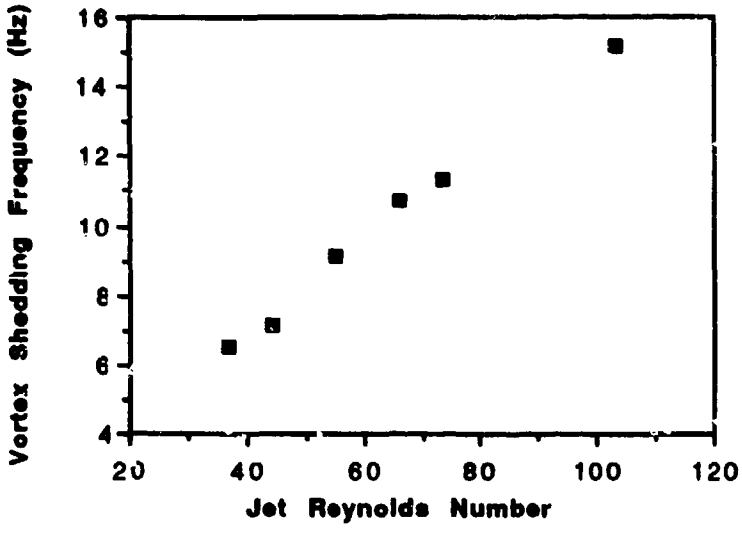

Figure 6.11 Vortex Shedding Frequencies

measurements. The statistical quantities obtained from the LDA data may provide important information on the interaction. The mean velocity profiles are important since they will identify, on the average, the flow's behavior. The ability to associate these mean flows with mean flows from different, simpler geometries could provide useful insight into the important factors governing the flow. The mean profiles for axial and transverse velocity are given in Figures 6.6 and 6.7, respectively. For the axial velocity cases, the mean flows above the centerbody at z = 6 mm resemble jet flows. By z = 20 mm, however, the flows (except for U_j = 51.8 cm/s) resemble wake flows. Sato (1960) studied various slot jets (without annulus flows) and got mean profiles like those shown in Figure 6.12. He also observed that the mean velocity distribution changed

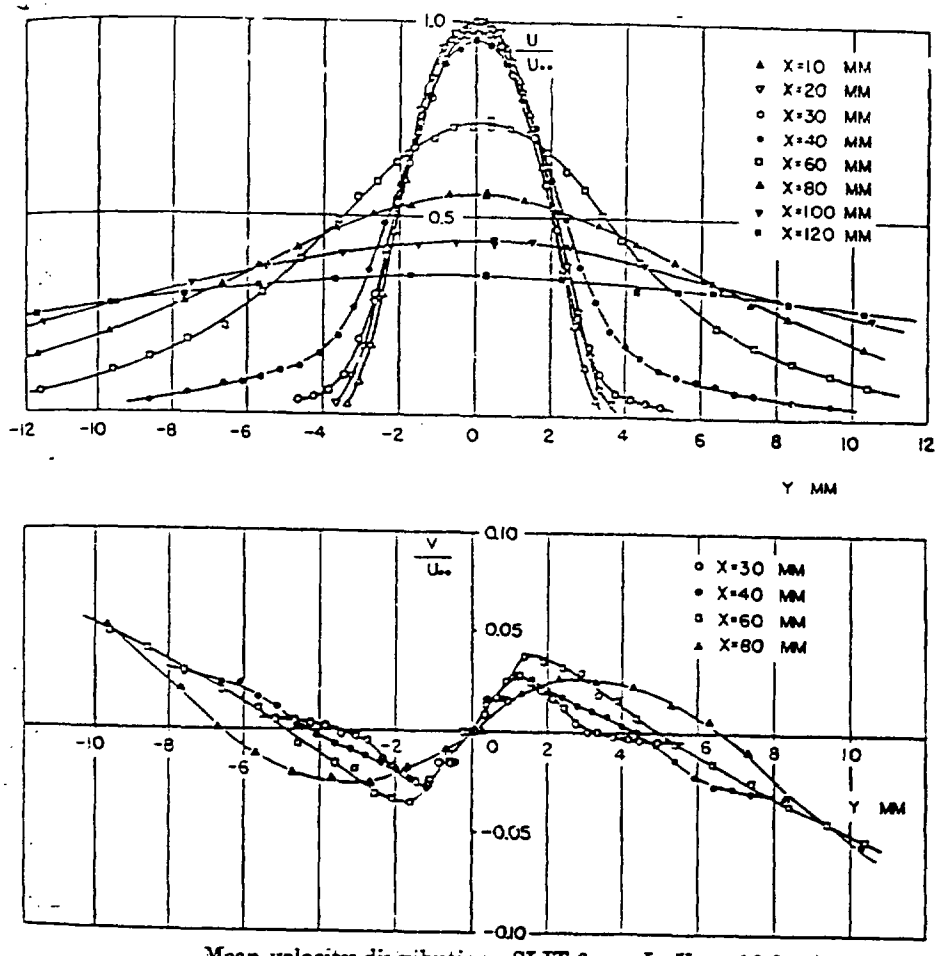

Mean-velocity distribution. SLIT 6 mm L. U_{00} = 10·0 m/sec.
X is measured from the slit.

Figure 6.12 Mean Velocity Distribution (Sato,1960)

drastically around z/D of 6 or 7. Figures 6.6 and 6.7 show behavior very similar to this, except these profiles are affected by the annulus flow. Transverse scans at z = 10 mm were not added on Figures 6.6 through 6.10 because the 3-D plot lost some of its clarity. The case where z = 10 mm does very closely resemble the case for z = 6 mm for all conditions. With the similarity seen in this comparison, two definitions of flow "regimes" will be made. The "jet field" is considered that region above (axial direction) the bluff body up to z/D of 6 or 7. The "annulus field" is that region above the "jet field." It is important to note that the "annulus field" is not just the region above the annulus. The "jet field" is the region where the jet's influence is strong, and the mean behavior of the flow is similar to that of a jet. The "annulus field" is the region where the influence of the annulus is strong, and the flow behaves like a wake. These definitions will be useful in later discussions.

It was hoped that the root mean square of the fluctuating velocities and the covariance could be used to help better define flow characteristics. As discussed earlier in the chapter, equation (6.2) could be used to estimate angular rotation rate for vortices assumed to be solid body rotators. Estimates of rotation rate for the cases where U_j = 27.8 and 33.3 cm/s are given in Figure 6.13. The vortex radii, r, were determined using

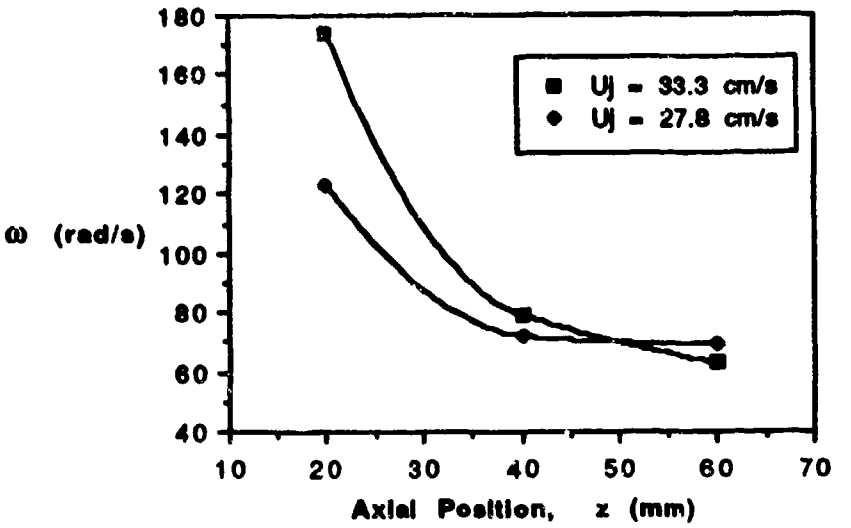

Figure 6.13 Estimation of Vortex Angular Rotation Rate

measurements based on the photographs. v_{rms} was taken from the data. The curves in Figure 6.13 provide a qualitative trend about the flowfield which may provide some insight into the bluff body/slot jet interaction. The covariance, shown in Figure 6.10, was typically very small (absolute values less than 0.05), so this parameter was not used to help better define the flowfields. No trends or distinct shifts in the parameter were seen, so little time was spent evaluating the impact of the covariance.

As just stated, however, the assumptions used to arrive at Eq. (6.2) may be able to help understand the jet/annulus interaction. Their significance may be brought out in the following way. The following development has been proposed by Hitchcock (1987). Consider the fully

developed duct flow shown in Figure 6.14. The angular rotation rate of the fluid, given by the curl of the velocity, is

$$\omega_z = \frac{1}{2}\left(\frac{\partial u}{\partial y} - \cancelto{0}{\frac{\partial v}{\partial x}}\right) \tag{6.3}$$

Knowing that

$$\frac{u}{\bar{u}} = \frac{3}{2}\left[1 - \left(\frac{y}{b}\right)^2\right] \tag{6.4}$$

one finds that

$$\omega_z = \frac{3\ y\ \bar{u}}{2\ b^2} \tag{6.5}$$

Since the maximum rotation speed will occur at y = b, Eq. (6.5) can be rewritten

$$\omega_{z\ max} = \frac{3\ \bar{u}}{2\ b} \tag{6.6}$$

If one then assumes $\bar{u} \sim U_j$, Eq. (6.6) becomes

$$\omega_{z\ max} = \frac{3\ U_j}{D} \tag{6.7}$$

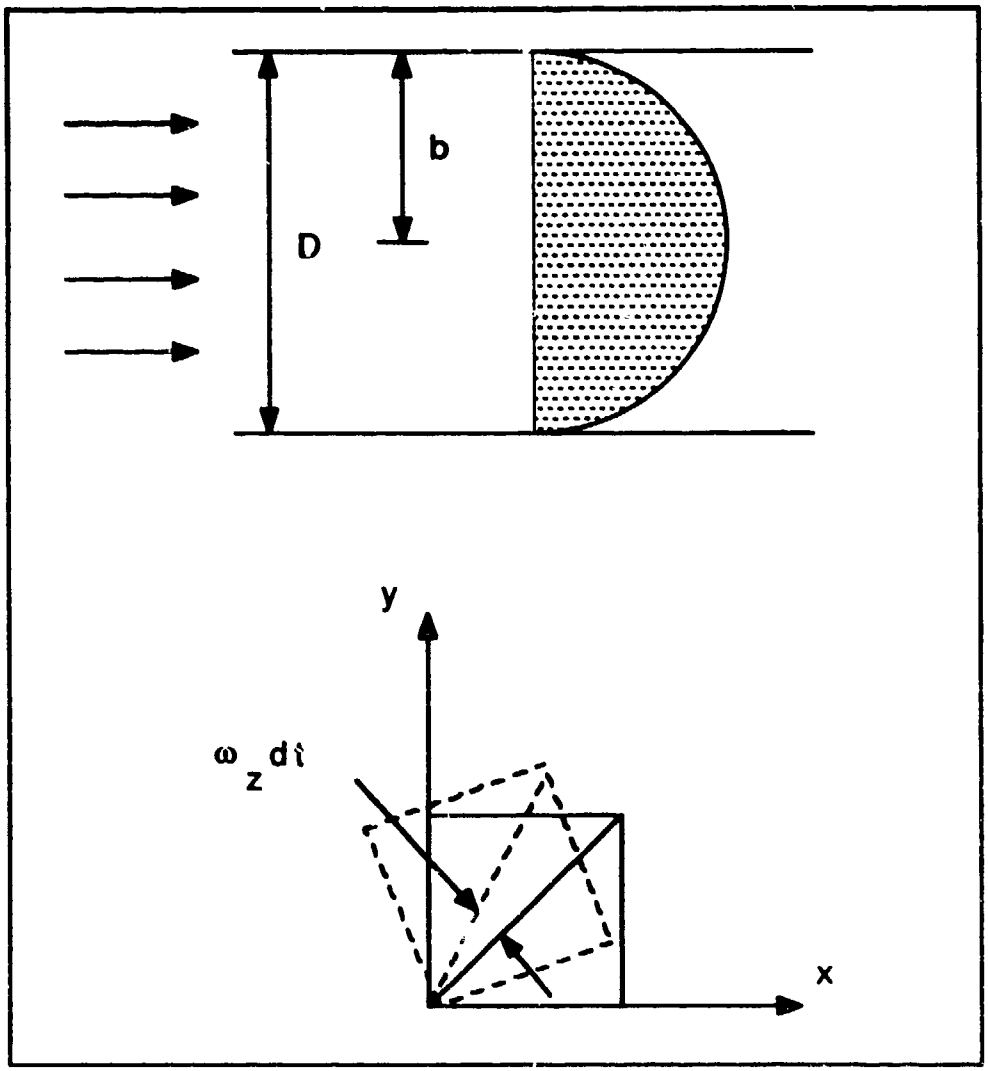

Figure 6.14 Duct Flow

Defining

$$f_r = \frac{\omega_{z\,max}}{2\pi} \sim \frac{U_j}{2\,D} \tag{6.8}$$

one can see that an estimate of angular rotation rate can be made based upon the "history" of the flow (i.e., before the flow exhausted into the ambient stream). This result is interesting for several reasons. The values of ω_z from Eq. (6.7) are generally within a factor of two of those shown in Figure 6.13. This result is encouraging considering the assumptions made to arrive at both results. (Whether the flow is fully developed in this investigation is a question which may be raised, but the exit profiles shown in Figure 6.6 show mean velocities that tend toward a fully developed duct flow.) One can also see that there is no dependence on viscosity in Eq. (6.8). For a developing flow, viscosity would be important, so parameters such as Reynolds number become important. This is an important point when considering Strouhal number, which will be discussed next.

It was mentioned in Chapter I that use of a parameter such as St or Re may be difficult in the present investigation. To consider Strouhal number, however, several factors point to the fact that U_j and slot width D would be the appropriate parameters for non-dimensionalizing the vortex shedding frequencies. Even though the mean velocity profiles have shown a combination of jet and wake-like flows (with the exception

of U_j = 51.8 cm/s), the vortex shedding frequency was the same in the jet and annulus "fields." These facts indicate that one is justified in assuming that the slot width and jet exit velocity would be appropriate parameters with which to non-dimensionalize the shedding frequencies (given in Figure 6.11). The Strouhal numbers for this configuration are plotted against jet Reynolds numbers (Re_j) in Figure 6.15. The value of St is nearly constant and has the value 0.098. The data Sato (1960) obtained for much higher Re (1500-8000) produced a Strouhal number of 0.14. This result shows, as Sato's did, that Strouhal number is independent of jet Reynolds number (for the range of Re_j investigated, with the exception of U_j = 51.8 cm/s). If one uses the definition of St, given by Eq. (1.1), and the approximation of f_r given by Eq. (6.8), it is easy to show that

$$St = \frac{f\,D}{U_j} \sim \frac{f}{2\,f_r} \tag{6.9}$$

which says that vortex shedding frequency f is proportional to the viscous rotation rate in fully developed duct flow. The absence of Reynolds number dependence again leads to the fact that the flow in the duct is fully developed. It is quite interesting that the flow history is so important. Recall that in Chapter I most of the articles that dealt

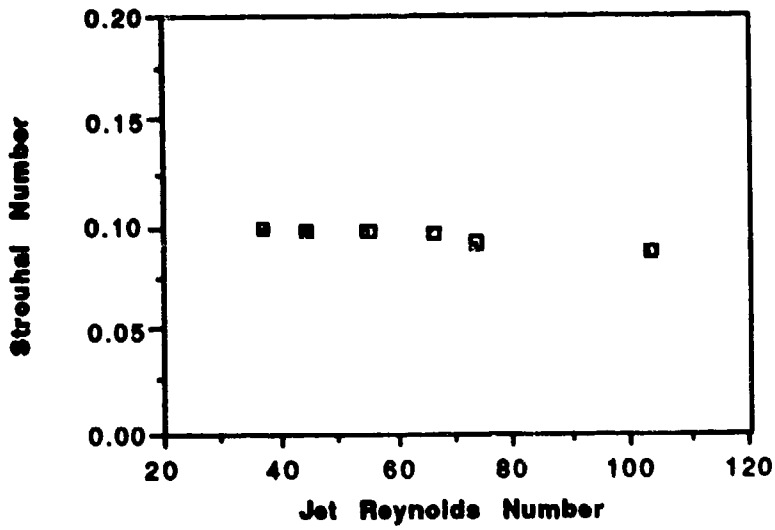

Figure 6.15 Variation of Strouhal Number with Reynolds Number

with the jet's near field focused on the jet boundary. This is certainly important, but the relation between the flow in the duct and the flow's evolution is certainly an interesting one. Having analyzed the data obtained from the LDA and the Mie scattering and having closely examined the flow visualizations, a description of the flowfield dynamics can now be presented.

The following description of the flowfield is presented. For velocity ratios U_j/U_a up to approximately 1.45, there exist a "jet field" and an "annulus field." Beyond this velocity ratio, the "jet field" extends into and eliminates the "annulus field." The source of the large-scale structures is the slot jet and not the annulus flow. Evidence to support this description will now be given.

Strouhal number based on the jet velocity and slot width was constant (for all cases except where U_j = 51.8 cm/s), and this supports the fact that the jet is responsible for producing the instability that results in vortex formation. If the annulus flow was responsible for vortex production, one would expect to see a constant Strouhal number based on annulus velocity and an appropriate length scale (such as the width of the bluff body) because, for low Re, this flow should be similar to shedding in the wake of a circular cylinder (a flow known to produce constant St for low Re). Annulus Strouhal numbers for this experiment, however, are not constant since U_a and D remain constant while f varies. Also, the "stable" configuration for a von Karman vortex street requires that b/a = 0.281, where b is the transverse separation between vortex centers, and a is the axial distance separating the centers. Evaluation of the quantity b/a, based on measurements of the structures in the photographs, did not yield values of 0.281. Deviations from this were sometimes as high as 100 percent, so the inaccuracy involved with measuring could be ignored.

The flow patterns seen in the photographs of Figure 6.4 do show stable configuration of the vortices. The vertical sheet light extends 210 mm in the axial direction, so one can view up to 70 slot widths. This stability in the "annulus field" is a result of the co-flowing stream's

influence on the jet. Looking at Figure 6.4, the "trunks" of the flows are like the one depicted in Figure 6.16(a). Figure 6.16(b) shows the stable configuration for a plane, free shear layer that was studied by Lasheras et al (1986). It is easy to imagine that a slight distortion (offset of alternating vortices) of the pattern in Figure 6.16(a) would yield the configuration in (b), which is the stable configuration for the 2-D centerbody. The geometry and flow conditions will dictate the precise shape of the configuration. The general shape, however, will remain the same, and is it the annulus flow that is responsible for this stabilization.

The "jet field" extends to z/D of approximately 6 or 7. It is here a significant redistribution of the mean axial velocity occurs. Structures formed in the "jet field" propagate through the annulus field without much change. However, as jet velocities increase, there is a point where the jet flow begins to dominate the dynamics of the entire flowfield. Looking at Figure 6.4 for U_j = 51.8 cm/s, one may be able to see the interaction of some of the vortices in what should be the "annulus field." Near the top of the sheet light there appears to be a break in the asymmetric pattern. This is the result of vortex interaction (this was very clear when one viewed the high speed movies of the flow). Vortex interaction is not expected when the annulus flow provides a stable configuration for the vortices, but

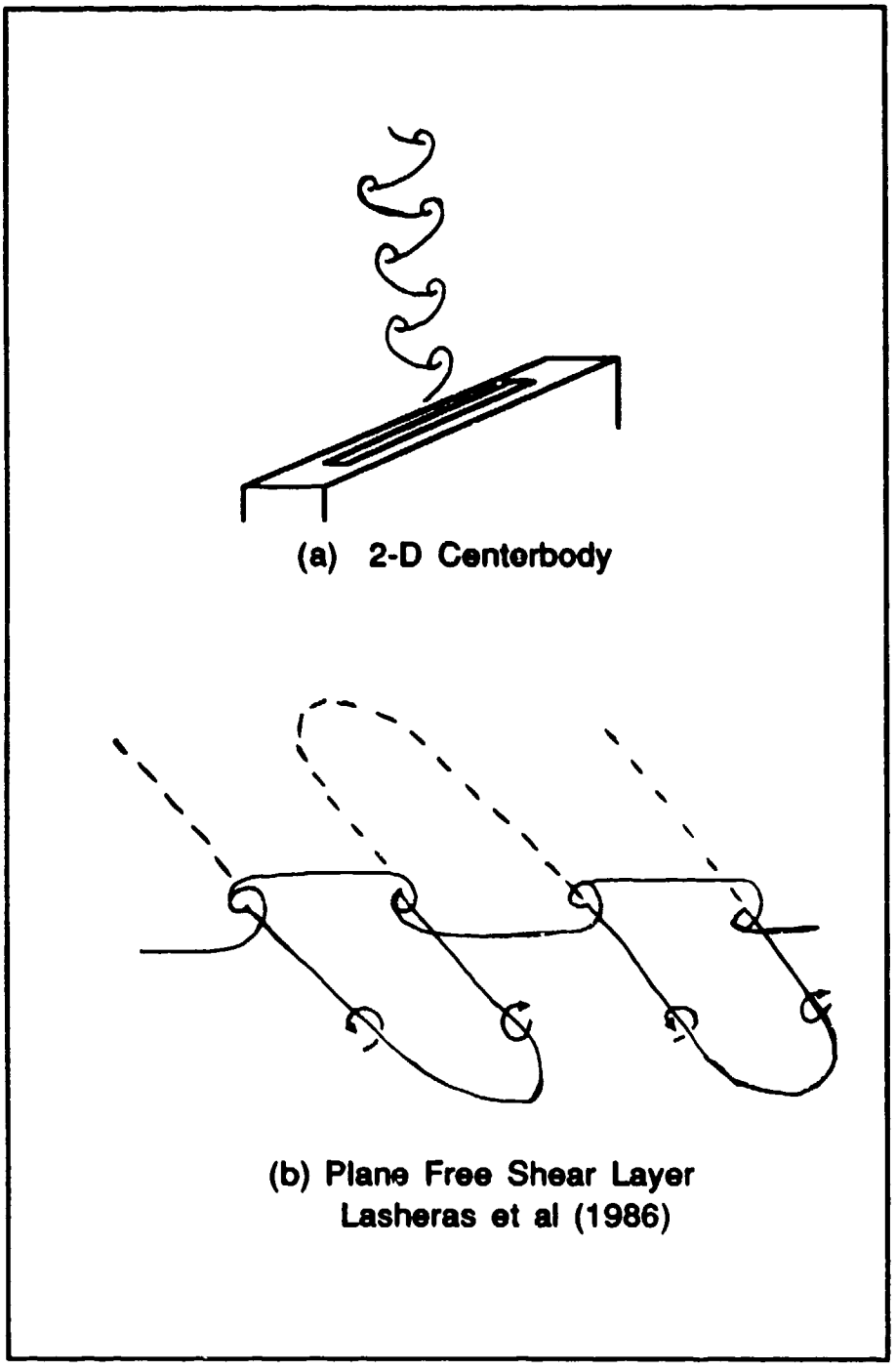

Figure 6.16 Stable Configurations

the jet now has sufficient energy to overcome a large portion of the annulus' influence. The jet's strength has now been able to eliminate, or at least subdue, the "annulus field."

Determination of the approximate point where the "annulus field" disappears was made possible by reanalyzing Mie scattering data of Tankin (1987) for 40.4 cm/s < U_j < 71.8 cm/s. The slight discontinuity in St for U_j = 51.8 cm/s given in Figure 6.14 indicated the change probably occurred between 37.0 and 51.8 cm/s, and Tankin's data covered this range. Figures 6.17(a) through 6.17(e) show the dominant frequencies (at z = 80 mm) in the flow. The peak frequency at each condition is given in Figure 6.18. Vortex shedding frequencies from this investigation are repeated to provide a comparison. Stepwise transitions in frequency indicate a jet flow is dominating the region. This stepwise behavior has been reported for various jet configurations by several authors, most recently Chen and Schmoll (1987). The frequency spectra in Figure 6.17 provide a beautiful example of the competing frequencies in the jet over the range of investigation. The dominant frequency remains dominant for relatively large jet velocity ranges before it eventually is overcome by another frequency. It is also interesting to note that the

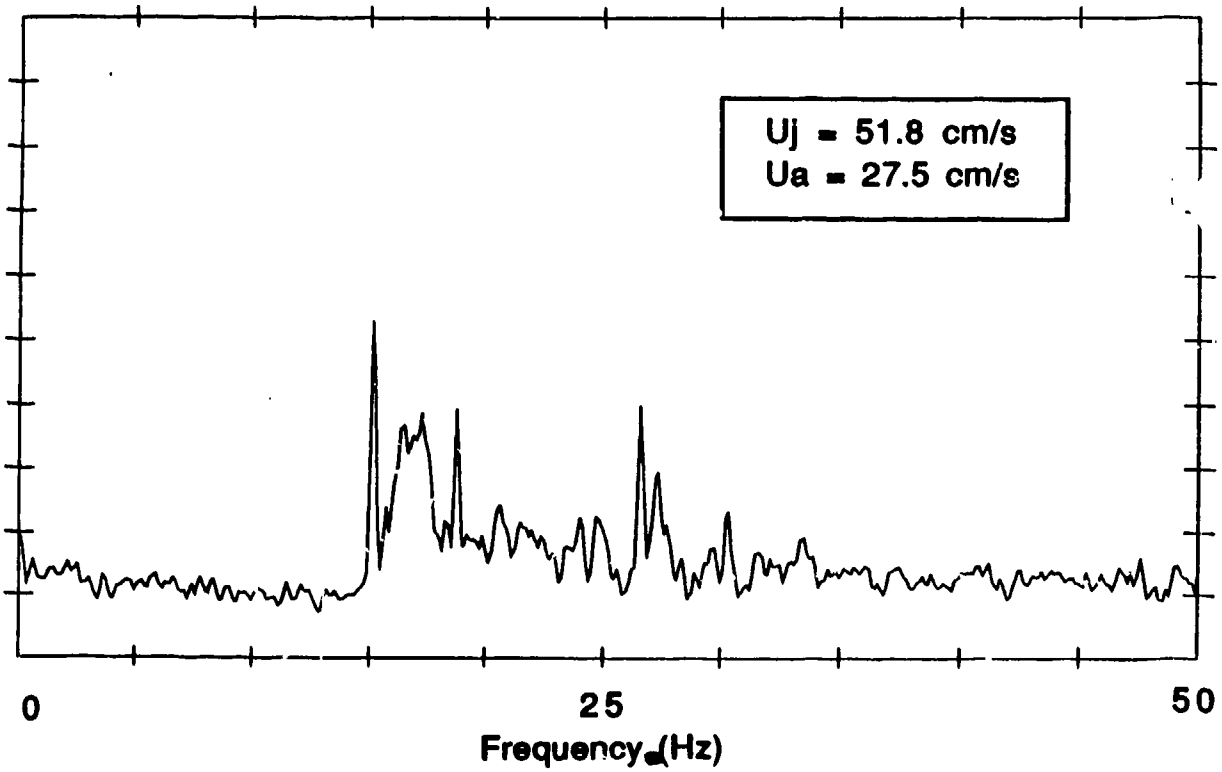

(b)

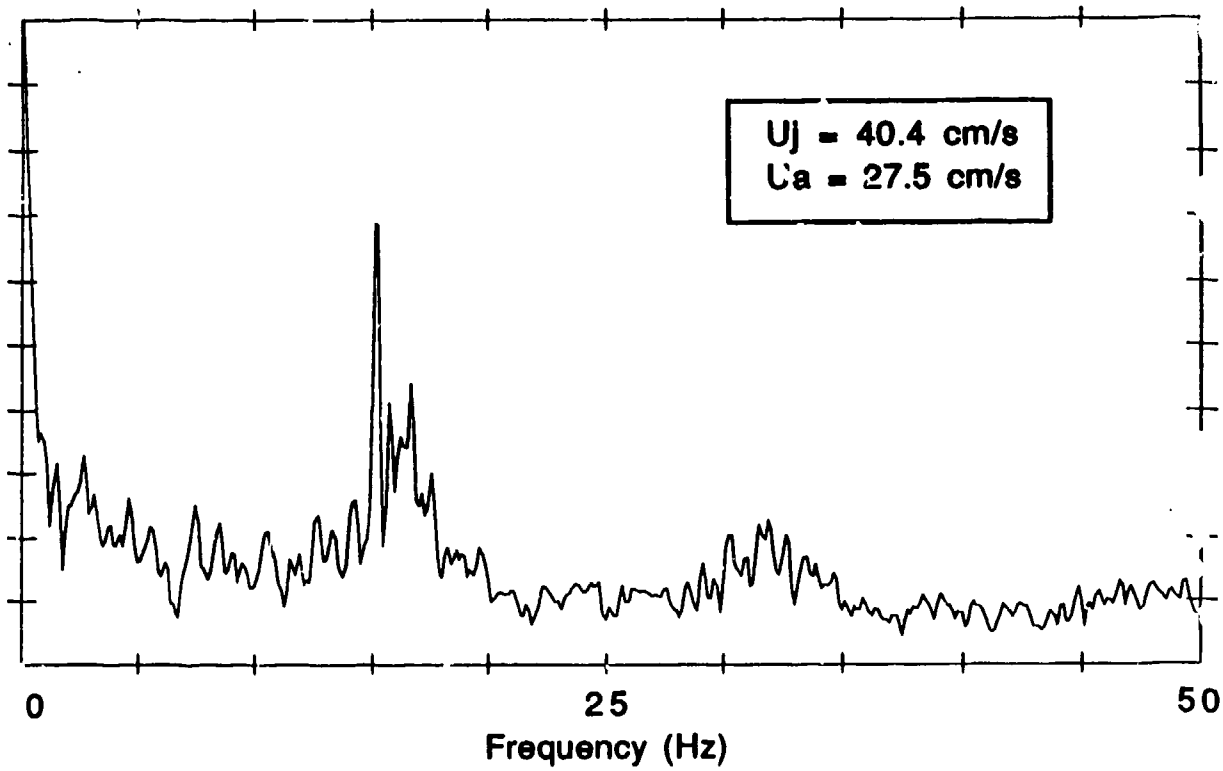

(a)

Figure 6.17 Frequency Spectra from Tankin (1987)

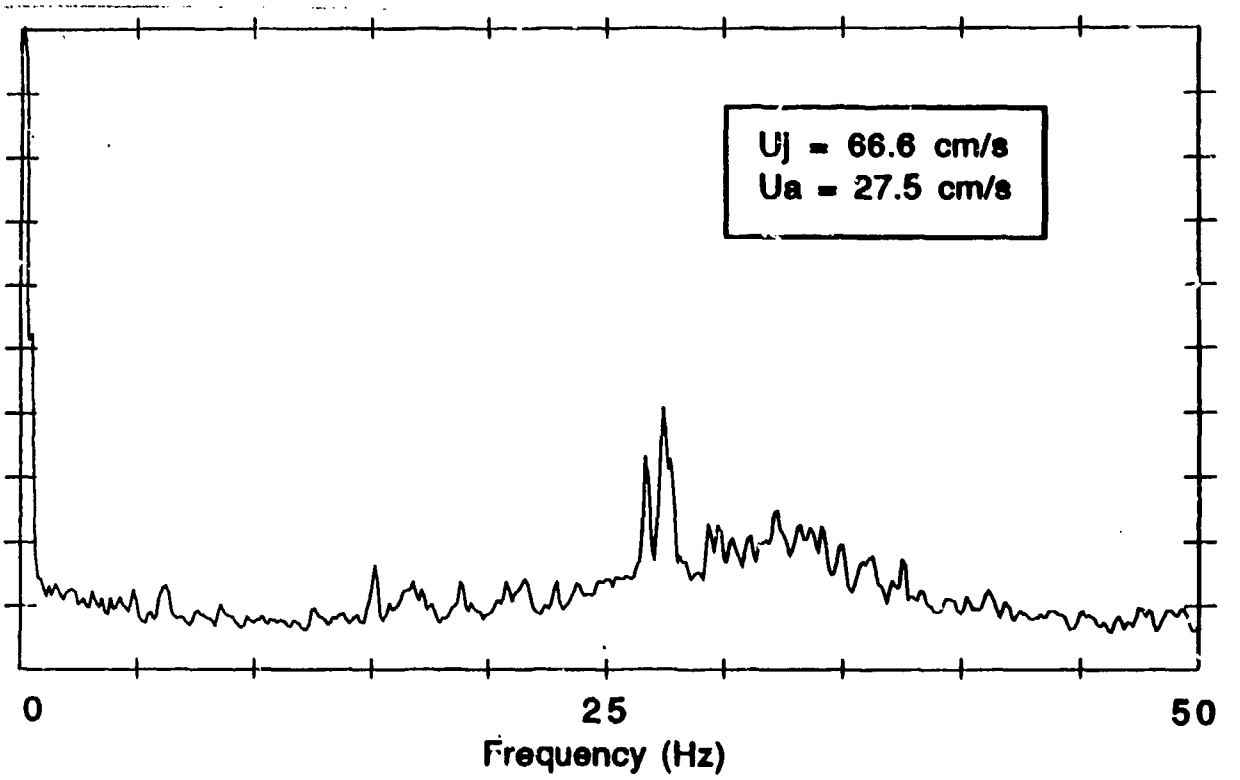

(d)

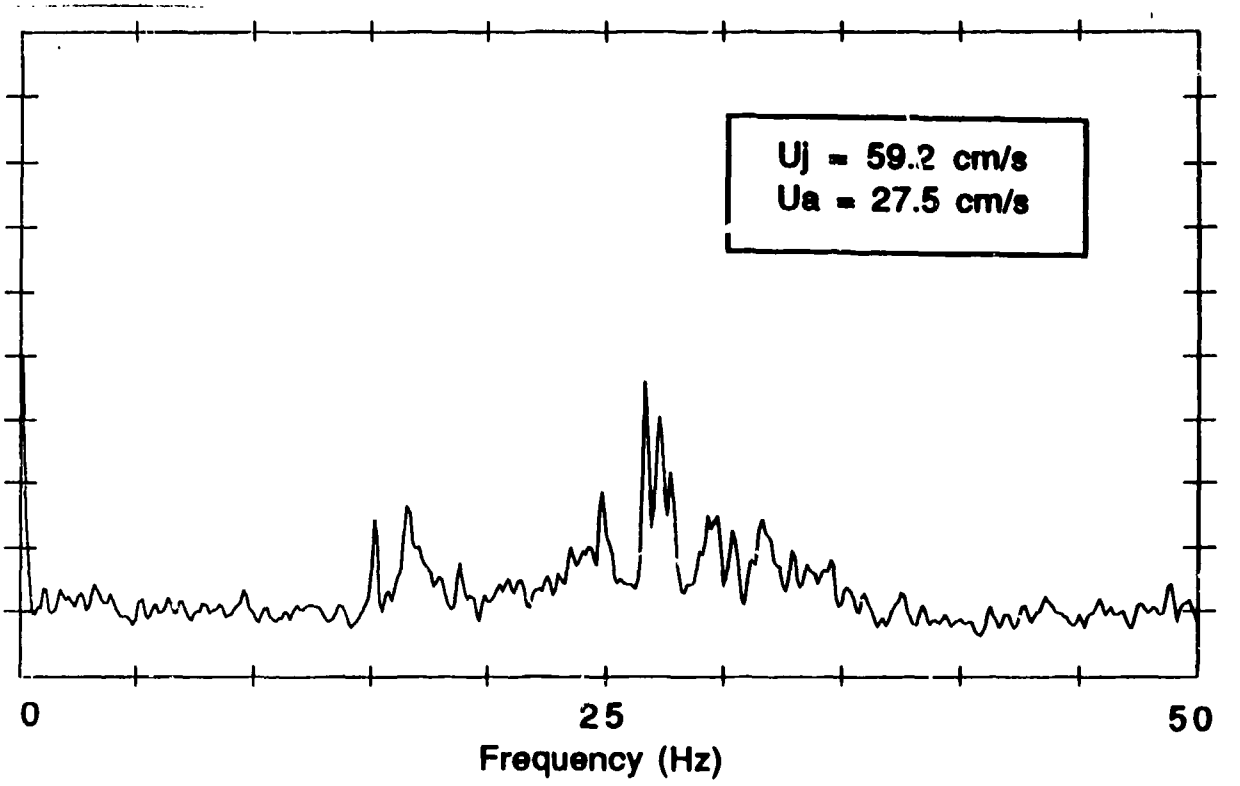

(c)

Figure 6.17 Frequency Spectra from Tankin (1987)

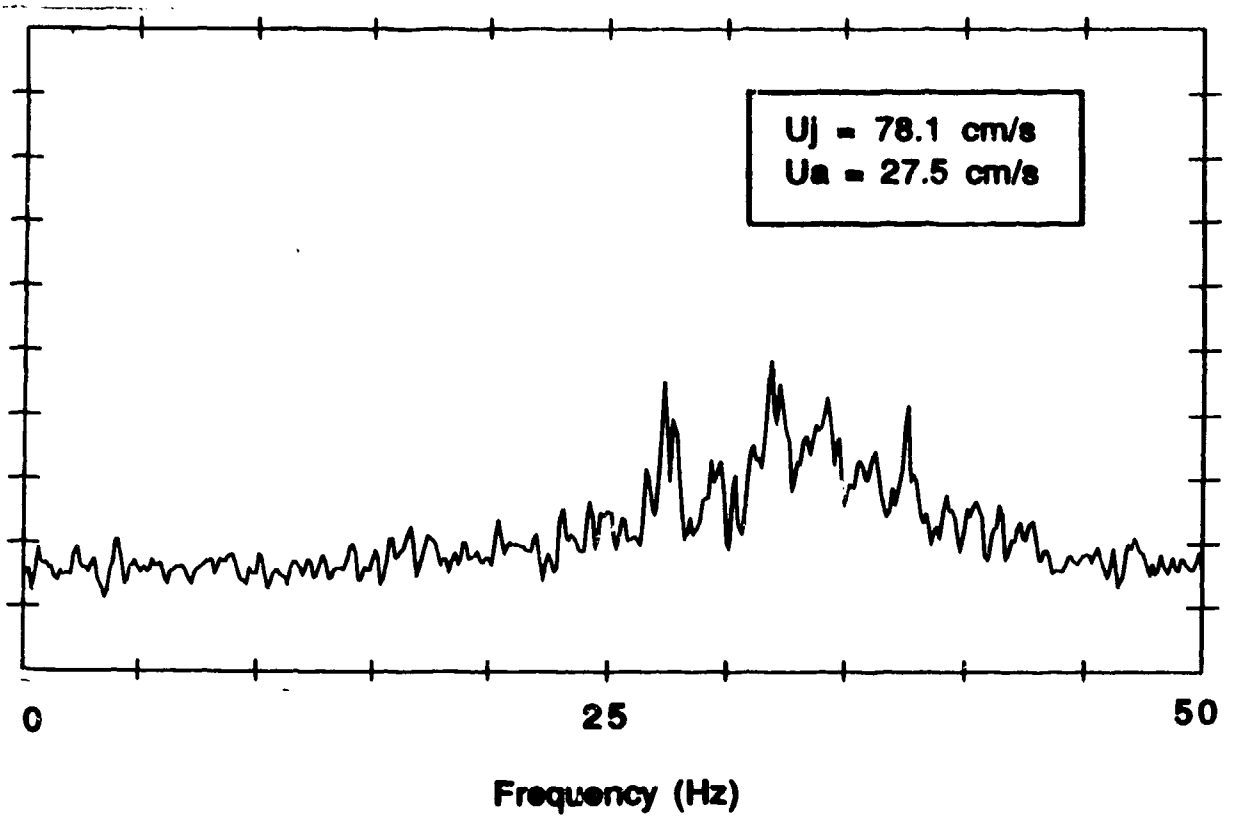

(e)

Figure 6.17 Frequency Spectra from Tankin (1987)

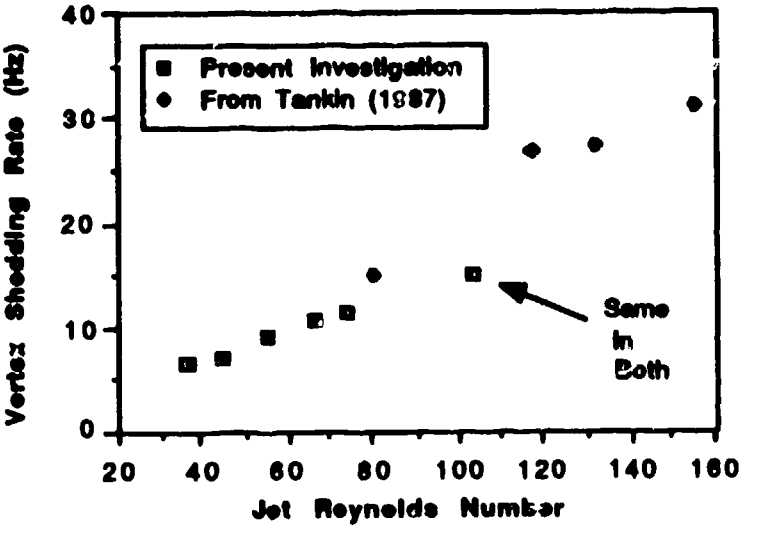

Figure 6.18 Vortex Shedding Rate for the Two-Dimensional Centerbody

frequency which will eventually dominate the flow appears well before it becomes dominant, thus providing a hint of what will soon follow if jet velocity is increased.

At U_j = 37.0 cm/s in the present experiment, the shedding frequency was 12.125 Hz. This condition was also tested by Tankin, and the same result was obtained. At 40.4 cm/s, a significant change in frequency has occurred. Shedding frequency is now 15.125 Hz, a value which remains the peak frequency until 59.2 cm/s. Because of the significant change at 40.4 cm/s, it was assumed that this signified the initiation of the jet's dominance over the entire flowfield. The approximate velocity ratio U_j/U_a at which this dominance is seen is 1.45. Velocity ratios less than this should produce jet and annulus "fields," while ratios greater than 1.45 should result in jet domination. This description does not ignore the influence of the annulus flow; its main point is simply that the "annulus field" has disappeared and lost some measure of its stabilizing strength.

Having completed the description of the flowfield dynamics, how can it be used to explain the observed bifurcations? Viewing Figure 6.4, one can see some patterns which are rather easily explained. At U_j = 18.5 cm/s, we see the strong influence of the annulus flow as it tries to wrap jet fluid around itself, thus forming the large vortex structures which are oriented "up." At U_j = 51.8 cm/s, the

jet fluid wraps ambient fluid around itself and vortices with a "down" orientation are formed. The flow pattern change at U_j = 22.2 cm/s results because of the interaction of the annulus and jet flows when their mean exit velocities are equal. Figure 6.19 shows that there is a difference between theoretical and actual mean velocities. At these low flow rates, it is expected that the flow profile would deviate from the idealized (1-D) case. At U_j = 22.2 cm/s, mean exit velocities for the annulus and jet are equal, and this results in the strange flow pattern. The transverse spread of the jet is very small. It appears like the jet is

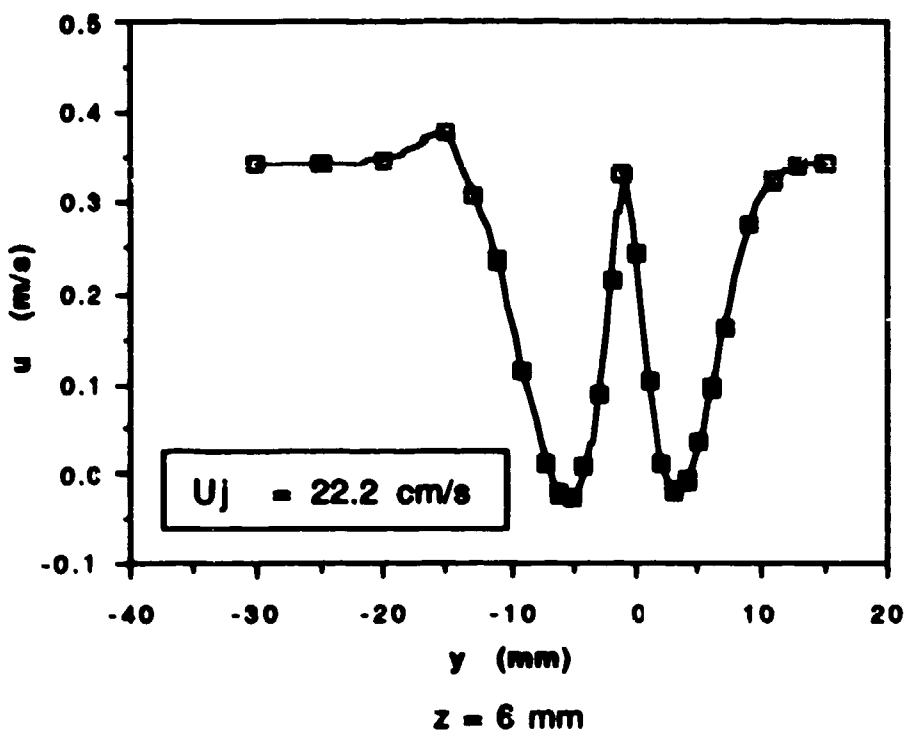

Figure 6.19 Axial Velocity Profile, Transverse Scan

confined to that space directly above the bluff body. The TiO_2 particles seem to act almost like a solid wall meant to separate the two annulus flows. With equal velocities, little entrainment is expected, so the transverse spread of the jet is minimized.

The bifurcation at U_j = 37.0 cm/s is quite interesting. This condition is very close to the point where the "annulus field" disappears. The nearly straight line pattern from Tankin (1987), shown in Figure 4.1(h), is not matched exactly in the present experiment (see Figure 6.4(e)), but the bifurcation can still be described. At this jet velocity, some small disturbances are seen in the form of small white "dots" which should be the beginnings of large-scale structures. These disturbances, however, are very weakly amplified. Inspection of the mean axial velocity profile at z = 60 mm, Figure 6.20, will help explain why this occurs. The flat velocity profile says there is no shear in the "annulus field." Therefore, the disturbance (which results from the jet flow but whose evolution is still governed by the annulus flow) is not amplified. If jet velocity is increased slightly (so U_j/U_a > 1.45), amplification of the disturbance will occur, and the jet flow will dominate the entire flowfield.

The flow pattern change at U_j = 22.2 cm/s is important, but the bifurcation at U_j = 37.0 cm/s is critical. While

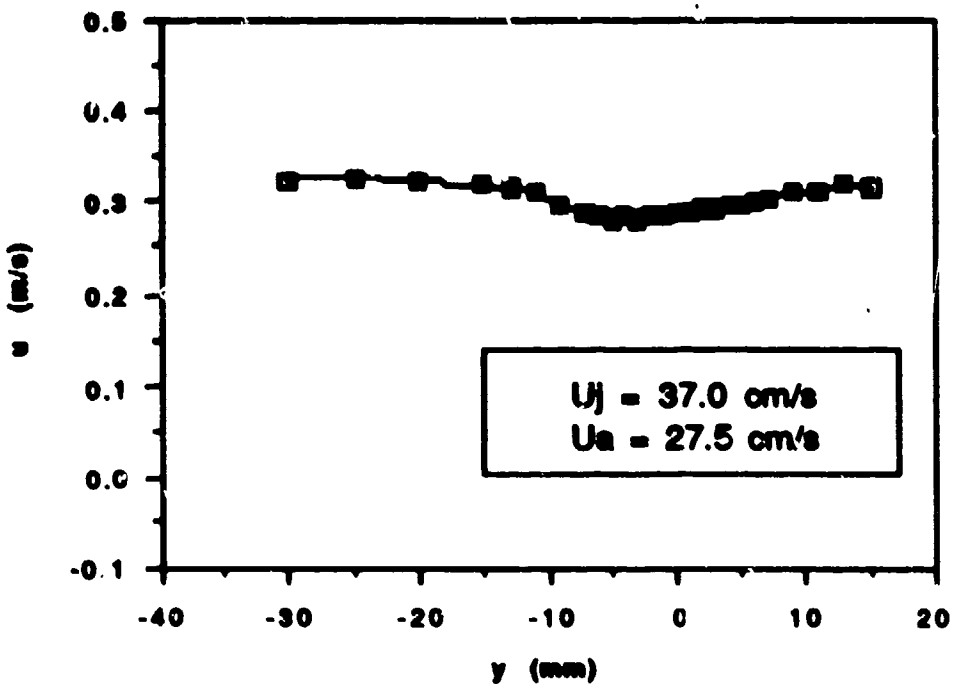

Figure 6.20 Axial Velocity Profile, Transverse Scan
z = 60 mm

the former bifurcation point occurs because of velocity counterposition, the latter represents a point around which the governing factors of the flowfield will change. Up to U_j = 37.0 cm/s, one expects the structures formed in the "jet field" to be carried by the stabilizing annulus flow without much change. Beyond this velocity, however, jet strength is sufficient to subdue the influence of the annulus flow, and a jet-dominated flow results. From the data taken, the flow pattern change at 22.2 cm/s did not reveal a change in the character of the flow similar to the one seen at 37.0 cm/s.

There is one more point which can be addressed. Flow patterns are always asymmetric (i.e., position of the structures alternates from side to side). Two explanations are offered. First, the analogy of an axisymmetric jet which is being squeezed may be used. The flow patterns during a simulated contraction process are shown in Figure 6.21. The vortices in (a) start to get closer and closer as the jet width narrows. At a certain point, (c), the vortices can no longer be brought closer. Since the vortices do not interact (coalesce), they must align themselves as in (d). The geometry, then, would specify whether or not symmetric patterns would be observed. Changing geometries (e.g., slot or bluff body widths) could change the patterns. This simplified analysis does not account for end effects which will play an important role in determining if the vortices can be shed symmetrically.

The second explanation involves a feedback mechanism. According to the description of the flowfield dynamics, the configuration shown in Figure 6.16(a) is stable. This asymmetric pattern will set up an induced pressure field that, even though it is very weak, can affect the flow at the jet exit. Ho and Nosseir (1982) used a jet impinging on a wall to show that resonance was established based on a feedback mechanism. A symmetric vortex shedding is unstable in the "annulus field," so asymmetric patterns are formed which create the induced pressure field that results in

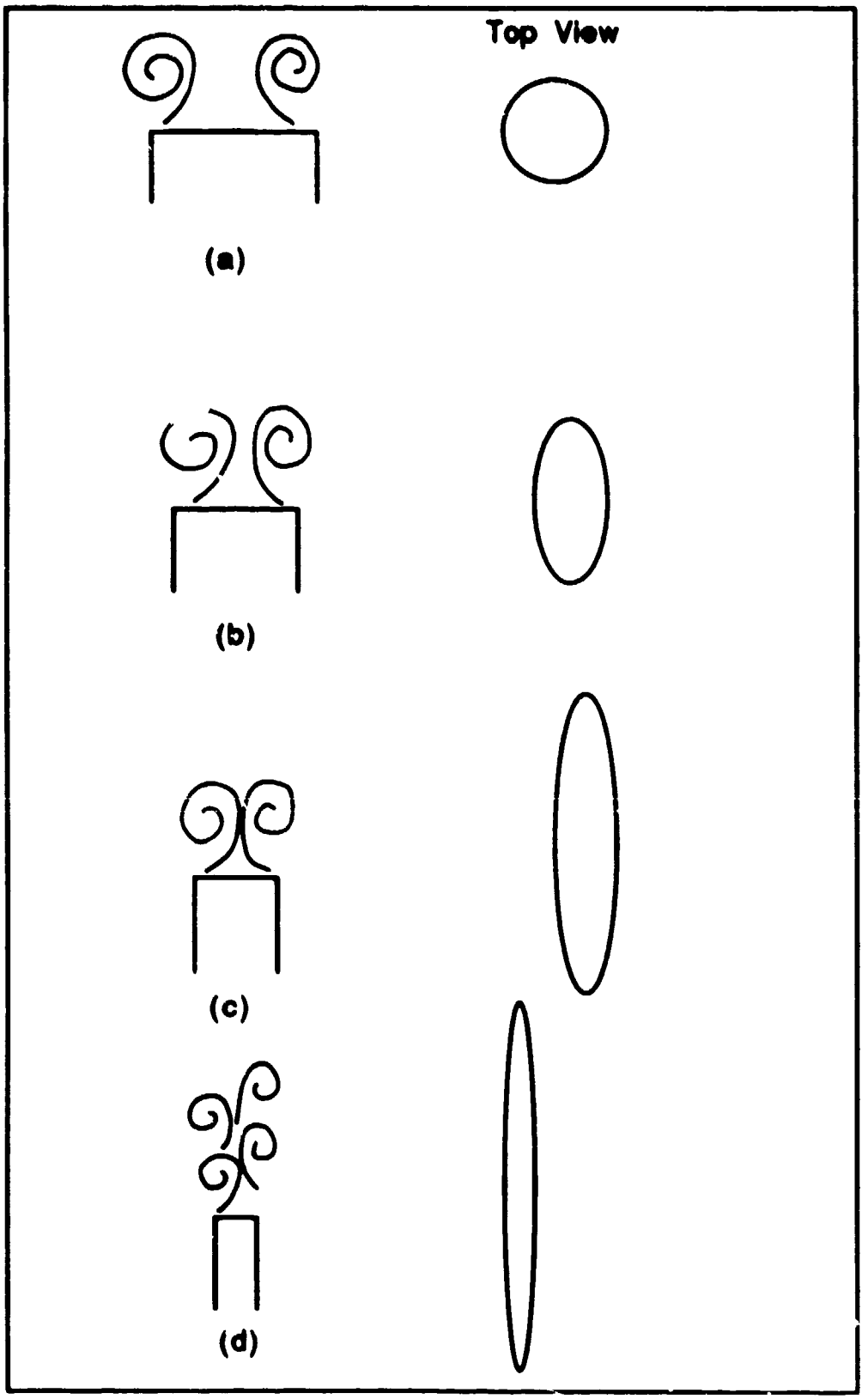

Figure 6.21 Conception of the Reason for Asymmetric Vortex Shedding in a Thin Slot Jet

asymmetric shedding at the jet exit. Strong evidence for the existence of this mechanism in this flow was seen in the Mie scattering experiments. For U_j = 33.3 cm/s, the measurement spot was located in a region (z = 20 mm) where no structures existed, although one could see that the "interface lines" were wavering. The frequency of this wavering, as determined by Mie scattering and shown in Figure 6.22, was 11.375 Hz. This is the same frequency determined when the data were taken in a region where structures did exist (z = 40 mm and z = 60 mm). This provides strong evidence for the existence of a feedback mechanism in the flows under investigation.

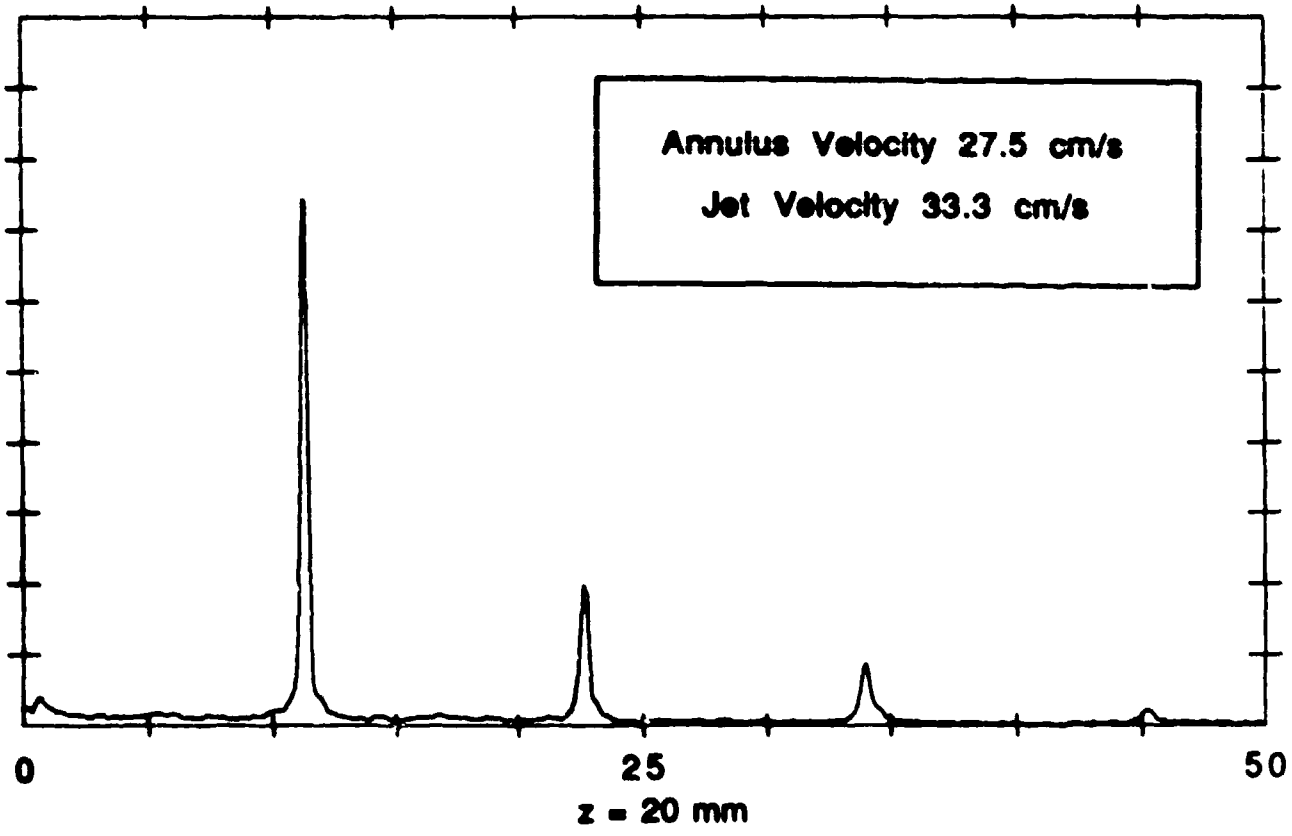

Figure 6.22 Vortex Shedding Frequency

VII. Conclusions and Recommendations

The character of the interaction between bluff body and jet flows has been determined. The concept of jet and annulus "fields" can be used to explain the interactions up to velocity ratios U_j/U_a of 1.45. Beyond this value, the flowfield dynamics are governed by the jet, but the annulus flow cannot be ignored. The jet determines the shedding frequencies of the large-scale structures and governs the flow in the region above the bluff body to z/D of approximately 6 or 7 (i.e., the "jet field"). The "annulus field" is that region above the "jet field" wherein the annulus flow creates a stable vortex configuration and governs the flow's dynamics.

The two observed flow pattern changes, bifurcations, were partially explained. The flow pattern at U_j = 22.2 cm/s resulted from flow conditions where jet and annulus velocities were nearly identical. The bifurcation at U_j = 37.0 cm/s was a critical one since it identified the point above which the "annulus field" has been eliminated. There are many important factors in the interaction of the jet and annulus flows, and flow pattern changes have been partially explained by using various labels. There are still many details of the flowfield which could be uncovered.

Recommendations for further research would be to investigate the interaction at higher velocities (one order

of magnitude at least) to determine if the same description is valid. Redesign of the centerbody should first be accomplished, however. Also, testing should be done in a low turbulence facility to avoid the problems with the annulus turbulence levels.

No point where the annulus flow dominates the entire flowfield was observed in this investigation. The visualizations from Tankin (1987), however, may suggest that there is a point where this does occur. Figure 4.1(a) shows the condition where U_j = 4 cm/s. No structures are seen emanating from the slot. As jet velocity is increased, structures formed at the slot exit become evident. The flow at U_j = 4 cm/s is much like the flow behind a bluff body (so the slot jet only acts as an orifice to provide the seed needed to visualize the flow). Experiments at very low U_j/U_a might provide information concerning the interactions of the annulus and jet flows where the annulus dominates the entire flowfield.

There are many other areas where these results could be applied. In Computational Fluid Dynamics, these incompressible, 2-D flows could be modelled, and those results could be compared with those from this experiment. For this reason all data collected during the LDA measurements are presented in Appendix C. Availability of data for a unique configuration is important, so these data are included in this thesis. Critical point theory

could be applied to further analyze these flowfields. Linear and non-linear instability analyses might provide insight in flow regimes where tractable.

APPENDIX A: DETERMINATION OF $TiCl_4$ CONCENTRATION

Flow visualization used in this experiment has been described in detail (Chen and Roquemore, 1986). Titanium tetrachloride ($TiCl_4$) is introduced to a dry fluid and exhausts as a mixture through the experimental apparatus (jet, etc). When the $TiCl_4$ contacts water vapor (H_2O), titanium dioxide (TiO_2) is formed. This reaction occurs under nearly isothermal conditions, so relatively little energy is lost or gained by the flow. The submicron TiO_2 particles respond to flow variations nearly instantaneously. Reactive flow visualization techniques like the one described above provide important insight to the processes occurring in various flows.

An important question concerning this flow visualization technique had not been answered: "What is the seed concentration?" Density, and more importantly density gradients, are critical factors in jet and wake flows; therefore, the seed concentration must be small so that density gradients are not introduced. A model to determine seed concentration for flow visualization has been developed.

A typical experimental set-up is shown in Figure A-1. Dry air passes through a flow meter and then to a seeding vessel. The seeding vessel is shown in greater detail in Figure A-2. Flow enters and can be bypassed to any degree desired (0-100 percent). Flow enters the container, wherein

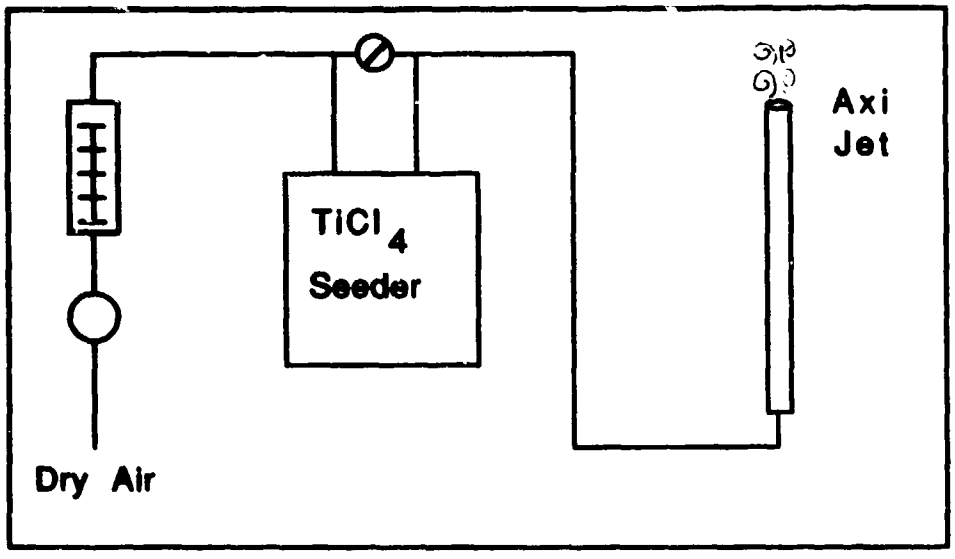

Figure A-1 Flow Visualization Test Arrangement

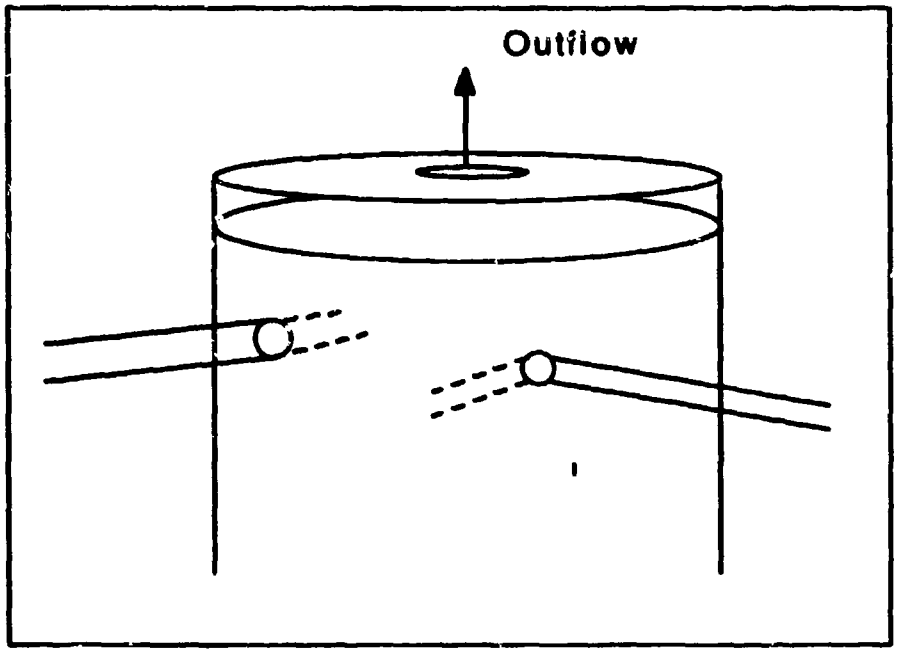

Figure A-2 $TiCl_4$ Seeding Vessel

liquid $TiCl_4$ is stored, through three 1/4 inch lines. Each of these lines has a ball valve so that flow may go through 1, 2, or 3 of the lines. Many different seeders have been built; most give adequate seeding rate with only one input line. This is what was used in this analysis. The lines inside the container are angled at -45 degrees from the horizontal and are canted so the flow leaves nearly parallel to the wall. The design enhances mixing and ensures adequate amounts of $TiCl_4$ get into the flow.

Mass transfer theory can be used to determine the seed concentration. The seeder is designed to get the liquid $TiCl_4$ rotating. This has been observed in a clear plexiglass seeder designed for water vapor uptake. Mass transfer for a laminar rotating disk has been analyzed (Levich, 1962) and was used to model the flow in the seeder. The mass flux from the surface to the fluid is given by

$$j = k\,(c_s - c_o) = .62\, D_{ab}^{2/3}\, \nu^{-1/6}\, \omega^{1/2}\, c_s \qquad (A.1)$$

where c_s is the surface concentration of $TiCl_4$, and c_o is the overall concentration of $TiCl_4$. ω is the angular rate at which the disk rotates (or the angular rate at which the flow passes the liquid surface). D_{ab} is the binary diffusion coefficient. The value of ν, the kinematic viscosity, is taken as that for air. If we assume $c_o/c_s << 1$, we get

$$k = .62\, D_{ab}^{2/3}\, \nu^{-1/6} \omega^{1/2} \qquad (A.2)$$

From a mass balance, we also know that

$$c_o V = A k (c_s - c_o) \tag{A.3}$$

where V is the volumetric flow rate of air, and A is the surface area of the liquid $TiCl_4$. The concentration of $TiCl_4$, in parts per thousand by volume, is thus

$$\frac{c_o}{c_s} = \left(\frac{A k}{V + Ak}\right) 1000 \tag{A.4}$$

In order to determine surface concentration we use

$$c_s = \frac{P_s}{R T} = \frac{P_{vp}}{R T} \tag{A.5}$$

where P_{vp} is the vapor pressure of $TiCl_4$, and R is the universal gas constant. Several methods for determining vapor pressure are available and are summarized by Reid et al (1977). One method was chosen that was simplest for computer application, although it was not designed as such (Reidel, 1954).

$$\ln P_{vp\ r} = A^+ - (B^+/T_r) + C^+ \ln T_r + D^+ T_r^6 \tag{A.6}$$

where the subscript r denotes a reduced property (i.e., one normalized by its appropriate critical property). We have

$$A^+ = -35\ Q \tag{A.7a}$$
$$B^+ = -36\ Q \tag{A.7b}$$
$$C^+ = 42\ Q + \alpha_c \tag{A.7c}$$
$$D^+ = -Q \tag{A.7d}$$

$$Q = .0838\ (3.758 - \alpha_c) \tag{A.8}$$

$$\alpha_c = \frac{0.315\ \psi_b + \ln P_c}{0.0838\ \psi_b - \ln T_{br}} \tag{A.9}$$

$$\psi_b = -35 + (36/T_{br}) + 42 \ln T_{br} - T_{br} \tag{A.10}$$

In order to determine the vapor pressure using equation (A.6), critical properties for $TiCl_4$ must be known. Boiling temperature was also required and was obtained from the Chemical Engineers' Handbook (1973). Critical temperature and pressure of $TiCl_4$ were determined using the method of Lydersen (1955). Critical properties are determined using structural contributions. We have

$$T_c = T_b\ (0.567 + \sum_i (\hat{}t)_i - [\sum_i (\hat{}t)_i^{\ 2}])^{-1} \tag{A.11}$$
$$P_c = M\ [0.34 + \sum_i (\hat{}p)_i^{\ -2}] \tag{A.12}$$

where T_c is in degrees Kelvin, and P_c is in atmospheres. M is the molecular weight, and ^t and ^p are the structural contributions. These values are given in Table A-I for Si and Cl. No data could be found for $TiCl_4$ or Ti, so approximations were made. Due to bonding similarity, use of

Si values should yield acceptable results. The desired answer need not be perfect, so little time was spent searching for a better model.

TABLE A-I Lydersen's Critical Contributions (Lydersen, 1955)

Increments	^t	^p
-- Cl	0.017	0.320
-- Si --	0.03	0.54

Using equations (A.11) and (A.12), one can find the critical properties for $TiCl_4$. The important properties of $TiCl_4$ are listed in Table A-II. Equations (A.6) through (A.10) are now used to determine vapor pressure after a temperature has been specified.

TABLE A-II $TiCl_4$ PROPERTIES

M (gm/mole)	189.71
T_b (°K)	409
T_c (°K)	624
P_c (atm)	40.5

Data for vapor pressure of $TiCl_4$ existed in the Chemical Engineers' Handbook (1973). These data and the model using (A.6) through (A.10) are shown in Figure A-3. A correction to the model was made to better match the data from the

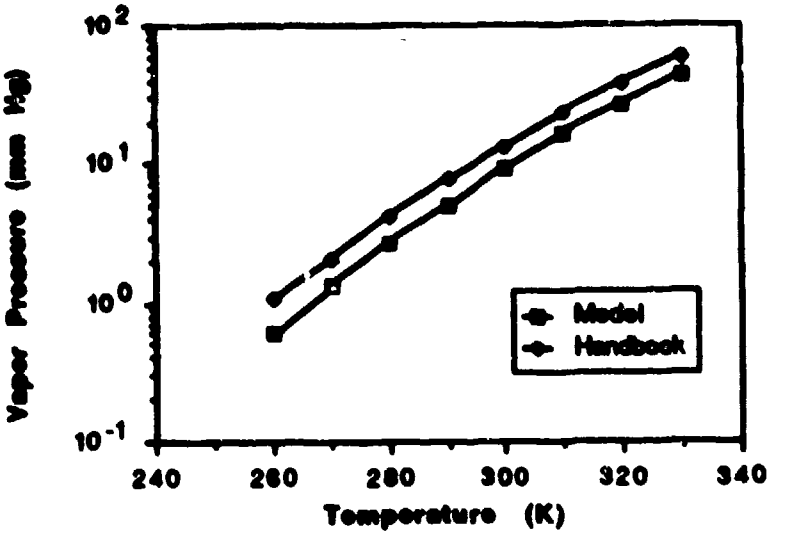

Figure A-3. TiCl4 Vapor Pressure

<u>Chemical Engineers' Handbook</u>. Since vapor pressure models are complex, it was decidedly easier to use the Reidel method and correct it instead of trying to curve fit the existing data. The model, with its correction, is

$$P_{vp} = [1.65 + 0.0046857\ (260 - T)]\ P_{vp\ c} \qquad (A.13)$$

which is valid from 260°K to 330°K. $P_{vp\ c}$ is the vapor pressure calculated with Reidel's method. The greatest error occurs at 260°K and is approximately 4.5 percent. The error quickly decreases with temperature increase and remains nearly constant at 1 percent over the remainder of the valid range.

The next step in determining concentration was to evaluate the diffusion coefficient, D_{ab}. Using the method of Bird et al (1960), we have

$$D_{ab} = .0018583 \frac{\{T^3[(1/M_a)+(1/M_b)]\}^{1/2}}{P\ \sigma_{ab}^2\ \Omega_{Dab}} \quad \left(\frac{cm\text{-}cm}{s}\right) \quad (A.14)$$

where T is temperature in ^oK, P is the pressure in atmospheres, M_a and M_b are molecular weights of the two molecules ($TiCl_4$ and air) in grams per mole, σ_{ab} is the characteristic dimension of the molecules in Angstroms, and Ω_{Dab} is the collision cross section for diffusion (dimensionless). To calculate σ_{ab}, we must use

$$\sigma_{ab} = 0.5\ (\sigma_a + \sigma_b) \quad (A.15)$$

where values of σ are given for various gases by Svehla (1962). For $TiCl_4$, the value of σ was assumed to be that for $SiCl_4$ since no data were available for $TiCl_4$. To calculate Ω, an empirical relation for nonpolar gases given by Neufeld et al (1972) was used.

$$\Omega_D = \frac{A}{T^{*B}} + \frac{C}{\exp(DT^*)} + \frac{E}{\exp(FT^*)} + \frac{G}{\exp(HT^*)} \quad (A.16)$$

where

$$T^* = \frac{k\ T}{\epsilon_{ab}} \quad (A.17)$$

and

$$A = 1.06036$$
$$B = 0.15610$$
$$C = 0.19300$$
$$D = 0.47635$$
$$E = 1.03587$$
$$F = 1.52996$$
$$G = 1.76474$$
$$H = 3.89411$$

k is the well-known Boltzmann constant, and ϵ_{ab} is an intermolecular force constant which is calculated as

$$\epsilon_{ab} = (\epsilon_a \ \epsilon_b)^{1/2} \tag{A.18}$$

Values for ϵ are given by Svehla (1962). Again, the value of ϵ for $TiCl_4$ was assumed the same as that for $SiCl_4$.

In order to calculate the mass transfer coefficient in equation (A.2), we must know the kinematic viscosity of the mixture. Assuming the concentration of $TiCl_4$ is low everywhere except very near the liquid, we need only calculate the kinematic viscosity of air. We know

$$\nu = \mu / \rho \tag{A.19}$$

where

$$\rho = \frac{P}{R\ T} \tag{A.20}$$

To calculate the viscosity, we must use the equation from Bird et al (1960)

$$\mu = 2.6693\times10^{-5} \frac{(M\ T)^{1/2}}{\sigma^2\ \Omega_\mu} \left(\frac{gm}{cm\text{-}s}\right) \qquad (A.21)$$

where M is the molecular weight of air in grams per mole, σ is the characteristic dimension of the air molecule in Angstroms, and Ω_μ is the collision cross section for viscosity. The collision cross section is a slowly varying function (near unity) which indicates how close the molecules under consideration behave like perfectly elastic spheres. To evaluate Ω_μ, we use an empirical relation proposed by Neufeld et al (1972).

$$\Omega_\mu = \frac{A}{T^{*B}} + \frac{C}{\exp(DT^*)} + \frac{E}{\exp(FT^*)} \qquad (A.22)$$

where

$$T^* = \frac{k\ T}{\epsilon} \qquad (A.23)$$

and

A = 1.16145
B = 0.14874
C = 0.52487
D = 0.77320
E = 2.16178
F = 2.43787

σ and ϵ can be obtained from existing data for air (Svehla, 1962).

We may now calculate k, the mass transfer coefficient, if we can evaluate the angular speed ω. An estimate of ω was used.

$$\omega = 0.25\ (v/C) \qquad (A.24)$$

where v is the velocity of air leaving the 1/4 inch line which enters the top of the canister (see Figure A-2), and C is the canister's inside circumference (πd).

One final adjustment must be made because the mass transfer model developed by Levich was valid only for laminar flow. To correct for turbulence, a flat plate analogy was used. Welty et al (1976) have given, for a flat plate,

$$k_{lam} = 0.332\ (D_{ab}/x)\ Re_x^{1/2}\ Sc^{1/3} \qquad (A.25)$$

and

$$k_{turb} = 0.0292\ (D_{ab}/x)\ Re_x^{4/5}\ Sc^{1/3} \qquad (A.26)$$

Forming a ratio, we have

$$\frac{k_{turb}}{k_{lam}} = 0.08795\ (Re_x)^{0.3} \qquad (A.27)$$

This factor varies from unity at Re_x of 3,300 to approximately 5.5 at Re_x of 1,000,000. Assuming the particle travels a distance d, the diameter of the canister, we find

$$Re_x = \frac{v_x\ d}{\nu_{air}} \qquad (A.28)$$

where v_x is the velocity in the canister and is assumed to be 25 percent of the velocity leaving the 1/4 inch inlet line (i.e., 0.25 v).

The equations in this appendix have been put in a computer program, CONCENTRATION, in order to quickly analyze the $TiCl_4$ concentration present in different flows under various conditions. One inputs temperature, pressure, and jet velocity (this specifies volumetric flow rate for the specific test arrangement). Some results are given in Table A-III. The concentration of $TiCl_4$, given in parts per thousand by volume, is small in all instances and can be justifiably ignored as an influence on the flow under study. This general statement is not applicable in flows of very low velocity (< 5 cm/s) and high seeding. Changes in flow patterns have been observed when seeding rates increased to a maximum value at these low velocities. The density and temperature gradients induced by adding the seed have a longer time over which to act, so natural convection can no longer be ignored. In other instances, however, the effect of the seed on the flow development and transport of mass, momentum, and energy can be ignored.

TABLE A-III CONCENTRATION OF $TiCl_4$

AXISYMMETRIC JET (D_e = 1 cm)

TEMP (^oK)	P (atm)	U_e (m/s)	k (cm/s)	C (ppt)
260	1	7.52	1.15	0.18
270	1	7.52	1.17	0.38
280	1	7.52	1.19	0.76
290	1	7.52	1.21	1.43
300	1	7.52	1.23	2.57
310	1	7.52	1.25	4.39
320	1	7.52	1.27	7.19
330	1	7.52	1.28	11.36
260	1	3.05	0.55	0.21
270	1	3.05	0.56	0.45
280	1	3.05	0.57	0.89
290	1	3.05	0.58	1.67
300	1	3.05	0.59	3.00
310	1	3.05	0.60	5.12
320	1	3.05	0.61	8.39
330	1	3.05	0.62	13.25

APPENDIX B: VALIDATION OF THE MIE SCATTERING METHOD

A set of experiments was designed to test the validity of the Mie scattering method (MSM) for determining the shedding frequency of vortex structures in various flows. The peak frequency of velocity fluctuations corresponds to the rate at which vortex structures pass and can provide important information for understanding flow dynamics. For example, vortex pairing has occurred when the frequency of the fluctuating velocity is halved (Chen and Schmoll, 1987). Frequency spectra can be obtained from LDA, hot wire, or hot/cold wire experiments. When LDA is used, seeding rates must be sufficient to ensure that data rates fulfill the Nyquist criterion (i.e., the data rate must be at least twice the highest frequency component one is trying to measure). This must be done to avoid losing any frequency higher than the Nyquist frequency (half the sampling rate) and avoid having the undersampled high frequencies show up as spurious low frequencies, a phenomenon known as aliasing (Malmstadt et al, 1981). As discussed in Section 4, seeding problems arise if flow rates are extremely low, such as those in the present study. Data rates are often too low to provide spectral information. The MSM could provide a viable way of determining important shedding frequencies. The method was never previously validated, so a set of experiments was designed to check its validity. Previous

use of the MSM for determining shedding frequencies was inconclusive because many frequencies often resulted from the Fourier analyses. Complex signals made it impossible to interpret the results in a satisfactory manner. If one could fix the vortex shedding frequency at a given value, the MSM could be used, and the results should be much easier to interpret.

An axisymmetric jet configuration was used to test the Mie scattering method. The test set-up is shown in Figures B-1 and B-2. A facility for diagnostic testing was being established by the project sponsor, and this is where the validation took place. The flow system used dry air brought through a flow meter (Fisher Porter model using Tube No. 85-27-10/77), through a seeder, and then through a 1 meter tube. Nozzle exit diameter was 1 centimeter. Acoustic forcing was used in this experiment in order to "drive" the flow. A sinusoidal input, one whose frequency and amplitude could be varied, is provided to the speaker. The acoustic wave is transmitted to the flow through a thin rubber membrane (part of a surgeons glove) which is placed over the line that fits into the bottom of the tee which is located at the bottom of the 1 meter tube. Flexible tubing was inserted in the inner horn of the speaker and led to the bottom of the tee fitting. The glove is used to protect the speaker and other equipment from potential contamination

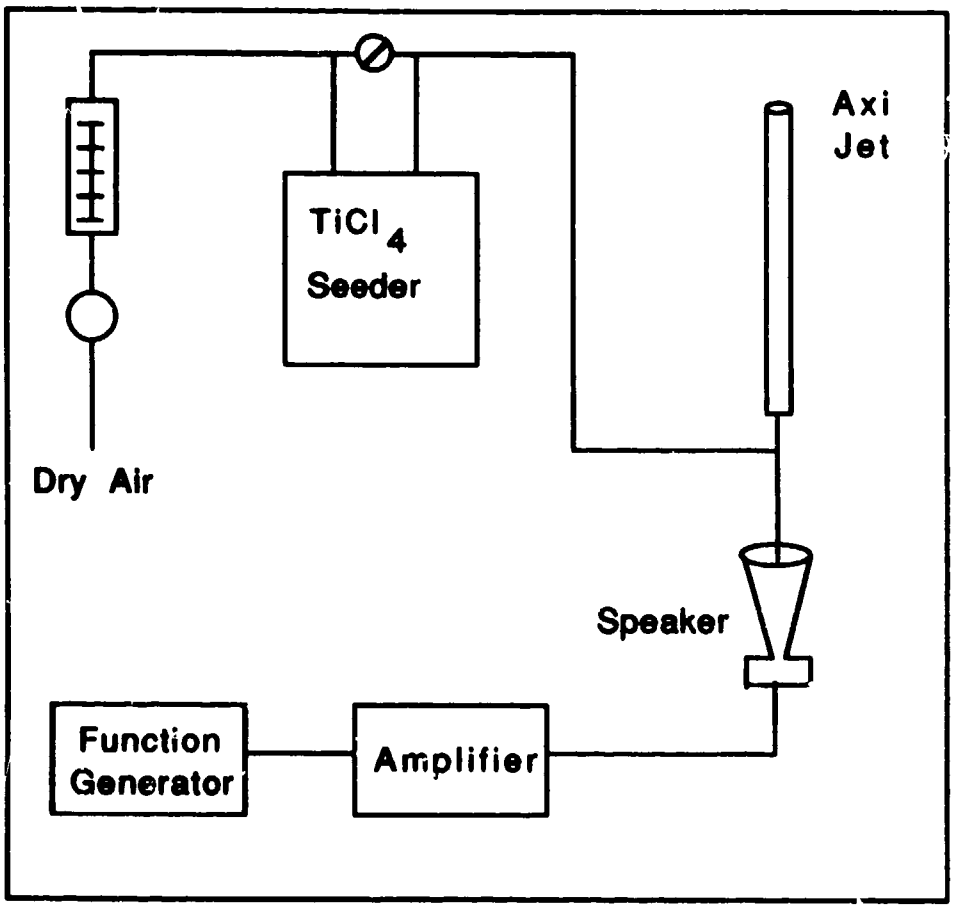

Figure B-1 Flow System for Mie Scattering Method Validation

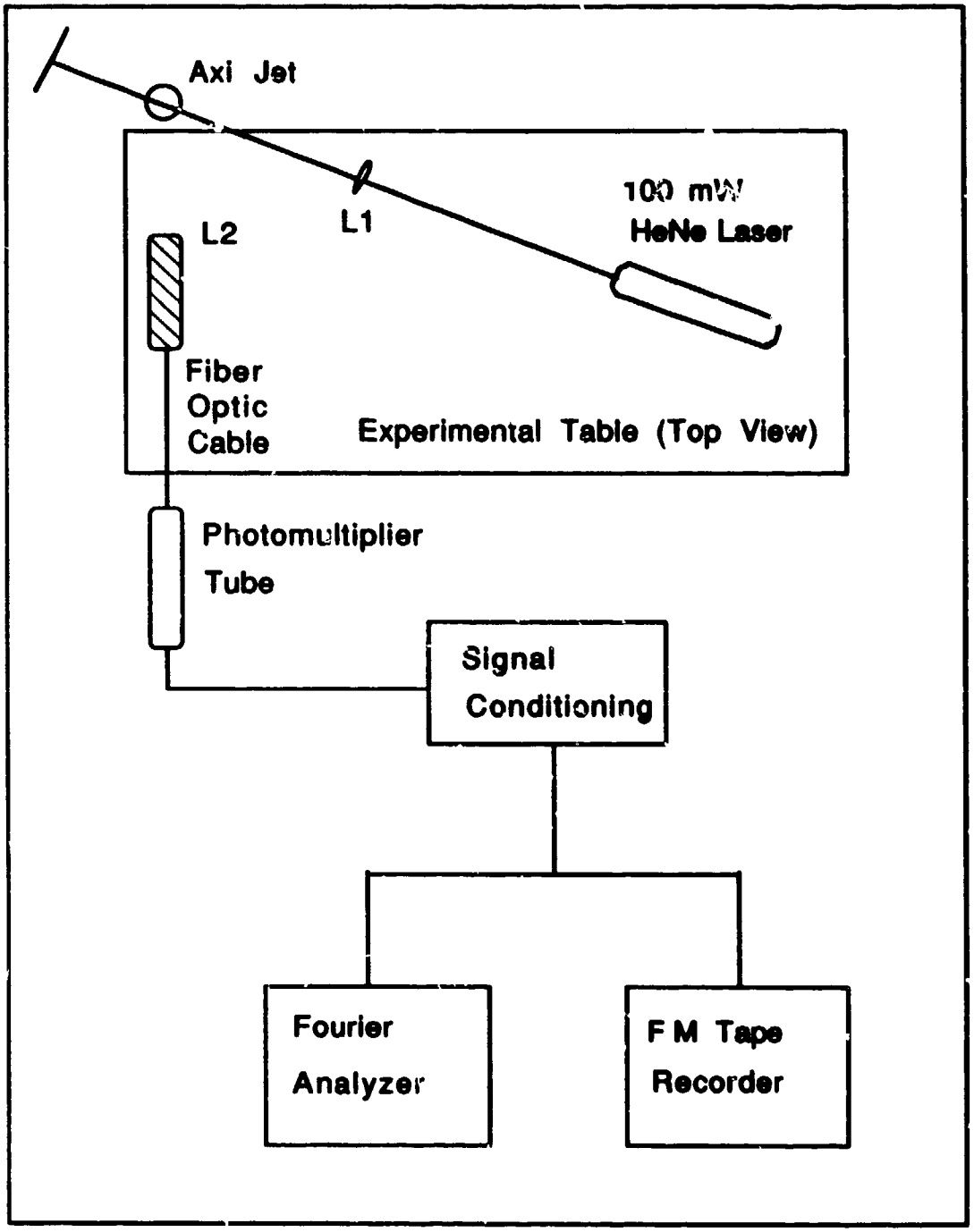

Figure B-2 Optical Arrangement for Mie Scattering Method Validation

from the HCl which is formed in the reaction of the $TiCl_4$. The optical arrangement is the same as the one described in Section 2.

A variable speed strobe was used to "freeze" the motion of the jet. This visualization technique helps identify the structures' shedding frequencies. A strobe and the MSM were used to determine the natural (i.e., unforced) shedding frequency of the jet shown in Figure B-1 with velocity 4 m/s. The facility used did not allow for the elimination of outside disturbances, so the presence of several different frequencies was expected. It was difficult to exactly "freeze" the jet motion using the strobe, and the Fourier transform of the light scattering signal, shown in Figure B-3, did contain several frequencies. The flow appeared closest to being frozen by the strobe at approximately 365 Hz. The value of 365 Hz is not seen exactly in Figure B-3, but the two strongest peaks surround that value. The peak at 437.5 Hz may result from external disturbances or the jet may be nearing a flow condition where transition to a higher shedding rate will take place. The frequency is certainly not negligible, but the MSM cannot tell the source of the various instabilities. This must be left to the investigator.

Acoustic forcing was then used to raise the level of the natural instability, assumed to be 365 Hz, well above

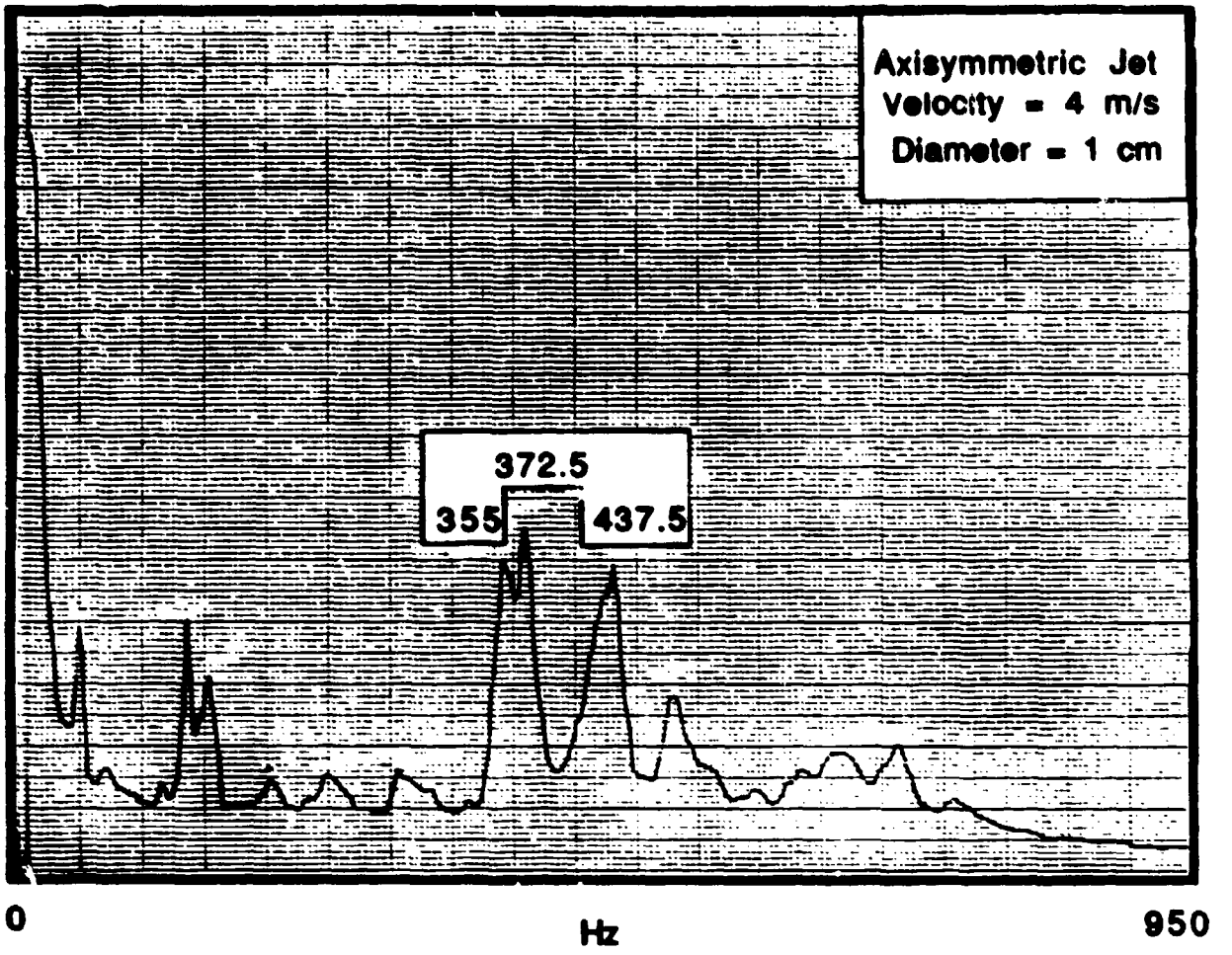

Figure B-3. Natural Jet Vortex Shedding Frequency Spectrum

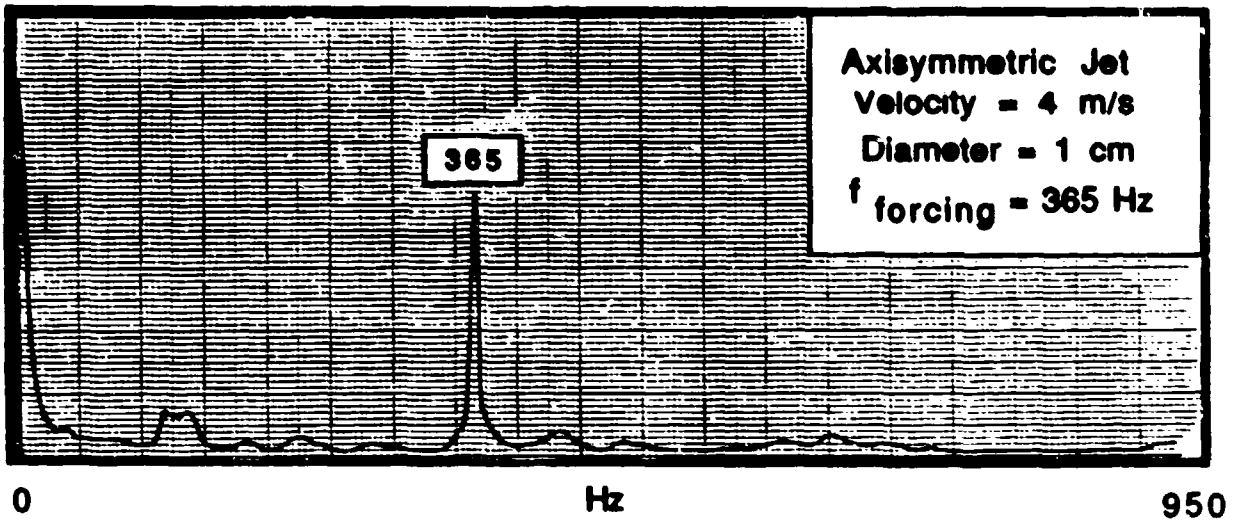

Figure B-4. Forced Jet Frequency Spectrum

the background noise and external disturbances. This is exactly what Crow and Champagne (1971) did in their classic experiment. If the MSM is unambiguous, only one frequency should be evident. If not, perhaps the additional frequencies would become clear. For example, one might speculate that both vortex size and spacing would yield frequencies when spectral analysis was performed. If two frequencies result when the jet is forced, one could measure vortex size and spacing and, with the velocity, see how close this is to the observed result.

Figure B-4 shows the frequency spectrum when the jet is forced at its natural frequency. Only one component of frequency exists, and it is the shedding frequency of the large scale structures. This fact was verified using the strobe (which was synchronized with the oscillator). Note the scales on the y-axes of Figures B-3 and B-4. Although the vertical scales in the two figures display arbitrary units, the scales may be compared against one another. The natural jet spectrum must be multiplied by a factor of 8 to achieve the levels shown, while the forced jet has a factor of only 2. Thus, forcing has effectively eliminated the background. These experiments prove the MSM is a useful tool in obtaining the shedding frequencies for the vortex structures in different flowfields.

APPENDIX C: LDA DATA SUMMARY

1. RUN SUMMARY OF THE 6 FLOW CONDITIONS IN THE PRESENT STUDY

2. DATA FOR ALL RUNS
   - SET UP AS 2 ROWS OF INFORMATION FOR EACH DATA POINT
   - SET UP IS AS FOLLOWS

X	Y	Z	u	v	u_{rms}	v_{rms}	$(\overline{u'v'})_n$
S_u	K_u	S_v	K_v	0	0	0	$(T.K.E.)_n$

u - Mean axial velocity

v - Mean transverse (radial) velocity

u_{rms} - Root mean square of fluctuating axial velocity

u_{rms} - Root mean square of fluctuating transverse velocity

$(\overline{u'v'})_n$ - Normalized Reynold stresses

S_u - Skewness of u

K_u - Kurtosis of u

S_v - Skewness of v

K_v - Kurtosis of v

$(T.K.E.)_n$ - Normalized turbulent kinetic energy

Table C-I LDA Run Summary

U_a (cm/s)	U_j (cm/s)	z (mm)	RUN SEQUENCE	DATA QUALITY
27.5	18.5	6	9029-9054	GOOD
		10	9055-9080	GOOD
		20	9081-9106	GOOD
		40	9107-9132	GOOD
		60	9133-9158	GOOD
	22.2	6	9159-9184	GOOD
		10	9185-9210	GOOD
		20	9211-9236	GOOD
		40	9237-9262	GOOD
		60	9263-9288	GOOD
	27.8	6	8924-8949	GOOD
		10	8898-8923	GOOD
		20	8950-8975	GOOD
		40	8976-9001	GOOD
		60	9002-9028	GOOD
	33.3	6	9289-9314	GOOD
		10	9315-9340	GOOD
		20	9341-9366	EXCELLENT
		40	9367-9392	EXCELLENT
		60	9393-9419	EXCELLENT
	37.0	6	9420-9445	EXCELLENT
		10	8798-8823	GOOD
		20	8824-8844	GOOD
		40	8845-8871	GOOD
		60	8872-8897	GOOD
	51.8	10	9446-9471	EXCELLENT
		20	9472-9497	EXCELLENT
		60	9502-9527	EXCELLENT
		120	9530-9551	EXCELLENT

Plot Number: [illegible]

-0.005	-[illegible]	5.995	0.543	0.040	0.1784E+00	0.2235E+00	-0.4730E-02
-0.004	[illegible]	0.000	4.405	0.000	0.0000E+00	0.0000E+00	0.2022E+00
-0.005	-24.995	5.995	0.543	0.043	0.1670E+00	0.2233E+00	0.2442E-01
0.004	2.936	0.079	4.113	0.000	0.0000E+00	0.0000E+00	0.1935E+00
-0.005	-19.995	5.995	0.339	0.044	0.1637E+00	0.2060E+00	-0.1411E-01
0.017	2.951	0.050	3.995	0.000	0.0000E+00	0.0000E+00	0.1575E+00
-0.005	-14.995	5.995	0.334	0.050	0.1535E+00	0.2027E+00	-0.7375E-02
0.025	2.819	0.073	3.951	0.000	0.0000E+00	0.0000E+00	0.1305E+00
-0.005	-13.005	5.995	0.303	0.044	0.1576E+00	0.1924E+00	-0.1119E-01
0.050	2.757	0.021	3.719	0.000	0.0000E+00	0.0000E+00	0.1734E+00
-0.005	-11.010	5.995	0.227	0.046	0.1563E+00	0.1865E+00	0.6471E-02
0.040	2.944	0.112	3.413	0.000	0.0000E+00	0.0000E+00	0.1732E+00
-0.005	-9.990	5.995	0.105	0.039	0.1631E+00	0.2093E+00	-0.3453E-02
0.012	3.034	0.126	4.053	0.000	0.0000E+00	0.0000E+00	0.1376E+00
-0.005	-6.990	5.995	0.013	0.025	0.1665E+00	0.2145E+00	-0.3990E-02
-0.010	2.967	0.236	4.217	0.000	0.0000E+00	0.0000E+00	0.1942E+00
-0.005	-4.000	5.995	-0.010	0.023	0.1645E+00	0.2066E+00	0.4315E-02
0.059	3.221	0.057	4.292	0.000	0.0000E+00	0.0000E+00	0.1655E+00
-0.005	-3.010	5.995	-0.024	0.015	0.1655E+00	0.2021E+00	0.1771E-01
-0.027	2.925	0.153	4.059	0.000	0.0000E+00	0.0000E+00	0.1[illegible]75E-00
-0.005	-4.005	5.995	-0.004	0.015	0.1731E+00	0.2080E+00	0.1655E-01
0.017	3.457	0.051	4.021	0.000	0.0000E+00	0.0000E+00	0.1913E+00
-0.005	-2.000	5.995	0.054	0.019	0.1745E+00	0.1973E+00	0.4344E-02
0.057	3.120	0.107	4.003	0.000	0.0000E+00	0.0000E+00	0.1[illegible]5E+00
-0.005	-0.005	5.995	0.159	0.032	0.2172E+00	0.2003E+00	0.1773E-01
0.245	2.581	0.104	4.104	0.000	0.0000E+00	0.0000E+00	0.2042E+00
-0.005	-1.005	5.995	0.297	0.040	0.2801E+00	0.2149E+00	0.5515E-01
0.255	2.511	0.251	4.327	0.000	0.0000E+00	0.0000E+00	0.2445E+00
-0.005	-0.010	5.995	0.203	0.040	0.2144E+00	0.2126E+00	0.7534E-02
0.175	3.217	0.259	4.375	0.000	0.0000E+00	0.0000E+00	0.2159E+00
-0.005	1.015	5.995	0.069	0.024	0.1797E+00	0.2121E+00	0.1037E-01
-0.017	3.454	-0.027	3.943	0.000	0.0000E+00	0.0000E+00	0.1956E+00
-0.005	2.005	5.995	-0.007	0.023	0.1753E+00	0.2160E+00	0.2045E-01
0.035	3.170	0.159	3.239	0.000	0.0000E+00	0.0000E+00	0.1957E+00
-0.005	2.995	5.995	-0.010	0.014	0.1622E+00	0.2014E+00	0.1025E-01
0.025	2.932	0.061	4.032	0.000	0.0000E+00	0.0000E+00	0.1929E+00
-0.005	4.000	5.995	0.004	0.021	0.1600E+00	0.1961E+00	0.5301E-01
0.050	2.994	0.065	3.330	0.000	0.0000E+00	0.0000E+00	0.1790E+00
0.000	5.005	5.995	0.039	0.004	0.1640E+00	0.2017E+00	0.1525E-01
0.026	2.745	-0.025	3.740	0.000	0.0000E+00	0.0000E+00	0.1833E+00
0.000	5.995	5.995	0.093	-0.009	0.1673E+00	0.2075E+00	-0.5323E-01
-0.029	2.935	0.095	3.890	0.000	0.0000E+00	0.0000E+00	0.1335E+00
0.000	6.995	5.995	0.165	-0.004	0.1672E+00	0.2127E+00	-0.1115E-01
0.020	2.978	-0.025	4.392	0.000	0.0000E+00	0.0000E+00	0.1913E+00
0.000	9.015	5.995	0.274	-0.015	0.1606E+00	0.1960E+00	-0.4339E-03
0.027	2.937	0.153	3.581	0.000	0.0000E+00	0.0000E+00	0.1792E+00
0.000	11.005	5.995	0.320	-0.021	0.1509E+00	0.1905E+00	0.1434E-01
-0.061	2.735	0.046	3.633	0.000	0.0000E+00	0.0000E+00	0.1719E+00
0.000	13.010	5.995	0.333	-0.016	0.1543E+00	0.2024E+00	-0.4957E-02
-0.008	2.630	0.195	4.227	0.000	0.0000E+00	0.0000E+00	0.1303E+00
0.000	14.990	5.995	0.339	-0.014	0.1591E+00	0.2010E+00	-0.9435E-02
0.046	2.994	-0.003	3.552	0.000	0.0000E+00	0.0000E+00	0.1313E+00

FILE NAME: 6J9D55AU

θ	2θ						
0.000	-29.990	9.995	0.333	0.041	0.1500E+00	0.2017E+00	0.1534E-02
-0.028	2.600	0.051	3.837	0.000	0.0000E+00	0.0000E+00	0.1777E+00
0.000	-23.000	9.995	0.345	0.053	0.1508E+00	0.1977E+00	0.3972E-02
0.040	2.988	0.012	3.934	0.000	0.0000E+00	0.0000E+00	0.1758E+00
0.000	-17.995	9.995	0.343	0.054	0.1531E+00	0.1966E+00	0.3759E-02
-0.017	2.832	-0.023	3.807	0.000	0.0000E+00	0.0000E+00	0.1752E+00
0.000	-14.990	9.995	0.332	0.059	0.1538E+00	0.1955E+00	0.1502E-01
-0.043	3.047	-0.032	4.072	0.000	0.0000E+00	0.0000E+00	0.1739E+00
0.000	-13.005	9.995	0.307	0.063	0.1557E+00	0.1929E+00	-0.2410E-01
0.028	2.995	0.117	4.253	0.000	0.0000E+00	0.0000E+00	0.1733E+00
0.000	-11.000	9.995	0.334	0.053	0.1547E+00	0.1913E+00	0.1153E-01
-0.037	2.918	-0.011	3.697	0.000	0.0000E+00	0.0000E+00	0.1742E+00
0.000	-9.000	9.995	0.123	0.047	0.1595E+00	0.1868E+00	0.6019E-02
0.000	2.896	0.044	3.692	0.000	0.0000E+00	0.0000E+00	0.1741E+00
0.000	-7.010	9.995	0.029	0.031	0.1609E+00	0.2006E+00	0.1636E-01
0.067	3.126	-0.049	4.214	0.000	0.0000E+00	0.0000E+00	0.1718E+00
0.000	-6.005	9.995	-0.001	0.033	0.1548E+00	0.2023E+00	-0.2400E-01
0.035	2.957	0.067	3.652	0.000	0.0000E+00	0.0000E+00	0.1801E+00
0.000	-5.005	9.995	0.005	0.018	0.1623E+00	0.1999E+00	0.2333E-03
-0.021	3.176	0.116	3.587	0.000	0.0000E+00	0.0000E+00	0.1821E+00
0.000	-4.005	9.995	0.056	0.006	0.1635E+00	0.1963E+00	-0.5337E-01
-0.027	2.892	0.035	3.841	0.000	0.0000E+00	0.0000E+00	0.1835E+00
0.005	-3.000	9.995	0.116	-0.002	0.1625E+00	0.1933E+00	-0.4396E-01
0.023	2.944	-0.011	3.761	0.000	0.0000E+00	0.0000E+00	0.1859E+00
0.005	-2.005	9.995	0.165	0.006	0.1536E+00	0.1951E+00	-0.4733E-01
-0.010	2.741	0.052	3.907	0.000	0.0000E+00	0.0000E+00	0.1759E+00
0.005	-1.005	9.995	0.135	0.018	0.1521E+00	0.1903E+00	0.1674E-01
0.057	2.943	-0.022	3.816	0.000	0.0000E+00	0.0000E+00	0.1725E+00
0.005	-0.005	9.995	0.153	0.030	0.1592E+00	0.1876E+00	0.2952E-01
0.008	2.349	0.023	3.451	0.000	0.0000E+00	0.0000E+00	0.1740E+00
0.000	0.995	9.995	0.045	0.034	0.1596E+00	0.1841E+00	0.7945E-01
0.072	2.555	0.040	4.071	0.000	0.0000E+00	0.0000E+00	0.1777E+00
0.005	1.995	9.995	0.043	0.049	0.1554E+00	0.1826E+00	0.2939E-01
-0.004	2.737	0.050	3.773	0.000	0.0000E+00	0.0000E+00	0.1750E+00
0.005	3.010	9.995	0.005	0.014	0.1549E+00	0.1934E+00	0.1016E-02
0.044	2.787	0.062	3.909	0.000	0.0000E+00	0.0000E+00	0.1752E+00
0.005	3.995	9.995	0.021	0.001	0.1515E+00	0.1898E+00	-0.1439E-01
-0.033	3.051	-0.097	3.595	0.000	0.0000E+00	0.0000E+00	0.1751E+00
0.005	5.000	9.995	0.072	-0.001	0.1562E+00	0.1859E+00	0.1596E-01
0.094	3.072	0.097	3.612	0.000	0.0000E+00	0.0000E+00	0.1717E+00
0.000	5.995	9.995	0.131	-0.011	0.1549E+00	0.1923E+00	0.3373E-02
0.062	2.911	0.094	4.273	0.000	0.0000E+00	0.0000E+00	0.1746E+00
0.005	6.995	9.995	0.192	-0.011	0.1515E+00	0.1830E+00	0.1935E-01
0.024	2.653	0.024	3.724	0.000	0.0000E+00	0.0000E+00	0.1753E+00
0.005	8.930	9.995	0.280	-0.020	0.1553E+00	0.1886E+00	-0.5404E-02
0.003	3.029	-0.042	3.706	0.000	0.0000E+00	0.0000E+00	0.1727E+00
0.005	10.970	9.995	0.312	-0.021	0.1559E+00	0.1865E+00	0.2943E-01
-0.027	2.945	0.006	4.315	0.000	0.0000E+00	0.0000E+00	0.1735E+00
0.005	13.005	9.995	0.337	-0.014	0.1564E+00	0.1944E+00	0.6512E-03
-0.015	2.633	0.095	4.053	0.000	0.0000E+00	0.0000E+00	0.1754E+00
0.005	14.995	9.995	0.335	-0.011	0.1524E+00	0.1942E+00	0.2375E-01
0.101	2.544	0.153	4.150	0.000	0.0000E+00	0.0000E+00	0.1745E+00

FILE NAME: SJ9J81K0

B	2θ						
0.000	-30.030	20.005	0.339	0.041	0.1497E+00	0.1892E+00	0.2595E-03
-0.024	2.831	-0.021	3.359	0.000	0.0000E+00	0.0000E+00	0.1706E+00
0.000	-24.990	20.003	0.337	0.046	0.1515E+00	0.1952E+00	0.3633E-03
0.002	2.812	-0.036	3.693	0.000	0.0000E+00	0.0000E+00	0.1747E+00
0.000	-20.000	20.000	0.334	0.059	0.1620E+00	0.2147E+00	-0.1930E-01
-0.003	3.019	-0.014	4.512	0.000	0.0000E+00	0.0000E+00	0.1913E+00
0.000	-15.000	20.000	0.325	0.054	0.1541E+00	0.1928E+00	0.3022E-02
0.041	2.767	0.117	3.495	0.000	0.0000E+00	0.0000E+00	0.1743E+00
0.000	-10.010	20.000	0.303	0.051	0.1585E+00	0.1942E+00	0.3034E-02
-0.002	3.030	-0.027	3.676	0.000	0.0000E+00	0.0000E+00	0.1773E+00
0.005	-11.010	20.000	0.261	0.055	0.1520E+00	0.1933E+00	0.2517E-01
0.010	2.887	0.022	3.981	0.000	0.0000E+00	0.0000E+00	0.1739E+00
0.005	-8.995	20.000	0.190	0.047	0.1537E+00	0.1946E+00	0.6143E-02
0.038	2.755	-0.032	3.565	0.000	0.0000E+00	0.0000E+00	0.1762E+00
0.000	-7.015	20.000	0.125	0.041	0.1559E+00	0.2012E+00	-0.1542E-01
-0.014	3.077	0.102	4.135	0.000	0.0000E+00	0.0000E+00	0.1600E+00
0.005	-5.000	20.000	0.090	0.026	0.1534E+00	0.1895E+00	-0.1190E-01
0.021	2.836	0.033	3.677	0.000	0.0000E+00	0.0000E+00	0.1724E+00
0.005	-5.005	20.000	0.074	0.023	0.1586E+00	0.1907E+00	-0.1223E-02
0.060	3.074	0.122	4.037	0.000	0.0000E+00	0.0000E+00	0.1734E+00
0.005	-4.010	20.000	0.070	0.017	0.1553E+00	0.1847E+00	-0.1029E-02
0.011	2.824	0.002	3.945	0.000	0.0000E+00	0.0000E+00	0.1709E+00
0.005	-3.010	20.000	0.036	0.015	0.1660E+00	0.1956E+00	-0.4393E-01
0.061	3.083	-0.019	3.533	0.000	0.0000E+00	0.0000E+00	0.1615E+00
0.005	-2.005	20.000	0.043	0.013	0.1749E+00	0.2166E+00	-0.2952E-01
0.110	3.633	0.036	4.074	0.000	0.0000E+00	0.0000E+00	0.1959E+00
0.005	-1.000	20.000	0.090	0.021	0.1476E+00	0.1665E+00	-0.2655E-01
-0.003	2.763	0.094	3.510	0.000	0.0000E+00	0.0000E+00	0.1632E+00
0.005	0.000	20.000	0.104	0.011	0.1535E+00	0.1945E+00	0.5143E-02
0.010	2.839	0.031	3.542	0.000	0.0000E+00	0.0000E+00	0.1593E+00
0.005	0.990	20.000	0.099	0.014	0.1528E+00	0.1929E+00	-0.3434E-01
0.009	3.165	0.000	4.053	0.000	0.0000E+00	0.0000E+00	0.1735E+00
0.005	1.995	20.000	0.094	0.008	0.1557E+00	0.1657E+00	0.2152E-01
-0.061	2.913	0.052	3.737	0.000	0.0000E+00	0.0000E+00	0.1730E+00
0.005	2.995	20.000	0.105	0.002	0.1657E+00	0.1967E+00	0.1477E-01
0.052	3.420	0.150	4.036	0.000	0.0000E+00	0.0000E+00	0.1329E+00
0.005	4.000	20.000	0.122	-0.004	0.1646E+00	0.2005E+00	-0.1015E-01
0.033	3.290	0.037	4.100	0.000	0.0000E+00	0.0000E+00	0.1834E+00
0.005	4.990	20.000	0.154	-0.003	0.1598E+00	0.1961E+00	0.1515E-01
0.014	2.951	0.042	3.609	0.000	0.0000E+00	0.0000E+00	0.1734E+00
0.005	6.000	20.000	0.200	-0.017	0.1601E+00	0.1944E+00	-0.2039E-02
0.040	2.924	0.065	4.115	0.000	0.0000E+00	0.0000E+00	0.1730E+00
0.005	7.000	20.000	0.235	-0.020	0.1580E+00	0.1953E+00	-0.3424E-03
0.030	2.894	-0.002	4.173	0.000	0.0000E+00	0.0000E+00	0.1793E+00
0.005	8.000	20.000	0.240	-0.012	0.1570E+00	0.1944E+00	-0.7695E-02
0.015	2.798	0.124	3.691	0.000	0.0000E+00	0.0000E+00	0.1797E+00
0.005	11.010	20.000	0.314	-0.011	0.1642E+00	0.2015E+00	-0.6433E-02
0.009	3.033	0.100	4.019	0.000	0.0000E+00	0.0000E+00	0.1738E+00
0.005	12.995	20.000	0.327	-0.013	0.1556E+00	0.2004E+00	-0.1350E-01
-0.025	2.866	-0.039	3.955	0.000	0.0000E+00	0.0000E+00	0.1837E+00
0.005	15.000	20.000	0.330	-0.016	0.1572E+00	0.1967E+00	0.2322E-01
-0.001	2.872	0.050	3.844	0.000	0.0000E+00	0.0000E+00	0.1730E+00

FILE NAME: 3J91J7X0

3	29						
0.000	-29.990	40.005	0.332	0.035	0.1530E+00	0.1916E+00	-0.1395E-01
0.006	2.750	0.015	3.687	0.000	0.0000E+00	0.0000E+00	0.1734E+00
0.000	-25.005	40.005	0.336	0.044	0.1549E+00	0.1894E+00	-0.2377E-02
0.029	2.957	0.039	3.694	0.000	0.0000E+00	0.0000E+00	0.1730E+00
0.000	-20.005	40.005	0.339	0.042	0.1494E+00	0.1855E+00	-0.1935E-01
-0.034	2.794	0.046	3.639	0.000	0.0000E+00	0.0000E+00	0.1734E+00
0.005	-15.005	40.005	0.315	0.043	0.1526E+00	0.1884E+00	0.1134E-01
-0.025	2.791	0.014	3.497	0.000	0.0000E+00	0.0000E+00	0.1713E+00
0.005	-12.990	40.005	0.303	0.037	0.1520E+00	0.1885E+00	-0.1638E-01
0.043	2.826	0.075	3.549	0.000	0.0000E+00	0.0000E+00	0.1712E+00
0.005	-11.010	40.005	0.277	0.052	0.1459E+00	0.2000E+00	0.2723E-01
0.007	3.040	0.043	3.575	0.000	0.0000E+00	0.0000E+00	0.1751E+00
0.005	-9.995	40.005	0.245	0.042	0.1517E+00	0.1954E+00	0.4166E-01
0.007	2.809	-0.045	3.750	0.000	0.0000E+00	0.0000E+00	0.1749E+00
0.005	-7.000	40.005	0.205	0.043	0.1538E+00	0.1894E+00	0.3665E-01
-0.047	2.913	-0.331	3.457	0.000	0.0000E+00	0.0000E+00	0.1725E+00
0.005	-6.000	40.005	0.190	0.046	0.1534E+00	0.2002E+00	0.1316E-01
0.001	2.919	0.108	3.667	0.000	0.0000E+00	0.0000E+00	0.1733E+00
0.005	-5.000	40.005	0.170	0.043	0.1516E+00	0.1952E+00	0.2003E-01
-0.019	2.775	-0.104	4.132	0.000	0.0000E+00	0.0000E+00	0.1765E+00
0.005	-4.010	40.005	0.156	0.036	0.1565E+00	0.1952E+00	0.4376E-02
0.000	2.957	0.129	4.102	0.000	0.0000E+00	0.0000E+00	0.1769E+00
0.005	-3.005	40.005	0.145	0.028	0.1538E+00	0.1930E+00	0.3474E-02
0.013	2.933	0.100	3.727	0.000	0.0000E+00	0.0000E+00	0.1745E+00
0.005	-2.010	40.005	0.144	0.015	0.1601E+00	0.2037E+00	0.1047E-01
0.023	3.120	0.056	4.005	0.000	0.0000E+00	0.0000E+00	0.1752E+00
0.005	-1.000	40.005	0.148	-0.002	0.1546E+00	0.1932E+00	-0.1312E-01
0.046	2.894	0.102	3.953	0.000	0.0000E+00	0.0000E+00	0.1750E+00
0.005	0.010	40.005	0.156	0.005	0.1525E+00	0.1965E+00	-0.3219E-02
0.010	2.935	0.030	3.947	0.000	0.0000E+00	0.0000E+00	0.1759E+00
0.005	0.985	40.005	0.157	-0.002	0.1644E+00	0.1932E+00	-0.2509E-03
-0.003	3.211	0.116	3.713	0.000	0.0000E+00	0.0000E+00	0.1744E+00
0.005	1.995	40.005	0.133	-0.009	0.1562E+00	0.1926E+00	-0.2125E-01
0.040	2.792	0.041	3.455	0.000	0.0000E+00	0.0000E+00	0.1754E+00
0.005	2.990	40.005	0.230	-0.014	0.1589E+00	0.1959E+00	-0.4410E-01
0.007	3.035	0.013	3.673	0.000	0.0000E+00	0.0000E+00	0.1733E+00
0.005	4.000	40.005	0.217	-0.012	0.1546E+00	0.1934E+00	-0.2350E-01
0.036	2.543	0.052	3.503	0.000	0.0000E+00	0.0000E+00	0.1750E+00
0.005	4.990	40.005	0.236	-0.013	0.1549E+00	0.1874E+00	-0.1377E-01
0.024	2.944	0.029	3.533	0.000	0.0000E+00	0.0000E+00	0.1719E+00
0.005	5.990	40.005	0.252	-0.008	0.1578E+00	0.1914E+00	-0.1073E-01
0.039	2.354	0.017	3.726	0.000	0.0000E+00	0.0000E+00	0.1754E+00
0.005	7.000	40.005	0.273	-0.011	0.1636E+00	0.2000E+00	-0.1532E-02
0.065	2.952	0.090	3.733	0.000	0.0000E+00	0.0000E+00	0.1814E+00
0.005	8.000	40.000	0.293	-0.008	0.1515E+00	0.1948E+00	0.1277E-01
0.058	2.751	0.009	3.739	0.000	0.0000E+00	0.0000E+00	0.1745E+00
0.005	11.015	40.005	0.313	-0.013	0.1557E+00	0.1976E+00	-0.9531E-03
0.022	2.824	0.041	4.042	0.000	0.0000E+00	0.0000E+00	0.1775E+00
0.005	13.010	40.005	0.319	-0.001	0.1519E+00	0.1911E+00	0.7312E-02
-0.003	2.884	0.154	3.971	0.000	0.0000E+00	0.0000E+00	0.1726E+00
0.005	14.990	40.005	0.323	-0.005	0.1535E+00	0.1935E+00	0.3445E-02
0.006	2.813	0.121	4.044	0.000	0.0000E+00	0.0000E+00	0.1749E+00

FILE NAME: SJ9133X0

0.000	-29.990	59.995	0.331	0.027	0.1547E+00	0.1582E+00	0.1193E-01
-0.065	2.836	-0.015	3.641	0.000	0.0000E+00	0.0000E+00	0.1723E+00
0.005	-25.005	59.995	0.332	0.028	0.1566E+00	0.1903E+00	0.1236E-01
0.005	3.012	0.130	3.733	0.000	0.0000E+00	0.0000E+00	0.1743E+00
0.005	-19.995	59.995	0.331	0.032	0.1499E+00	0.1759E+00	-0.1461E-02
-0.011	2.720	0.157	3.891	0.000	0.0000E+00	0.0000E+00	0.1744E+00
0.005	-14.995	59.995	0.313	0.027	0.1502E+00	0.1855E+00	0.2393E-01
-0.017	2.715	0.029	3.473	0.000	0.0000E+00	0.0000E+00	0.1693E+00
0.005	-13.005	59.995	0.303	0.031	0.1509E+00	0.1572E+00	0.7171E-02
-0.058	2.754	0.229	3.410	0.000	0.0000E+00	0.0000E+00	0.1700E+00
0.005	-10.995	59.995	0.230	0.035	0.1565E+00	0.1937E+00	0.3751E-01
-0.005	2.876	-0.005	3.721	0.000	0.0000E+00	0.0000E+00	0.1751E+00
0.005	-9.005	59.995	0.254	0.033	0.1480E+00	0.1891E+00	0.4525E-01
-0.050	2.740	0.011	3.452	0.000	0.0000E+00	0.0000E+00	0.1698E+00
0.005	-6.990	59.995	0.225	0.027	0.1589E+00	0.1924E+00	0.2539E-01
-0.009	2.997	-0.033	3.695	0.000	0.0000E+00	0.0000E+00	0.1755E+00
0.005	-5.005	59.995	0.218	0.032	0.1548E+00	0.1937E+00	0.2633E-01
0.043	2.572	0.040	3.690	0.000	0.0000E+00	0.0000E+00	0.1754E+00
0.005	-3.010	59.995	0.202	0.026	0.1557E+00	0.1675E+00	0.5150E-01
-0.000	2.803	-0.031	3.259	0.000	0.0000E+00	0.0000E+00	0.1723E+00
0.005	-4.005	59.995	0.197	0.025	0.1521E+00	0.1930E+00	0.1703E-01
0.005	2.730	0.119	3.645	0.000	0.0000E+00	0.0000E+00	0.1737E+00
0.005	-3.005	59.995	0.187	0.019	0.1582E+00	0.1914E+00	0.4078E-02
-0.041	2.934	0.066	3.615	0.000	0.0000E+00	0.0000E+00	0.1756E+00
0.005	-2.010	59.995	0.185	0.012	0.1558E+00	0.1947E+00	0.1510E-01
0.045	3.030	0.097	3.680	0.000	0.0000E+00	0.0000E+00	0.1753E+00
0.005	-1.005	59.995	0.159	0.006	0.1597E+00	0.1928E+00	-0.5297E-02
0.016	3.039	-0.099	3.950	0.000	0.0000E+00	0.0000E+00	0.1756E+00
0.005	-0.010	59.995	0.195	0.011	0.1714E+00	0.2133E+00	-0.3314E-01
-0.049	3.152	0.014	4.391	0.000	0.0000E+00	0.0000E+00	0.1733E+00
0.005	0.990	59.995	0.207	-0.001	0.1552E+00	0.1987E+00	-0.2221E-01
0.013	2.613	0.009	3.927	0.000	0.0000E+00	0.0000E+00	0.1735E+00
0.005	1.990	59.995	0.217	-0.001	0.1621E+00	0.1946E+00	-0.2193E-01
-0.056	2.938	-0.030	3.635	0.000	0.0000E+00	0.0000E+00	0.1792E+00
0.005	2.995	59.995	0.234	0.000	0.1598E+00	0.1935E+00	-0.1309E-01
0.000	2.843	-0.036	3.935	0.000	0.0000E+00	0.0000E+00	0.1775E+00
0.005	3.995	59.995	0.247	0.004	0.1617E+00	0.1927E+00	-0.5253E-02
0.025	2.943	0.039	3.543	0.000	0.0000E+00	0.0000E+00	0.1779E+00
0.005	4.995	59.995	0.269	-0.002	0.1553E+00	0.1900E+00	-0.1951E-01
-0.001	2.936	0.091	3.754	0.000	0.0000E+00	0.0000E+00	0.1735E+00
0.005	5.990	59.995	0.274	0.007	0.1539E+00	0.1912E+00	-0.2874E-01
0.025	2.907	0.071	3.604	0.000	0.0000E+00	0.0000E+00	0.1736E+00
0.005	7.000	59.995	0.235	0.000	0.1511E+00	0.1923E+00	-0.3533E-01
-0.001	2.554	0.043	3.629	0.000	0.0000E+00	0.0000E+00	0.1729E+00
0.005	9.005	59.995	0.308	-0.005	0.1505E+00	0.1953E+00	0.2335E-01
0.092	2.845	0.065	3.819	0.000	0.0000E+00	0.0000E+00	0.1743E+00
0.005	10.995	59.995	0.312	0.004	0.1574E+00	0.1919E+00	0.2297E-01
0.002	2.903	0.006	3.625	0.000	0.0000E+00	0.0000E+00	0.1753E+00
0.005	13.000	59.995	0.323	0.001	0.1516E+00	0.1907E+00	0.2153E-01
-0.056	2.709	0.065	3.684	0.000	0.0000E+00	0.0000E+00	0.1723E+00
0.005	14.995	59.995	0.325	0.010	0.1517E+00	0.1873E+00	-0.2193E-02
0.017	2.862	0.100	3.859	0.000	0.0000E+00	0.0000E+00	0.1705E+00

FILE NAME: SJ9159X0

o	2o						
0.000	-30.020	5.000	0.344	0.046	0.1527E+00	0.1901E+00	0.5636E-02
0.005	2.846	0.020	3.707	0.000	0.0000E+00	0.0000E+00	0.1724E+00
0.005	-25.000	5.995	0.343	0.042	0.1529E+00	0.1915E+00	0.2955E-01
-0.031	2.813	0.077	3.699	0.000	0.0000E+00	0.0000E+00	0.1735E+00
0.005	-19.995	5.995	0.348	0.045	0.1585E+00	0.1922E+00	0.2133E-02
0.006	2.973	-0.041	4.137	0.000	0.0000E+00	0.0000E+00	0.1761E+00
0.005	-14.995	5.995	0.337	0.048	0.1528E+00	0.1871E+00	0.1182E-01
0.001	2.750	0.020	3.232	0.000	0.0000E+00	0.0000E+00	0.1705E+00
0.005	-12.995	5.995	0.310	0.047	0.1546E+00	0.1923E+00	0.2564E-01
0.006	2.770	-0.042	3.842	0.000	0.0000E+00	0.0000E+00	0.1745E+00
0.005	-11.005	5.995	0.237	0.043	0.1578E+00	0.1906E+00	0.1232E-01
0.056	2.941	-0.061	4.103	0.000	0.0000E+00	0.0000E+00	0.1750E+00
0.005	-9.000	5.995	0.115	0.031	0.1545E+00	0.1883E+00	-0.1472E-01
0.019	2.877	-0.025	4.201	0.000	0.0000E+00	0.0000E+00	0.1722E+00
0.005	-7.005	5.995	0.009	0.025	0.1578E+00	0.1931E+00	-0.1259E-01
0.019	3.166	0.079	3.879	0.000	0.0000E+00	0.0000E+00	0.1753E+00
0.005	-5.005	5.995	-0.023	0.023	0.1569E+00	0.1896E+00	-0.2599E-02
0.013	2.940	0.097	4.109	0.000	0.0000E+00	0.0000E+00	0.1740E+00
0.005	-3.010	5.995	-0.029	0.022	0.1599E+00	0.1924E+00	-0.3353E-02
-0.003	3.245	0.041	3.716	0.000	0.0000E+00	0.0000E+00	0.1759E+00
0.005	-4.005	5.995	0.006	0.019	0.1512E+00	0.1890E+00	0.3307E-03
0.028	2.849	-0.015	3.649	0.000	0.0000E+00	0.0000E+00	0.1711E+00
0.005	-5.000	5.995	0.087	0.017	0.1574E+00	0.1854E+00	0.2009E-01
0.053	2.978	0.025	3.491	0.000	0.0000E+00	0.0000E+00	0.1720E+00
0.005	-2.010	5.995	0.213	0.025	0.1921E+00	0.2296E+00	0.6018E-02
-0.007	3.554	0.266	3.553	0.000	0.0000E+00	0.0000E+00	0.2117E+00
0.005	-0.995	5.995	0.332	0.039	0.2329E+00	0.2209E+00	0.5197E-01
0.102	2.995	0.065	5.005	0.000	0.0000E+00	0.0000E+00	0.2270E+00
0.005	-0.005	5.995	0.245	0.047	0.2136E+00	0.2329E+00	0.2338E-01
0.013	3.619	0.063	5.534	0.000	0.0000E+00	0.0000E+00	0.2235E+00
0.005	0.990	5.995	0.103	0.030	0.1715E+00	0.2036E+00	0.1431E-02
0.005	5.326	-0.032	4.356	0.000	0.0000E+00	0.0000E+00	0.1832E+00
0.005	2.000	5.995	0.009	0.017	0.1691E+00	0.1698E+00	0.1097E-01
0.119	3.355	0.105	3.317	0.000	0.0000E+00	0.0000E+00	0.1797E+00
0.005	2.990	5.995	-0.015	0.006	0.1557E+00	0.1591E+00	-0.2772E-02
0.024	2.893	0.013	3.683	0.000	0.0000E+00	0.0000E+00	0.1732E+00
0.005	4.005	5.995	-0.008	0.011	0.1562E+00	0.1882E+00	0.1733E-01
0.076	2.990	0.107	3.905	0.000	0.0000E+00	0.0000E+00	0.1729E+00
0.005	4.935	5.995	0.032	0.002	0.1526E+00	0.1877E+00	-0.1154E-02
-0.035	2.819	-0.043	3.957	0.000	0.0000E+00	0.0000E+00	0.1711E+00
0.005	5.995	5.995	0.095	-0.009	0.1557E+00	0.1932E+00	-0.7905E-02
0.045	2.853	0.051	4.412	0.000	0.0000E+00	0.0000E+00	0.1754E+00
0.005	7.005	5.995	0.158	-0.017	0.1529E+00	0.1663E+00	-0.3322E-02
-0.002	2.837	0.039	4.020	0.000	0.0000E+00	0.0000E+00	0.1704E+00
0.005	5.995	5.995	0.276	-0.021	0.1540E+00	0.1880E+00	0.1153E-01
0.046	2.713	0.032	3.657	0.000	0.0000E+00	0.0000E+00	0.1713E+00
0.005	11.005	5.995	0.326	-0.014	0.1509E+00	0.1909E+00	-0.7123E-02
-0.056	2.747	-0.006	3.293	0.000	0.0000E+00	0.0000E+00	0.1721E+00
0.005	12.990	5.995	0.340	-0.013	0.1567E+00	0.1926E+00	-0.2483E-03
0.027	2.683	0.000	3.629	0.000	0.0000E+00	0.0000E+00	0.1757E+00
0.005	14.990	5.995	0.343	-0.011	0.1528E+00	0.1963E+00	0.3063E-01
0.008	2.834	-0.037	3.977	0.000	0.0000E+00	0.0000E+00	0.1759E+00

FILE NAME: SJ9125XO

θ	2θ						
0.005	-30.020	10.005	0.340	0.045	0.1518E+00	0.1941E+00	0.2106E-01
-0.012	2.750	0.131	4.171	0.000	0.0000E+00	0.0000E+00	0.1742E+00
0.005	-24.995	10.005	0.342	0.041	0.1577E+00	0.1927E+00	0.2095E-01
-0.014	2.930	-0.071	3.631	0.000	0.0000E+00	0.0000E+00	0.1761E+00
0.005	-19.995	10.005	0.347	0.039	0.1510E+00	0.1930E+00	0.6760E-02
-0.011	2.793	0.106	3.711	0.000	0.0000E+00	0.0000E+00	0.1733E+00
0.005	-14.990	10.005	0.338	0.050	0.1506E+00	0.1902E+00	-0.1363E-01
0.025	2.839	-0.005	3.728	0.000	0.0000E+00	0.0000E+00	0.1716E+00
0.005	-12.985	10.005	0.309	0.062	0.1493E+00	0.1879E+00	-0.7952E-02
0.061	2.723	0.075	3.704	0.000	0.0000E+00	0.0000E+00	0.1697E+00
0.005	-11.005	10.005	0.246	0.059	0.1485E+00	0.1859E+00	-0.7663E-02
0.025	2.733	0.011	3.593	0.000	0.0000E+00	0.0000E+00	0.1632E+00
0.005	-9.000	10.005	0.133	0.045	0.1594E+00	0.1901E+00	-0.5659E-03
0.053	3.022	0.061	4.471	0.000	0.0000E+00	0.0000E+00	0.1754E+00
0.005	-7.000	10.005	0.026	0.032	0.1548E+00	0.1881E+00	-0.2515E-01
0.054	3.018	0.067	3.747	0.000	0.0000E+00	0.0000E+00	0.1723E+00
0.005	-5.005	10.005	-0.002	0.025	0.1568E+00	0.1960E+00	-0.2932E-01
-0.011	2.894	0.057	4.129	0.000	0.0000E+00	0.0000E+00	0.1775E+00
0.005	-3.010	10.005	-0.011	0.018	0.1666E+00	0.2018E+00	-0.1513E-01
-0.003	3.128	0.067	3.777	0.000	0.0000E+00	0.0000E+00	0.1359E+00
0.005	-4.000	10.005	0.013	0.011	0.1597E+00	0.2017E+00	-0.1226E-01
0.014	2.992	-0.092	4.621	0.000	0.0000E+00	0.0000E+00	0.1319E+00
0.005	-3.000	10.005	0.092	0.010	0.1795E+00	0.2114E+00	-0.1599E-01
0.050	3.205	0.123	4.736	0.000	0.0000E+00	0.0000E+00	0.1951E+00
0.005	-2.010	10.005	0.194	0.018	0.2009E+00	0.2114E+00	0.1548E-01
0.052	3.304	0.191	4.764	0.000	0.0000E+00	0.0000E+00	0.2062E+00
0.005	-0.995	10.005	0.265	0.036	0.2323E+00	0.2596E+00	0.3505E-01
0.252	3.329	0.134	9.681	0.000	0.0000E+00	0.0000E+00	0.2453E+00
0.005	0.015	10.005	0.219	0.039	0.2144E+00	0.2115E+00	0.6711E-01
0.107	3.066	0.268	5.619	0.000	0.0000E+00	0.0000E+00	0.2130E+00
0.005	0.995	10.005	0.131	0.041	0.1862E+00	0.2198E+00	0.1555E-01
0.145	3.318	0.272	5.095	0.000	0.0000E+00	0.0000E+00	0.2037E+00
0.005	2.005	10.005	0.041	0.023	0.1703E+00	0.1967E+00	0.1055E-01
0.072	3.172	0.004	3.793	0.000	0.0000E+00	0.0000E+00	0.1540E+00
0.005	3.005	10.005	0.013	0.016	0.1619E+00	0.1984E+00	-0.3305E-02
0.042	2.931	-0.026	3.810	0.000	0.0000E+00	0.0000E+00	0.1311E+00
0.005	3.995	10.005	0.025	0.008	0.1592E+00	0.1906E+00	0.6931E-02
-0.003	2.937	0.172	3.864	0.000	0.0000E+00	0.0000E+00	0.1756E+00
0.005	5.000	10.005	0.074	-0.006	0.1643E+00	0.1876E+00	-0.3354E-01
0.039	3.108	0.058	3.493	0.000	0.0000E+00	0.0000E+00	0.1764E+00
0.005	5.995	10.005	0.133	-0.021	0.1649E+00	0.2068E+00	-0.2674E-01
0.066	3.072	0.014	4.262	0.000	0.0000E+00	0.0000E+00	0.1570E+00
0.005	6.995	10.005	0.192	-0.030	0.1681E+00	0.2092E+00	-0.1156E-01
0.085	3.163	0.017	4.321	0.000	0.0000E+00	0.0000E+00	0.1393E+00
0.005	8.995	10.005	0.289	-0.023	0.1569E+00	0.1947E+00	0.1710E-02
0.058	2.830	0.035	4.133	0.000	0.0000E+00	0.0000E+00	0.1738E+00
0.005	10.995	10.005	0.322	-0.021	0.1546E+00	0.1667E+00	0.1274E-01
0.069	2.866	-0.088	3.636	0.000	0.0000E+00	0.0000E+00	0.1714E+00
0.005	12.990	10.005	0.335	-0.015	0.1528E+00	0.1664E+00	-0.1456E-01
0.040	2.791	0.155	3.695	0.000	0.0000E+00	0.0000E+00	0.1704E+00
0.005	14.995	10.005	0.338	-0.018	0.1513E+00	0.1909E+00	-0.2914E-02
0.019	2.741	-0.015	4.152	0.000	0.0000E+00	0.0000E+00	0.1722E+00

FILE NAME: SJ9211X0

J	26						
0.005	-29.990	20.005	0.339	0.044	0.1663E+00	0.2127E+00	0.1222E-01
0.026	3.000	0.212	4.945	0.000	0.0000E+00	0.0000E+00	0.1910E+00
0.005	-25.000	20.005	0.335	0.047	0.1681E+00	0.2[illegible]54E+00	0.9[illegible]E-02
0.051	3.066	0.134	4.145	0.000	0.0000E+00	0.0000E+00	0.1938E+00
0.005	-20.005	20.005	0.328	0.045	0.1563E+00	0.1911E+00	0.1035E-01
-0.001	2.790	0.052	4.009	0.000	0.0000E+00	0.0000E+00	0.1746E+00
0.005	-14.995	20.005	0.320	0.051	0.1600E+00	0.1897E+00	-0.1133E-01
0.063	3.119	0.028	3.944	0.000	0.0000E+00	0.0000E+00	0.1755E+00
0.005	-13.010	20.005	0.310	0.056	0.1527E+00	0.1869E+00	-0.2537E-01
-0.014	2.779	0.230	4.212	0.000	0.0000E+00	0.0000E+00	0.1707E+00
0.005	-10.985	20.000	0.257	0.057	0.1515E+00	0.1864E+00	0.3057E-01
0.028	2.766	0.166	3.819	0.000	0.0000E+00	0.0000E+00	0.1693E+00
0.005	-8.990	20.000	0.184	0.048	0.1477E+00	0.1931E+00	0.1135E-01
0.036	2.712	0.092	3.780	0.000	0.0000E+00	0.0000E+00	0.1719E+00
0.005	-7.005	20.005	0.115	0.034	0.1562E+00	0.1950E+00	0.2808E-01
0.036	2.953	0.027	3.587	0.000	0.0000E+00	0.0000E+00	0.1735E+00
0.005	-5.995	20.000	0.083	0.036	0.1623E+00	0.2004E+00	0.7779E-02
0.013	3.026	0.024	3.703	0.000	0.0000E+00	0.0000E+00	0.1824E+00
0.005	-5.010	20.000	0.080	0.029	0.1728E+00	0.2109E+00	0.3475E-01
0.073	3.142	0.174	4.311	0.000	0.0000E+00	0.0000E+00	0.1928E+00
0.005	-4.005	20.000	0.074	0.023	0.1639E+00	0.2011E+00	-0.1728E-01
0.046	2.965	-0.014	3.973	0.000	0.0000E+00	0.0000E+00	0.1835E+00
0.005	-2.990	20.000	0.033	0.011	0.1785E+00	0.1954E+00	-0.1569E-01
0.157	3.053	0.057	4.023	0.000	0.0000E+00	0.0000E+00	0.1871E+00
0.005	-2.010	20.000	0.102	0.011	0.1756E+00	0.1993E+00	0.1342E-01
0.115	2.821	-0.023	3.992	0.000	0.0000E+00	0.0000E+00	0.1878E+00
0.005	-0.995	20.000	0.113	0.013	0.1910E+00	0.2022E+00	0.3433E-01
0.100	3.083	0.144	4.086	0.000	0.0000E+00	0.0000E+00	0.1967E+00
0.005	0.005	20.000	0.122	0.013	0.1948E+00	0.2076E+00	0.3929E-01
0.165	3.172	0.065	4.870	0.000	0.0000E+00	0.0000E+00	0.2013E+00
0.005	0.995	20.000	0.105	0.003	0.1674E+00	0.1998E+00	0.3233E-01
0.143	3.073	-0.137	3.921	0.000	0.0000E+00	0.0000E+00	0.1843E+00
0.005	1.990	20.000	0.102	0.001	0.1634E+00	0.1907E+00	0.2140E-01
0.051	2.984	0.037	3.582	0.000	0.0000E+00	0.0000E+00	0.1776E+00
0.005	2.995	20.005	0.113	-0.002	0.1615E+00	0.2046E+00	0.1293E-01
-0.010	3.149	0.157	4.270	0.000	0.0000E+00	0.0000E+00	0.1343E+00
0.005	3.995	20.000	0.135	-0.011	0.1607E+00	0.1973E+00	-0.2034E-01
-0.013	2.877	0.039	4.249	0.000	0.0000E+00	0.0000E+00	0.1799E+00
0.005	4.995	20.000	0.169	-0.015	0.1583E+00	0.1866E+00	-0.2270E-01
0.017	2.934	0.015	3.811	0.000	0.0000E+00	0.0000E+00	0.1741E+00
0.005	5.995	20.000	0.197	-0.017	0.1526E+00	0.1811E+00	-0.3506E-01
-0.036	2.922	-0.121	3.742	0.000	0.0000E+00	0.0000E+00	0.1674E+00
0.005	6.995	20.000	0.235	-0.024	0.1598E+00	0.1841E+00	0.4693E-03
0.046	2.941	-0.017	3.752	0.000	0.0000E+00	0.0000E+00	0.1724E+00
0.005	9.010	20.000	0.290	-0.021	0.1546E+00	0.1841E+00	0.2039E-02
-0.015	2.841	0.069	3.795	0.000	0.0000E+00	0.0000E+00	0.1700E+00
0.005	11.010	20.000	0.308	-0.019	0.1488E+00	0.1659E+00	0.2525E-01
0.034	2.732	-0.053	3.525	0.000	0.0000E+00	0.0000E+00	0.1634E+00
0.005	13.000	20.000	0.326	-0.015	0.1551E+00	0.1806E+00	-0.2302E-01
-0.019	3.038	0.089	3.474	0.000	0.0000E+00	0.0000E+00	0.1694E+00
0.005	14.995	20.000	0.323	-0.019	0.1482E+00	0.1657E+00	0.3953E-01
0.018	2.743	0.120	3.955	0.000	0.0000E+00	0.0000E+00	0.1630E+00

FILE NAME: SJ9237X0

ω	2θ						
0.005	-29.990	40.005	0.331	0.026	0.1546E+00	0.1893E+00	-0.3157E-01
0.019	2.542	-0.039	3.750	0.000	0.0000E+00	0.0000E+00	0.1723E+00
0.005	-25.000	40.005	0.329	0.035	0.1515E+00	0.1927E+00	-0.2163E-01
-0.017	2.717	0.046	4.077	0.000	0.0000E+00	0.0000E+00	0.1733E+00
0.005	-19.995	40.000	0.325	0.036	0.1521E+00	0.1914E+00	-0.4472E-02
0.021	2.800	0.104	3.674	0.000	0.0000E+00	0.0000E+00	0.1729E+00
0.005	-14.995	40.005	0.315	0.027	0.1494E+00	0.1841E+00	-0.5250E-02
0.013	2.779	0.054	3.600	0.000	0.0000E+00	0.0000E+00	0.1676E+00
0.005	-13.010	40.000	0.306	0.038	0.1524E+00	0.1894E+00	-0.9319E-02
-0.073	2.775	0.066	3.757	0.000	0.0000E+00	0.0000E+00	0.1719E+00
0.005	-11.010	40.000	0.273	0.034	0.1531E+00	0.1927E+00	0.2791E-01
-0.006	2.809	-0.003	3.639	0.000	0.0000E+00	0.0000E+00	0.1740E+00
0.005	-8.970	40.000	0.250	0.040	0.1616E+00	0.1855E+00	0.3750E-01
0.025	3.043	0.059	3.427	0.000	0.0000E+00	0.0000E+00	0.1739E+00
0.005	-7.010	40.000	0.208	0.043	0.1572E+00	0.1951E+00	0.2258E-02
-0.038	2.848	0.003	3.496	0.000	0.0000E+00	0.0000E+00	0.1772E+00
0.005	-5.005	40.000	0.191	0.034	0.1550E+00	0.1870E+00	0.7348E-02
-0.010	2.805	0.013	3.639	0.000	0.0000E+00	0.0000E+00	0.1718E+00
0.005	-5.010	40.000	0.169	0.030	0.1526E+00	0.1905E+00	0.9438E-02
-0.024	2.685	-0.027	3.643	0.000	0.0000E+00	0.0000E+00	0.1726E+00
0.005	-4.005	40.000	0.159	0.018	0.1640E+00	0.2025E+00	0.1290E-01
-0.012	2.949	-0.107	4.518	0.000	0.0000E+00	0.0000E+00	0.1843E+00
0.005	-3.000	40.000	0.148	0.027	0.1726E+00	0.2102E+00	0.3639E-01
0.026	3.126	-0.052	4.410	0.000	0.0000E+00	0.0000E+00	0.1823E+00
0.005	-1.990	40.000	0.147	0.025	0.1625E+00	0.1951E+00	-0.6347E-02
0.039	3.052	-0.015	3.560	0.000	0.0000E+00	0.0000E+00	0.1795E+00
0.005	-1.005	40.000	0.150	0.015	0.1629E+00	0.2061E+00	0.2325E-01
0.031	2.991	0.015	3.378	0.000	0.0000E+00	0.0000E+00	0.1824E+00
0.005	0.015	40.000	0.154	0.011	0.1733E+00	0.2107E+00	0.7352E-03
0.046	3.146	0.165	4.965	0.000	0.0000E+00	0.0000E+00	0.1729E+00
0.005	1.000	-0.000	0.168	0.000	0.1601E+00	0.1947E+00	-0.1796E-01
-0.050	2.853	0.016	3.793	0.000	0.0000E+00	0.0000E+00	0.1782E+00
0.005	1.995	40.000	0.185	-0.006	0.1542E+00	0.1931E+00	-0.7390E-02
-0.037	2.806	-0.002	3.454	0.000	0.0000E+00	0.0000E+00	0.1747E+00
0.005	2.995	40.000	0.208	-0.011	0.1522E+00	0.1902E+00	-0.1343E-01
0.038	2.733	0.005	3.758	0.000	0.0000E+00	0.0000E+00	0.1722E+00
0.005	3.995	40.000	0.218	-0.015	0.1521E+00	0.1899E+00	-0.7742E-02
-0.042	2.820	0.095	3.685	0.000	0.0000E+00	0.0000E+00	0.1721E+00
0.005	4.985	40.000	0.244	-0.006	0.1558E+00	0.1919E+00	-0.1633E-01
-0.023	2.747	0.044	3.834	0.000	0.0000E+00	0.0000E+00	0.1748E+00
0.005	5.995	40.000	0.263	-0.014	0.1499E+00	0.1886E+00	-0.4407E-02
0.033	2.941	0.052	3.683	0.000	0.0000E+00	0.0000E+00	0.1734E+00
0.005	6.995	40.000	0.276	-0.007	0.1514E+00	0.1861E+00	0.2101E-01
0.024	2.724	0.034	3.710	0.000	0.0000E+00	0.0000E+00	0.1695E+00
0.005	6.990	40.000	0.300	-0.004	0.1517E+00	0.1851E+00	0.2720E-02
0.020	2.730	0.065	3.680	0.000	0.0000E+00	0.0000E+00	0.1692E+00
0.005	11.010	40.000	0.312	-0.002	0.1546E+00	0.1872E+00	-0.7911E-02
0.040	2.902	0.023	3.865	0.000	0.0000E+00	0.0000E+00	0.1721E+00
0.005	13.010	40.000	0.318	-0.004	0.1467E+00	0.1897E+00	-0.6130E-02
-0.006	2.846	0.026	3.617	0.000	0.0000E+00	0.0000E+00	0.1695E+00
0.005	15.005	40.000	0.321	-0.006	0.1516E+00	0.1840E+00	0.3254E-01
-0.010	2.885	0.025	3.762	0.000	0.0000E+00	0.0000E+00	0.1736E+00

FILE NAME: SJ9263X0

J	2S						
0.005	-29.990	59.995	0.335	0.027	0.1536E+00	0.1896E+00	0.1798E-01
0.007	2.751	0.100	3.802	0.000	0.0000E+00	0.0000E+00	0.1726E+00
0.005	-25.005	59.995	0.331	0.027	0.1555E+00	0.2014E+00	-0.4231E-01
0.038	2.911	-0.033	4.149	0.000	0.0000E+00	0.0000E+00	0.1799E+00
0.005	-20.000	59.995	0.329	0.034	0.1524E+00	0.1958E+00	0.5444E-02
0.013	2.817	0.076	3.795	0.000	0.0000E+00	0.0000E+00	0.1754E+00
0.005	-14.995	59.995	0.317	0.027	0.1552E+00	0.1907E+00	0.5045E-02
0.070	2.855	0.110	3.623	0.000	0.0000E+00	0.0000E+00	0.1738E+00
0.005	-13.010	59.995	0.308	0.031	0.1501E+00	0.1891E+00	0.9403E-02
-0.013	2.797	0.060	3.940	0.000	0.0000E+00	0.0000E+00	0.1707E+00
0.005	-11.015	59.995	0.289	0.032	0.1512E+00	0.1856E+00	0.4528E-01
0.017	2.856	0.005	3.438	0.000	0.0000E+00	0.0000E+00	0.1672E+00
0.005	-9.005	59.995	0.261	0.032	0.1535E+00	0.1846E+00	0.8303E-02
0.024	2.794	0.024	3.376	0.000	0.0000E+00	0.0000E+00	0.1699E+00
0.005	-7.025	59.995	0.230	0.021	0.1541E+00	0.1924E+00	0.3224E-01
0.024	2.850	0.106	3.792	0.000	0.0000E+00	0.0000E+00	0.1743E+00
0.005	-6.005	59.995	0.224	0.023	0.1496E+00	0.1879E+00	0.5070E-01
-0.010	2.693	0.007	3.603	0.000	0.0000E+00	0.0000E+00	0.1699E+00
0.005	-5.010	59.995	0.217	0.027	0.1529E+00	0.1906E+00	0.4531E-01
0.019	2.590	0.082	3.458	0.000	0.0000E+00	0.0000E+00	0.1729E+00
0.005	-4.005	59.995	0.211	0.028	0.1512E+00	0.1929E+00	0.3910E-01
0.025	2.792	0.077	3.716	0.000	0.0000E+00	0.0000E+00	0.1733E+00
0.005	-3.005	59.995	0.204	0.024	0.1473E+00	0.1897E+00	0.1778E-01
0.053	2.773	0.000	3.379	0.000	0.0000E+00	0.0000E+00	0.1693E+00
0.005	-2.005	59.995	0.193	0.015	0.1463E+00	0.1925E+00	-0.4373E-02
0.052	2.659	0.062	3.639	0.000	0.0000E+00	0.0000E+00	0.1710E+00
0.005	-1.005	59.995	0.204	0.006	0.1558E+00	0.1884E+00	0.4243E-02
0.043	2.856	-0.002	3.552	0.000	0.0000E+00	0.0000E+00	0.1729E+00
0.005	-0.005	59.995	0.207	0.006	0.1502E+00	0.1866E+00	-0.3356E-01
0.009	2.814	0.141	3.562	0.000	0.0000E+00	0.0000E+00	0.1694E+00
0.005	0.995	59.995	0.216	0.003	0.1507E+00	0.1906E+00	0.9077E-02
0.011	2.694	0.107	3.634	0.000	0.0000E+00	0.0000E+00	0.1713E+00
0.005	1.995	59.995	0.227	-0.002	0.1535E+00	0.1831E+00	-0.1534E-02
0.022	2.794	0.079	3.515	0.000	0.0000E+00	0.0000E+00	0.1716E+00
0.005	2.995	59.995	0.241	-0.003	0.1509E+00	0.1864E+00	-0.4623E-01
-0.002	2.735	0.047	3.455	0.000	0.0000E+00	0.0000E+00	0.1696E+00
0.005	3.995	59.995	0.260	0.004	0.1526E+00	0.1835E+00	-0.3010E-01
0.050	2.624	-0.021	3.415	0.000	0.0000E+00	0.0000E+00	0.1697E+00
0.005	5.005	59.995	0.270	0.004	0.1539E+00	0.1902E+00	-0.1124E-01
0.036	2.721	-0.020	3.752	0.000	0.0000E+00	0.0000E+00	0.1730E+00
0.005	5.995	59.995	0.285	-0.001	0.1623E+00	0.2034E+00	-0.1536E-01
0.062	2.661	0.119	4.546	0.000	0.0000E+00	0.0000E+00	0.1840E+00
0.005	6.995	59.995	0.292	0.003	0.1563E+00	0.1886E+00	0.1953E-01
-0.010	2.796	0.147	3.762	0.000	0.0000E+00	0.0000E+00	0.1732E+00
0.005	8.995	59.995	0.303	0.000	0.1527E+00	0.1911E+00	-0.2365E-01
0.000	2.685	0.035	4.260	0.000	0.0000E+00	0.0000E+00	0.1730E+00
0.005	11.000	59.995	0.316	-0.001	0.1531E+00	0.1669E+00	0.1575E-01
-0.007	2.813	-0.013	3.634	0.000	0.0000E+00	0.0000E+00	0.1738E+00
0.005	13.010	59.995	0.319	0.007	0.1507E+00	0.1860E+00	-0.1575E-01
0.045	2.626	0.060	3.734	0.000	0.0000E+00	0.0000E+00	0.1593E+00
0.005	15.005	59.995	0.325	0.006	0.1502E+00	0.1669E+00	0.3694E-02
-0.021	2.769	0.087	3.790	0.000	0.0000E+00	0.0000E+00	0.1695E+00

FILE NAME: SJ6944KO

e	2b						
0.005	-30.030	5.995	0.340	0.043	0.1563E+00	0.2040E+00	-0.1255E-01
0.044	2.630	-0.014	3.969	0.000	0.0000E+00	0.0000E+00	0.1817E+00
0.005	-24.995	5.995	0.343	0.052	0.1596E+00	0.2047E+00	0.5505E-02
0.045	2.691	0.070	4.115	0.000	0.0000E+00	0.0000E+00	0.1835E+00
0.005	-19.990	5.995	0.344	0.051	0.1561E+00	0.2027E+00	-0.1077E-01
-0.031	2.697	0.049	3.932	0.000	0.0000E+00	0.0000E+00	0.1809E+00
0.005	-14.990	5.995	0.342	0.061	0.1526E+00	0.1932E+00	-0.9378E-02
0.033	2.776	0.045	3.398	0.000	0.0000E+00	0.0000E+00	0.1741E+00
0.005	-13.005	5.995	0.314	0.053	0.1559E+00	0.1911E+00	0.6503E-02
0.049	2.852	0.000	3.519	0.000	0.0000E+00	0.0000E+00	0.1744E+00
0.005	-11.000	5.995	0.244	0.052	0.1506E+00	0.1932E+00	-0.1432E-01
-0.012	2.812	0.118	3.731	0.000	0.0000E+00	0.0000E+00	0.1733E+00
0.005	-9.000	5.995	0.117	0.044	0.1559E+00	0.1935E+00	-0.2255E-01
0.044	2.884	-0.117	3.768	0.000	0.0000E+00	0.0000E+00	0.1737E+00
0.005	-7.005	5.995	0.007	0.029	0.1512E+00	0.1877E+00	0.9975E-02
0.044	2.717	0.089	3.372	0.000	0.0000E+00	0.0000E+00	0.1705E+00
0.005	-6.005	5.995	-0.023	0.025	0.1567E+00	0.1916E+00	-0.3632E-01
0.015	2.941	0.022	3.375	0.000	0.0000E+00	0.0000E+00	0.1750E+00
0.005	-5.005	5.995	-0.034	0.025	0.1471E+00	0.1960E+00	0.7875E-02
0.037	2.757	-0.034	3.709	0.000	0.0000E+00	0.0000E+00	0.1753E+00
0.000	-4.000	5.995	0.006	0.020	0.1546E+00	0.1946E+00	-0.7613E-02
0.016	2.674	-0.053	3.850	0.000	0.0000E+00	0.0000E+00	0.1757E+00
0.000	-3.000	5.995	0.099	0.020	0.1617E+00	0.1924E+00	0.2307E-01
0.031	2.783	0.059	3.457	0.000	0.0000E+00	0.0000E+00	0.1777E+00
0.000	-1.990	5.995	0.336	0.034	0.2092E+00	0.2096E+00	-0.6346E-02
0.054	2.886	0.036	4.425	0.000	0.0000E+00	0.0000E+00	0.2094E+00
0.000	-1.005	5.995	0.482	0.046	0.2433E+00	0.2219E+00	0.3024E-01
0.095	2.739	0.010	4.512	0.000	0.0000E+00	0.0000E+00	0.2329E+00
0.000	-0.010	5.995	0.275	0.037	0.2015E+00	0.2160E+00	0.3531E-01
0.078	2.933	0.186	4.247	0.000	0.0000E+00	0.0000E+00	0.2105E+00
0.000	0.990	5.995	0.093	0.024	0.1658E+00	0.1992E+00	0.5239E-02
0.003	2.813	0.069	4.443	0.000	0.0000E+00	0.0000E+00	0.1833E+00
0.000	2.000	5.995	-0.009	0.012	0.1592E+00	0.1945E+00	0.2359E-01
-0.009	2.903	0.005	3.556	0.000	0.0000E+00	0.0000E+00	0.1777E+00
0.000	3.015	5.995	-0.036	0.007	0.1555E+00	0.1923E+00	-0.2505E-01
0.011	2.715	0.073	3.644	0.000	0.0000E+00	0.0000E+00	0.1749E+00
0.000	4.000	5.995	-0.009	-0.001	0.1578E+00	0.1902E+00	0.2943E-02
-0.023	2.670	-0.014	3.545	0.000	0.0000E+00	0.0000E+00	0.1749E+00
0.000	5.010	5.995	0.049	-0.004	0.1542E+00	0.1960E+00	-0.4323E-03
0.077	2.810	0.037	3.892	0.000	0.0000E+00	0.0000E+00	0.1753E+00
0.000	5.995	5.995	0.112	-0.023	0.1540E+00	0.1922E+00	-0.1337E-01
0.036	2.776	0.057	3.503	0.000	0.0000E+00	0.0000E+00	0.1741E+00
0.000	6.995	5.995	0.154	-0.020	0.1499E+00	0.1946E+00	-0.6736E-03
-0.103	2.773	0.081	3.770	0.000	0.0000E+00	0.0000E+00	0.1737E+00
0.000	8.995	5.995	0.291	-0.029	0.1530E+00	0.1955E+00	0.2935E-01
-0.015	2.631	0.004	3.475	0.000	0.0000E+00	0.0000E+00	0.1755E+00
0.000	11.010	5.995	0.331	-0.026	0.1606E+00	0.2055E+00	-0.1531E-01
0.057	2.746	-0.010	3.713	0.000	0.0000E+00	0.0000E+00	0.1844E+00
0.000	12.990	5.995	0.337	-0.017	0.1601E+00	0.2093E+00	-0.1667E-01
0.039	2.343	0.071	3.793	0.000	0.0000E+00	0.0000E+00	0.1554E+00
0.000	15.015	5.995	0.336	-0.019	0.1539E+00	0.1992E+00	-0.2543E-02
-0.030	2.938	-0.029	3.624	0.000	0.0000E+00	0.0000E+00	0.1730E+00

FILE NAME: SJ3393X0

0.	2θ						
0.000	-29.990	9.995	0.340	0.046	0.1637E+00	0.2164E+00	0.1031E-01
0.037	2.770	0.243	4.643	0.000	0.0000E+00	0.0000E+00	0.1919E+00
0.005	-24.995	9.995	0.339	0.048	0.1575E+00	0.2136E+00	-0.5431E-02
0.043	2.784	0.020	3.770	0.000	0.0000E+00	0.0000E+00	0.1377E+00
0.005	-19.995	9.995	0.345	0.056	0.1638E+00	0.2142E+00	-0.1742E-01
-0.018	3.034	0.036	3.761	0.000	0.0000E+00	0.0000E+00	0.1907E+00
0.005	-14.990	9.995	0.333	0.058	0.1743E+00	0.2127E+00	0.2313E-02
-0.003	3.157	0.071	4.286	0.000	0.0000E+00	0.0000E+00	0.1944E+00
0.005	-13.005	9.995	0.316	0.064	0.1665E+00	0.2113E+00	-0.1657E-01
0.006	2.937	0.145	3.937	0.000	0.0000E+00	0.0000E+00	0.1902E+00
0.005	-11.000	9.995	0.257	0.063	0.1629E+00	0.2070E+00	0.1002E-02
-0.010	2.918	0.029	3.611	0.000	0.0000E+00	0.0000E+00	0.1353E+00
0.005	-9.000	9.995	0.152	0.054	0.1635E+00	0.2007E+00	-0.1237E-01
-0.003	2.934	0.022	4.206	0.000	0.0000E+00	0.0000E+00	0.1331E+00
0.005	-7.005	9.995	0.029	0.035	0.1562E+00	0.1997E+00	0.2537E-01
0.005	2.987	0.043	3.623	0.000	0.0000E+00	0.0000E+00	0.1792E+00
0.005	-5.005	9.995	-0.011	0.030	0.1543E+00	0.2039E+00	0.4146E-01
-0.011	2.722	0.069	3.691	0.000	0.0000E+00	0.0000E+00	0.1608E+00
0.005	-3.005	9.995	-0.018	0.026	0.1663E+00	0.2057E+00	0.1321E-01
0.004	3.192	0.065	3.978	0.000	0.0000E+00	0.0000E+00	0.1370E+00
0.005	-1.000	9.995	0.016	0.016	0.1759E+00	0.2018E+00	-0.3146E-02
0.100	3.110	0.066	3.329	0.000	0.0000E+00	0.0000E+00	0.1393E+00
0.005	-3.000	9.995	0.130	0.014	0.1532E+00	0.1953E+00	-0.1335E-01
0.120	3.239	0.070	4.095	0.000	0.0000E+00	0.0000E+00	0.1693E+00
0.005	-1.995	9.995	0.105	0.025	0.2151E+00	0.2151E+00	-0.6504E-02
0.174	2.953	0.199	3.939	0.000	0.0000E+00	0.0000E+00	0.2151E+00
0.005	-1.005	9.995	0.421	0.041	0.2453E+00	0.2316E+00	0.1453E-01
0.101	4.895	0.327	4.972	0.000	0.0000E+00	0.0000E+00	0.2335E+00
0.005	0.010	9.995	0.323	0.049	0.2199E+00	0.2197E+00	0.3726E-01
0.145	3.157	0.242	4.493	0.000	0.0000E+00	0.0000E+00	0.2198E+00
0.005	0.995	9.995	0.155	0.036	0.1842E+00	0.2098E+00	0.6133E-01
0.075	3.127	0.091	4.561	0.000	0.0000E+00	0.0000E+00	0.1974E+00
0.005	2.005	9.995	0.030	0.018	0.1737E+00	0.2033E+00	0.2762E-01
0.038	3.417	0.013	3.573	0.000	0.0000E+00	0.0000E+00	0.1591E+00
0.005	2.995	9.995	0.007	-0.002	0.1571E+00	0.2003E+00	0.2537E-02
0.030	2.327	0.006	3.601	0.000	0.0000E+00	0.0000E+00	0.1603E+00
0.005	3.995	9.995	0.030	-0.013	0.1592E+00	0.1927E+00	-0.1134E-01
0.039	2.536	0.009	3.692	0.000	0.0000E+00	0.0000E+00	0.1767E+00
0.005	5.010	9.995	0.097	-0.026	0.1593E+00	0.1932E+00	-0.3650E-01
-0.002	2.623	-0.028	3.500	0.000	0.0000E+00	0.0000E+00	0.1771E+00
0.005	6.005	9.995	0.165	-0.032	0.1543E+00	0.1901E+00	-0.3999E-01
-0.015	2.677	0.127	3.639	0.000	0.0000E+00	0.0000E+00	0.1731E+00
0.005	7.005	9.995	0.214	-0.026	0.1666E+00	0.1895E+00	-0.2233E-01
0.003	2.913	0.092	3.646	0.000	0.0000E+00	0.0000E+00	0.1734E+00
0.005	9.015	9.995	0.293	-0.037	0.1543E+00	0.1882E+00	-0.5735E-02
0.050	2.732	0.019	3.778	0.000	0.0000E+00	0.0000E+00	0.1721E+00
0.005	11.020	9.995	0.321	-0.024	0.1568E+00	0.1956E+00	0.2237E-01
-0.010	2.718	0.052	3.556	0.000	0.0000E+00	0.0000E+00	0.1773E+00
0.005	13.010	9.995	0.329	-0.029	0.1546E+00	0.1926E+00	-0.7552E-02
0.012	2.758	0.069	3.831	0.000	0.0000E+00	0.0000E+00	0.1746E+00
0.005	15.015	9.995	0.332	-0.024	0.1540E+00	0.1906E+00	-0.2633E-02
0.020	2.675	-0.003	3.654	0.000	0.0000E+00	0.0000E+00	0.1732E+00

FILE NAME: SJ3930KD

θ	2θ						
0.000	-29.995	20.000	0.334	0.045	0.1540E+00	0.1996E+00	-0.1439E-01
-0.005	2.620	-0.030	3.713	0.000	0.0000E+00	0.0000E+00	0.1733E+00
0.000	-25.000	20.000	0.334	0.042	0.1549E+00	0.2053E+00	-0.3513E-02
0.023	2.643	0.040	3.725	0.000	0.0000E+00	0.0000E+00	0.1719E+00
0.000	-19.995	20.000	0.324	0.052	0.1527E+00	0.2001E+00	-0.1055E-01
0.021	2.729	-0.025	3.630	0.000	0.0000E+00	0.0000E+00	0.1730E+00
0.000	-14.995	20.000	0.319	0.054	0.1520E+00	0.1966E+00	-0.1904E-01
0.006	2.813	-0.005	3.822	0.000	0.0000E+00	0.0000E+00	0.1764E+00
0.000	-13.005	20.000	0.295	0.054	0.1547E+00	0.1966E+00	0.2625E-01
0.012	2.762	0.010	3.757	0.000	0.0000E+00	0.0000E+00	0.1769E+00
0.000	-11.000	20.000	0.262	0.060	0.1590E+00	0.1944E+00	0.3563E-02
-0.015	2.751	0.105	3.951	0.000	0.0000E+00	0.0000E+00	0.1776E+00
0.000	-9.000	20.000	0.193	0.054	0.1583E+00	0.1947E+00	0.3691E-01
-0.037	2.917	-0.004	3.603	0.000	0.0000E+00	0.0000E+00	0.1775E+00
0.000	-7.010	20.000	0.128	0.040	0.1570E+00	0.1931E+00	0.4395E-01
-0.023	2.685	0.015	3.574	0.000	0.0000E+00	0.0000E+00	0.1760E+00
0.000	-5.005	20.000	0.095	0.033	0.1573E+00	0.1962E+00	0.1534E-01
0.049	2.792	0.026	3.557	0.000	0.0000E+00	0.0000E+00	0.1776E+00
0.000	-5.010	20.000	0.073	0.024	0.1567E+00	0.1959E+00	-0.4144E-02
0.069	2.683	-0.020	3.640	0.000	0.0000E+00	0.0000E+00	0.1774E+00
0.000	-3.995	20.000	0.051	0.021	0.1639E+00	0.1948E+00	-0.1774E-01
0.093	2.797	0.001	3.565	0.000	0.0000E+00	0.0000E+00	0.1800E+00
0.000	-3.000	20.000	0.131	0.013	0.2123E+00	0.2178E+00	-0.4990E-01
0.135	3.153	0.065	4.625	0.000	0.0000E+00	0.0000E+00	0.2151E+00
0.000	-2.010	20.000	0.141	0.020	0.2169E+00	0.2076E+00	0.4835E-02
0.265	3.025	0.140	3.809	0.000	0.0000E+00	0.0000E+00	0.2123E+00
0.000	-1.005	20.000	0.151	0.013	0.2201E+00	0.2014E+00	-0.1192E-01
0.359	2.627	-0.001	3.769	0.000	0.0000E+00	0.0000E+00	0.2110E+00
0.000	0.015	20.000	0.140	0.009	0.2080E+00	0.1984E+00	0.4519E-01
0.263	2.858	-0.075	3.753	0.000	0.0000E+00	0.0000E+00	0.2033E+00
0.000	0.995	20.000	0.111	0.001	0.1902E+00	0.1965E+00	0.3833E-03
0.151	2.888	-0.054	3.703	0.000	0.0000E+00	0.0000E+00	0.1876E+00
0.000	1.995	20.000	0.121	0.009	0.1928E+00	0.2035E+00	0.1076E-01
0.163	3.403	-0.046	5.921	0.000	0.0000E+00	0.0000E+00	0.2141E+00
0.000	3.010	20.000	0.135	-0.014	0.1756E+00	0.2262E+00	-0.3545E-01
0.017	2.936	0.023	4.326	0.000	0.0000E+00	0.0000E+00	0.2025E+00
0.000	3.995	19.995	0.156	-0.021	0.1610E+00	0.2040E+00	-0.4251E-01
-0.050	2.623	0.055	4.331	0.000	0.0000E+00	0.0000E+00	0.1838E+00
0.000	5.005	20.000	0.181	-0.030	0.1605E+00	0.1967E+00	-0.3110E-02
0.014	2.677	0.037	3.615	0.000	0.0000E+00	0.0000E+00	0.1806E+00
0.000	5.995	20.000	0.219	-0.029	0.1555E+00	0.1965E+00	-0.1992E-01
0.051	2.744	-0.027	4.095	0.000	0.0000E+00	0.0000E+00	0.1774E+00
0.000	6.995	19.995	0.246	-0.021	0.1596E+00	0.1909E+00	-0.2337E-01
-0.002	2.951	0.124	3.638	0.000	0.0000E+00	0.0000E+00	0.1760E+00
0.000	7.015	19.995	0.287	-0.026	0.1582E+00	0.1972E+00	-0.4029E-03
0.058	2.739	0.042	4.645	0.000	0.0000E+00	0.0000E+00	0.1733E+00
0.000	10.995	20.000	0.305	-0.020	0.1547E+00	0.1870E+00	-0.4326E-02
0.047	2.673	0.079	3.504	0.000	0.0000E+00	0.0000E+00	0.1716E+00
0.000	13.020	19.995	0.315	-0.016	0.1539E+00	0.1913E+00	-0.1315E-01
-0.003	2.716	0.067	3.488	0.000	0.0000E+00	0.0000E+00	0.1736E+00
0.000	15.015	19.995	0.319	-0.021	0.1566E+00	0.1935E+00	0.4664E-02
0.046	2.792	0.023	3.697	0.000	0.0000E+00	0.0000E+00	0.1760E+00

FILE NAME: SJ5976XO

6	26						
-0.005	-29.995	40.005	0.321	0.035	0.1578E+00	0.1976E+00	-0.6793E-02
0.029	2.739	0.019	3.649	0.000	0.0000E+00	0.0000E+00	0.1733E+00
-0.005	-25.000	40.000	0.314	0.042	0.1543E+00	0.2046E+00	-0.5776E-02
0.045	2.751	-0.016	3.957	0.000	0.0000E+00	0.0000E+00	0.1812E+00
-0.005	-20.000	40.000	0.312	0.034	0.1590E+00	0.1975E+00	0.2443E-02
0.014	2.877	0.056	3.656	0.000	0.0000E+00	0.0000E+00	0.1793E+00
-0.005	-14.995	40.000	0.303	0.034	0.1540E+00	0.1916E+00	0.1308E-02
-0.013	2.745	0.013	3.686	0.000	0.0000E+00	0.0000E+00	0.1732E+00
-0.005	-13.005	40.000	0.286	0.044	0.1553E+00	0.1909E+00	0.2507E-01
0.008	2.653	0.041	3.856	0.000	0.0000E+00	0.0000E+00	0.1740E+00
-0.005	-11.000	40.000	0.275	0.039	0.1548E+00	0.1959E+00	0.1526E-01
-0.007	2.826	0.090	3.615	0.000	0.0000E+00	0.0000E+00	0.1732E+00
-0.005	-9.000	40.000	0.247	0.037	0.1777E+00	0.2212E+00	0.1253E-01
-0.005	3.147	-0.010	4.155	0.000	0.0000E+00	0.0000E+00	0.2039E+00
-0.005	-5.990	40.000	0.220	0.039	0.1569E+00	0.2069E+00	0.2591E-01
0.059	2.650	0.125	3.870	0.000	0.0000E+00	0.0000E+00	0.1935E+00
-0.005	-5.000	40.000	0.211	0.035	0.1557E+00	0.1996E+00	0.1590E-01
0.006	2.750	-0.030	3.827	0.000	0.0000E+00	0.0000E+00	0.1791E+00
-0.005	-3.010	40.000	0.192	0.030	0.1627E+00	0.2018E+00	0.1035E-01
0.015	2.847	0.024	3.874	0.000	0.0000E+00	0.0000E+00	0.1833E+00
-0.005	-3.995	40.000	0.185	0.024	0.1659E+00	0.2016E+00	-0.2595E-01
0.051	2.809	0.044	3.605	0.000	0.0000E+00	0.0000E+00	0.1865E+00
-0.005	-3.000	40.000	0.190	0.019	0.1795E+00	0.2045E+00	-0.2593E-01
0.096	2.822	0.016	3.844	0.000	0.0000E+00	0.0000E+00	0.1927E+00
-0.005	-2.010	40.000	0.189	0.007	0.1782E+00	0.1995E+00	-0.1150E-01
0.023	2.795	0.066	3.485	0.000	0.0000E+00	0.0000E+00	0.1892E+00
-0.005	-1.005	40.000	0.185	-0.002	0.1702E+00	0.1977E+00	0.1321E-01
0.105	2.904	-0.009	3.677	0.000	0.0000E+00	0.0000E+00	0.1844E+00
-0.005	-0.010	40.000	0.189	0.002	0.1622E+00	0.2166E+00	0.2498E-01
0.046	3.146	0.197	4.541	0.000	0.0000E+00	0.0000E+00	0.2031E+00
-0.005	0.990	40.000	0.195	-0.003	0.1649E+00	0.2033E+00	-0.2941E-01
0.063	2.743	0.059	3.539	0.000	0.0000E+00	0.0000E+00	0.1851E+00
-0.005	2.000	40.000	0.217	-0.001	0.1633E+00	0.1977E+00	0.1073E-02
0.090	2.850	0.045	3.556	0.000	0.0000E+00	0.0000E+00	0.1814E+00
-0.005	3.010	40.000	0.223	-0.008	0.1606E+00	0.1965E+00	-0.1055E-01
0.008	2.735	0.040	3.734	0.000	0.0000E+00	0.0000E+00	0.1775E+00
-0.005	3.995	40.000	0.235	-0.009	0.1616E+00	0.1990E+00	-0.1550E-01
0.017	2.973	0.125	3.692	0.000	0.0000E+00	0.0000E+00	0.1812E+00
-0.005	4.995	40.000	0.249	-0.010	0.1543E+00	0.1931E+00	-0.1757E-01
-0.003	2.637	0.010	3.962	0.000	0.0000E+00	0.0000E+00	0.1747E+00
-0.005	6.005	40.000	0.265	-0.011	0.1563E+00	0.1951E+00	-0.4994E-01
-0.043	2.919	0.022	3.800	0.000	0.0000E+00	0.0000E+00	0.1767E+00
-0.005	6.995	40.000	0.275	-0.008	0.1596E+00	0.1963E+00	0.4749E-02
0.037	2.757	0.167	3.732	0.000	0.0000E+00	0.0000E+00	0.1739E+00
-0.005	8.995	40.000	0.289	-0.009	0.1521E+00	0.1873E+00	-0.5577E-02
0.017	2.771	0.002	3.414	0.000	0.0000E+00	0.0000E+00	0.1736E+00
-0.005	10.995	40.000	0.299	-0.005	0.1576E+00	0.1907E+00	-0.2736E-01
-0.028	2.934	0.017	3.555	0.000	0.0000E+00	0.0000E+00	0.1749E+00
-0.005	13.010	40.000	0.305	-0.006	0.1607E+00	0.2085E+00	-0.2052E-02
-0.059	2.973	0.055	3.986	0.000	0.0000E+00	0.0000E+00	0.1852E+00
-0.005	14.990	40.000	0.307	-0.006	0.1706E+00	0.2222E+00	-0.6139E-03
-0.027	2.964	0.152	4.512	0.000	0.0000E+00	0.0000E+00	0.1981E+00

FILE NAME: 3J9J0240

6	27						
-0.005	-29.993	60.005	0.323	0.026	0.1590E+00	0.2000E+00	-0.3148E-01
0.012	2.732	0.056	3.936	0.000	0.0000E+00	0.0000E+00	0.1807E+00
-0.005	-24.990	60.000	0.319	0.031	0.1564E+00	0.2050E+00	-0.1917E-01
0.047	2.671	0.072	4.246	0.000	0.0000E+00	0.0000E+00	0.1840E+00
-0.005	-19.995	60.000	0.314	0.024	0.1615E+00	0.1953E+00	-0.6523E-02
-0.038	3.049	0.130	3.941	0.000	0.0000E+00	0.0000E+00	0.1792E+00
-0.005	-14.995	60.000	0.306	0.026	0.1574E+00	0.1977E+00	0.1223E-01
-0.039	2.759	0.021	3.744	0.000	0.0000E+00	0.0000E+00	0.1736E+00
-0.005	-13.005	60.000	0.299	0.026	0.1540E+00	0.1937E+00	-0.6622E-02
-0.036	2.727	-0.011	3.677	0.000	0.0000E+00	0.0000E+00	0.1750E+00
-0.005	-11.000	60.000	0.287	0.036	0.1756E+00	0.2226E+00	-0.5292E-02
-0.041	3.264	0.077	4.481	0.000	0.0000E+00	0.0000E+00	0.2005E+00
-0.005	-6.990	60.000	0.266	0.019	0.1861E+00	0.2354E+00	0.6024E-02
0.002	3.159	0.113	4.767	0.000	0.0000E+00	0.0000E+00	0.2131E+00
-0.005	-6.990	60.000	0.250	0.016	0.1799E+00	0.2195E+00	-0.7914E-03
0.095	3.295	0.170	5.075	0.000	0.0000E+00	0.0000E+00	0.2007E+00
-0.005	-5.005	60.000	0.249	0.029	0.1640E+00	0.2053E+00	-0.1213E-01
0.001	2.565	0.036	3.649	0.000	0.0000E+00	0.0000E+00	0.1959E+00
-0.005	-3.010	60.000	0.241	0.020	0.1625E+00	0.1992E+00	0.2197E-02
0.015	2.767	0.070	3.429	0.000	0.0000E+00	0.0000E+00	0.1513E+00
-0.005	-3.995	60.000	0.235	0.018	0.1593E+00	0.2029E+00	0.5034E-02
0.068	2.735	0.051	3.275	0.000	0.0000E+00	0.0000E+00	0.1824E+00
-0.005	-3.000	60.000	0.230	0.015	0.1595E+00	0.1944E+00	-0.1502E-01
0.053	2.659	0.055	3.775	0.000	0.0000E+00	0.0000E+00	0.1778E+00
-0.005	-2.010	60.000	0.227	0.018	0.1505E+00	0.1956E+00	-0.7201E-02
0.016	2.656	0.075	3.564	0.000	0.0000E+00	0.0000E+00	0.1307E+00
-0.005	-1.005	60.000	0.230	0.013	0.1640E+00	0.1962E+00	-0.1275E-02
-0.026	2.918	-0.025	3.274	0.000	0.0000E+00	0.0000E+00	0.1603E+00
-0.005	-0.010	60.000	0.231	0.015	0.1654E+00	0.1978E+00	-0.9509E-02
0.011	2.645	0.022	3.746	0.000	0.0000E+00	0.0000E+00	0.1523E+00
-0.005	1.005	60.000	0.236	0.010	0.1572E+00	0.1977E+00	0.4144E-02
-0.016	2.760	0.081	3.480	0.000	0.0000E+00	0.0000E+00	0.1756E+00
-0.005	1.993	60.000	0.245	0.001	0.1592E+00	0.1962E+00	-0.2241E-01
0.077	2.778	0.019	3.509	0.000	0.0000E+00	0.0000E+00	0.1736E+00
-0.005	2.990	60.000	0.252	0.002	0.1671E+00	0.2046E+00	-0.4395E-01
0.013	2.521	0.017	3.608	0.000	0.0000E+00	0.0000E+00	0.1637E+00
-0.005	3.995	60.000	0.263	0.006	0.2045E+00	0.2513E+00	-0.2048E-01
0.004	3.175	-0.162	5.537	0.000	0.0000E+00	0.0000E+00	0.2292E+00
-0.005	4.995	60.000	0.271	0.000	0.1792E+00	0.2219E+00	-0.4573E-01
0.061	3.070	0.197	4.135	0.000	0.0000E+00	0.0000E+00	0.2012E+00
-0.005	5.005	60.000	0.273	0.002	0.1651E+00	0.2023E+00	-0.3930E-01
0.006	2.854	0.112	4.052	0.000	0.0000E+00	0.0000E+00	0.1846E+00
-0.005	5.995	60.000	0.276	-0.001	0.1612E+00	0.1934E+00	-0.4016E-01
0.010	2.791	-0.061	3.365	0.000	0.0000E+00	0.0000E+00	0.1750E+00
-0.005	6.995	60.000	0.287	-0.005	0.1573E+00	0.1981E+00	-0.9527E-02
0.041	2.536	0.069	3.674	0.000	0.0000E+00	0.0000E+00	0.1739E+00
-0.005	8.970	60.000	0.292	0.002	0.1534E+00	0.1989E+00	-0.3532E-02
0.021	2.742	0.116	3.676	0.000	0.0000E+00	0.0000E+00	0.1793E+00
-0.005	10.995	60.000	0.306	0.000	0.1602E+00	0.1961E+00	-0.1717E-01
-0.016	2.572	0.016	4.142	0.000	0.0000E+00	0.0000E+00	0.1302E+00
-0.005	13.005	60.000	0.311	0.008	0.1596E+00	0.1973E+00	-0.4103E-03
0.054	2.657	0.129	3.574	0.000	0.0000E+00	0.0000E+00	0.1794E+00
-0.005	14.990	60.000	0.316	0.004	0.1548E+00	0.1964E+00	-0.5412E-02
0.001	2.510	0.137	3.742	0.000	0.0000E+00	0.0000E+00	0.1755E+00

FILE NAME: SJ9239X0

0.005	-30.035	5.995	0.342	0.040	0.1475E+00	0.1376E+00	0.1350E-01
0.030	2.754	0.006	3.541	0.000	0.0000E+00	0.0000E+00	0.1537E+00
0.005	-24.990	5.995	0.347	0.044	0.1518E+00	0.1914E+00	0.1010E-01
-0.033	2.370	0.103	3.625	0.000	0.0000E+00	0.0000E+00	0.1727E+00
0.005	-20.005	5.995	0.352	0.055	0.1502E+00	0.1889E+00	0.1643E-02
-0.034	2.787	0.064	3.573	0.000	0.0000E+00	0.0000E+00	0.1705E+00
0.005	-16.995	5.995	0.345	0.056	0.1529E+00	0.1916E+00	0.2370E-02
-0.034	2.834	0.050	3.557	0.000	0.0000E+00	0.0000E+00	0.1680E+00
0.005	-13.010	5.995	0.319	0.059	0.1479E+00	0.1827E+00	-0.3993E-02
0.027	2.895	0.023	3.564	0.000	0.0000E+00	0.0000E+00	0.1652E+00
0.005	-11.010	5.995	0.255	0.045	0.1493E+00	0.1831E+00	-0.1701E-01
-0.012	2.796	0.010	3.591	0.000	0.0000E+00	0.0000E+00	0.1673E+00
0.005	-5.990	5.995	0.128	0.045	0.1552E+00	0.1801E+00	0.1339E-01
-0.010	3.020	0.067	3.464	0.000	0.0000E+00	0.0000E+00	0.1531E+00
0.005	-7.005	5.995	0.010	0.025	0.1489E+00	0.1823E+00	0.1259E-01
-0.032	2.719	0.169	3.911	0.000	0.0000E+00	0.0000E+00	0.1554E+00
0.005	-5.995	5.995	-0.023	0.023	0.1567E+00	0.1694E+00	-0.1330E-01
-0.003	2.890	-0.021	3.602	0.000	0.0000E+00	0.0000E+00	0.1735E+00
0.005	-4.985	5.995	-0.039	0.024	0.1509E+00	0.1875E+00	-0.2356E-01
0.037	2.837	0.037	3.512	0.000	0.0000E+00	0.0000E+00	0.1732E+00
0.005	-4.005	5.995	-0.010	0.028	0.1568E+00	0.1540E+00	0.9070E-02
0.034	2.750	0.105	3.621	0.000	0.0000E+00	0.0000E+00	0.1715E+00
0.005	-3.000	5.995	0.094	0.024	0.1544E+00	0.1547E+00	-0.2250E-01
0.032	2.318	0.131	3.639	0.000	0.0000E+00	0.0000E+00	0.1732E+00
0.005	-2.015	5.995	0.309	0.032	0.2066E+00	0.2473E+00	0.5556E-02
0.235	4.093	0.176	5.359	0.000	0.0000E+00	0.0000E+00	0.2279E+00
0.005	-1.005	5.995	0.455	0.056	0.2138E+00	0.2412E+00	-0.2152E-02
0.001	3.477	0.229	5.318	0.000	0.0000E+00	0.0000E+00	0.2239E+00
0.005	0.015	5.995	0.353	0.054	0.2049E+00	0.2512E+00	0.5026E-02
0.043	3.476	0.275	5.672	0.000	0.0000E+00	0.0000E+00	0.2292E+00
0.005	0.995	5.995	0.125	0.031	0.1520E+00	0.1889E+00	0.4266E-02
0.032	2.755	0.153	3.923	0.000	0.0000E+00	0.0000E+00	0.1715E+00
0.005	2.005	5.995	-0.008	0.013	0.1574E+00	0.1841E+00	0.1574E-01
0.029	2.952	0.021	3.659	0.000	0.0000E+00	0.0000E+00	0.1713E+00
0.005	3.010	5.995	-0.035	0.010	0.1559E+00	0.1843E+00	0.5733E-02
0.044	3.010	0.144	3.456	0.000	0.0000E+00	0.0000E+00	0.1707E+00
0.005	3.995	5.995	-0.016	0.000	0.1500E+00	0.1814E+00	0.3545E-02
-0.020	2.655	0.031	3.440	0.000	0.0000E+00	0.0000E+00	0.1665E+00
0.005	4.995	5.995	0.035	-0.007	0.1518E+00	0.1797E+00	-0.2052E-01
0.022	2.757	0.035	3.434	0.000	0.0000E+00	0.0000E+00	0.1653E+00
0.005	6.000	5.995	0.104	-0.009	0.1536E+00	0.1841E+00	0.5295E-02
-0.039	2.834	0.013	3.643	0.000	0.0000E+00	0.0000E+00	0.1675E+00
0.005	5.995	5.995	0.179	-0.020	0.1573E+00	0.1863E+00	-0.2077E-01
-0.035	2.758	0.119	4.095	0.000	0.0000E+00	0.0000E+00	0.1724E+00
0.005	7.015	5.995	0.291	-0.025	0.1522E+00	0.1860E+00	-0.2120E-01
0.016	2.653	0.038	3.615	0.000	0.0000E+00	0.0000E+00	0.1711E+00
0.005	11.000	5.995	0.332	-0.031	0.1539E+00	0.1881E+00	-0.5005E-02
0.034	2.787	0.046	3.470	0.000	0.0000E+00	0.0000E+00	0.1718E+00
0.005	12.935	5.995	0.342	-0.023	0.1515E+00	0.1872E+00	0.2368E-02
0.036	2.683	0.090	3.602	0.000	0.0000E+00	0.0000E+00	0.1703E+00
0.005	15.000	5.995	0.342	-0.020	0.1520E+00	0.1895E+00	-0.1071E-01
0.002	2.796	0.031	3.433	0.000	0.0000E+00	0.0000E+00	0.1713E+00

FILE NAME: SJ9315X0

J	25						
0.005	-27.990	10.005	0.341	0.042	0.1466E+00	0.1662E+00	0.2213E-01
0.019	2.639	-0.037	3.357	0.000	0.0000E+00	0.0000E+00	0.1676E+00
0.005	-25.000	10.005	0.344	0.045	0.1481E+00	0.1665E+00	0.9890E-02
0.015	2.799	0.043	3.639	0.000	0.0000E+00	0.0000E+00	0.1675E+00
0.005	-23.005	10.005	0.343	0.053	0.1468E+00	0.1633E+00	-0.3132E-03
0.007	2.675	-0.004	3.650	0.000	0.0000E+00	0.0000E+00	0.1650E+00
0.005	-15.005	10.005	0.339	0.066	0.1520E+00	0.1660E+00	0.2203E-02
-0.029	2.758	-0.023	3.683	0.000	0.0000E+00	0.0000E+00	0.1699E+00
0.005	-12.990	10.005	0.321	0.062	0.1466E+00	0.1690E+00	-0.3177E-02
0.037	2.663	0.022	3.914	0.000	0.0000E+00	0.0000E+00	0.1700E+00
0.005	-11.010	10.005	0.269	0.070	0.1428E+00	0.1642E+00	0.5961E-02
0.008	2.757	0.013	3.394	0.000	0.0000E+00	0.0000E+00	0.1549E+00
0.005	-9.990	10.005	0.161	0.061	0.1498E+00	0.1542E+00	-0.1032E-01
-0.024	2.810	-0.038	3.442	0.000	0.0000E+00	0.0000E+00	0.1679E+00
0.005	-7.010	10.005	0.054	0.033	0.1487E+00	0.1905E+00	0.5529E-02
0.042	2.713	-0.110	4.057	0.000	0.0000E+00	0.0000E+00	0.1739E+00
0.005	-5.995	10.005	-0.013	0.038	0.1611E+00	0.1693E+00	-0.5549E-02
-0.010	3.039	0.015	3.636	0.000	0.0000E+00	0.0000E+00	0.1753E+00
0.005	-5.005	10.005	-0.034	0.025	0.1563E+00	0.1695E+00	-0.3074E-01
-0.029	2.879	0.045	3.713	0.000	0.0000E+00	0.0000E+00	0.1737E+00
0.005	-4.005	10.005	0.008	0.019	0.1546E+00	0.1911E+00	-0.7316E-02
-0.039	2.601	-0.065	3.764	0.000	0.0000E+00	0.0000E+00	0.1738E+00
0.005	-3.000	10.005	0.123	0.021	0.1594E+00	0.1857E+00	0.2386E-01
-0.017	2.718	0.067	3.963	0.000	0.0000E+00	0.0000E+00	0.1752E+00
0.005	-1.990	10.005	0.299	0.028	0.2007E+00	0.2285E+00	-0.2511E-02
0.146	3.335	-0.041	5.133	0.000	0.0000E+00	0.0000E+00	0.2151E+00
0.005	-1.000	10.005	0.427	0.044	0.2207E+00	0.2473E+00	0.3296E-02
0.027	3.527	0.295	5.275	0.000	0.0000E+00	0.0000E+00	0.2344E+00
0.005	0.015	10.005	0.533	0.048	0.2003E+00	0.2334E+00	0.5530E-01
0.037	3.082	0.324	5.715	0.000	0.0000E+00	0.0000E+00	0.2175E+00
0.005	0.995	10.005	0.153	0.014	0.1676E+00	0.1965E+00	0.3933E-01
0.042	3.025	0.019	4.034	0.000	0.0000E+00	0.0000E+00	0.1837E+00
0.005	2.005	10.005	0.021	0.016	0.1630E+00	0.1916E+00	0.4235E-01
0.020	3.047	0.091	4.053	0.000	0.0000E+00	0.0000E+00	0.1779E+00
0.005	2.995	10.005	-0.003	0.006	0.1674E+00	0.1991E+00	0.1393E-01
-0.046	2.989	0.075	3.623	0.000	0.0000E+00	0.0000E+00	0.1859E+00
0.005	3.985	10.005	0.019	-0.010	0.1581E+00	0.1999E+00	-0.7372E-02
0.004	2.812	-0.009	4.207	0.000	0.0000E+00	0.0000E+00	0.1802E+00
0.005	4.985	10.005	0.077	-0.017	0.1609E+00	0.1942E+00	-0.1636E-01
0.071	2.959	-0.015	3.943	0.000	0.0000E+00	0.0000E+00	0.1733E+00
0.005	5.000	10.005	0.146	-0.029	0.1568E+00	0.1907E+00	-0.2214E-01
-0.021	2.896	0.135	3.804	0.000	0.0000E+00	0.0000E+00	0.1745E+00
0.005	7.000	10.005	0.205	-0.029	0.1609E+00	0.1854E+00	0.2934E-02
-0.017	2.995	0.119	3.542	0.000	0.0000E+00	0.0000E+00	0.1736E+00
0.005	9.010	10.005	0.285	-0.034	0.1547E+00	0.1896E+00	0.1073E-02
-0.037	2.653	0.041	3.987	0.000	0.0000E+00	0.0000E+00	0.1731E+00
0.005	11.010	10.005	0.325	-0.036	0.1525E+00	0.1875E+00	-0.4930E-01
0.006	2.693	0.024	3.634	0.000	0.0000E+00	0.0000E+00	0.1709E+00
0.005	12.990	10.005	0.334	-0.029	0.1565E+00	0.1854E+00	0.1459E-01
0.005	2.756	0.013	3.707	0.000	0.0000E+00	0.0000E+00	0.1715E+00
0.005	14.935	10.005	0.335	-0.022	0.1517E+00	0.1930E+00	0.5504E-02
-0.043	2.751	0.165	3.876	0.000	0.0000E+00	0.0000E+00	0.1735E+00

FILE NAME: SJ9341XD

a	2a						
0.005	-29.995	20.005	0.339	0.045	0.1557E+00	0.1562E+00	0.1413E-02
0.003	2.334	0.150	3.731	0.000	0.0000E+00	0.0000E+00	0.1715E+00
0.005	-24.990	[illegible]	[illegible]	0.049	0.1434E+00	0.1920E+00	0.1323E-01
-0.027	[illegible]	[illegible]	[illegible]	0.000	0.0000E+00	0.0000E+00	0.1720E+00
[illegible]	-1[illegible]	[illegible]	0.330	0.051	0.1530E+00	0.1911E+00	0.1530E-01
-0.007	[illegible]	[illegible]	3.633	0.000	0.0000E+00	0.0000E+00	0.1731E+00
[illegible]	-14.995	[illegible]	0.322	0.060	0.1362E+00	0.1942E+00	-0.2751E-02
[illegible]	[illegible]	0.[illegible]	3.903	0.000	0.0000E+00	0.0000E+00	0.1753E+00
0.005	-13.025	20.005	0.305	0.062	0.1531E+00	0.1840E+00	0.3104E-03
0.005	[illegible]	0.032	3.272	0.000	0.0000E+00	0.0000E+00	0.1535E+00
0.005	-12.995	20.005	0.272	0.064	0.1489E+00	0.1870E+00	-0.1740E-02
0.005	2.733	0.004	3.650	0.000	0.0000E+00	0.0000E+00	0.1691E+00
0.005	-7.005	20.005	0.205	0.065	0.1502E+00	0.2265E+00	0.1821E-01
0.005	5.252	0.315	3.317	0.000	0.0000E+00	0.0000E+00	0.2053E+00
0.003	-5.990	20.005	0.139	0.058	0.1704E+00	0.2153E+00	0.9350E-02
0.075	5.125	0.043	4.790	0.000	0.0000E+00	0.0000E+00	0.1942E+00
0.005	-5.990	20.000	0.135	0.045	0.1604E+00	0.2102E+00	-0.2935E-01
0.030	2.817	0.118	4.127	0.000	0.0000E+00	0.0000E+00	0.1870E+00
0.005	-5.015	20.005	0.155	0.021	0.1754E+00	0.2144E+00	-0.1258E+00
0.060	2.878	0.076	3.483	0.000	0.0000E+00	0.0000E+00	0.1959E+00
0.005	-4.005	20.005	0.191	0.005	0.1810E+00	0.2265E+00	-0.1354E+00
0.024	2.755	0.135	3.904	0.000	0.0000E+00	0.0000E+00	0.2052E+00
0.005	-3.000	20.005	0.215	-0.003	0.1807E+00	0.2178E+00	-0.1233E+00
0.005	2.945	0.107	3.744	0.000	0.0000E+00	0.0000E+00	0.2031E+00
0.005	-2.005	20.005	0.218	0.005	0.1693E+00	0.2155E+00	-0.3542E-01
-0.025	3.233	-0.107	3.847	0.000	0.0000E+00	0.0000E+00	0.1940E+00
0.005	-1.010	20.005	0.221	0.025	0.1633E+00	0.2151E+00	0.5939E-01
-0.007	3.073	0.039	3.795	0.000	0.0000E+00	0.0000E+00	0.1910E+00
0.005	-0.010	20.005	0.237	0.035	0.1692E+00	0.2097E+00	0.3775E-01
0.093	2.641	0.202	4.439	0.000	0.0000E+00	0.0000E+00	0.1905E+00
0.005	0.990	20.005	0.217	0.040	0.1825E+00	0.2155E+00	0.1531E+00
0.040	2.900	0.111	3.963	0.000	0.0000E+00	0.0000E+00	0.1997E+00
0.005	2.000	20.005	0.195	0.029	0.1803E+00	0.2129E+00	0.1593E+00
0.071	2.952	0.160	4.014	0.000	0.0000E+00	0.0000E+00	0.1973E+00
0.005	3.010	20.005	0.151	0.011	0.1647E+00	0.2002E+00	0.5417E-01
-0.024	2.895	0.063	3.499	0.000	0.0000E+00	0.0000E+00	0.1533E+00
0.005	5.995	20.005	0.139	-0.008	0.1595E+00	0.1926E+00	-0.5750E-02
-0.011	2.987	0.013	3.645	0.000	0.0000E+00	0.0000E+00	0.1759E+00
0.005	5.010	20.005	0.171	-0.024	0.1523E+00	0.1938E+00	-0.3324E-01
0.000	2.634	-0.055	4.053	0.000	0.0000E+00	0.0000E+00	0.1743E+00
0.005	5.995	20.005	0.211	-0.027	0.1538E+00	0.1855E+00	-0.1330E-01
-0.007	2.769	0.011	3.785	0.000	0.0000E+00	0.0000E+00	0.1704E+00
0.005	7.015	20.005	0.243	-0.030	0.1524E+00	0.1659E+00	0.5013E-02
0.011	2.921	0.082	3.931	0.000	0.0000E+00	0.0000E+00	0.1599E+00
0.005	5.995	20.005	0.275	-0.029	0.1513E+00	0.1565E+00	0.6133E-02
0.054	2.770	0.054	4.003	0.000	0.0000E+00	0.0000E+00	0.1593E+00
0.005	11.010	20.005	0.303	-0.026	0.1526E+00	0.1892E+00	0.1139E-01
0.057	2.807	0.053	3.709	0.000	0.0000E+00	0.0000E+00	0.1719E+00
0.005	12.990	20.005	0.319	-0.026	0.1490E+00	0.1876E+00	0.3799E-02
0.020	2.764	0.022	3.537	0.000	0.0000E+00	0.0000E+00	0.1594E+00
0.005	14.995	20.005	0.320	-0.018	0.1524E+00	0.1911E+00	-0.3431E-01
0.024	2.782	-0.007	3.515	0.000	0.0000E+00	0.0000E+00	0.1729E+00

FILE NAME: SJ9367X0

θ	2θ						
0.005	-30.010	40.005	0.337	0.032	0.1534E+00	0.1831E+00	-0.4157E-02
0.050	2.737	-0.040	3.775	0.000	0.0000E+00	0.0000E+00	0.1579E+00
0.005	-25.000	40.000	0.332	0.035	0.1527E+00	0.1661E+00	0.2790E-02
0.024	2.738	0.069	3.601	0.000	0.0000E+00	0.0000E+00	0.1702E+00
0.005	-19.995	40.000	0.329	0.033	0.1500E+00	0.1914E+00	0.1125E-01
0.002	2.777	0.006	3.748	0.000	0.0000E+00	0.0000E+00	0.1719E+00
0.005	-14.995	40.000	0.318	0.033	0.1517E+00	0.1831E+00	-0.1203E-01
-0.011	2.746	0.172	3.613	0.000	0.0000E+00	0.0000E+00	0.1681E+00
0.005	-13.010	40.000	0.312	0.033	0.1525E+00	0.1876E+00	0.2493E-01
0.054	2.862	-0.042	3.394	0.000	0.0000E+00	0.0000E+00	0.1710E+00
0.005	-11.010	40.000	0.295	0.025	0.1507E+00	0.1667E+00	0.2767E-01
-0.017	2.927	0.032	3.522	0.000	0.0000E+00	0.0000E+00	0.1697E+00
0.005	-8.990	40.000	0.271	0.030	0.1591E+00	0.1887E+00	0.1798E-01
-0.016	2.901	0.019	3.648	0.000	0.0000E+00	0.0000E+00	0.1745E+00
0.005	-7.000	40.000	0.254	0.031	0.1566E+00	0.1941E+00	-0.2572E-01
0.049	2.790	-0.043	4.064	0.000	0.0000E+00	0.0000E+00	0.1763E+00
0.005	-5.995	40.000	0.237	0.029	0.1597E+00	0.1949E+00	-0.1343E-01
-0.041	3.037	0.027	3.760	0.000	0.0000E+00	0.0000E+00	0.1782E+00
0.005	-5.010	40.000	0.219	0.027	0.1558E+00	0.1996E+00	0.6334E-02
-0.004	2.540	0.044	3.710	0.000	0.0000E+00	0.0000E+00	0.1790E+00
0.005	-4.010	40.000	0.203	0.023	0.1567E+00	0.2048E+00	0.1740E-01
-0.004	2.936	-0.057	3.946	0.000	0.0000E+00	0.0000E+00	0.1523E+00
0.005	-3.005	40.000	0.195	0.024	0.1601E+00	0.2045E+00	0.1553E-01
0.009	3.122	0.024	3.678	0.000	0.0000E+00	0.0000E+00	0.1356E+00
0.005	-2.005	40.000	0.189	0.014	0.1575E+00	0.2087E+00	-0.3355E-01
0.003	3.151	0.067	3.747	0.000	0.0000E+00	0.0000E+00	0.1349E+00
0.005	-1.010	40.000	0.200	0.023	0.1571E+00	0.2053E+00	0.2203E-01
0.005	3.050	0.059	3.795	0.000	0.0000E+00	0.0000E+00	0.1323E+00
0.005	-0.020	40.000	0.203	0.016	0.1545E+00	0.1956E+00	-0.6773E-02
0.035	2.796	0.095	3.642	0.000	0.0000E+00	0.0000E+00	0.1779E+00
0.005	0.995	40.000	0.212	0.018	0.1588E+00	0.1984E+00	0.2792E-01
-0.041	3.049	0.130	4.050	0.000	0.0000E+00	0.0000E+00	0.1797E+00
0.005	1.990	40.000	0.233	0.011	0.1638E+00	0.2023E+00	0.1760E-01
0.033	2.922	0.127	3.881	0.000	0.0000E+00	0.0000E+00	0.1841E+00
0.005	2.995	40.000	0.250	0.012	0.1586E+00	0.1947E+00	0.2212E-01
0.030	2.753	0.009	3.555	0.000	0.0000E+00	0.0000E+00	0.1775E+00
0.005	3.995	40.000	0.263	0.015	0.1592E+00	0.1920E+00	0.3310E-02
0.011	2.636	0.023	3.497	0.000	0.0000E+00	0.0000E+00	0.1764E+00
0.005	5.010	40.000	0.267	0.010	0.1559E+00	0.1909E+00	0.1338E-01
-0.033	2.972	-0.069	4.246	0.000	0.0000E+00	0.0000E+00	0.1743E+00
0.005	6.000	40.000	0.276	0.009	0.1587E+00	0.1915E+00	-0.2503E-01
0.065	2.938	0.025	4.106	0.000	0.0000E+00	0.0000E+00	0.1759E+00
0.005	6.995	40.000	0.283	0.003	0.1509E+00	0.1648E+00	-0.3563E-02
0.026	2.780	-0.045	3.798	0.000	0.0000E+00	0.0000E+00	0.1687E+00
0.005	9.010	40.000	0.303	-0.003	0.1514E+00	0.1627E+00	-0.1069E-02
-0.016	2.738	-0.120	3.552	0.000	0.0000E+00	0.0000E+00	0.1673E+00
0.005	11.010	40.000	0.312	0.001	0.1486E+00	0.1871E+00	-0.6591E-02
0.008	2.740	-0.039	3.513	0.000	0.0000E+00	0.0000E+00	0.1689E+00
0.005	12.995	40.000	0.320	0.007	0.1600E+00	0.1903E+00	-0.2532E-01
0.063	2.993	0.037	3.639	0.000	0.0000E+00	0.0000E+00	0.1758E+00
0.005	15.010	40.000	0.322	-0.001	0.1572E+00	0.1860E+00	-0.9007E-02
0.012	2.849	-0.053	4.016	0.000	0.0000E+00	0.0000E+00	0.1735E+00

FILE NAME: SJ9393X0

3 27

0.005	-50.015	59.995	0.336	0.023	0.1478E+00	0.1519E+00	-0.9021E-02
0.051	2.772	0.070	3.490	0.000	0.0000E+00	0.0000E+00	0.1657E+00
0.005	-25.010	59.995	0.332	0.029	0.1499E+00	0.1806E+00	0.1412E-01
0.057	2.742	0.033	3.459	0.000	0.0000E+00	0.0000E+00	0.1660E+00
0.005	-19.995	59.995	0.334	0.025	0.1527E+00	0.1865E+00	-0.1307E-01
0.025	2.828	0.030	3.827	0.000	0.0000E+00	0.0000E+00	0.1715E+00
0.005	-14.990	60.000	0.321	0.023	0.1508E+00	0.1826E+00	0.1755E-01
0.003	2.790	0.001	3.852	0.000	0.0000E+00	0.0000E+00	0.1674E+00
0.005	-13.010	60.000	0.320	0.020	0.1535E+00	0.1814E+00	0.4701E-03
0.002	2.766	0.026	3.437	0.000	0.0000E+00	0.0000E+00	0.1630E+00
0.005	-11.005	60.000	0.310	0.029	0.1562E+00	0.1927E+00	0.6062E-02
0.076	2.963	-0.022	3.691	0.000	0.0000E+00	0.0000E+00	0.1754E+00
0.005	-8.995	60.000	0.286	0.024	0.1591E+00	0.1921E+00	0.5656E-02
0.038	2.808	0.003	4.004	0.000	0.0000E+00	0.0000E+00	0.1754E+00
0.005	-7.010	60.000	0.257	0.016	0.1540E+00	0.1946E+00	0.5103E-02
0.017	2.783	-0.032	3.704	0.000	0.0000E+00	0.0000E+00	0.1755E+00
0.005	-5.005	60.000	0.244	0.022	0.1526E+00	0.1931E+00	-0.3313E-02
-0.002	2.836	-0.040	3.717	0.000	0.0000E+00	0.0000E+00	0.1741E+00
0.005	-3.005	60.000	0.239	0.019	0.1540E+00	0.1919E+00	0.1668E-01
-0.024	2.895	0.076	3.678	0.000	0.0000E+00	0.0000E+00	0.1740E+00
0.005	-4.000	60.000	0.223	0.020	0.1579E+00	0.1981E+00	0.1555E-01
0.053	2.840	0.094	3.765	0.000	0.0000E+00	0.0000E+00	0.1791E+00
0.005	-2.995	60.000	0.228	0.018	0.1561E+00	0.1932E+00	0.1513E-01
-0.005	2.958	0.031	3.598	0.000	0.0000E+00	0.0000E+00	0.1756E+00
0.005	-2.015	60.000	0.225	0.017	0.1581E+00	0.1937E+00	-0.3231E-02
-0.033	3.110	-0.019	3.416	0.000	0.0000E+00	0.0000E+00	0.1763E+00
0.005	-1.005	60.000	0.222	0.015	0.1517E+00	0.1949E+00	-0.9743E-03
-0.020	2.836	0.033	3.983	0.000	0.0000E+00	0.0000E+00	0.1746E+00
0.005	0.000	60.000	0.234	0.009	0.1556E+00	0.1975E+00	0.2853E-02
-0.026	2.860	0.001	3.655	0.000	0.0000E+00	0.0000E+00	0.1779E+00
0.005	0.995	60.000	0.238	0.013	0.1534E+00	0.2001E+00	-0.2235E-01
0.045	2.814	0.134	3.935	0.000	0.0000E+00	0.0000E+00	0.1733E+00
0.005	1.995	60.000	0.243	0.011	0.1741E+00	0.2155E+00	-0.3235E-01
-0.056	3.195	0.075	4.626	0.000	0.0000E+00	0.0000E+00	0.1959E+00
0.005	2.020	60.000	0.249	0.013	0.1591E+00	0.1985E+00	0.2172E-01
0.053	2.538	0.062	3.878	0.000	0.0000E+00	0.0000E+00	0.1799E+00
0.005	3.000	60.000	0.262	0.007	0.1582E+00	0.1911E+00	-0.2955E-01
-0.037	2.923	0.059	3.319	0.000	0.0000E+00	0.0000E+00	0.1754E+00
0.005	4.000	60.000	0.279	0.013	0.1548E+00	0.1996E+00	-0.3356E-01
0.027	2.862	0.154	4.030	0.000	0.0000E+00	0.0000E+00	0.1736E+00
0.005	4.990	60.000	0.285	0.004	0.1553E+00	0.1939E+00	0.1045E-01
0.007	2.748	0.153	3.586	0.000	0.0000E+00	0.0000E+00	0.1757E+00
0.005	5.985	60.000	0.290	0.005	0.1543E+00	0.1650E+00	-0.1449E-01
0.020	2.811	0.051	3.413	0.000	0.0000E+00	0.0000E+00	0.1733E+00
0.005	6.995	60.000	0.305	0.009	0.1543E+00	0.1932E+00	0.4033E-02
-0.002	2.817	0.182	4.009	0.000	0.0000E+00	0.0000E+00	0.1749E+00
0.005	9.010	60.000	0.311	0.010	0.1547E+00	0.1876E+00	0.5339E-02
0.053	2.848	-0.034	3.540	0.000	0.0000E+00	0.0000E+00	0.1719E+00
0.005	10.990	60.000	0.325	0.011	0.1466E+00	0.1833E+00	0.9990E-02
-0.033	2.748	0.140	3.489	0.000	0.0000E+00	0.0000E+00	0.1669E+00
0.005	12.995	60.000	0.324	0.009	0.1543E+00	0.1859E+00	-0.4035E-02
0.010	2.731	0.098	3.756	0.000	0.0000E+00	0.0000E+00	0.1708E+00
0.005	14.990	60.000	0.327	0.011	0.1535E+00	0.1862E+00	0.1974E-01
0.013	2.791	0.035	3.707	0.000	0.0000E+00	0.0000E+00	0.1705E+00

FILE NAME: SJ9420X0

0.005	-29.990	5.995	0.349	0.051	0.1503E+00	0.1943E+00	-0.6907E-02
0.004	2.539	0.095	3.609	0.000	0.0000E+00	0.0000E+00	0.1737E+00
0.005	-25.010	5.995	0.348	0.048	0.1543E+00	0.1946E+00	0.2933E-01
-0.016	2.859	0.066	3.739	0.000	0.0000E+00	0.0000E+00	0.1756E+00
0.005	-19.995	5.995	0.355	0.054	0.1462E+00	0.1924E+00	0.1104E-01
-0.005	2.742	0.041	4.023	0.000	0.0000E+00	0.0000E+00	0.1709E+00
0.005	-14.995	5.995	0.349	0.055	0.1573E+00	0.1866E+00	-0.1394E-01
0.032	2.954	-0.001	3.642	0.000	0.0000E+00	0.0000E+00	0.1726E+00
0.005	-13.005	5.995	0.329	0.064	0.1572E+00	0.1868E+00	0.3491E-01
0.013	2.920	0.101	3.791	0.000	0.0000E+00	0.0000E+00	0.1727E+00
0.005	-10.995	5.995	0.262	0.051	0.1585E+00	0.1860E+00	-0.6736E-02
0.042	3.115	0.112	3.725	0.000	0.0000E+00	0.0000E+00	0.1723E+00
0.005	-8.990	5.995	0.130	0.038	0.1574E+00	0.1862E+00	-0.2457E-01
-0.021	2.900	0.052	3.654	0.000	0.0000E+00	0.0000E+00	0.1724E+00
0.005	-7.010	5.995	0.017	0.021	0.1574E+00	0.1962E+00	0.1354E-02
0.065	2.734	-0.015	3.471	0.000	0.0000E+00	0.0000E+00	0.1779E+00
0.005	-5.000	5.995	-0.029	0.021	0.1542E+00	0.1837E+00	-0.9151E-02
0.068	2.923	0.012	3.513	0.000	0.0000E+00	0.0000E+00	0.1695E+00
0.005	-4.935	5.995	-0.045	0.029	0.1539E+00	0.1880E+00	0.1619E-01
0.004	2.903	0.004	3.837	0.000	0.0000E+00	0.0000E+00	0.1719E+00
0.005	-3.995	5.995	-0.016	0.031	0.1554E+00	0.1869E+00	0.2965E-02
-0.004	2.854	0.088	3.766	0.000	0.0000E+00	0.0000E+00	0.1719E+00
0.005	-3.005	5.995	0.093	0.022	0.1549E+00	0.1832E+00	-0.7032E-03
-0.021	2.827	0.020	3.695	0.000	0.0000E+00	0.0000E+00	0.1697E+00
0.005	-2.005	5.995	0.338	0.025	0.1555E+00	0.1977E+00	0.3365E-01
0.045	3.106	0.017	3.905	0.000	0.0000E+00	0.0000E+00	0.1823E+00
0.005	-1.000	5.995	0.537	0.046	0.1699E+00	0.2047E+00	-0.1622E-01
-0.011	2.937	0.065	4.013	0.000	0.0000E+00	0.0000E+00	0.1831E+00
0.005	0.000	5.995	0.595	0.047	0.1653E+00	0.1979E+00	0.9435E-02
0.041	3.044	0.059	4.094	0.000	0.0000E+00	0.0000E+00	0.1823E+00
0.005	1.005	5.995	0.132	0.018	0.1500E+00	0.1810E+00	0.2013E-01
-0.012	2.754	-0.030	4.123	0.000	0.0000E+00	0.0000E+00	0.1652E+00
0.005	2.030	5.995	-0.010	0.007	0.1527E+00	0.1659E+00	-0.7773E-02
0.020	2.746	0.056	3.515	0.000	0.0000E+00	0.0000E+00	0.1670E+00
0.005	2.995	5.995	-0.042	0.010	0.1473E+00	0.1526E+00	0.2197E-02
0.071	2.578	0.233	3.724	0.000	0.0000E+00	0.0000E+00	0.1659E+00
0.005	4.005	5.995	-0.015	0.004	0.1481E+00	0.1545E+00	0.7525E-02
0.002	2.591	0.060	3.536	0.000	0.0000E+00	0.0000E+00	0.1673E+00
0.005	4.995	5.995	0.038	0.000	0.1544E+00	0.1767E+00	-0.2244E-01
0.046	2.770	0.040	3.217	0.000	0.0000E+00	0.0000E+00	0.1670E+00
0.005	5.990	5.995	0.106	-0.008	0.1497E+00	0.1781E+00	-0.2941E-01
0.041	2.755	0.044	3.590	0.000	0.0000E+00	0.0000E+00	0.1645E+00
0.005	7.005	5.995	0.183	-0.023	0.1506E+00	0.1830E+00	-0.3057E-01
-0.022	2.742	0.019	3.432	0.000	0.0000E+00	0.0000E+00	0.1676E+00
0.005	5.995	5.995	0.291	-0.025	0.1514E+00	0.1824E+00	0.1394E-01
0.021	2.673	0.079	3.421	0.000	0.0000E+00	0.0000E+00	0.1676E+00
0.005	11.020	5.995	0.331	-0.024	0.1526E+00	0.1952E+00	0.7225E-02
0.007	2.739	-0.073	3.917	0.000	0.0000E+00	0.0000E+00	0.1752E+00
0.005	12.990	5.995	0.348	-0.025	0.1520E+00	0.1917E+00	-0.1714E-01
-0.006	2.796	0.065	3.650	0.000	0.0000E+00	0.0000E+00	0.1730E+00
0.005	15.015	5.995	0.343	-0.022	0.1526E+00	0.1895E+00	-0.1840E-01
-0.013	2.739	-0.062	3.794	0.000	0.0000E+00	0.0000E+00	0.1720E+00

FILE NAME: SJ.879BYJ

0.005	-30.010	9.995	0.327	0.048	0.1569E+00	0.2056E+00	0.5733E-03
0.032	2.730	-0.045	3.962	0.000	0.0000E+00	0.0000E+00	0.1529E+00
0.005	-24.990	9.995	0.334	0.052	0.1535E+00	0.2115E+00	0.2654E-01
-0.032	2.773	0.069	3.952	0.000	0.0000E+00	0.0000E+00	0.1343E+00
0.005	-19.990	9.995	0.333	0.058	0.1571E+00	0.2008E+00	-0.7290E-03
-0.038	2.775	0.077	3.906	0.000	0.0000E+00	0.0000E+00	0.1503E+00
0.005	-14.990	9.995	0.327	0.062	0.1546E+00	0.2056E+00	0.1313E-01
0.019	2.766	-0.069	3.846	0.000	0.0000E+00	0.0000E+00	0.1219E+00
0.005	-12.990	9.995	0.312	0.065	0.1614E+00	0.1947E+00	0.1197E-01
-0.009	2.800	-0.044	3.924	0.000	0.0000E+00	0.0000E+00	0.1733E+00
0.005	-10.995	9.995	0.268	0.070	0.1583E+00	0.2014E+00	-0.1341E-01
0.039	2.764	-0.043	3.709	0.000	0.0000E+00	0.0000E+00	0.1812E+00
0.005	-9.005	9.995	0.164	0.059	0.1579E+00	0.2047E+00	-0.3294E-02
-0.013	2.822	0.149	4.166	0.000	0.0000E+00	0.0000E+00	0.1828E+00
0.005	-6.995	9.995	0.035	0.037	0.1522E+00	0.1909E+00	0.2752E-01
0.041	2.716	-0.106	3.864	0.000	0.0000E+00	0.0000E+00	0.1727E+00
0.005	-5.995	9.995	-0.016	0.032	0.1547E+00	0.1941E+00	-0.5041E-02
0.002	2.793	0.132	3.411	0.000	0.0000E+00	0.0000E+00	0.1755E+00
0.005	-5.010	9.995	-0.043	0.031	0.1546E+00	0.1961E+00	-0.2305E-02
0.015	2.731	-0.007	3.603	0.000	0.0000E+00	0.0000E+00	0.1756E+00
0.005	-4.005	9.995	-0.004	0.023	0.1524E+00	0.1958E+00	-0.2223E-02
-0.001	2.926	0.077	3.804	0.000	0.0000E+00	0.0000E+00	0.1755E+00
0.005	-3.005	9.995	0.149	0.019	0.1557E+00	0.1669E+00	-0.9233E-02
0.029	2.725	0.057	3.549	0.000	0.0000E+00	0.0000E+00	0.1720E+00
0.005	-2.010	9.995	0.399	0.031	0.1725E+00	0.2022E+00	0.6250E-02
-0.006	3.113	0.225	4.261	0.000	0.0000E+00	0.0000E+00	0.1880E+00
0.005	-1.005	9.995	0.555	0.046	0.1904E+00	0.2253E+00	-0.1351E-01
-0.022	3.192	0.224	4.178	0.000	0.0000E+00	0.0000E+00	0.2035E+00
0.005	-0.010	9.995	0.421	0.046	0.1760E+00	0.2036E+00	0.1233E-01
0.003	3.208	0.133	4.290	0.000	0.0000E+00	0.0000E+00	0.1903E+00
0.005	1.010	9.995	0.154	0.023	0.1587E+00	0.1877E+00	-0.1355E-01
0.009	2.760	0.023	3.715	0.000	0.0000E+00	0.0000E+00	0.1734E+00
0.005	2.000	9.995	0.006	0.014	0.1545E+00	0.1925E+00	0.3525E-02
-0.001	2.803	0.062	3.654	0.000	0.0000E+00	0.0000E+00	0.1747E+00
0.005	2.990	9.995	-0.025	0.004	0.1531E+00	0.1921E+00	-0.1113E-01
-0.001	2.871	0.046	3.273	0.000	0.0000E+00	0.0000E+00	0.1737E+00
0.005	3.995	9.995	0.024	-0.011	0.1553E+00	0.1957E+00	-0.3457E-02
0.002	2.751	-0.091	4.044	0.000	0.0000E+00	0.0000E+00	0.1765E+00
0.005	5.005	9.995	0.039	-0.024	0.1578E+00	0.1941E+00	0.2946E-01
0.040	2.692	0.063	3.639	0.000	0.0000E+00	0.0000E+00	0.1769E+00
0.005	5.995	9.995	0.160	-0.030	0.1565E+00	0.1956E+00	-0.2993E-01
-0.075	2.773	0.063	3.965	0.000	0.0000E+00	0.0000E+00	0.1771E+00
0.005	7.005	9.995	0.218	-0.044	0.1607E+00	0.1925E+00	0.2039E-01
0.024	3.012	-0.031	3.539	0.000	0.0000E+00	0.0000E+00	0.1773E+00
0.005	9.010	9.995	0.292	-0.035	0.1599E+00	0.1940E+00	-0.2177E-02
-0.016	2.835	0.133	3.886	0.000	0.0000E+00	0.0000E+00	0.1777E+00
0.005	10.945	9.995	0.318	-0.035	0.1582E+00	0.1986E+00	0.5615E-02
-0.016	2.745	-0.017	3.492	0.000	0.0000E+00	0.0000E+00	0.1795E+00
0.005	12.990	9.995	0.329	-0.026	0.1596E+00	0.1942E+00	0.4334E-02
0.003	2.775	-0.036	3.933	0.000	0.0000E+00	0.0000E+00	0.1777E+00
0.005	14.990	9.995	0.329	-0.027	0.1557E+00	0.2005E+00	0.9843E-02
-0.004	2.832	0.033	3.793	0.000	0.0000E+00	0.0000E+00	0.1795E+00

FILE NAME: SJ8324X0

d 21

0.000	-29.995	20.000	0.335	0.048	0.1565E+00	0.2016E+00	0.1520E-01
-0.050	2.780	-0.018	3.853	0.000	0.0000E+00	0.0000E+00	0.1806E+00
0.000	-25.000	19.995	0.335	0.058	0.1539E+00	0.2008E+00	-0.2304E-02
0.007	2.694	0.060	3.775	0.000	0.0000E+00	0.0000E+00	0.1789E+00
0.000	-20.000	19.995	0.332	0.062	0.1540E+00	0.2502E+00	0.9750E-02
0.010	3.081	0.278	4.838	0.000	0.0000E+00	0.0000E+00	0.2196E+00
0.005	-15.000	19.995	0.325	0.066	0.1577E+00	0.1960E+00	0.2490E-01
0.059	2.729	0.140	3.722	0.000	0.0000E+00	0.0000E+00	0.1779E+00
0.005	-12.990	19.995	0.300	0.066	0.1536E+00	0.1912E+00	-0.3453E-04
0.000	2.724	-0.041	3.737	0.000	0.0000E+00	0.0000E+00	0.1734E+00
0.005	-11.010	19.995	0.272	0.066	0.1479E+00	0.1894E+00	-0.1287E-01
0.051	2.736	0.053	3.452	0.000	0.0000E+00	0.0000E+00	0.1699E+00
0.005	-9.020	19.995	0.209	0.063	0.1561E+00	0.2001E+00	0.1020E-01
-0.029	2.855	0.037	3.738	0.000	0.0000E+00	0.0000E+00	0.1793E+00
0.005	-6.985	19.995	0.123	0.055	0.1601E+00	0.2012E+00	-0.2055E-01
0.006	2.844	-0.003	3.444	0.000	0.0000E+00	0.0000E+00	0.1818E+00
0.005	-5.995	19.995	0.082	0.045	0.1599E+00	0.2097E+00	-0.1526E-01
0.012	2.547	0.125	4.179	0.000	0.0000E+00	0.0000E+00	0.1565E+00
0.005	-5.015	19.995	0.070	0.033	0.1606E+00	0.2001E+00	0.3148E-02
-0.004	2.844	-0.020	3.595	0.000	0.0000E+00	0.0000E+00	0.1814E+00
0.005	-4.010	5.995	-0.007	0.032	0.1835E+00	0.2266E+00	0.1577E-01
0.003	3.130	-0.032	4.293	0.000	0.0000E+00	0.0000E+00	0.2052E+00
0.005	2.035	20.005	0.109	-0.003	0.1569E+00	0.1911E+00	0.1353E-01
0.012	2.903	0.050	3.333	0.000	0.0000E+00	0.0000E+00	0.1749E+00
0.005	2.990	20.005	0.105	-0.009	0.1546E+00	0.1679E+00	0.6375E-02
-0.007	2.695	0.094	3.945	0.000	0.0000E+00	0.0000E+00	0.1720E+00
0.005	4.000	20.005	0.144	-0.015	0.1516E+00	0.1953E+00	0.1250E-01
0.006	2.728	0.082	3.376	0.000	0.0000E+00	0.0000E+00	0.1745E+00
0.005	5.010	20.005	0.190	-0.021	0.1528E+00	0.1980E+00	-0.4016E-01
0.004	2.620	0.161	4.205	0.000	0.0000E+00	0.0000E+00	0.1755E+00
0.005	5.990	20.005	0.226	-0.026	0.1573E+00	0.1929E+00	-0.2002E-01
0.051	2.725	0.134	3.615	0.000	0.0000E+00	0.0000E+00	0.1760E+00
0.005	6.995	20.005	0.256	-0.033	0.1533E+00	0.1946E+00	-0.5201E-02
-0.001	2.715	-0.043	3.635	0.000	0.0000E+00	0.0000E+00	0.1752E+00
0.005	8.985	20.005	0.291	-0.036	0.1515E+00	0.1933E+00	-0.1522E-01
-0.026	2.679	0.052	3.695	0.000	0.0000E+00	0.0000E+00	0.1735E+00
0.005	11.010	20.005	0.312	-0.033	0.1655E+00	0.2116E+00	0.2993E-01
-0.030	2.913	0.014	3.734	0.000	0.0000E+00	0.0000E+00	0.1900E+00
0.005	12.995	20.005	0.312	-0.028	0.1589E+00	0.1966E+00	0.8341E-02
-0.005	2.834	-0.060	3.651	0.000	0.0000E+00	0.0000E+00	0.1737E+00
0.005	15.005	20.005	0.322	-0.027	0.1614E+00	0.2012E+00	0.2612E-01
-0.002	2.936	0.054	3.609	0.000	0.0000E+00	0.0000E+00	0.1824E+00

FILE NAME: SJ5345X0

0	27						
0.005	-29.993	40.005	0.326	0.032	0.1696E+00	0.2137E+00	0.6650E-03
-0.013	2.957	0.039	3.754	0.000	0.0000E+00	0.0000E+00	0.1929E+00
0.005	-25.000	40.005	0.323	0.043	0.1617E+00	0.2169E+00	-0.7004E-02
0.048	2.973	0.133	4.523	0.000	0.0000E+00	0.0000E+00	0.1924E+00
0.005	-19.995	40.005	0.324	0.040	0.1564E+00	0.2005E+00	0.1456E-03
0.035	2.832	0.072	3.801	0.000	0.0000E+00	0.0000E+00	0.1792E+00
0.005	-15.000	40.005	0.315	0.039	0.1542E+00	0.1956E+00	0.5456E-02
0.059	2.832	0.008	3.579	0.000	0.0000E+00	0.0000E+00	0.1752E+00
0.005	-13.010	40.005	0.301	0.038	0.1539E+00	0.1949E+00	0.1653E-01
-0.016	2.734	0.063	3.641	0.000	0.0000E+00	0.0000E+00	0.1756E+00
0.005	-11.010	40.005	0.293	0.041	0.1614E+00	0.2121E+00	0.5146E-02
-0.063	2.545	0.063	3.933	0.000	0.0000E+00	0.0000E+00	0.1334E+00
0.005	-9.005	40.005	0.271	0.039	0.1600E+00	0.1994E+00	-0.1272E-01
0.055	2.921	0.045	3.807	0.000	0.0000E+00	0.0000E+00	0.1303E+00
0.005	-7.005	40.005	0.252	0.037	0.1569E+00	0.2022E+00	0.1237E-01
0.037	2.769	-0.002	3.828	0.000	0.0000E+00	0.0000E+00	0.1309E+00
0.005	-5.000	40.005	0.249	0.030	0.1625E+00	0.2062E+00	-0.1986E-01
0.039	2.839	0.003	3.664	0.000	0.0000E+00	0.0000E+00	0.1653E+00
0.005	-3.000	40.000	0.256	0.034	0.1614E+00	0.2079E+00	-0.1729E-01
0.042	2.502	0.052	3.663	0.000	0.0000E+00	0.0000E+00	0.1351E+00
0.005	-4.005	40.005	0.266	0.023	0.1601E+00	0.2134E+00	-0.2910E-01
0.011	2.793	0.021	3.334	0.000	0.0000E+00	0.0000E+00	0.1655E+00
0.005	-3.005	40.000	0.272	0.027	0.1580E+00	0.2159E+00	0.3904E-02
0.040	2.718	0.020	3.543	0.000	0.0000E+00	0.0000E+00	0.1592E+00
0.005	-2.010	40.005	0.273	0.014	0.1543E+00	0.2095E+00	-0.2112E-01
-0.007	2.757	0.060	3.470	0.000	0.0000E+00	0.0000E+00	0.1543E+00
0.005	-1.000	40.005	0.276	0.011	0.1560E+00	0.2081E+00	0.1432E-01
0.031	2.503	0.057	3.525	0.000	0.0000E+00	0.0000E+00	0.1448E+00
0.005	-0.010	40.000	0.272	0.018	0.1781E+00	0.2316E+00	0.2910E-01
-0.022	3.031	0.304	5.113	0.000	0.0000E+00	0.0000E+00	0.2067E+00
0.005	1.010	40.000	0.270	0.014	0.1747E+00	0.2165E+00	0.5531E-01
0.014	2.453	-0.043	4.193	0.000	0.0000E+00	0.0000E+00	0.1975E+00
0.005	1.995	40.000	0.260	-0.007	0.1635E+00	0.2025E+00	0.5125E-01
-0.013	2.793	0.017	3.555	0.000	0.0000E+00	0.0000E+00	0.1340E+00
0.005	3.000	40.000	0.252	-0.001	0.1657E+00	0.2065E+00	0.2642E-01
0.033	2.921	0.099	3.994	0.000	0.0000E+00	0.0000E+00	0.1573E+00
0.005	4.000	40.000	0.254	-0.003	0.1685E+00	0.2057E+00	0.7979E-02
-0.039	3.053	0.041	3.790	0.000	0.0000E+00	0.0000E+00	0.1332E+00
0.005	5.005	40.000	0.262	-0.003	0.1670E+00	0.2002E+00	0.3153E-01
-0.006	2.911	0.172	4.395	0.000	0.0000E+00	0.0000E+00	0.1344E+00
0.005	5.000	40.000	0.269	-0.006	0.1605E+00	0.1970E+00	0.9712E-02
-0.020	2.999	-0.003	3.956	0.000	0.0000E+00	0.0000E+00	0.1797E+00
0.005	5.995	40.000	0.263	-0.004	0.1591E+00	0.1923E+00	0.1243E-01
-0.013	2.867	-0.057	3.949	0.000	0.0000E+00	0.0000E+00	0.1755E+00
0.005	7.000	40.000	0.284	-0.001	0.1571E+00	0.1970E+00	0.3501E-02
-0.004	2.752	0.021	3.715	0.000	0.0000E+00	0.0000E+00	0.1751E+00
0.005	9.015	40.000	0.304	0.002	0.1533E+00	0.1944E+00	-0.1733E-01
0.016	2.726	0.109	3.565	0.000	0.0000E+00	0.0000E+00	0.1750E+00
0.005	10.990	40.000	0.305	-0.006	0.1529E+00	0.1937E+00	-0.2913E-02
0.046	2.833	0.017	3.727	0.000	0.0000E+00	0.0000E+00	0.1745E+00
0.005	12.990	40.000	0.313	-0.009	0.1496E+00	0.1919E+00	0.9073E-02
-0.042	2.749	-0.024	3.344	0.000	0.0000E+00	0.0000E+00	0.1720E+00
0.005	14.990	40.000	0.310	-0.004	0.1498E+00	0.1894E+00	0.1343E-01
-0.059	2.795	0.031	3.770	0.000	0.0000E+00	0.0000E+00	0.1707E+00

FILE NAME: SJ5372X0

b	2b						
0.005	-24.990	59.995	0.326	0.034	0.1602E+00	0.2077E+00	0.1138E-01
0.003	[illegible]	0.115	4.019	0.000	0.0000E+00	0.0000E+00	0.1357E+00
0.005	-25.000	59.995	0.327	0.032	0.1571E+00	0.2111E+00	-0.4975E-02
0.046	[illegible]	-0.012	3.741	0.000	0.0000E+00	0.0000E+00	0.1561E+00
0.005	-17.995	59.995	0.324	0.026	0.1652E+00	0.2041E+00	0.5345E-02
-0.003	2.971	0.015	3.978	0.000	0.0000E+00	0.0000E+00	0.1537E+00
0.005	-14.995	59.995	0.319	0.026	0.1595E+00	0.1996E+00	0.7332E-02
0.010	2.995	0.026	3.973	0.000	0.0000E+00	0.0000E+00	0.1537E+00
0.005	-13.005	59.995	0.317	0.031	0.1577E+00	0.1954E+00	-0.5659E-02
-0.025	2.939	-0.017	3.935	0.000	0.0000E+00	0.0000E+00	0.1731E+00
0.005	-11.005	59.995	0.313	0.030	0.1538E+00	0.1930E+00	-0.4340E-02
0.003	2.750	0.150	3.833	0.000	0.0000E+00	0.0000E+00	0.1745E+00
0.005	-9.030	59.995	0.297	0.033	0.1858E+00	0.2296E+00	0.2240E-02
-0.020	3.391	0.215	4.692	0.000	0.0000E+00	0.0000E+00	0.2059E+00
0.005	-8.990	60.000	0.289	0.036	0.1863E+00	0.2346E+00	0.1466E-01
0.051	3.033	0.143	4.275	0.000	0.0000E+00	0.0000E+00	0.2114E+00
0.005	-5.995	59.995	0.287	0.028	0.1798E+00	0.2200E+00	0.1913E-01
-0.031	3.223	0.099	4.134	0.000	0.0000E+00	0.0000E+00	0.2039E+00
0.005	-5.010	59.995	0.281	0.026	0.1660E+00	0.2174E+00	-0.1334E-01
0.025	3.077	0.017	3.902	0.000	0.0000E+00	0.0000E+00	0.1934E+00
0.005	-3.995	59.995	0.286	0.027	0.1602E+00	0.2077E+00	-0.2005E-01
-0.001	2.711	0.025	3.361	0.000	0.0000E+00	0.0000E+00	0.1855E+00
0.005	-3.000	59.995	0.233	0.016	0.1603E+00	0.2055E+00	0.9463E-02
0.008	2.878	0.019	3.559	0.000	0.0000E+00	0.0000E+00	0.1845E+00
0.005	-2.005	59.995	0.235	0.014	0.1618E+00	0.2065E+00	-0.5058E-03
-0.001	2.943	-0.003	3.641	0.000	0.0000E+00	0.0000E+00	0.1855E+00
0.005	-1.005	59.995	0.237	0.018	0.1566E+00	0.2073E+00	0.5746E-02
0.077	2.966	-0.007	3.403	0.000	0.0000E+00	0.0000E+00	0.1841E+00
0.005	-0.010	59.995	0.239	0.011	0.1571E+00	0.1970E+00	0.1237E-01
0.010	2.875	0.016	3.313	0.000	0.0000E+00	0.0000E+00	0.1732E+00
0.005	1.010	59.995	0.291	0.011	0.1546E+00	0.1963E+00	0.2205E-01
-0.002	2.927	-0.033	3.482	0.000	0.0000E+00	0.0000E+00	0.1754E+00
0.005	2.000	59.995	0.294	0.012	0.1555E+00	0.1990E+00	-0.2055E-02
0.011	2.544	0.005	3.345	0.000	0.0000E+00	0.0000E+00	0.1735E+00
0.005	2.993	60.000	0.294	0.011	0.1553E+00	0.1991E+00	-0.2205E-02
0.052	2.791	0.079	3.477	0.000	0.0000E+00	0.0000E+00	0.1735E+00
0.005	3.995	59.995	0.297	0.008	0.1574E+00	0.1927E+00	-0.1236E-01
-0.026	2.774	0.040	3.677	0.000	0.0000E+00	0.0000E+00	0.1750E+00
0.005	4.995	59.995	0.298	0.013	0.1537E+00	0.1892E+00	-0.5131E-02
-0.017	2.664	0.152	3.463	0.000	0.0000E+00	0.0000E+00	0.1724E+00
0.005	5.005	60.000	0.301	0.001	0.1488E+00	0.1906E+00	0.1555E-01
-0.015	2.731	-0.023	3.564	0.000	0.0000E+00	0.0000E+00	0.1710E+00
0.005	7.000	59.995	0.304	0.009	0.1523E+00	0.1855E+00	-0.3709E-01
-0.046	2.709	-0.060	3.549	0.000	0.0000E+00	0.0000E+00	0.1697E+00
0.005	8.995	59.995	0.314	0.009	0.1529E+00	0.1915E+00	0.4504E-02
-0.027	2.725	-0.084	3.375	0.000	0.0000E+00	0.0000E+00	0.1733E+00
0.005	10.995	60.000	0.314	0.006	0.1547E+00	0.1919E+00	-0.1848E-01
0.037	2.790	0.027	3.638	0.000	0.0000E+00	0.0000E+00	0.1743E+00
0.005	13.005	59.995	0.319	0.009	0.1539E+00	0.1901E+00	0.9725E-02
-0.014	2.725	-0.010	3.256	0.000	0.0000E+00	0.0000E+00	0.1730E+00
0.005	14.990	59.995	0.317	0.005	0.1534E+00	0.1912E+00	-0.2807E-02
-0.016	2.656	0.052	3.524	0.000	0.0000E+00	0.0000E+00	0.1733E+00

FILE NAME: SJ446XU

δ	2θ						
0.005	-23.990	10.000	0.343	0.052	0.1530E+00	0.1856E+00	0.2153E-01
0.016	2.838	-0.071	3.781	0.000	0.0000E+00	0.0000E+00	0.1701E+00
0.005	-25.010	9.995	0.341	0.051	0.1536E+00	0.1903E+00	0.2233E-01
0.002	2.502	-0.002	3.925	0.000	0.0000E+00	0.0000E+00	0.1729E+00
0.005	-14.995	9.995	0.347	0.056	0.1474E+00	0.1892E+00	0.5002E-02
-0.020	2.709	0.024	3.546	0.000	0.0000E+00	0.0000E+00	0.1596E+00
0.005	-14.990	9.995	0.343	0.063	0.1560E+00	0.1865E+00	0.4595E-03
0.013	2.923	0.070	3.615	0.000	0.0000E+00	0.0000E+00	0.1719E+00
0.005	-13.005	9.995	0.331	0.068	0.1510E+00	0.1823E+00	-0.4985E-02
0.006	2.923	-0.041	3.466	0.000	0.0000E+00	0.0000E+00	0.1574E+00
0.005	-11.005	9.995	0.277	0.057	0.1512E+00	0.1847E+00	-0.1205E-01
0.040	2.769	-0.001	3.508	0.000	0.0000E+00	0.0000E+00	0.1533E+00
0.005	-9.000	9.995	0.173	0.060	0.1475E+00	0.1867E+00	0.2594E-02
-0.034	2.836	0.049	3.931	0.000	0.0000E+00	0.0000E+00	0.1594E+00
0.005	-6.995	9.995	0.042	0.036	0.1520E+00	0.1866E+00	-0.3759E-02
0.022	2.905	-0.017	3.954	0.000	0.0000E+00	0.0000E+00	0.1713E+00
0.005	-6.005	9.995	-0.020	0.033	0.1571E+00	0.1663E+00	-0.6043E-03
0.042	2.953	-0.004	3.742	0.000	0.0000E+00	0.0000E+00	0.1723E+00
0.005	-5.010	9.995	-0.055	0.028	0.1549E+00	0.1622E+00	-0.1593E-01
0.063	2.930	0.016	3.522	0.000	0.0000E+00	0.0000E+00	0.1591E+00
0.005	-4.005	9.995	-0.023	0.026	0.1489E+00	0.1840E+00	-0.1895E-02
-0.045	2.836	-0.025	3.395	0.000	0.0000E+00	0.0000E+00	0.1574E+00
0.005	-3.000	9.995	0.138	0.018	0.1529E+00	0.1635E+00	0.5040E-02
0.052	2.852	0.004	3.869	0.000	0.0000E+00	0.0000E+00	0.1539E+00
0.005	-2.005	9.995	0.449	0.031	0.1624E+00	0.2045E+00	-0.2016E-01
-0.009	2.854	0.200	3.979	0.000	0.0000E+00	0.0000E+00	0.1345E+00
0.005	-0.995	9.995	0.693	0.036	0.1690E+00	0.2087E+00	-0.1763E-01
-0.038	2.922	0.135	3.584	0.000	0.0000E+00	0.0000E+00	0.1599E+00
0.005	-0.005	9.995	0.547	0.042	0.1689E+00	0.2045E+00	0.5595E-03
-0.001	3.072	0.057	3.675	0.000	0.0000E+00	0.0000E+00	0.1367E+00
0.005	0.990	9.995	0.210	0.022	0.1477E+00	0.1605E+00	0.9133E-02
-0.004	2.710	0.044	3.791	0.000	0.0000E+00	0.0000E+00	0.1651E+00
0.005	2.005	9.995	0.001	0.010	0.1552E+00	0.1633E+00	0.1011E-02
-0.014	2.964	0.100	3.562	0.000	0.0000E+00	0.0000E+00	0.1595E+00
0.005	3.010	9.995	-0.035	-0.001	0.1546E+00	0.1797E+00	0.3647E-02
-0.011	2.711	0.011	3.500	0.000	0.0000E+00	0.0000E+00	0.1575E+00
0.005	3.995	9.995	0.016	-0.014	0.1523E+00	0.1637E+00	-0.5630E-02
-0.006	2.816	0.022	3.492	0.000	0.0000E+00	0.0000E+00	0.1537E+00
0.005	4.935	9.995	0.087	-0.029	0.1556E+00	0.1886E+00	0.2133E-01
0.036	2.974	0.015	4.173	0.000	0.0000E+00	0.0000E+00	0.1730E+00
0.005	5.005	9.995	0.161	-0.037	0.1503E+00	0.1830E+00	-0.4896E-02
-0.017	2.543	0.046	3.540	0.000	0.0000E+00	0.0000E+00	0.1574E+00
0.005	7.005	9.995	0.223	-0.047	0.1524E+00	0.1821E+00	0.1523E-01
0.052	2.774	0.011	3.722	0.000	0.0000E+00	0.0000E+00	0.1579E+00
0.005	9.015	9.995	0.302	-0.041	0.1513E+00	0.1833E+00	0.5519E-02
-0.007	2.733	0.051	3.474	0.000	0.0000E+00	0.0000E+00	0.1631E+00
0.005	11.010	9.995	0.328	-0.044	0.1516E+00	0.1862E+00	0.2725E-01
0.103	2.809	0.072	3.819	0.000	0.0000E+00	0.0000E+00	0.1599E+00
0.005	13.005	9.995	0.342	-0.036	0.1509E+00	0.1844E+00	0.2635E-02
0.035	2.810	0.025	3.879	0.000	0.0000E+00	0.0000E+00	0.1635E+00
0.005	14.995	9.995	0.337	-0.030	0.1546E+00	0.1817E+00	0.1515E-01
0.001	2.757	0.004	3.555	0.000	0.0000E+00	0.0000E+00	0.1538E+00

FILE NAME: SJ9472X0

0	25						
0.005	-29.990	20.005	0.336	0.048	0.1547E+00	0.1874E+00	0.1173E-01
0.058	2.837	-0.011	3.595	0.000	0.0000E+00	0.0000E+00	0.1713E+00
0.005	-25.000	20.005	0.331	0.055	0.1462E+00	0.1862E+00	0.1556E-02
-0.003	2.745	0.120	3.523	0.000	0.0000E+00	0.0000E+00	0.1674E+00
0.005	-19.990	20.005	0.332	0.066	0.1515E+00	0.1817E+00	-0.1332E-01
-0.052	2.839	0.052	3.544	0.000	0.0000E+00	0.0000E+00	0.1674E+00
0.005	-15.000	20.005	0.319	0.076	0.1484E+00	0.1660E+00	0.2154E-01
-0.052	2.699	0.145	3.401	0.000	0.0000E+00	0.0000E+00	0.1632E+00
0.005	-13.020	20.005	0.307	0.067	0.1483E+00	0.1819E+00	-0.5957E-02
-0.004	2.737	0.072	3.503	0.000	0.0000E+00	0.0000E+00	0.1650E+00
0.005	-11.010	20.005	0.285	0.067	0.1505E+00	0.1798E+00	0.7937E-03
0.024	2.783	0.034	3.614	0.000	0.0000E+00	0.0000E+00	0.1653E+00
0.005	-8.990	20.005	0.235	0.068	0.1518E+00	0.1546E+00	0.1266E-01
-0.005	2.771	0.115	3.767	0.000	0.0000E+00	0.0000E+00	0.1690E+00
0.005	-7.035	20.005	0.141	0.048	0.1582E+00	0.1834E+00	0.1191E-01
0.071	3.072	-0.040	3.599	0.000	0.0000E+00	0.0000E+00	0.1713E+00
0.005	-5.995	20.005	0.087	0.041	0.1521E+00	0.1804E+00	0.2124E-01
0.004	2.851	-0.011	3.159	0.000	0.0000E+00	0.0000E+00	0.1659E+00
0.005	-5.010	20.005	0.052	0.032	0.1443E+00	0.1664E+00	0.4750E-02
0.024	2.707	0.064	3.542	0.000	0.0000E+00	0.0000E+00	0.1656E+00
0.005	-4.035	20.005	0.072	0.023	0.1515E+00	0.1575E+00	-0.4342E-02
0.005	2.817	0.185	3.745	0.000	0.0000E+00	0.0000E+00	0.1704E+00
0.005	-3.030	20.000	0.217	0.015	0.1490E+00	0.1871E+00	-0.2171E-01
0.049	2.727	0.165	3.817	0.000	0.0000E+00	0.0000E+00	0.1692E+00
0.005	-2.020	20.000	0.447	0.022	0.1624E+00	0.1969E+00	0.1104E-01
0.020	2.892	0.158	4.277	0.000	0.0000E+00	0.0000E+00	0.1605E+00
0.005	-0.995	20.000	0.534	0.025	0.1692E+00	0.2156E+00	-0.2912E-01
0.026	2.652	0.255	4.418	0.000	0.0000E+00	0.0000E+00	0.1933E+00
0.005	-0.035	20.000	0.503	0.034	0.1686E+00	0.2071E+00	0.5929E-04
-0.026	2.875	0.171	4.103	0.000	0.0000E+00	0.0000E+00	0.1833E+00
0.005	0.990	20.000	0.275	0.015	0.1587E+00	0.1795E+00	-0.4733E-02
0.041	2.955	0.045	3.515	0.000	0.0000E+00	0.0000E+00	0.1694E+00
0.005	2.000	20.000	0.119	0.008	0.1499E+00	0.1801E+00	-0.1929E-01
0.032	2.778	0.135	3.655	0.000	0.0000E+00	0.0000E+00	0.1657E+00
0.005	2.995	20.000	0.098	-0.004	0.1545E+00	0.1542E+00	0.2652E-02
0.026	2.941	0.097	3.851	0.000	0.0000E+00	0.0000E+00	0.1700E+00
0.005	3.995	20.000	0.138	-0.010	0.1522E+00	0.1813E+00	-0.1149E-03
0.060	2.823	0.015	3.595	0.000	0.0000E+00	0.0000E+00	0.1674E+00
0.005	5.010	20.000	0.185	-0.024	0.1529E+00	0.1900E+00	-0.1839E-02
0.026	2.850	0.017	4.424	0.000	0.0000E+00	0.0000E+00	0.1725E+00
0.005	6.995	20.000	0.230	-0.031	0.1558E+00	0.1816E+00	-0.6251E-02
0.010	2.837	0.045	4.091	0.000	0.0000E+00	0.0000E+00	0.1692E+00
0.005	7.035	20.000	0.258	-0.030	0.1559E+00	0.1861E+00	-0.2440E-01
0.043	2.876	0.049	3.735	0.000	0.0000E+00	0.0000E+00	0.1716E+00
0.005	8.950	20.000	0.297	-0.035	0.1549E+00	0.1865E+00	0.7334E-02
0.039	2.740	0.001	3.710	0.000	0.0000E+00	0.0000E+00	0.1725E+00
0.005	11.010	20.000	0.309	-0.034	0.1584E+00	0.1833E+00	0.1751E-01
0.015	2.913	0.101	3.705	0.000	0.0000E+00	0.0000E+00	0.1713E+00
0.005	12.995	20.000	0.323	-0.029	0.1538E+00	0.1845E+00	-0.9387E-02
0.007	2.744	0.035	3.666	0.000	0.0000E+00	0.0000E+00	0.1699E+00
0.005	14.995	20.000	0.324	-0.022	0.1517E+00	0.1668E+00	0.1845E-01
0.053	2.735	0.082	3.772	0.000	0.0000E+00	0.0000E+00	0.1702E+00

FILE NAME: SJ9502XO

θ	2θ						
0.003	-50.035	60.005	0.330	0.031	0.1600E+00	0.1976E+00	-0.2340E-01
0.033	2.920	0.114	4.730	0.000	0.0000E+00	0.0000E+00	0.1799E+00
0.005	-20.995	60.005	0.325	0.030	0.1609E+00	0.1981E+00	-0.3335E-01
0.031	2.775	0.149	3.963	0.000	0.0000E+00	0.0000E+00	0.1604E+00
0.005	-19.990	60.005	0.326	0.033	0.1542E+00	0.1978E+00	0.2330E-02
-0.039	2.724	0.093	3.974	0.000	0.0000E+00	0.0000E+00	0.1773E+00
0.005	-14.990	60.005	0.318	0.025	0.1546E+00	0.1921E+00	-0.1239E-01
-0.016	2.759	0.051	4.033	0.000	0.0000E+00	0.0000E+00	0.1743E+00
0.005	-13.010	60.005	0.318	0.026	0.1559E+00	0.1834E+00	0.1605E-02
0.036	2.752	0.051	3.841	0.000	0.0000E+00	0.0000E+00	0.1702E+00
0.005	-10.995	60.005	0.303	0.029	0.1533E+00	0.1654E+00	0.3491E-02
-0.013	2.702	0.084	3.719	0.000	0.0000E+00	0.0000E+00	0.1701E+00
0.005	-5.995	60.005	0.296	0.024	0.1545E+00	0.1863E+00	0.4359E-01
-0.011	2.751	0.042	3.750	0.000	0.0000E+00	0.0000E+00	0.1711E+00
0.005	-5.935	60.005	0.273	0.025	0.1538E+00	0.1861E+00	-0.5555E-02
0.054	2.500	0.060	3.800	0.000	0.0000E+00	0.0000E+00	0.1718E+00
0.005	-5.010	60.005	0.267	0.025	0.1537E+00	0.1619E+00	0.3770E-02
-0.003	2.764	0.019	3.513	0.000	0.0000E+00	0.0000E+00	0.1634E+00
0.005	-4.995	60.005	0.292	0.021	0.1514E+00	0.1791E+00	-0.6593E-02
0.071	2.717	-0.048	3.479	0.000	0.0000E+00	0.0000E+00	0.1633E+00
0.005	-4.005	60.005	0.345	0.019	0.1584E+00	0.1665E+00	-0.2459E-01
0.035	2.775	0.145	3.636	0.000	0.0000E+00	0.0000E+00	0.1730E+00
0.005	-3.000	60.005	0.404	0.027	0.1654E+00	0.1954E+00	-0.5027E-02
-0.017	2.874	0.153	3.780	0.000	0.0000E+00	0.0000E+00	0.1810E+00
0.005	-2.005	60.005	0.429	0.028	0.1633E+00	0.1992E+00	0.3397E-02
0.048	2.923	0.119	4.101	0.000	0.0000E+00	0.0000E+00	0.1821E+00
0.005	-0.995	60.005	0.437	0.027	0.1643E+00	0.1974E+00	-0.7639E-02
-0.032	2.699	0.039	3.938	0.000	0.0000E+00	0.0000E+00	0.1816E+00
0.005	-0.005	60.005	0.400	0.024	0.1646E+00	0.1918E+00	0.3537E-01
0.026	2.543	0.069	3.720	0.000	0.0000E+00	0.0000E+00	0.1757E+00
0.005	0.990	60.005	0.335	0.010	0.1526E+00	0.1535E+00	0.2051E-01
-0.005	2.735	0.064	3.631	0.000	0.0000E+00	0.0000E+00	0.1633E+00
0.005	2.000	60.005	0.294	0.016	0.1536E+00	0.1786E+00	0.1057E-01
0.005	2.736	0.064	3.437	0.000	0.0000E+00	0.0000E+00	0.1555E+00
0.005	3.000	60.005	0.253	0.014	0.1464E+00	0.1776E+00	-0.4121E-02
0.059	2.753	0.074	3.385	0.000	0.0000E+00	0.0000E+00	0.1529E+00
0.005	4.020	60.005	0.276	0.007	0.1511E+00	0.1769E+00	-0.6379E-02
0.045	2.777	0.033	3.354	0.000	0.0000E+00	0.0000E+00	0.1536E+00
0.005	5.010	60.005	0.288	0.002	0.1507E+00	0.1821E+00	-0.2161E-01
0.015	2.653	-0.045	3.576	0.000	0.0000E+00	0.0000E+00	0.1571E+00
0.005	5.995	60.005	0.295	0.004	0.1541E+00	0.1821E+00	-0.1725E-01
-0.021	2.796	0.135	3.785	0.000	0.0000E+00	0.0000E+00	0.1647E+00
0.005	7.005	60.005	0.307	0.006	0.1543E+00	0.1814E+00	0.3867E-03
-0.045	2.602	0.095	3.497	0.000	0.0000E+00	0.0000E+00	0.1534E+00
0.005	8.990	60.000	0.311	0.001	0.1490E+00	0.1606E+00	-0.1336E-01
0.043	2.521	-0.004	3.433	0.000	0.0000E+00	0.0000E+00	0.1559E+00
0.005	10.970	60.000	0.320	0.007	0.1492E+00	0.1830E+00	0.1334E-01
0.008	2.729	0.035	3.398	0.000	0.0000E+00	0.0000E+00	0.1570E+00
0.005	13.005	60.005	0.322	0.005	0.1506E+00	0.1781E+00	0.6250E-02
0.020	2.669	0.060	3.749	0.000	0.0000E+00	0.0000E+00	0.1649E+00
0.005	14.995	60.000	0.318	0.001	0.1502E+00	0.1794E+00	0.2533E-01
0.024	2.732	0.050	3.400	0.000	0.0000E+00	0.0000E+00	0.1654E+00

FILE NAME: SJ952540

0.005	-30.010	119.995	0.329	0.011	0.1542E+00	0.1963E+00	0.3035E-01
-0.005	2.855	0.048	3.946	0.000	0.0000E+00	0.0000E+00	0.1733E+00
0.005	-24.990	119.995	0.336	0.016	0.1575E+00	0.1868E+00	0.7399E-02
0.014	2.906	0.045	3.732	0.000	0.0000E+00	0.0000E+00	0.1734E+00
0.005	-19.990	119.995	0.329	0.025	0.1559E+00	0.1857E+00	0.2593E-02
-0.006	2.795	0.108	3.741	0.000	0.0000E+00	0.0000E+00	0.1731E+00
0.005	-14.990	119.995	0.324	0.003	0.1535E+00	0.1851E+00	0.1340E-02
0.016	2.934	-0.044	3.612	0.000	0.0000E+00	0.0000E+00	0.1700E+00
0.005	-12.985	119.995	0.322	0.019	0.1575E+00	0.1846E+00	0.1645E-01
0.035	2.753	0.034	3.613	0.000	0.0000E+00	0.0000E+00	0.1717E+00
0.005	-11.010	119.995	0.323	0.020	0.1579E+00	0.1667E+00	-0.1230E-01
-0.035	2.915	0.004	3.617	0.000	0.0000E+00	0.0000E+00	0.1729E+00
0.005	-9.015	119.995	0.333	0.019	0.1580E+00	0.1837E+00	-0.1744E-01
0.046	2.903	0.011	3.595	0.000	0.0000E+00	0.0000E+00	0.1713E+00
0.005	-7.010	119.995	0.340	0.030	0.1556E+00	0.1874E+00	-0.9453E-02
0.030	2.727	0.108	3.551	0.000	0.0000E+00	0.0000E+00	0.1722E+00
0.005	-5.995	119.995	0.357	0.018	0.1515E+00	0.1875E+00	-0.1151E-01
-0.058	2.764	0.026	3.415	0.000	0.0000E+00	0.0000E+00	0.1705E+00
0.005	-5.005	119.995	0.360	0.022	0.1577E+00	0.1894E+00	-0.3107E-01
0.069	2.737	0.057	3.936	0.000	0.0000E+00	0.0000E+00	0.1742E+00
0.005	-4.005	119.995	0.374	0.015	0.1575E+00	0.1912E+00	-0.2576E-03
0.030	2.722	0.036	3.743	0.000	0.0000E+00	0.0000E+00	0.1752E+00
0.005	-3.000	119.995	0.371	0.025	0.1567E+00	0.1896E+00	-0.2364E-01
0.034	2.756	0.035	3.693	0.000	0.0000E+00	0.0000E+00	0.1739E+00
0.005	-2.005	119.995	0.359	0.021	0.1551E+00	0.1876E+00	-0.3611E-02
0.007	2.745	0.010	3.659	0.000	0.0000E+00	0.0000E+00	0.1721E+00
0.005	-0.995	119.995	0.371	0.019	0.1568E+00	0.1901E+00	0.4171E-02
0.065	2.915	-0.016	3.293	0.000	0.0000E+00	0.0000E+00	0.1743E+00
0.005	-0.005	119.995	0.366	0.014	0.1543E+00	0.1852E+00	0.2757E-01
0.015	2.832	-0.077	3.393	0.000	0.0000E+00	0.0000E+00	0.1727E+00
0.005	0.995	119.995	0.358	0.016	0.1532E+00	0.1874E+00	0.3625E-01
0.050	2.841	0.074	3.677	0.000	0.0000E+00	0.0000E+00	0.1735E+00
0.005	2.010	119.995	0.349	0.011	0.1536E+00	0.1863E+00	0.4039E-02
-0.014	2.546	-0.027	3.573	0.000	0.0000E+00	0.0000E+00	0.1707E+00
0.005	3.010	119.995	0.335	0.010	0.1553E+00	0.1812E+00	0.3197E-04
0.004	2.820	-0.003	3.175	0.000	0.0000E+00	0.0000E+00	0.1537E+00
0.005	3.995	119.995	0.336	0.010	0.1564E+00	0.1843E+00	0.4325E-01
-0.023	2.718	0.076	3.401	0.000	0.0000E+00	0.0000E+00	0.1716E+00
0.005	5.010	119.995	0.331	0.014	0.1540E+00	0.1832E+00	0.2654E-03
-0.045	2.775	0.194	3.753	0.000	0.0000E+00	0.0000E+00	0.1692E+00
0.005	5.995	119.995	0.326	0.014	0.1519E+00	0.1802E+00	0.5056E-02
-0.045	2.680	0.071	3.640	0.000	0.0000E+00	0.0000E+00	0.1665E+00
0.005	7.005	119.995	0.323	0.008	0.1553E+00	0.1804E+00	-0.1322E-01
0.002	2.724	-0.014	3.320	0.000	0.0000E+00	0.0000E+00	0.1633E+00

BIBLIOGRAPHY

Ballal, D.R., A.J. Lightman, and P.P. Yaney, "Development of Test Facility and Optical Instrumentation for Turbulent Combustion Research," AIAA-86-0045, AIAA, New York, 1986.

Ballal, D.R. and T.H. Chen, "Studies of a CO_2 Slot Jet Using an Integrated Raman-LDA System," AIAA-87-0375, AIAA, New York, 1987.

Beavers, G.S. and T.A. Wilson, "Vortex Growth in Jets," JFM 44: 97-112, 1970.

Becker, H.A., H.C. Hottel, and G.C. Williams, "On the Light Scatter Technique for the Study of Turbulence and Mixing," JFM 30: 259, 1967.

Becker, H.A. and J.A. Massaro, "Vortex Evolution in a Round Jet," JFM 31: 435-448, 1968.

Bird, R.B., W.E. Stewart, and E.N. Lightfoot, Transport Phenomena, John Wiley & Sons, New York, 1960.

Bradbury, L.J.S., "The Structure of a Self-Preserving Turbulent Plane Jet," JFM 23: 31-64, 1965.

Bradbury, L.J.S. and J. Riley, "The Spread of a Turbulent Plane Jet Issuing into a Parallel Moving Airstream," JFM 27: 381-394, 1967.

Britton, R.L., Private Communication, 1987.

Chen, L.-D. and W.M. Roquemore, "Visualization of Jet Flames," Combustion and Flame 66: 81-86, 1986.

Chen, T.H. and W.J. Schmoll, "Development of Structures in the Near Field of Round Jets," to be published, 1987.

Crow, S.C. and F.H. Champagne, "Orderly Structure in Jet Turbulence," Journal of Fluid Mechanics 48: 547-591, 1971.

Everitt, K.W. and A.G. Robins, "The Development and Structure of Turbulent Plane Jets," JFM 88: 563-583, 1978.

Ghoniem, A.F., H.M. Aly, and O.M. Knio, "Three Dimensional Vortex Simulation with Application to Axisymmetric Shear Layers," AIAA-87-0397, AIAA, New York, 1987.

Hitchcock, J.E., Private communication, 1987.

Ho, C.-M. and N.S. Nosseir, "Dynamics of an Impinging Jet, Part 1: The Feedback Phenomenon," JFM 105: 119-142, 1981.

Holman, J.P., Experimental Methods for Engineers, McGraw-Hill, New York, 1984.

Hussain, A.K.M.F., "Coherent Structures and Turbulence," JFM 173: 303-356, 1986.

Lasheras, J.C., J.S. Cho, and T. Maxworthy, "On the Origin and Evolution of Streamwise Vortical Structures in a Plane, Free Shear Layer," JFM 172: 231-258, 1986.

Laufer, J., "Instability and Turbulence in Jets," in Transition and Turbulence, edited by R.E. Meyer, Academic Press, New York, 1981, pp 63-76.

Levich, V.G., Physicochemical Hydrodynamics, Prentice-Hall, Inc., Englewood Cliffs, N.J., 1962.

List, E.J., "Turbulent Jets and Plumes," Annual Review of Fluid Mechanics 14: 189-212, 1982.

Lydersen, A.L., "Estimation of Critical Properties of Organic Compounds," University of Wisconsin College of Engineering, Engineering Experiments Standard Report 3, Madison, April 1955.

Malmstadt, H.V., C.G. Enke, and S.R. Crouch, Electronics and Instrumentation for Scientists, The Benjamin/Cummings Publishing Company, Reading, MA, 1981.

Miksad, R.W., "Experiments on Nonlinear Interactions in the Transition of a Free Shear Layer," JFM 59: 1-21. 1973.

Neufeld, P.D., A.R. Janzen, and R.A. Aziz, Journal of Chemical Physics 57: 1100, 1972.

Perry, A.E. and T.R. Steiner, "Large-Scale Vortex Structures in Turbulent Wakes Behind Bluff Bodies. Part 1. Vortex Formation Processes," JFM 174: 233-270, 1987.

Perry, A.E. and M.S. Chong, "A Description of Eddying Motions and Flow Patterns Using Critical-Point Concepts," Annual Review of Fluid Mechanics 19: 125-155, 1987.

Reid, R.C., J.M. Prausnitz, and T.K. Sherwood, The Properties of Gases and Liquids, McGraw-Hill, New York, 1977.

Reidel, L., Chem Ing Tech 26: 83, 1954.

Roquemore, W.M., R.S. Tankin, H.H. Chui, and S.A. Lottes, "A Study of Bluff-Body Combustor Using Laser Sheet Lighting," Experiments in Fluids 4: 205-213, 1986.

Roquemore, W.M., Private communication, 1987.

Sato, H., "The Stability and Transition of a Two-Dimensional Jet," JFM 7: 53-80, 1960.

Steiner, T.R. and A.E. Perry, "Large-Scale Vortex Structures in Turbulent Wakes Behind Bluff Bodies. Part 2. Far-Wake Structures," JFM 174: 271-298, 1987.

Svehla, R.A., Estimated Viscosities and Thermal Conductivities of Gases at High Temperatures, NASA TR R-132, 1962.

Tankin, R.S., Visualization, Velocity, and Frequency Measurements of a Two-Dimensional Jet, 1987 USAF-UES Summer Faculty Research Program Graduate Student Summer Support Program Final Report, September, 1987.

Tennekes, H. and J.L. Lumley, A First Course in Turbulence, The MIT Press, Cambridge, 1972.

Welty, J.R., C.E. Wicks, and R.E. Wilson, Fundamentals of Momentum, Heat, and Mass Transfer, John Wiley and Sons, New York, 1976.

-----. Chemical Engineers' Handbook, edited by C.H. Chilton and R.H. Perry, McGraw-Hill, New York, 1973.

VITA

Captain Christopher A. Boedicker was born on 28 September 1961 in Saint Louis, Missouri. He graduated from DeSmet Jesuit High School in Saint Louis in 1979 and attended the United States Air Force Academy, from which he received the degree of Bachelor of Science in Aeronautical Engineering in June 1983. Upon graduation, he also received a commission in the USAF. He worked as an Airframe Propulsion Integration Engineer in the Aeronautical Systems Division's Flight Dynamics Laboratory from July 1983 until May 1986. He entered the School of Engineering, Air Force Institute of Technology, in May 1986.

Permanent Address: 11053 Quebec Court
Saint Ann, Missouri 63074

UNCLASSIFIED
SECURITY CLASSIFICATION OF THIS PAGE

REPORT DOCUMENTATION PAGE

Form Approved
OMB No. 0704-0188

1a. REPORT SECURITY CLASSIFICATION Unclassified	1b. RESTRICTIVE MARKINGS None
2a. SECURITY CLASSIFICATION AUTHORITY	3. DISTRIBUTION/AVAILABILITY OF REPORT Approved for public release; distribution unlimited
2b. DECLASSIFICATION/DOWNGRADING SCHEDULE	
4. PERFORMING ORGANIZATION REPORT NUMBER(S) AFIT/GAE/AA/87D-2	5. MONITORING ORGANIZATION REPORT NUMBER(S)
6a. NAME OF PERFORMING ORGANIZATION School of Engineering 6b. OFFICE SYMBOL (If applicable) AFIT/ENY	7a. NAME OF MONITORING ORGANIZATION
6c. ADDRESS (City, State, and ZIP Code) Air Force Institute of Technology Wright-Patterson AFB OH 45433-6583	7b. ADDRESS (City, State, and ZIP Code)
8a. NAME OF FUNDING/SPONSORING ORGANIZATION Air Force Wright Aero Lab 8b. OFFICE SYMBOL (If applicable) AFWAL/POSF	9. PROCUREMENT INSTRUMENT IDENTIFICATION NUMBER
8c. ADDRESS (City, State, and ZIP Code) AFWAL/POSF Wright-Patterson AFB OH 45433-6563	10. SOURCE OF FUNDING NUMBERS PROGRAM ELEMENT NO. / PROJECT NO. / TASK NO. / WORK UNIT ACCESSION NO.
11. TITLE (Include Security Classification) See box 19	
12. PERSONAL AUTHOR(S) Christopher A. Boedicker	
13a. TYPE OF REPORT MS Thesis 13b. TIME COVERED FROM _____ TO _____	14. DATE OF REPORT (Year, Month, Day) 1987 December 15. PAGE COUNT 164
16. SUPPLEMENTARY NOTATION	

17. COSATI CODES			18. SUBJECT TERMS (Continue on reverse if necessary and identify by block number)
FIELD	GROUP	SUB-GROUP	Fluid Dynamics, Fluid Mechanics,
20	04		

19. ABSTRACT (Continue on reverse if necessary and identify by block number)

TITLE : INTERACTION OF A TWO-DIMENSIONAL BLUFF BODY AND INCOMPRESSIBLE JET AND ANNULUS FLOWS

Thesis Chairman : James B. Planeaux, Lt, USAF
Assistant Professor of Aerospace Engineering

over

Approved for public release: IAW AFR 190-1
LYNN E. WOLAVER 31 Dec 87
Dean for Research and Professional Development
Air Force Institute of Technology (AU)
Wright-Patterson AFB OH 45433

20. DISTRIBUTION/AVAILABILITY OF ABSTRACT UNCLASSIFIED/UNLIMITED ☒ SAME AS RPT. ☐ DTIC USERS	21. ABSTRACT SECURITY CLASSIFICATION
22a. NAME OF RESPONSIBLE INDIVIDUAL James B. Planeaux, Lt,	22b. TELEPHONE (Include Area Code) 513-255-3517 22c. OFFICE SYMBOL AFIT/ENY

DD Form 1473, JUN 86 Previous editions are obsolete. SECURITY CLASSIFICATION OF THIS PAGE

Box 19 :

A particular interaction of bluff body and jet flows was studied using a two-dimensional slot jet (aspect ratio = 50) surrounded by a two-dimensional bluff body. The co-flowing system used air in the annulus and nitrogen in the jet. Flow visualization identified flow patterns containing large vortex structures. With a fixed annulus velocity, drastic changes in thd flow's structure were observed as jet velocities changed. Laser Doppler Anemometry measurements of instantaneous velocities were examined to characterize the flowfield details, and high speed movies provided qualitative insight into flow dynamics. The concept of jet and annulus "fields" is introduced. The "jet field" is the region above the bluff body that extends six or seven slot widths downstream, and the "annulus field" is the region above the jet field. The annulus flow dictates the flowfield dynamics in the annulus field up to jet-to-annulus velocity ratios of 1.45. The jet is responsible for the formation of the large-scale structures and dominates the flow in the jet field. Jet domination of the entire flowfield is seen at velocity ratios of 1.45 and above. Mie scattering was used to determine shedding frequencies of the large structures; Strouhal number based on jet velocity and slot width was a constant 0.098. (Thesis)